An investigation into the role of optineurin in macrophage-mediated acute antibacterial response in inflammatory bowel disease

By

Thean Soon Chew

A thesis submitted to UCL for the degree of

Doctor of Philosophy

Division of Medicine

2015

I, Thean Soon Chew confirm that the work presented in this thesis is my own. Where information has been derived from other sources, I confirm that this has been indicated in the thesis.

ex nihilo nihil fit

Abstract

Crohn's disease (CD) is now recognised to be due to defective host responses to bacteria in genetically susceptible individuals. Others in our research group previously found defective neutrophil recruitment, bacterial clearance and monocyte-derived macrophage (MDM) proinflammatory cytokine secretion in CD. To investigate the defective cytokine secretion, we performed transcriptomic analysis and identified reduced MDM optineurin (*OPTN*) expression in 10% CD patients. Here, I show that macrophages stimulated with *E. coli*, bacterial Toll-like and NOD-like receptor ligands upregulate OPTN, a Golgi complex protein that regulates vesicle transport. *In vitro*, *Optn*$^{-/-}$ bone marrow-derived macrophages (BMDM) stimulated with *E. coli* secrete significantly lower levels of proinflammatory TNF and IL6 cytokines, which is normalised to wildtype levels on addition of lysosomal function inhibitors. *In vivo*, *Optn*$^{-/-}$ mice develop a more severe *Citrobacter* colitis with greater mortality, an early defective neutrophil recruitment to the bowel and lower levels of serum proinflammatory cytokines. The *Optn*$^{-/-}$ mice also demonstrated a similar phenotype of defective neutrophil recruitment and lower serum proinflammatory cytokines in an *E. coli*-induced peritonitis. These results indicate that the low *OPTN* expression originally identified in CD macrophages has likely contributed to an attenuated antibacterial response, which potentially led to the development of bowel inflammation.

Table of Contents

Table of Figures

Table of Tables

Acknowledgements

This work was supported by the Wellcome Trust and Medical Research Council, United Kingdom. I would like to thank and acknowledge the following people who have contributed to this body of work:

- Dr Li-Shan Yeoh and Miss Sophie Chew – my wife and daughter for their patience and love.
- Professor Anthony W Segal – for his supervision and direction.
- Dr Andrew M Smith – for his supervision, guidance and support.
- Dr Nuala R O'Shea – for the laughter and tears we shared in working out and performing the experiments that needed doing.
- Mr Adam P Levine – for his support with bioinformatics, statistics and his critical eye on science.
- Dr Jenny Dunne – for her support with quantitative PCR and teaching me robust and tested scientific protocols.
- Dr Gavin W Sewell and Dr Carol McDonald – for their support with cell culture and molecular cloning.
- Ms Penelope Harrison – for excellent management of the lab, which allowed us to carry out experiments.
- Ms Rebecca Marnane, Ms Bernadette Petersen, Ms Sabrina Pacheco, Ms Janne Plugge – for excellent technical support, assistance and for keeping me in line.
- Dr Stuart L Bloom, Dr Sara McCartney and Dr Roser Vega – for sharing their patients with us and assisting with patient recruitment.
- Professor Marco Novelli and Mr Dahmane Oukrif – for reviewing histological specimens and sharing their expertise in histology.
- Mr Mark Turmaine – for his support with electron microscopy.
- UCLH histopathology department and UCL-Advanced Diagnostics – for their services with histology and immunohistochemistry.
- Mrs Sophia Joyce – for her administrative support.

Statement of Collaborative Work

A number of aspects of the work presented in this thesis were conducted as part of a collaboration. These include

- *Optn* zebrafish in situ hybridisation, stimulation with *Salmonella* and morpholino knockdown was performed by Dr Stefan H Oehlers and Professor Philip S Crosier, Department of Molecular Medicine and Pathology, School of Medical Sciences, The University of Auckland, Auckland 1142, New Zealand.
- Immunoprecipitation of OPTN in THP-1 cells was done by Dr Andrew M Smith and shotgun proteomics by mass spectrometry was performed by Dr Claire Mulvey and Professor Jasminka Godovac-Zimmermann, Proteomics and Molecular Cell Dynamics, Division of Medicine, University College London.
- Electron microscopy of macrophages was done by Mr Mark Turmaine, Division of Biosciences, University College London.
- H&E and immunohistochemistry optimisation and staining were performed by the UCLH histopathology department and UCL-Advanced Diagnostics under my direction.
- Optineurin expression in human monocyte-derived macrophages were performed jointly with Dr Gavin W Sewell, Dr Nuala O'Shea, Dr Carol McDonald, Dr Philip J Smith, Dr Farooq Rahman, Dr Daniel Marks, Dr Bu-Hayee Hussein, Ms Penelope Harrison, Ms Rebecca Marnane, Ms Bernadette Petersen.
- Subcellular fractionation of THP-1 cells was done by Dr Jenny Dunne and Dr Nuala O'Shea.

List of Abbreviations

- ADAM A disintegrin and metalloproteinase
- ADAMDEC1 ADAM-like, decysin 1
- ALS amyotrophic lateral sclerosis
- BMDM bone marrow-derived macrophages
- BSA bovine serum albumin
- CD Crohn’s disease
- cDNA complementary DNA
- CCL C-C chemokine ligand
- CXCL C-X-C chemokine ligand
- DNA deoxyribonucleic acid
- DSS dextran sodium sulphate
- EEA1 early endosome antigen 1
- eQTL expression quantitative trait locus
- ER endoplasmic reticulum
- FACS fluorescence activated cell sorting
- FBS foetal bovine serum
- FIP 14.7K interacting protein
- gDNA genomic DNA
- GI gastrointestinal
- GWAS genome-wide association study
- H&E haematoxylin and eosin
- HC healthy control
- HkEc heat-killed *E. coli*
- IBD inflammatory bowel disease
- IFN interferon
- Ig immunoglobulin
- IL interleukin
- IP immunoprecipitation

- IRF3 interferon regulatory factor 3
- K63-pUb Lysine-63 polyubiquitin chain
- LPS lipopolysaccharide
- M-CSF macrophage-colony stimulating factor
- MDM monocyte derived macrophages
- MDP muramyl dipeptide
- MOI multiplicity of infection
- MPS mononuclear phagocytic system
- mRNA messenger RNA
- MyoVI myosin VI
- NEMO NF-κB essential modulator
- NLR NOD-like receptor
- NOD nucleotide oligomerisation binding domain
- NRP NEMO-related protein
- optineurin optic neuropathy inducing
- OPTN human and mouse optineurin protein
- *OPTN* human optineurin gene
- *Optn* mouse optineurin gene
- *optn* zebrafish optineurin gene
- Optn zebrafish optineurin protein
- PAMP pathogen associated molecular pattern
- PBMC peripheral blood mononuclear cell
- PCR polymerase chain reaction
- PMN polymorphonuclear leukocyte
- POAG primary open angle glaucoma
- PRR pattern recognition receptor
- qRT-PCR quantitative reverse transcription-PCR
- RNA ribonucleic acid
- RNAi RNA interference
- siRNA small interfering RNA

- SNARE Soluble NSF attachment protein receptor
- SNP single nucleotide polymorphism
- SPF specified pathogen free
- T3SS type 3 secretion system
- TACE Tumour necrosis factor-α converting enzyme
- TBK1 TANK-binding kinase
- TEM transmission electron microscopy
- TiPM thioglycollate-induced peritoneal macrophages
- TIR Toll interleukin-1 receptor
- TLR Toll-like receptor
- TNF tumour necrosis factor α
- Ub ubiquitin
- UC ulcerative colitis
- UPR unfolded protein response
- WTSI Wellcome Trust Sanger Institute

Chapter 1 Introduction

Idiopathic inflammatory bowel disease (IBD) is a chronic relapsing systemic inflammatory disorder, primarily affecting the gastrointestinal tract (GI) but is associated with extraintestinal manifestations as well as other inflammatory diseases [1]. IBD consists of two predominant phenotypes, Crohn's disease (CD) and ulcerative colitis (UC), which are differentiated by their distinct inflammatory pattern and distribution of disease [2].

1.1 Diagnosis and natural history of inflammatory bowel disease

The diagnosis of CD or UC in patients with symptoms of bowel disease is dependent on the clinical history, disease presentation on endoscopy and imaging as well as biopsy histology. Crohn's disease presents with transmural inflammation of the GI mucosa that can affect the entire GI tract from the mouth to the anus [3] (Figure 1.1). By contrast, ulcerative colitis presents with superficial to deep ulceration and inflammation of the GI mucosa that affects only the colon to varying extents from the distal rectum to the proximal caecum [4].

1.1.1 Natural history of Crohn's disease

CD most commonly presents with patchy discontinuous inflammatory skip lesions that affects the terminal ileum only (45% patients), colon (32%) or ileum and colon i.e. ileocolonic (19%) (Figure 1.1) [5]. The majority of patients are diagnosed between the ages of 17 to 40 (56%), with a smaller percentage diagnosed above 40 (32%) and below 17 years of age (11%). In the majority of CD patients (81%), the mucosal disease is purely inflammatory, with a minority having more severe stricturing (5%) or penetrating/fistulating disease (19%) [3].

Endoscopically, the inflamed CD bowel presents on a spectrum from small discrete aphthous ulcers, patchy well demarcated skip lesions to deep serpiginous and linear cobblestone ulcers (Figure 1.1). One of the hallmarks of CD is the finding of granulomas on bowel biopsy, which are collections of macrophages and lymphocytes.

The clinical presentation is largely dependent on disease location and behaviour, which may include symptoms of diarrhoea, abdominal pain, vomiting, bowel obstruction, weight loss, haematochezia and mucochezia.

Whilst the anatomical location affected by CD remains relatively unchanged [6], the behaviour of the disease can change substantially with time. Three months after diagnosis, almost a fifth (19%) of patients and at 20 years, more than half (51%) developed a more aggressively behaving disease [5]. In a different cohort, over a 10 year period, 27% of patients with purely inflammatory CD developed stricturing disease whilst 29% developed penetrating disease over a median of 6 years [7].

After the first year, only 55–65% achieve remission, 15–25% continue with low levels of disease activity whilst the remaining 10–30% develop a further exacerbation. In the long term, only 10–13% remain in remission for several years, 13–20% continue to have active disease whilst the vast majority, 67–73% have a chronic intermittent disease course [8].

The life expectancy of CD patients today is no different from the general population. This is in contrast to older studies and is likely due to improved treatment options available now [9, 10].

a

b

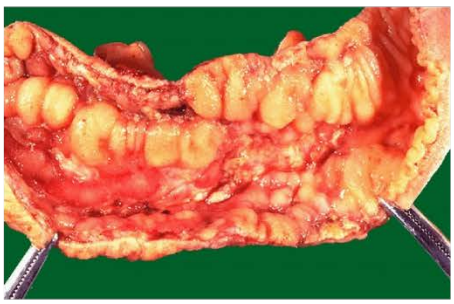

c

d

e

f

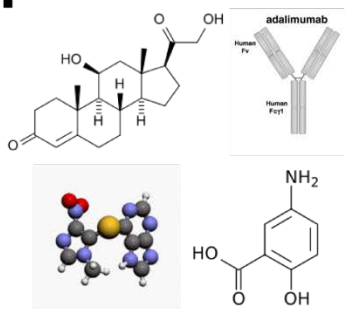

g

Montreal classification of Crohn's disease		
Age at diagnosis	A1	≤16 years of age
	A2	between 17- 40 years of age
	A3	>40 years of age
Location	L1	ileal
	L2	colonic
	L3	ileocolonic
	L4	isolated upper disease*
Behaviour	B1	non-stricturing, non-penetrating
	B2	stricturing
	B3	penetrating
	p	perianal disease modifier†

*L4 is a modifier that can be added to to L1-L3 when concomitant upper gastrointestinal disease is present.

†p is added to B1-B3 when concomitant perianal disease is present.

h

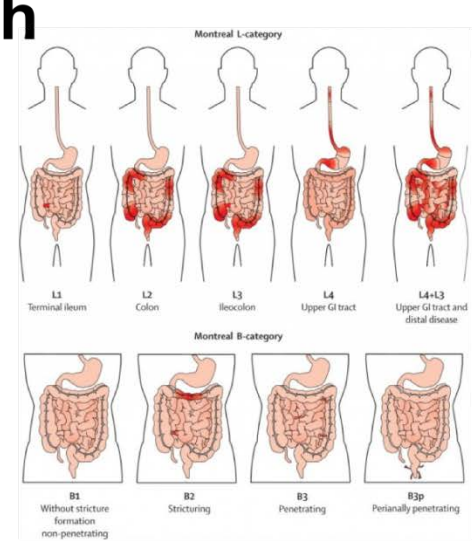

i

j

k

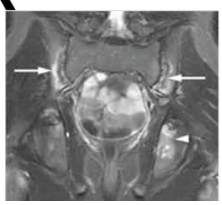

l

Figure 1.1 The various manifestations of Crohn's disease. (a) Burrill B. Crohn who presented a case series of patients with terminal ileitis, whom the disease has been named after, (b) resection specimen of the terminal ileum showing cobblestoning and ulceration of the mucosa, (c) endoscopic view of patchy ulcerated mucosa, (d) barium follow through of the small bowel showing stricturing of the terminal ileum (arrow), (e) H&E stain showing transmural inflammation and a non-caseating granuloma in CD, (f) drugs used in the treatment of Crohn's disease, clockwise from top left corticosteroids, adalimumab anti-TNF, mesalazine, azathioprine, (g) Montreal classification of Crohn's disease, (h) pictorial representation of location and behaviour of Crohn's disease, (i) extraintestinal manifestations of Crohn's disease, namely uveitis, (j) pyoderma gangrenosum, (k) magnetic resonance image of sacroiliac joints showing sacroiliitis (arrows) and (l) oral Crohn's disease (See Image references).

1.1.2 Natural history of ulcerative colitis

By contrast, UC presents with inflammation in the distal rectum that extends continuously to varying extents to involve just the rectum (proctitis, 32% patients), rectum, sigmoid and descending colon (left-sided colitis, 31%) or the whole colon including the transverse, ascending colon and caecum (pancolitis, 31%) [11, 12]. The clinical presentation in UC is largely dependent on the extent and severity of the disease, with symptoms and signs of bloody diarrhoea, abdominal cramps, weight loss, passage of pus and mucus, proximal constipation, toxic megacolon and bowel perforation in the extreme. Most patients present with mild (no signs of systemic toxicity and up to 4 bloody stools daily, 51% patients) and moderate UC (more than 4 bloody stools daily, 40%). Only a minority present with severe UC (signs of systemic toxicity and more than 6 bloody stools daily, 9%) [11].

Endoscopically, the bowel in UC presents on a spectrum from mild erythema, oedema and loss of vascular markings, mucosal granularity, friability and spontaneous bleeding, erosions to large ulcers. Histologically, in contrast to CD, there is marked involvement of the mucosal crypts with

visible crypt architectural distortion, cryptitis and crypt abscesses in the UC mucosa but no granulomas, suggesting a different aetiology.

The natural history of UC over 10 years is good, with the majority of patients (55%) achieving remission, 37% having intermittent exacerbations and only 6% developing chronic continuous symptoms [13]. One fifth of patients with proctitis or left-sided colitis at diagnosis progressed to pancolitis over a 10-year period. Conversely, the probability of regression of the pancolitis over 25 years was calculated to be 75% in another study [14]. The overall colectomy rate in UC over 10 years was 9.8% and overall mortality risk was not increased compared to the general population.

1.2 Epidemiology and burden of inflammatory bowel disease

1.2.1 Healthcare cost of inflammatory bowel disease

The natural history of CD and UC highlight the potential impact of these two inflammatory diseases on the population. It inflicts a chronic recurrent debilitating illness on a relatively young population affecting physical growth and education in children [15], work productivity and fertility in adults [16] and mortality in the elderly [17]. The healthcare cost of IBD was calculated to be £500 million in 2000 and £720 million per year in 2006 for the UK National Health Service, C$753 million in 2008 and C$1.2 billion per year in 2012 in Canada, €4.6 to 5.6 billion per year in 2012 in Europe and US$1.4 billion in 1990 and US$6.3 billion in 2008 in USA [18-22]. The total economic burden for CD and UC is estimated to be US$10.9-15.5 billion and US$3.4-8.6 billion in USA and €2.1-16.7 billion and €5.4-12.6 billion in Europe [23, 24].

The trend of rising healthcare and total costs is made worse by the increasing incidence of IBD with time and also geographical location [25, 26]. The highest annual incidence for CD was 12.7, 5.0 and 20.2 per 100,000 person-years and for UC was 24.3, 6.3 and 19.2 per 100,000 person-years in

Europe, Asia and North America respectively. The prevalence for CD was 322 and 319 per 100,000 persons and for UC was 505 and 249 per 100,000 persons in Europe and North America. 75% and 60% of CD and UC epidemiological studies identified a rising disease incidence with an average annual percentage rise of 1.2% to 23.3% in CD and 2.4% to 18.2% in UC. By contrast, no CD and only 6% of UC studies showed decreasing incidence [26].

1.2.2 Rising incidence and prevalence of IBD

CD and UC was traditionally a disease of the western developed world. However, with globalisation and westernisation of lifestyle, IBD is rising in Asia [27]. In developing countries where CD and UC were previously rarely reported, IBD has also emerged. IBD in Asia and these developing countries seems to be following a similar pattern of progression in developed countries in the 20th century with an initial rise in UC incidence that stabilises followed by a rise in CD incidence 15 to 20 years later [26-28].

By example, in Asia the prevalence of CD in Japan has risen from 2.9 to 13.5 per 100,000 persons over 12 years and from 1.3 to 7.2 per 100,000 persons over 14 years in Singapore. The prevalence of UC has quadrupled from 7.6 to 30.9 per 100,000 over 8 years in South Korea, tripled from 2.3 to 6.3 per 100,000 over 9 years in Hong Kong and quadrupled over 10 years in China. Due to its recent emergence in developing countries, currently there is little time lapse data to confirm this trend. Incidence and prevalence is still low relative to developed Western countries. The prevalence of CD and UC was 1.2 and 5.3 per 100,000 persons in 2008 in Sri Lanka, 16.7 and 44.3 per 100,000 persons in 2004 in Barbados and 15 and 76 per 100,000 persons in 2009 in Argentina [29-31].

The prevalence of UC was 3.7 in Malays, 11.2 in Chinese and 17.9 in Indians per 100,000 persons in Malaysia and 44.3 per 100,000 persons in

India [32, 33]. The disparity in prevalence amongst different ethnic groups in a single location and of a single ethnic group i.e. Indians in different locations reflects the contribution of genetic susceptibility and the environment to the development and prevalence of disease. Unfortunately, genetic data from patients in developing countries is not currently available.

1.3 Environmental effects on IBD

1.3.1 Smoking

To date, the strongest associated environmental factor in IBD is smoking. In Caucasians, smoking is detrimental in CD and protective in UC, increasing the risk of CD (OR 1.76) and decreasing the risk of UC (0.58) [34]. However, the increased risk of CD with smoking has not been reproduced in Israeli Jews and the Chinese although the protective effect of smoking has been reproduced in the Japanese. It is postulated that smoking may not cause but modulate disease via immunosuppressive effects on immune cells such as macrophages and T cells, further strengthening the case for a macrophage defect in IBD immunopathogenesis [35].

1.3.2 Diet

The association of diet and IBD has been around since the time of Bonnie Prince Charlie (1720-1788), who likely suffered from ulcerative colitis. He treated himself by adopting a milk free diet in 1745 [36]. More recently two meta-analyses looking at dietary intake and IBD identified a higher risk of CD and UC with high fat and meat intake, whilst a high intake of fruit and fibre was protective for CD and a high vegetable intake was protective for UC [37, 38]. It is unclear how these dietary antigens may increase the risk of disease or be protective but may alter the expression of transcription factors that regulate inflammation, affect mediators of inflammation such as short chain fatty acids or alter the gut microflora [38]. Additionally, whilst these

results may be important in the development of disease, the effect of diet on disease progression is not clear.

The role of probiotics and prebiotics in modulating the gut microflora in IBD is discussed below. It is well accepted that enteral nutrition can be used as first-line therapy in children with CD to induce remission, which adds to the argument that dietary content can influence the mucosal inflammatory process [39-42]. Although enteral therapy is widely used in children, its mechanism of action is not known and in adults there is limited efficacy [43]. It has always been argued that the lack of effect in adults is due to poorer compliance with an exclusive enteral therapy regimen but this difference in effect may be due to differences in the inflammatory process in adults vs children, although this has not been conclusively shown.

1.4 Treatment of inflammatory bowel disease

The rise in healthcare costs of IBD is in part due to the rising cost of drug treatment and the availability of endoscopic as well as surgical therapies. Endoscopy does not just have a role in diagnosis of the disease but in the monitoring of remission, surveillance of cancer, diagnosis of disease exacerbations and treatment of strictures. Surgery has a role not just when drug treatment has failed and bowel resection is required but also in the treatment of fistulae and insertion of feeding lines. However, the mainstay of IBD treatment is with drug therapy to modulate inflammation (Figure 1.1).

1.4.1 5-Aminosalicylates

5-Aminosalicylates (5-ASA) in the form of sulphasalazine were first used in the early 1950s and forms the mainstay of treatment in induction and maintenance of remission in mild to moderate UC. Its exact mechanism of action is unknown but it is thought to exert a topical effect on the bowel via a combination of inhibition of cytokine, prostaglandin and leukotriene synthesis,

inhibition of leukocyte adhesion and function, macrophage chemotaxis [44] and prevention of clonal expansion of T and B cells. Many formulations of mesalazine exist with long acting single dose varieties as well as topical enemas and suppositories for distal proctitis. There is less evidence for the use of 5-ASA in CD except in ileal and right sided colonic disease [45].

1.4.2 Corticosteroids

Corticosteroids form the main acute therapeutic option in a flare of UC or CD and was first used in the 1950s to treat UC and reduced mortality from 24% to 7% [46]. Steroids function by switching off proinflammatory genes that encode cytokines, chemokines and adhesions molecules via NF-κB and switching on anti-inflammatory genes. In UC, steroids will successfully induce a remission in up to 70% patients. Steroids are twice as effective in inducing remission in CD compared to placebo and more than one and half times more effective than 5-ASA [47].

1.4.3 Thiopurine analogues

The main drug treatment to maintain remission in moderate to severe UC and CD are the thiopurine analogues azathioprine (AZA) and 6-mercaptopurine (6-MP). The thiopurine analogues are generally used as steroid-sparing agents in maintaining the remission achieved by steroids and ciclosporin thereby preventing the long term complications associated with steroid and ciclosporin toxicity. They act as purine antimetabolites that are falsely incorporated into dividing immune cells, hence has a slow mode of action taking months to be efficacious. They have been shown to reduce the number of lamina propria plasma cells and impair intracellular replication of *E. coli* in macrophages [48].

1.4.4 Anti-TNF therapy

The newest class of drugs in IBD are the biologics that target specific cytokines, receptors or molecules with antibodies. The most widely used biologics in CD are the anti-TNF antibodies infliximab and adalimumab. The exact mechanism of action of anti-TNFs in CD is unknown but may be through direct blockade of TNF or the induction of apoptosis in immune cells [49-52]. It is important to note that although anti-TNF therapy is efficacious in the setting of chronic CD inflammation there have been reports of new onset CD during anti-TNF therapy for ankylosing spondylitis and juvenile arthritis [53-61]. As such, whilst anti-TNFs may have a therapeutic role in the chronic inflammation of CD in inducing apoptosis of immune cells that perpetuate the inflammation [62], in the acute setting, TNF may be important in bacterial clearance in the bowel and its blockade then results in CD.

1.5 Pathogenesis of Crohn's disease

The earliest description of Crohn's disease was by the anatomical pathologist Giovanni Battista Morgagni who described an eroded and ulcerated ileum in 1769 in *De sedibus et causis morborum per anatomen indagatis* or 'Of the seats and causes of disease investigated through anatomy' [63, 64]. However, the most widely quoted description that gave name to the disease was in 1932 by Burrill Crohn (Figure 1.1), together with Leon Ginzburg and Gordon Oppenheimer, who presented a case series of patients with terminal ileitis to the Gastroenterological and Pathology section of the American Medical Association meeting in New Orleans [65, 66].

1.5.1 Infectious aetiology

Although the disease was first described more than 200 years ago, the cause of Crohn's disease is still not known [67]. There have been many proposed theories of causation including bacterial and viral agents, diet, poor

nutrition, imbalances in gut microflora, dysfunctional mucosal barrier, allergies, autoimmunity or immunodeficiency. Whilst there is evidence to support each theory there is no overwhelmingly proven hypothesis identifying a single cause of CD. It is likely that the cause of CD is complex and that as a syndrome, the collective signs and symptoms of CD may be the manifestation of multiple different defective processes resulting in a common expression of dysfunctional physiology that is the phenotype of CD. It is therefore plausible that different factors may play a role in different patients but result in the same phenotype of CD.

CD commonly affects the terminal ileum. This area of the bowel constitutes the area with the largest change in the number of intraluminal bacteria from the relatively sterile proximal small bowel (10^4 bacteria) to the colon (10^{12} bacteria) [68]. Antibiotics have had a beneficial role in the induction and maintenance of remission in CD albeit to only a limited extent further supporting a role for intraluminal bacteria in the pathogenesis and maintenance of inflammation in CD [69]. Additionally, diversion of the faecal stream results in improvement of CD inflammation [70], which all point to a role for bacteria in the aetiopathogenesis of CD.

An association between *Mycobacterium avium* subspecies *paratuberculosis* (MAP) and CD was made in the early 20th century by Dr T. K. Dalziel who noted the similarity between bovine Johne's disease caused by MAP and human CD although no visible mycobacterium were seen in CD tissue unlike in cattle [71]. Unfortunately, the causal association remains controversial and is unsupported due to clinicopathological differences between Johne's disease and CD [72], the inability to find MAP in bowel biopsies and in CD granulomas [73], and the lack of difference between relapse rates in MAP treated vs. placebo treated CD patients [74].

By contrast, stronger evidence is available for the role of adherent invasive *E. coli* (AIEC) in CD. The most convincing evidence for this is the

discovery of AIEC in 21.7% of CD chronic inflamed ileum versus only 6.2% in controls [75]. The invasion of AIEC is with its type 1 pili [76] that bind and invade the mucosal epithelium via CEACAM6, a carcinoembryonic antigen upregulated by proinflammatory cytokines and AIEC itself [77, 78] or via long polar fimbriae binding to M cells and invasion into Peyer's patches [79]. AIEC was also able to survive in macrophages and initiate inflammation [80]. Additionally, *E. coli* DNA has been found on PCR from microdissected CD granulomas [81].

1.5.2 Dysbiosis

Recently the focus has been on the changes in diversity of the bowel microflora that may be associated with CD causation [82]. Dysbiosis of the gut microflora has become a major focus of investigation in an attempt to identify qualitative and quantitative changes in gut microflora diversity, metabolic activity and distribution [83]. These findings identified a reduced complexity in the Fermicute phylum in CD patients [84, 85]. Twins with CD were found to have microbial compositions that were different from healthy controls (HC) and were different depending on whether the ileum or colon was affected by CD [86]. Additionally, a reduction in the abundance of *Faecalibacterium prausnitzii* was associated with a higher risk of post-operative recurrence of ileal CD and was anti-inflammatory in mouse models of colitis [87]. Of note there is evidence that diet can modify the gut microflora, which may be the mechanism by which diet modifies the risk of developing CD [88].

1.6 Genetic factors in Crohn's disease

Whilst the rising incidence of CD points to an environmental factor in causation, family and racial aggregation of CD points to a genetic contribution to aetiology. In first-degree relatives, the age-adjusted relative risk of developing the same type of IBD is 5 to 10 in CD and 2 to 8 for UC

[89-91]. IBD concordance rates in monozygotic twins was 20% to 50% for CD and 14% to 19% in UC but less than 7% in dizygotic twins for both CD and UC [92-96]. Finally, Jews have a two-fold increase risk of developing CD if they have affected family members compared to non-Jews [91].

The investigation into the genetic causation of CD has seen an unprecedented explosion in discovery over the past decade, beginning with the discovery of an association with CARD15/NOD2 [97, 98] till the more recent discoveries of genome wide association studies (GWAS) that has identified single nucleotide polymorphisms (SNP) within 163 different gene susceptibility loci [99-102].

1.6.1 NOD2

Nucleotide-binding oligomerisation domain-containing protein 2 (NOD2) was the first gene to be associated with CD and to date confers the greatest risk of developing CD. Using positional cloning and candidate gene approaches, two groups identified *NOD2* as a susceptibility gene in CD [97, 98]. NOD2 is a cytosolic receptor protein that recognises the ubiquitous bacterial peptidoglycan muramyl dipeptide (MDP), a pathogen associated molecular pattern. Unlike *NOD1*, *NOD2* expression is more restricted to haematopoietic cells such as myeloid and lymphoid cells, as well as intestinal epithelium [103] and Paneth cells [104]. Expression of *NOD2* is upregulated on exposure to lipopolysaccharide (LPS), tumour necrosis factor α (TNF) and interferon γ (IFNγ).

The NOD2 protein has a leucine-rich repeat (LRR) region that senses MDP, which results in oligomerisation at the central nucleotide-binding domain (NBD) and interaction of its multiple caspase-recruitment domains (CARD) with downstream adaptors such as receptor-interacting protein-2 (RIP2) [105]. This results in downstream nuclear factor-κB (NF-κB) and mitogen-activated protein kinase (MAPK) dependent gene transcription. Of

note, only loss of function variants in *NOD2* are associated with CD, whilst gain of function variants in *NOD2* are associated with Blau syndrome, a granulomatous disease with arthritis, uveitis and dermatitis. The three NOD2 loss of function variants associated with CD are 2104C>T/Arg702Trp (SNP8, in exon 4), 2722G>C/Gly908Arg (SNP12, in exon 8) and 3020insC/Leu1007fsinsC (SNP13, in exon 11. All three CD variants result in loss of function and impaired induction of pro-inflammatory cytokines [106-109]. Individuals who are heterozygous for one of the variants have a two to four fold risk of developing CD, whilst individuals who are homozygous or compound heterozygous have a 20 to 40 fold risk [110].

Despite this, the overall effect of NOD2 variants on inflammation and CD remains controversial. It is unclear if the NOD2 variants act via intestinal Paneth cells or myeloid cells or what the mechanism of action that results in increased CD risk is. NOD2 variants have been shown to regulate Toll-like receptor 2-mediated T helper type 1 responses, transcription of IL10 and expression of α-defensins [111-114]. Additionally, NOD2 variants are associated with increased ileal permeability, ileal only CD, penetrating and stenosing disease and acts as a marker of severity and need for surgery [115-117]. Whilst NOD2 confers the highest heritable risk of developing CD, the allele frequency in the healthy Caucasian population for SNP8, SNP12 and SNP13 are 4.3%, 1.2% and 2.3% implying that NOD2 alone may not be sufficient to result in CD but interacts with other as yet unknown risk factors [118]. Finally, whilst NOD2 increases the risk of developing CD, it is protective in UC, indicating that CD and UC may be pathophysiologically different [100].

1.6.2 ATG16L1

A nonsynonymous SNP resulting in a threonine to alanine substitution (1338A>G/Thr300Ala) in the autophagy-related 16-like 1 (*ATG16L1*) gene was also identified on GWAS to be associated with CD [102, 119]. The

1338A/A homozygous genotype of the risk allele has been reported to confer a 1.65-fold risk of developing CD, with a 2.2-fold risk of ileal disease [120]. However, similar to *NOD2*, the *ATG16L1* disease conferring allele frequency in the healthy Caucasian population is 50.4% vs. 58.1% in the CD cohort, indicating that the *ATG16L1* disease conferring allele is not sufficient to result in CD alone [121].

Autophagy, or simply self-eating, is the term used to describe the intracellular processes that degrade and recycle unwanted macromolecules, organelles and cellular components via lysosomes. There are at least three main types of autophagy, microautophagy, macroautophagy and chaperone-mediated autophagy [122]. Microautophagy is the uptake and degradation of cytoplasm by invagination of the lysosome, whilst chaperone-mediated autophagy is the import and degradation of cytosolic proteins by chaperones that are directly translocated across the lysosomal membrane independent of autophagosome [123]. Macroautophagy, commonly referred to as just autophagy is the sequestration of cytoplasm into double or multiple-membrane autophagosomes and its subsequent degradation by lysosomes. A specific subtype of autophagy is xenophagy, which is the selective degradation of microbes through an autophagy related mechanism.

Macroautophagy, here on just referred to as autophagy involves the initiation, elongation, completion steps of the double membrane autophagosome, then fusion and cargo degradation with lysosomes. After induction of autophagy, the ULK1 complex (ULK1-ATG13-FIP200-ATG101) in the endoplasmic reticulum recruits phosphatidylinositol-3-OH kinase (PI(3)K) complex, which forms phosphatidylinositol-3-phosphate that recruits double membrane vesicles containing ATG18, ATG12-ATG5-ATG16L1 and LC3 (Figure 1.2). The induction of starvation autophagy results in the inclusion of organelles and macromolecules for recycling. By contrast, LC3 present on the double membrane autophagosome can bind adaptor molecules such as p62, neighbour of BRCA1 gene 1 (NBR1), nuclear dot

protein 52 (NDP52) and optineurin (OPTN) carrying cargo such as ubiquitinated bacteria in selective autophagy (Figure 1.3) [124, 125]. Completion of the autophagosome occurs, which then fuses with lysosomes to form autophagolysosomes where contents are degraded. Autophagy is likely to have evolved as a response to nutrient starvation and allows unicellular organism to recycle damaged organelles and misfolded proteins, hence is upregulated upon starvation, endoplasmic reticulum (ER) stress and also infection [122, 123].

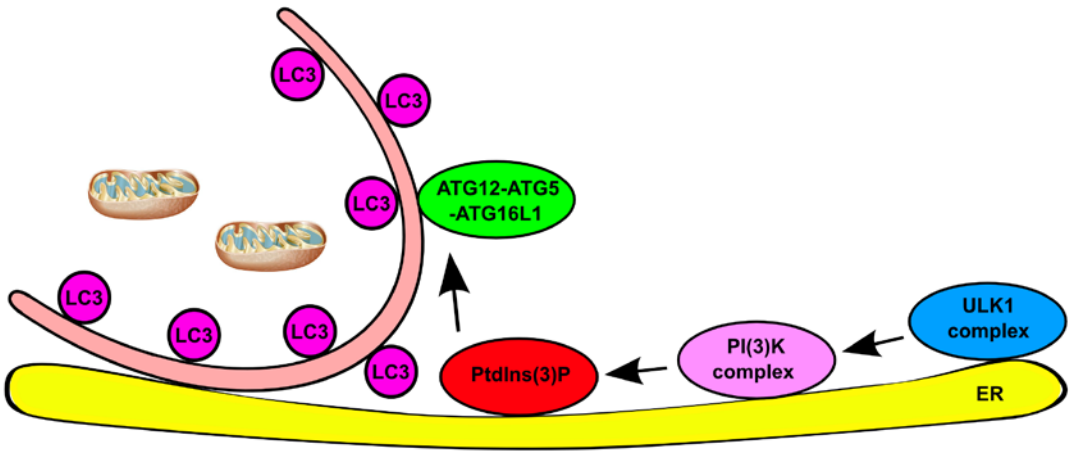

Figure 1.2 Induction of starvation autophagy. Induction of starvation autophagy results in the inclusion of organelles and macromolecules from the cytoplasm for degradation in double membrane autophagosomes.

Whilst autophagy was initially discovered in yeast cells as a response to starvation, autophagy has been linked to phagocytosis and bacterial handling. Particles that stimulate Toll-like receptors (TLR) whilst it is phagocytosed by murine macrophages recruit LC3 to the phagosome, which was associated with enhanced killing of phagocytosed microbes [126]. The discovery of an association between ATG16L1 and CD identifies autophagy as a process that may be defective in CD but the exact mechanism by which ATG16L1 increases the risk of CD remains unanswered. Human intestinal

cells with the T300A variant or that had *ATG16L1* knocked down were found to have impaired autophagy of internalized *Salmonella* within autophagosomes [102, 127], while ATG16L1 deficient murine macrophages stimulated with LPS were found to secrete high levels of the inflammasome associated pro-inflammatory cytokines IL1β and IL18 [128]. ATG16L1 hypomorphic mice were found to exhibit abnormalities in the granule exocytosis pathways in Paneth cells, which secrete antimicrobial peptides into the intestine, findings that were replicated in humans carrying the T300A variant [129]. However, the findings in the mice were later found to be associated with coinfection with murine norovirus [130].

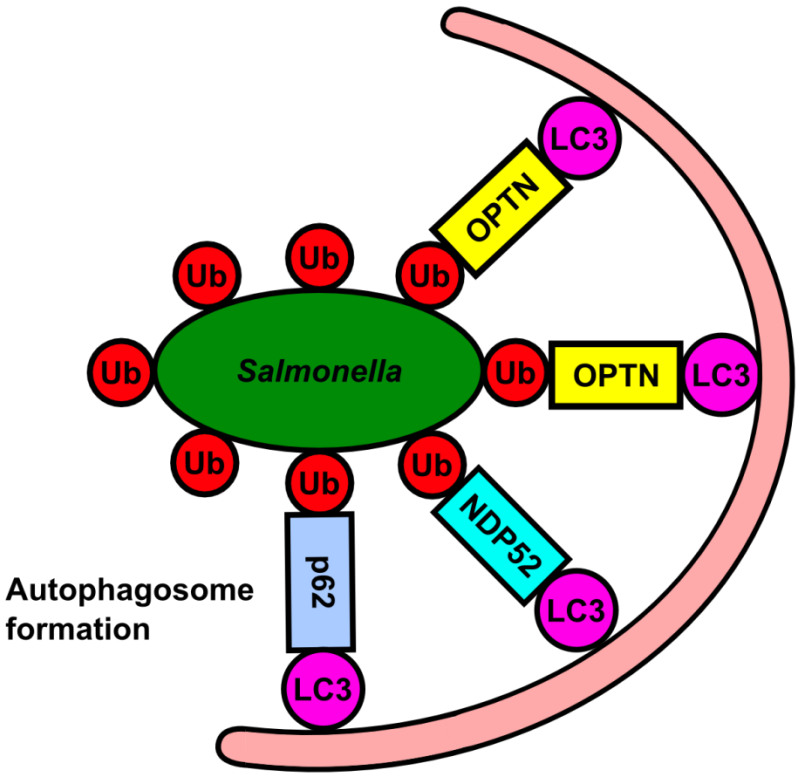

Figure 1.3 Selective autophagy and the role of adaptors in bringing cargo to autophagosomes. OPTN, optineurin; Ub, ubiquitin; p62/SQSTM1, protein 62/sequestosome1; NDP52, nuclear dot protein 52.

More recently, an association between NOD2 and ATG16L1 has been found. NOD2 stimulation by MDP induced autophagy in dendritic cells and was required for MHC Class II $CD4^+$ T cell responses whilst NOD2 stimulation in peripheral blood mononuclear cells from humans with the ATG16L1 T300A variant produced more inflammasome associated IL1β [131, 132].

1.6.3 The missing heritability in CD

GWAS are powered with large numbers of healthy versus affected individuals to identify disease susceptibility genes using the hypothesis that common complex diseases are due to relatively few common variants of small effect [133]. However, as discussed above, the collective signs and symptoms that make up the phenotypic syndrome of CD may be the result of multiple different rare variant-causing pathophysiological pathways. Given the GWAS limitation and the heterogeneity of the phenotype of CD it is therefore not surprising that the GWAS CD associated variants is calculated to account for only 23% of the total CD heritability and the recent discussion of the missing heritability unaccounted for in GWAS of complex diseases [99, 134].

1.7 Innate immunity in the gastrointestinal tract

Acute inflammation is the bodies' immediate reaction to trauma or infection and involves the classic signs of *calor, dolor, rubor, tumor* and *functio laesa* i.e. heat, pain, redness, swelling and loss of function first described by Celsus in *De Medicina* in the 1st century BC [135]. This acute inflammatory response is mediated by 'wandering cells' first identified by the Nobel laureate and Father of Cellular Innate Immunity, Elie Metchnikoff who had observed phagocytic cells in starfish larvae [136]. These phagocytes would later make up cells of the innate immune system consisting monocytes and

macrophages of the mononuclear phagocyte system as well as polymorphonuclear leukocytes or neutrophils.

1.7.1 Macrophages and neutrophils in gut mucosa

When bacteria breach our mucosal barrier they come into contact with tissue-resident macrophages, which are sentinels positioned and programmed to detect and deal with invading organisms [137]. Macrophages are specialised cells that are equipped with a wide range of pattern recognition receptors (PRR) that detect microbes. These PRR include the TLR that recognise pathogen associated molecular patterns (PAMP), which were discovered by Jules Hoffmann in fruit flies and Bruce Beutler in human macrophages, who were jointly awarded the Nobel Prize in 2011 [138, 139]. The Nod-like receptor NOD2 recognises muramyl dipeptide (MDP) as discussed earlier whilst the TLR recognise other PAMP such as the lipopeptide Pam_3CSK_4 by TLR2, double-stranded RNA by TLR3, lipopolysaccharide (LPS) by TLR4, flagellin by TLR5, single-stranded RNA by TLR7 and single-stranded DNA by TLR9 (Figure 1.4) [140].

The TLR are divided into two groups, TLR 2, 4 and 5 that are expressed on the cell surface and recognise mainly bacterial PAMP and TLR 3, 7 and 9 that are expressed on intracellular vesicles and mainly recognise microbial nucleic acids. The TLR are type 1 transmembrane proteins with an extracellular/intravesicular LRR domain that recognises PAMP, a transmembrane domain and an intracellular Toll-interleukin 1 receptor (TIR) domain for downstream signalling. Signalling of TLR occur via the TIR domain-containing adaptor molecules MyD88 and TIRAP down the MyD88-dependent pathway or via TRAM and TRIF, down the MyD88-independent pathway. For example, TLR4 in complex with MD2 binds LPS and recruits the adaptors TIRAP and MyD88, which activates a MyD88-dependent early NF-κB mediated inflammatory cytokine pathway. The internalised TLR4-MD2-LPS complex can then recruit TRAM and TRIF that activates the

IRF3/TRIF-dependent type I interferon pathway as well as a TRIF-dependent late NF-κB inflammatory cytokine pathway. In contrast to TLR4, TLR2, 5, 7 and 9 only activates the MyD88-dependent inflammatory cytokine pathway and TLR3 the TRIF pathway.

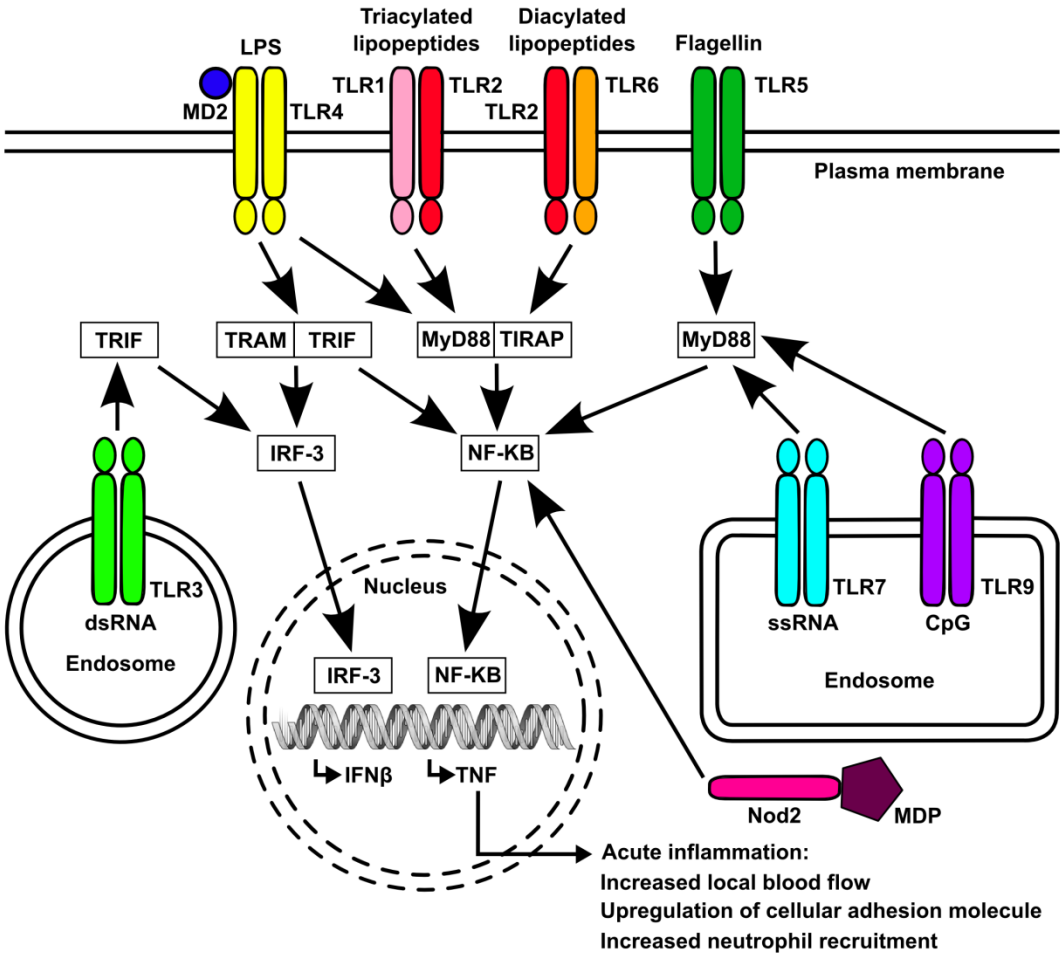

Figure 1.4 TLR and NLR activation by PAMP in macrophages. Activation of the NF-κB and IRF-3 pathway results in induction of pro-inflammatory cytokine gene transcription.

NF-κB activation is rapid and results in the transcription of proinflammatory cytokines, chemokines and adhesion molecules whilst type I interferon responses are aimed at limiting the spread of infectious agents

such as intracellular viruses, promoting antigen presentation and activating the adaptive immune system [141]. The resulting TLR activation of macrophages by bacterial PAMP is the release of proinflammatory cytokines such as TNF and chemokines such as CXCL1 that mediate acute inflammation and the recruitment of neutrophils. Blood flow to the site of infection increases and TNF results in increased expression of cellular adhesion molecules on endothelial cells. Initial capture and rolling adhesion is facilitated by transitory adhesion between selectins on neutrophils and endothelial cells, which is then reinforced by tighter adhesion between integrins CD11a/lymphocyte function-associated antigen-1 (LFA-1), CD11b/macrophage antigen 1 (Mac-1) and LPAM-1 (integrin $\alpha_4\beta_7$) with intercellular cell adhesion molecule-1 (ICAM-1), vascular cell adhesion molecule-1 (VCAM-1) and mucosal vascular addressin cell adhesion molecule-1 (MAdCAM-1). Transmigration through the endothelium then occurs through the interaction of platelet-endothelial cell adhesion molecules (PECAM) on neutrophils and endothelial cells [142].

Neutrophils are recruited to sites of infection within minutes and response peaks at 24 to 48 hours [143]. Neutrophils are the army of first responders that are efficient phagocytes at killing microbes using the NADPH oxidative burst as well as its arsenal of antimicrobial peptides such as myeloperoxidase, Cathepsin G, elastase and defensins [144, 145]. It has been shown that neutrophil depletion worsens the colitis in a DSS, TNBS and T cell transfer model of colitis, reinforcing the importance of neutrophils in the containment of infection and prevention of subsequent intestinal inflammation [146-148]. Additionally, mice lacking the neutrophil chemokine CXCL1 are more susceptible to a DSS colitis [149]. Finally, as discussed above, patients with monogenic deficiencies of neutrophil function commonly manifest intestinal inflammation that is similar to CD.

Tissue resident neutrophils have a short lifespan of a few days, undergo apoptosis and are cleared by macrophages to allow for resolution of

inflammation and wound healing. Indeed, the depletion of intestinal mononuclear phagocytes alone in contrast to depletion of neutrophils and mononuclear phagocytes has been shown to worsen a DSS induced colitis, suggesting that mononuclear cells have a role in the resolution of neutrophil-led inflammation [150]. Finally, it is important to note that the origin of tissue resident macrophages remains controversial. It was widely accepted for a long time that all tissue resident macrophages originated from peripheral blood monocytes [151]. However, more recent fate mapping studies in mice show that resident macrophages in the liver, lung, spleen and peritoneum are established from the primitive yolk sac prior to birth and subsequently maintain themselves independent of blood monocytes [152], whilst intestinal macrophages during inflammation derive from blood $Ly6C^+$ monocytes [153]. Whilst there is agreement on the origins of tissue resident macrophages in some organs, their origins in other organs particularly during inflammation remains hotly debated [154-157].

1.7.2 Cytokine trafficking in macrophages

Whilst extensive work has been done on the stimulation, signalling pathways and transcriptional mechanisms that result in the release of cytokines from macrophages as well as the effect of these cytokines on target receptors and cells, only recently has more been discovered about the pathways and mechanisms that control cytokine trafficking and vesicle fusion within cells. These discoveries earned James Rothman, Randy Schekman and Thomas Sudhof the Nobel Prize in 2013 for their role in identifying the function of SNARE proteins as well as the genes that control and time vesicle fusion.

1.7.2.1 TNF

The intracellular trafficking of cytokines in macrophages is most widely studied in TNF, which has shed light on the complex and tightly regulated trafficking of cytokines from the *trans*-Golgi network (TGN) to the plasma

membrane [158]. TNF secretion is non-constitutive and is tightly regulated at the transcriptional and translational levels to deliver a large bolus when macrophages are activated [159, 160], but unlike other cytokines is trafficked as a transmembrane precursor. On LPS stimulation, membrane-bound TNF can be found at the Golgi complex by 20 minutes and TNF secreted by 40 minutes [161]. After processing through the Golgi complex, TNF is packaged in tubulo-vesicular carriers and transported to the recycling endosome en route to the plasma membrane [162]. The packaging of TNF into tubulo-vesicular carriers at the Golgi complex is controlled by golgin-245/p230, a member of the golgin family of proteins that function in membrane fusion events and structural support at the Golgi [163]. The exact role of p230 in TNF exit from the Golgi is still unclear, but live imaging indicates that p230 largely remains at the Golgi suggesting that p230 has a role in TNF sorting but not vesicle scission. Similarly, Rab6 that localises to the TGN may have a role in stabilising p230 on the tubule-vesicular carriers and when depleted, like p230 resulted in attenuated TNF secretion [164]. By contrast, scission of these carriers at the Golgi is controlled by phosphoinositide-3-kinase (PI3K) p110δ isoform and dynamin 2 [165]. The TGN is a complex dynamic structure and major sorting centre at the crossroads of the endocytic and exocytic pathways, utilising numerous molecular machineries and proteins to correctly direct cytokines and cellular products to their destination [166].

TNF carriers exit the TGN and fuse with the recycling endosomes [162]. TNF carriers contain the SNARE complex, Stx6/Stx7/Vti1b that pairs with its R-SNARE partner VAMP3 on recycling endosomes for carrier-endosome fusion [167]. The final fusion step for delivery of TNF to the plasma membrane is facilitated by pairing of VAMP3 on the recycling endosome and Q-SNARE complex, Stx4/SNAP23 on the plasma membrane [168]. Syntaxin 4 (Stx4) and ADAM17/TACE (TNF converting enzyme) are sequestered to cholesterol-rich lipid rafts that result in the delivery of TNF carriers to these discrete punctae and their subsequent rapid cleavage into

soluble TNF and release into the extracellular environment [169, 170]. Interestingly, if an activated macrophage is phagocytosing a microbe, TNF and VAMP3 positive endosomes are delivered to the phagocytic cup providing membrane for an expanding cup and release of TNF [162].

1.7.2.2 IL6

IL6 is also a proinflammatory cytokine secreted by macrophages on stimulation with LPS. The trafficking of IL6 share many similarities with TNF [171]. Newly synthesised IL6 exits the TGN in transport vesicles either alone or together with TNF, and like TNF utilises similar SNAREs to fuse with recycling endosomes. It is within the endosomal compartment that their paths separate with TNF directed to phagocytic cups but not IL6, suggesting an important role for the endosomal system in sorting cargo for delivery to the plasma membrane. The location or nature of the cell surface sites that IL6 are directed to is still unclear. As such, IL6 can be transported in two distinct pathways that diverge at the endosomal compartment.

1.7.2.3 IL10

By contrast, the anti-inflammatory cytokine IL10 is secreted in two distinct pathways in macrophages, which are either endosome dependent or independent [172]. On LPS stimulation, a significant proportion of IL10 is trafficked in similar pathways to TNF and IL6, exiting the Golgi in p230 dependent carriers. The IL10 is then delivered to the endosomal compartment where sorting occurs then release. Another portion of IL10 exits the TGN in golgin-97 positive carriers, which bypasses the endosomal compartment.

1.7.3 The innate immune system and Crohn's disease

The GWAS discovery of NOD2, ATG16L1 as well as the autophagy gene IRGM as well as smaller studies that found associations with variants in CD14, TLR4, 5, 9 and 10 all suggest a role of the innate immune system and acute inflammation in CD [173-177]. In addition to GWAS, congenital monogenic innate immunodeficiencies affecting neutrophils have also provided strong evidence to support a role for defective innate immunity in CD. Failure of neutrophils to accumulate in sufficient numbers (leukocyte adhesion deficiency) [178], impaired vesicle trafficking and fusion (Chediak-Higashi and Hermansky-Pudlak syndromes) [179, 180] or poor digestion of bacteria within excessively acidic phagolysosomes (chronic granulomatous disease and glycogen storage disease-1b) [181-184] commonly develop granulomatous bowel inflammation that is indistinguishable from CD [185, 186]. These findings provide further evidence to support the hypothesis that defective innate immunity and acute inflammation increases the probability of developing CD.

1.8 Defective innate immunity in Crohn's disease

Following from the observation that patients with congenital neutrophil immunodeficiencies present with a CD-like colitis, others in our research group investigated neutrophil recruitment in the bowel of CD patients and found impaired neutrophil recruitment at sites of trauma [107]. This was associated with lower levels of the neutrophil chemokine CXCL8 in skin windows of CD patients. To investigate the effects of this impaired neutrophil recruitment, others in our group investigated bacterial clearance by injecting heat-killed *E. coli* (HkEc) subcutaneously into the forearm of CD patients and HCs [187]. Local blood flow at the injection site determined by laser Doppler scanning and accumulation of radioactively labelled autologous neutrophils as markers of acute inflammation was significantly attenuated in CD patients. The clearance rate of radioactively labelled heat-killed *E. coli* from the site of

injection was significantly reduced in CD patients but not in UC patients (inflammatory disease control) or healthy controls, with an extrapolated total clearance time of 44.3 days in CD versus 10.2 days in healthy controls. The local blood flow and bacterial clearance rates were dose dependent and was similar below 10^7 HkEc but significantly attenuated in CD patients above 10^7 HkEc.

To investigate this common phenotype of impaired bacterial clearance in CD, others in our group stimulated CD macrophages with HkEc and looked at cytokine and chemokine secretion [187]. The secretion of proinflammatory cytokines TNF, IL4, IL5, IL13, IL15 and IFNγ were *lower* in the HkEc stimulated ileal and colonic CD macrophages whilst IL6, IL12p70, GCSF and GMCSF were only lower in colonic CD and IL17 in ileal CD. By contrast, proinflammatory cytokine secretion in UC macrophages were similar to or greater than healthy controls. Secretion of chemokines CCL5, CXCL10, CCL2 and CXCL8 and anti-inflammatory cytokines IL1Ra and IL10 were similar in CD macrophages compared to healthy controls. The defective TNF secretion was replicated in a further cohort of 101 CD patients [188].

This defective TNF secretion on HkEc stimulation was not due to impaired cytokine gene transcription or mRNA stability [187]. Intracellular TNF levels were lower in HkEc stimulated CD macrophages which normalised to healthy control levels on addition of the ER to Golgi transport inhibitor brefeldin A, which indicated that TNF translation was also normal. In light of the normal TNF transcription and translation we stimulated CD macrophages with HkEc with and without the lysosomal function inhibitors monensin, chloroquine and NH_4Cl and found that the intracellular TNF levels normalised to healthy control levels, suggesting that the low TNF levels were due to misdirected trafficking of TNF to lysosomes for destruction.

These findings have led us to propose a 3-stage model of Crohn's disease pathogenesis, occurring in three temporally distinct but related

stages (Figure 1.5). Stage 1 involves the penetration of luminal contents such as bacteria and faeces into the normally sterile lamina propria that occur in the presence of an abnormal mucosal barrier. In stage 2, macrophages in healthy individuals mount a strong acute inflammatory cytokines response resulting in robust neutrophil recruitment, clearance of luminal contents and resolution of inflammation. However, CD macrophages mount an attenuated acute inflammatory response characterised by defective cytokine secretion resulting in poor neutrophil recruitment and inadequate bacterial clearance. The residual bacteria and faeces acts as a focus for the formation of granulomas and stage 3, which is a compensatory adaptive immune response exemplified by high levels of proinflammatory cytokines and the phenotype of CD that responds to immunosuppressive and anti-TNF therapy.

To investigate this trafficking defect, myself and others in our group performed microarray analysis of macrophage gene expression in CD patients and HCs, using UC patients as an inflammatory disease control. Mean and standard deviation of expression in the healthy control cohort was used to detect under expressed genes in individual CD patients using customised software [189]. This approach of outlier gene expression analysis has been used in cancer studies to identify candidate genes of pathological relevance [190]. Using this approach, we identified seven CD patients with abnormally low expression of optineurin (*OPTN*^{low}) in their macrophages in our initial cohort [191]. A further cohort replicated these results and identified four further CD patients to a total of eleven *OPTN*^{low} CD patients out of 105 CD patients, but none in the 75 healthy controls or 49 UC patients.

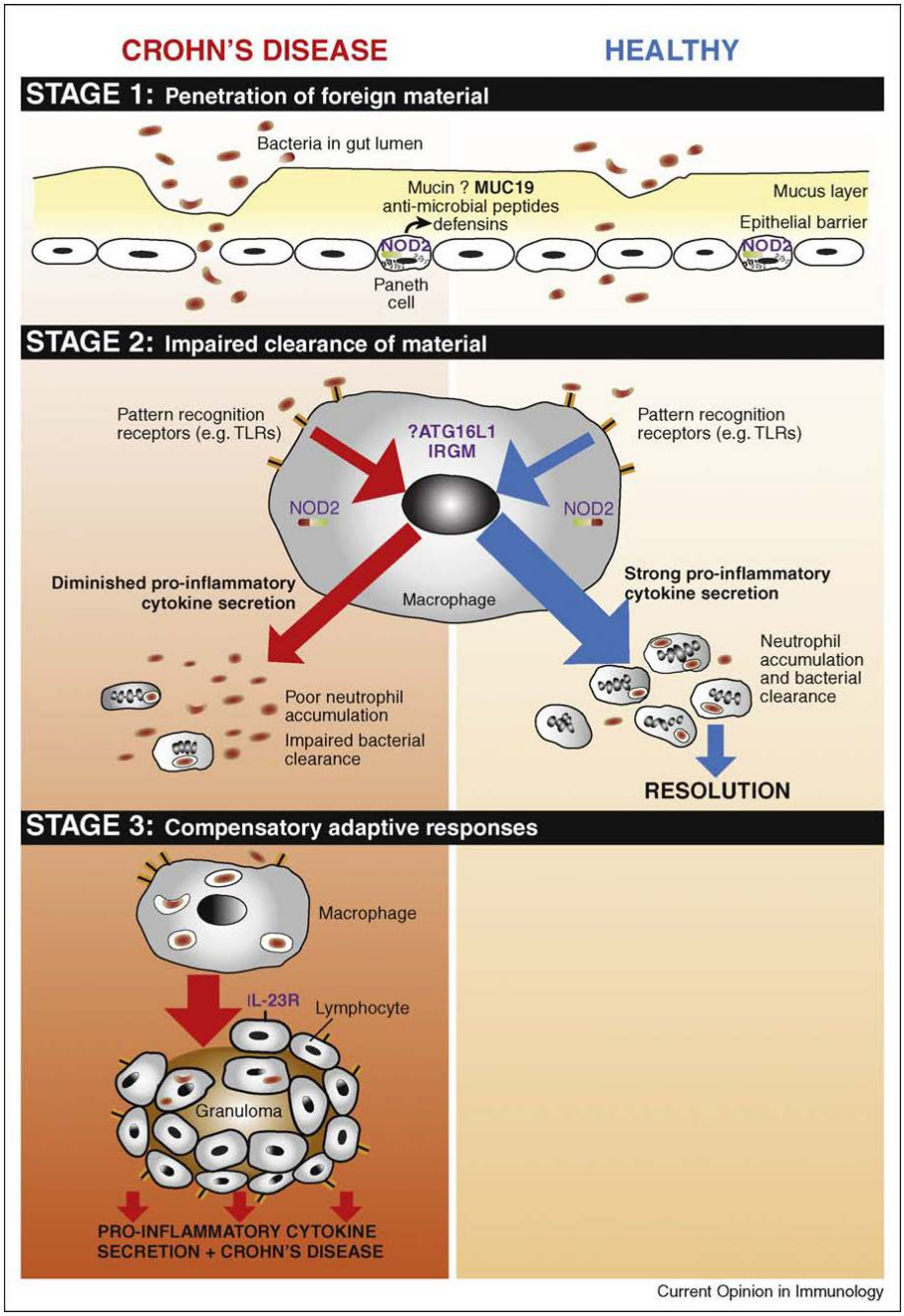

Figure 1.5 Three-stage model of Crohn's disease pathogenesis. Stage 1 is the penetration of faeces and bacteria into the bowel mucosa, stage 2 is the impaired proinflammatory cytokine secretion by macrophages and resultant attenuated neutrophil recruitment and stage 3 is the resulting compensatory adaptive immune response to uncleared bacteria and faeces [192].

1.9 Optineurin

1.9.1 Optineurin structure and function

Optineurin (OPTN) was originally isolated in a yeast two-hybrid screen of a HeLa cell cDNA library as a binding partner of the adenoviral TNF inhibitor E3-14.7K and named FIP2 (14.7K interacting protein 2) [193]. In 2002, mutations in FIP2 were found to be associated with autosomal dominant adult-onset primary open angle glaucoma (POAG) in 54 different families and named optineurin (*opti*c *neu*ropathy *in*ducing) [194].

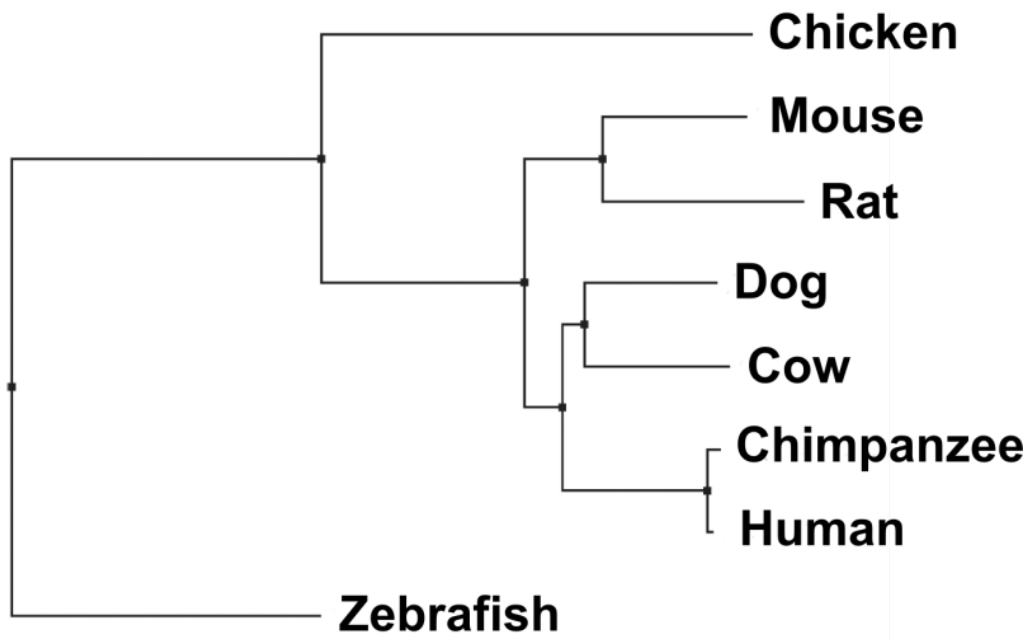

Figure 1.6 Phylogenetic tree of optineurin protein in different species. Adapted from Ying et al, 2012 [195].

OPTN homologs have been identified in many species including zebrafish and mice (Figure 1.6). In humans, OPTN is a 67 kD protein made up of 577 amino acids and the *OPTN* gene comprises 13 exons that spans 37 kilobases on chromosome 10. In mice, OPTN is predicted to be a 67 kD

protein made up of 584 amino acids sharing 78% homology with human OPTN. The mouse *Optn* gene comprises 13 exons on chromosome 2 [196]. In zebrafish, Optn is predicted to be 60 kD and is made up of 524 amino acids. The zebrafish *optn* gene comprises 13 exons and is on chromosome 4.

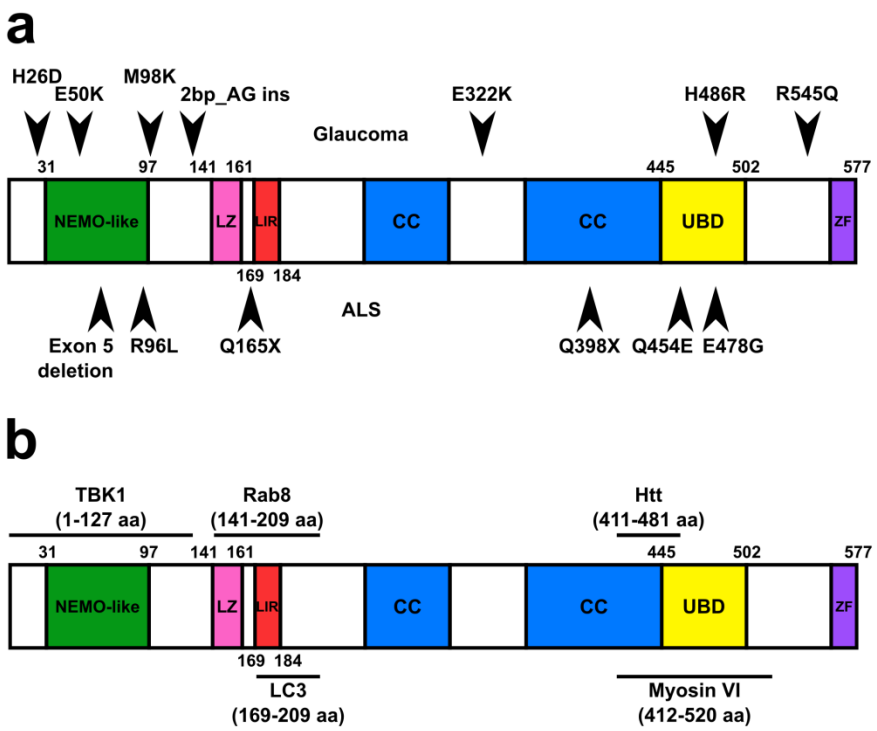

Figure 1.7 OPTN protein domains, mutation and binding partner sites. (a) Diagram depicting mutation sites for glaucoma (above) and ALS (below). (b) OPTN amino acid binding partner sites. CC, coiled-coils; ZF, zinc-finger; UBD, ubiquitin-binding domain; LZ, leucine zipper; LIR, LC3-interacting region. Adapted from Ying et al, 2012 [195].

The human OPTN protein is made up of multiple coiled-coil domains (CC), a zinc-finger (ZnF) domain, a ubiquitin-binding domain (UBD), a leucine-zipper (LZ) domain and an LC3-interacting region (LIR) (Figure 1.7). OPTN shares 53% similarity with NEMO (NF-κB essential modulator). Like

NEMO, OPTN is found in complexes with other interacting proteins [197] and is involved in multiple cellular functions beyond NF-κB signalling.

OPTN is ubiquitously expressed in many different organs and is upregulated by TNF and LPS via NF-κB signalling [198-200]. OPTN's main role is in vesicle trafficking and autophagy via its binding partners myosin VI, rab8, huntingtin (HTT) and LC3.

1.9.2 Optineurin in vesicle trafficking

OPTN was first identified as a binding partner of myosin VI using a yeast two-hybrid system (Figure 1.8) [201]. OPTN was found to bind myosin VI between amino acids 412 to 520 and together colocalise to the Golgi complex and vesicles at the plasma membrane in HeLa cells. RNA interference of OPTN resulted in loss of myosin VI from the Golgi complex and Golgi fragmentation. OPTN was also previously found to bind Rab8 [202]. Overexpression of Rab8 alone results in recruitment of myosin VI to Rab8 vesicles but overexpression of Rab8 in the presence of OPTN RNAi blocked myosin VI recruitment, suggesting that OPTN links myosin VI to the Golgi complex and has a role in maintaining the Golgi structure.

Additionally, OPTN in complex with myosin VI and Rab8 has a role in post-Golgi membrane trafficking since OPTN RNAi resulted in reduced transport of the VZV-G protein from the Golgi to the plasma membrane in nonpolarised HeLa cells and corrected aberrant transport introduced by a mutant C-terminal tail myosin VI in polarised MDCK kidney epithelial cells [203]. OPTN and its binding partners myosin VI and Rab8 were also shown to have a role in polarised delivery of EGFR to the leading edge of A549 human alveolar epithelial cells resulting in impaired lamellipodia formation [204]. Finally, using live-cell fluorescence microscopy in HeLa cells, OPTN and myosin VI depletion was found to reduce secretory vesicle fusion events

at the plasma membrane but have no effect on vesicle formation events at the trans-Golgi network [205].

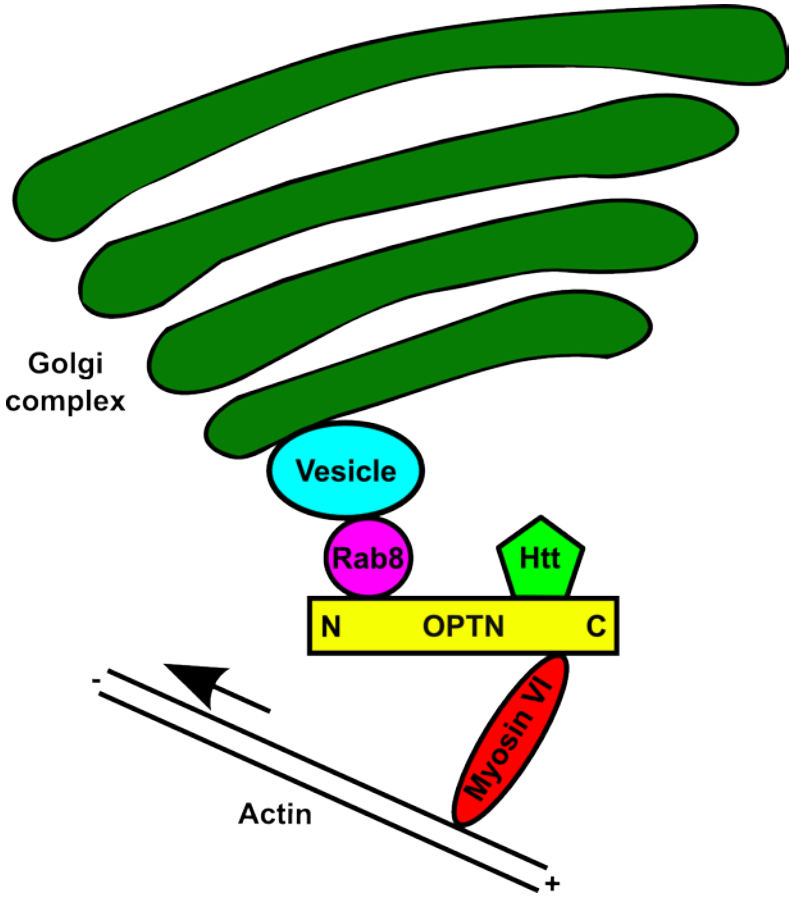

Figure 1.8 OPTN and its binding partners myosin VI, Rab8 and Htt. Illustration shows the binding of OPTN with its binding partners and how OPTN may act as a bridge binding vesicles to actin filaments via myosin VI to facilitate vesicle transport. Adapted from Sahlender et al, 2005 [201].

OPTN was also colocalised with huntingtin (HTT) to the Golgi complex in rat striatal cells that was dependent on expression of wildtype Htt in contrast to a 111Q polyglutamine Htt mutant [206]. RNAi of wildtype Htt and expression of mutant Htt resulted in impaired post-Golgi trafficking to

lysosomes, which was dependent on the expression of wildtype Rab8 and OPTN and resulted in the accumulation of the lysosome bound mannose-6-phosphate receptor at the TGN and reduced lysosomal DQ-collagen VI proteolysis. By contrast, Htt RNAi in HeLa cells resulted in endosome and lysosome dispersion that was dynein dependent with minimal defects in intracellular trafficking [207].

OPTN has also been shown to regulate endocytic trafficking of transferrin receptor at the recycling endosome in rat RGC5 retinal ganglion and human retinal pigment epithelial cells, a process impaired by expression of the glaucoma associated E50K mutation in the proximal NEMO-like TBK1 binding site domain of OPTN [208, 209]. A consequence of OPTN RNAi in RGC5 cells is the reduced secretion of neurotrophin-3 (NT-3) and ciliary neurotrophic factor that resulted in increased apoptotic cell death, which was reversed with exogenous NT-3 [210].

1.9.3 Optineurin and autophagy

As discussed above, autophagy is the term used to describe the intracellular processes that degrade and recycle unwanted cytosolic macromolecules, organelles and cellular components via lysosomes. Autophagy involves the formation of double membrane autophagosomes covered with LC3 that bind cargo carrying molecules such as NDP52 and p62 in selective autophagy (Figure 1.3) or degrades cytosolic macromolecules and organelles in non-selective autophagy under conditions of starvation (Figure 1.2).

Optineurin was found to be associated with the LC3 autophagy protein using a yeast two-hybrid system and verified by pull-down assays. The LC3-interacting region (LIR) in OPTN (Figure 1.7) was mapped to amino acids 169 to 209 [125]. Phosphorylation of OPTN within the LIR at serine-177 by TANK binding kinase 1 (TBK1) enhanced binding of OPTN to LC3 and autophagic clearance of ubiquitin-coated cytosolic *Salmonella enterica*

(Figure 1.3). Conversely, OPTN with ubiquitin and LC3 binding domain mutations as well as silencing of OPTN or TBK1 resulted in impaired *Salmonella* autophagy and intracellular bacterial proliferation.

Additionally, in RGC5 cells endogenous OPTN is mainly turned over by the ubiquitin-proteosome pathway but when the OPTN E50K mutant is overexpressed in these cells, the ubiquitin-proteosome pathway is compromised and autophagy is induced [211].

1.9.4 Optineurin and the type I interferon response

The type I interferon response aims to improve presentation and clearance of intracellular viruses. The OPTN type I interferon response involves TANK-binding kinase 1 (TBK1), a member of the IκB-kinase family involved in activation of interferon regulatory factor 3 (IRF3) and production of interferon β (IFNβ) [212].

OPTN shares 53% homology with NEMO and contains a ubiquitin-binding domain (UBD) (Figure 1.7), hence is also called NEMO-related protein (NRP). Mice containing a knockin defect at the UBD of OPTN were used to generate bone marrow derived macrophages (BMDM), which were stimulated with LPS. Defective pUb binding in these LPS stimulated BMDM containing UBD-mutant OPTN resulted in impaired phosphorylation of IRF3 and production of IFNβ suggesting that OPTN binding to K63-pUb chains at its UBD is required for the activation of OPTN's binding partner TBK1 [200, 212, 213].

By contrast, in another study OPTN was functioning as a negative regulator of the antiviral response. OPTN overexpression in human embryonic kidney cells inhibited Sendai virus triggered induction of IFNβ and conversely RNAi promoted viral induced IFNβ production and impaired Bunyamwera viral replication [214]. It is not clear why these results are

seemingly contradictory but may be related to variations in the response to viral infection in different cell types or non-specific effect of RNAi beyond just OPTN knock down.

1.9.5 Optineurin and disease

Mutations in *OPTN* have been associated with glaucoma, amyotrophic lateral sclerosis (ALS) and Paget's disease of the bone. Mutations in *OPTN* was first associated with ALS in six affected subjects from consanguineous marriages in four different families [215]. Two affected siblings from a single family were found to have a deletion of exon 5, two unrelated subjects, one from a consanguineous marriage were found to be homozygous for a nonsense mutation 1502C>T/Q398X (exon 12) and two sibling pairs from unrelated families were heterozygous for a missense mutation 1743A>G/E478G (exon 14). OPTN was colocalised with disease associated superoxide dismutase 1 (SOD1) and fused in sarcoma (FUS) in inclusion bodies of patients with ALS [215, 216]. Additionally, the Q398X and E478G ALS mutations were associated with impaired inhibition of IRF3, suggesting a viral aetiology [217]. A further six novel variants were identified in an Italian cohort and a further two in a Dutch cohort with familial and sporadic ALS [218, 219]. By contrast, three other studies in did not support the association of OPTN with ALS [220-222]. The involvement of OPTN in ALS therefore remains to be further elucidated.

Four mutations in OPTN were originally identified that were linked to POAG [194]. They are 458G>A/E50K (exon 4), which was the commonest variant affecting 13.5% of familial POAG patients, 691_692insAG/premature stop (exon 6), 1944G>A/R545Q (exon 16) and 603T>A/M98K (exon 5), which was only associated in South Asian families. Further disease associated variants have been found but only account for <1% of cases. Most of the OPTN associated mutations are missense mutations with one frameshift nonsense mutation and a silent mutation.

The most widely studied OPTN mutant is the E50K mutation. Mice overexpressing OPTN with the E50K mutation had thinner retina with loss of RGCs [223]. OPTN was shown to translocate to the nucleus when exposed to an apoptotic stimulus in a Rab8 dependent manner in fibroblasts. Overexpression of wildtype OPTN protected cells from the apoptotic stimulus in contrast to E50K-OPTN that did not translocate to the nucleus or maintain mitochondrial membrane integrity resulting in decreased survival [224]. Additionally, E50K-OPTN has been shown to impair post Golgi trafficking in human retinal pigment epithelium and RGC as discussed above.

In 2010, a GWAS into Paget's disease of the bone, a disease of increased and dysorganised bone remodelling in British patients identified three candidate loci, one of which was mapped to OPTN on chromosome 10p13 [225]. The association of Paget's with OPTN has since been validated in a French-Canadian cohort of patients [226]. Interestingly, the 10p13 chromosomal region had already been linked to familial Paget's disease in 2008 although the candidate gene was not identified [227]. However, to date the disease associated variant in OPTN has not been identified nor the functional consequences that results in Paget's disease.

1.10 Outline of thesis

1.10.1 Summary of background information

CD is a chronic, relapsing, systemic inflammatory disorder that predominantly affects the GI tract. The incidence of CD is rising with time and in places previously unknown to have CD. The aetiology of CD is unknown, but recent GWAS studies have implicated NOD2, which detects intracytoplasmic pathogens and ATG16L1, a gene involved in autophagy, implicating the innate immune system in the pathogenesis of this disease. Furthermore, individual with inherited neutrophil immunodeficiencies commonly manifest in colitis that is indistinguishable from CD.

Others in our research group previously identified an impaired acute inflammatory response in CD patients exposed to *E. coli*. CD patients had impaired neutrophil recruitment to sites of infection and delayed clearance of radioactively labelled *E. coli*. This defect was associated with impaired proinflammatory cytokine secretion in macrophages. This led our group to propose a 3-stage model for the pathogenesis of CD. The central causal phase of incomplete bacterial clearance by neutrophils follows the initial phase of faecal and bacterial penetration into the bowel wall. The incomplete clearance of bowel contents from the tissues results in the final phase involving a secondary adaptive immune response and the phenotype of CD.

Previous work from our group to investigate the defective proinflammatory cytokine secretion identified genes involved in vesicle trafficking. Myself and others in our group found optineurin expression in human macrophages to be significantly lower in 10% of CD patients in our cohort. Optineurin is an intracellular adaptor molecule that forms a complex with myosin VI, Rab8, HTT and LC3. It has been found to localise to the Golgi complex and plasma membrane in non-immune cells with a role in protein sorting at the Golgi and vesicle fusion at the membrane. This makes optineurin an exciting candidate for further investigation in macrophages to identify if optineurin has a role in bowel inflammation.

1.10.2 Summary of investigations and hypothesis

In this thesis, the discovery of abnormally low expression of OPTN in human macrophages is replicated and validated in a separate cohort of CD patients and healthy controls by myself and others in our group. Demographic data of the *OPTN*^{low} CD patients were analysed by myself to identify any predisposing factors that may be causal in the abnormal expression of OPTN.

The role of OPTN in macrophages *in vitro* was studied by myself using bacteria and TLR stimulation assays to investigate gene transcription, cytokine secretion, vesicle trafficking, autophagy, ER stress, phagocytosis and killing whilst its intracellular location in macrophages elucidated using colocalisation analysis on confocal immunofluorescence microscopy. This was aided by studies using subcellular fractionation, immunoprecipitation and shotgun proteomics by others in our group.

Finally, the role of OPTN in infection and colitis *in vivo* was investigated using *optn* knockdown zebrafish injected with *Salmonella* by our collaborators and an *Optn*$^{-/-}$ mouse model of intraperitoneal infection and *Citrobacter rodentium* colitis by myself to look at differences in susceptibility to infection, immune cell recruitment and cytokine secretion.

The null hypothesis of this thesis is that there is no association between low *OPTN* expression in MDM and the development of CD. I investigated this hypothesis by exploring these statements:

1. Low OPTN expression in human monocyte-derived macrophages is specific to CD patients and not in HC or UC patients (Chapter 3).
2. Low or deficient OPTN in macrophages is important in proinflammatory cytokine secretion and trafficking (Chapter 4).
3. *In vivo*, OPTN deficient mice developed a more severe colitis that is associated with impaired neutrophil recruitment to site of infection (Chapter 5).

Chapter 2 Materials and Methods

2.1 CD patient and healthy control recruitment

CD patients were recruited from the University College London Hospital Inflammatory Bowel Disease clinic. Patients had definitive diagnoses of CD, which were confirmed using standard diagnostic criteria and the Montreal classification for Crohn's disease [228]. All CD patients were between 18 and 75 years of age and were free of Hepatitis B, Hepatitis C and Human Immunodeficiency Virus (HIV). CD patients in the first cohort had quiescent disease (Harvey-Bradshaw index <3) [229] and on either no medication or a stable maintenance dose of 5-aminosalicylates for the previous 3 months. CD patients in the second cohort also had quiescent disease (Harvey-Bradshaw index <3) but could be on any medication for their CD except treatment dose steroids at the time of venesection. CD patients who met the inclusion criteria were recruited to participate in the study.

Matched HC from the Division of Medicine, University College London staff and student population were recruited. HCs were between 18 and 75 years of age, did not have CD or UC and were not on immunosuppressants. No CD patient or HC was studies more than once in the 2 different cohorts.

Details of CD patients and HCs are provided (Table 3-2). Signed informed consent was obtained from all participants at each meeting, which includes consent for venesection, release of tissue obtained at endoscopy or surgery and review of medical notes. Clinical details of CD patients and HCs were recorded in a password protected Excel spreadsheet, registered and covered by the Data Protection Act 1998. Clinical details include name, hospital number, date of birth, Montreal classification for Crohn's disease, smoking status, family history, date of venesection, current and previous medication and Harvey-Bradshaw were obtained from the CD patients or

their clinical records.

2.2 gDNA extraction, *OPTN* sequencing and SNP genotyping.

Genomic DNA (gDNA) was extracted from peripheral venous blood using the QIAamp DNA blood Mini Kit (Qiagen). Sequencing of the *OPTN* gene in *OPTN*^{low} CD patients and genotyping of the rs12415716 SNP in HC and CD patients was performed as previously described [191].

2.3 *Optn*$^{-/-}$ mouse generation and verification

2.3.1 *Optn*$^{-/-}$ mouse generation

Optn$^{+/-}$ mice on a C57BL/6 background were obtained from the Wellcome Trust Sanger Institute (WTSI), Cambridge, UK. The C57BL/6NTac-Optn$^{tm1a(EUCOMM)Wtsi}$ mice were generated by targeted mutagenesis of the *Optn* gene on Chromosome 2 using a 'knockout first', conditional targeting allele strategy by insertion of an IRES/lacZ – promoter-driven Neo targeting cassette upstream of critical exon 3 [230].

2.3.2 Mouse husbandry

Mice were bred to obtain *Optn*$^{+/+}$ and *Optn*$^{-/-}$ mice in specific-pathogen free (SPF) cages in the Biological Sciences Unit, University College London. Colonies were generated by keeping *Optn*$^{+/+}$ and *Optn*$^{-/-}$ breeding pairs to produce pure *Optn*$^{+/+}$ and *Optn*$^{-/-}$ litters. Mouse stocks were fed with Harlan 2018 Teklad Global 18% protein rodent diet whilst breeders were fed with Harlan 2019 Teklad Global 19% protein rodent diet.

2.3.3 Mouse genotyping

Mice were genotyped using *Optn*_47570_F, *Optn*_47570_R and

CAS_R1_Term_x primers (Appendix 1) provided by the WTSI from ear clip derived gDNA with the HotStar Taq Mastermix kit (Qiagen 203445). Mouse gDNA was extracted from ear clips by incubating the ear clips overnight at 55 °C in 95 µl of DNA extraction buffer (Section 2.6 Reagents) containing 5 µl of 4 mg/ml proteinase K (Qiagen). The samples were vortexed at 1400 rpm at 55 °C for 10 minutes in an Eppendorf Thermomixer comfort then centrifuged at 28,000 *g* for 10 minutes to pellet hair. The samples were transferred into new tubes and boiled at 95 °C for 5 minutes.

The PCR reaction volume was made up of 12.5 µl HotStar Taq Mastermix, 1 µl forward primer, 1 µl reverse primer, 1 µl gDNA and 9.5 µl RNase-free water, to a total volume of 25 µl. The final concentration in the reaction volume was 2.5 U HotStar Taq DNA polymerase, 1× PCR buffer containing 1.5 mM $MgCl_2$, 200 µM of each dNTP, 0.4 µM of each primer and a variable amount of gDNA. The PCR mix was activated at 95 °C for 15 minutes, denatured at 95 °C for 45 s, annealed at 60 °C for 45 s, extended at 72 °C for 45 s, for a total of 28 cycles, then extended for a final time at 72 °C for 10 minutes before being cooled to 4 °C on a DNA Engine Tetrad 2® Peltier Thermal Cycler (Bio-Rad). The annealing temperature of 60 °C was chosen after a temperature gradient was run for each primer pair. 5 µl Orange J was added to each 25 µl reaction mix and 15 µl was run on a 1% agarose gels then viewed with a ChemiDoc™ Imager (Bio-Rad).

2.3.4 *Optn*$^{-/-}$ mouse verification

Primers that spanned exon 2 to 4 of the *Optn* gene (Figure 4.12) were created using Primer 3 (Appendix 1). Stock primers were made up to 100 µM in RNase-free water as per manufacturer's instructions (Eurofins and Sigma) and further diluted to 10 µM in RNase-free water for PCR. Total RNA from *Optn*$^{+/+}$ and *Optn*$^{-/-}$ mouse small bowel was harvested and converted into cDNA (Section 2.9 Quantitative Reverse Transcription PCR). RT-PCR was performed with 25 µl HotStar Taq Mastermix, 2 µl forward primer, 2 µl

reverse primer, 2 µl cDNA and 19 µl RNase-free water, to a total volume of 50 µl and final concentration of 2.5 U HotStar Taq DNA polymerase, 1× PCR buffer containing 1.5 mM $MgCl_2$, 200 µM of each dNTP, 0.4 µM of each primer and ~40 ng/µl of cDNA. The RT-PCR was activated at 95 °C for 15 minutes, denatured at 95 °C for 30 s, annealed at 56 °C for 45 s, extended at 72 °C for 60 s, for a total of 35 cycles, then extended for a final time at 72 °C for 10 minutes before being cooled to 4 °C on a DNA Engine Tetrad 2® Peltier Thermal Cycler (Bio-Rad), which revealed a larger amplicon in the *Optn*$^{-/-}$ small bowel (Figure 4.15). The annealing temperature of 56 °C was chosen after a temperature gradient was run for the primer pair.

The RT-PCR reaction was repeated and the knockout Optn+ and wildtype amplicon were purified using QIAquick® PCR purification columns (Qiagen 28104) as per manufacturer's instructions and sequenced with the same primers using a BigDye® Terminator v3.1 Cycle Sequencing kit on an Applied Biosystems 3730XL DNA Analyzer.

Whole cell lysates of *Optn*$^{+/+}$ and *Optn*$^{-/-}$ thioglycollate-induced peritoneal macrophages in Laemlli buffer were made and immunoblotted (Section 2.10 Immunoblot), which confirmed the absence of OPTN in the *Optn*$^{-/-}$ mice.

2.3.5 Investigating the naïve *Optn*$^{-/-}$ phenotype

2.3.5.1 Naïve *Optn*$^{+/+}$ and *Optn*$^{-/-}$ organs

Naïve *Optn*$^{+/+}$ and *Optn*$^{-/-}$ large bowel, small bowel, spleen, kidney, liver, stomach, brain, heart, lung and thymus were harvested and fixed overnight in 10% neutral buffered formalin (CellPath). The organs were embedded, sectioned and stained with haematoxylin and eosin (H&E) (Figure 4.19).

To make H&E slides of the bone marrow, *Optn*$^{+/+}$ and *Optn*$^{-/-}$ hind legs

were dislocated at the hip joint and removed, overlying muscle and tendons were cut off and hind leg bones were fixed in 10% neutral buffered formalin overnight. Femurs and tibiae were decalcified in PBS containing 5% EDTA for 14 days on a Stuart SRT6 analogue rocker and roller mixer. The PBS containing 5% EDTA was made using tetrasodium EDTA (Sigma), which is more soluble and was changed daily.

2.3.5.2 Flow cytometry of peripheral blood

Naïve *Optn*$^{+/+}$ and *Optn*$^{-/-}$ were culled with CO_2 and cervical dislocation. A midline thoracotomy was performed and a cardiac puncture using a 1 ml syringe attached to a 26 G needle containing 100 µl of 0.3% citrate in PBS was carried out. Blood was transferred into Falcon tubes and kept on ice.

Red blood cells were lysed by adding 1 ml of red cell lysing solution (Sigma R7757) to citrated blood for 3 minutes at room temperature. Cells were washed in 10 ml of FACS buffer (PBS containing 1% BSA, 0.01% azide), centrifuged at 500 *g* for 5 minutes at 4 °C and resuspended in 200 µl of FACS buffer containing 2.0 µg/ml anti-CD16/CD32 Fc block for 20 minutes. Cells were washed in 1 ml of FACS buffer then stained in 100 µl FACS buffer containing 0.5 µg/ml CD11b V450, 0.25 µg/ml Gr1 PE, 0.25 µg/ml CD3 PE-Cy™7, 0.25 µg/ml CD19 PerCP-Cy™5.5, 0.25 µg/ml Ly-6C APC and 0.5 µg/ml F4/80 FITC antibodies for 30 minutes in the dark at room temperature then fixed in 1% formaldehyde in PBS for 10 minutes.

Compensation particles (BD 552845) were prepared by adding each antibody above to 100 µl of FACS buffer containing 1 drop of positive particles (~60 µl) and 1 drop of negative particles (~60 µl) to the same final concentration of antibodies. Particles were incubated in the dark at room temperature for 20 minutes then washed with 1 ml FACS buffer, centrifuged at 500 *g* for 5 minutes and resuspended in 300 µl of FACS buffer. Cells were

run on a BD LSRFortessa after compensation with antibody labelled particles and analysed with FlowJo (Tree Star, Inc).

2.3.5.3 Flow cytometry of blood and bone marrow

Naïve *Optn*$^{+/+}$ and *Optn*$^{-/-}$ were culled with CO_2 and cervical dislocation. Their hind legs were dislocated at the hips, removed and transported on ice. The overlying muscle and tendons were cut off. The cleaned bones were cut at either end and the bone marrow cavity was flushed through with ice cold sterile PBS in a 10 ml syringe attached to a 26 G needle into sterile petri dishes. The bone marrow cells were transferred into 50 ml Falcon tubes and centrifuged at 500 *g* for 5 minutes at 4 °C.

Red blood cells were lysed by adding 1 ml of red cell lysing solution (Sigma R7757) to citrated blood for 3 minute at room temperature. Cells were washed in 10 ml of FACS buffer (PBS containing 1% BSA, 0.01% azide), centrifuged at 500 *g* for 5 minutes at 4 °C and resuspended in 200 µl of FACS buffer containing 2.0 µg/ml anti-CD16/CD32 Fc block for 20 minutes. Cells were washed in 1 ml of FACS buffer then stained in 100 µl FACS buffer containing 0.5 µg/ml CD11b V450, 0.25 µg/ml Gr1 PE, 0.25 µg/ml CD3 PE-Cy™7, 0.25 µg/ml CD19 PerCP-Cy™5.5, 0.25 µg/ml Ly-6C APC and 0.5 µg/ml F4/80 FITC antibodies for 30 minutes in the dark at room temperature then fixed in 1% formaldehyde in PBS for 10 minutes.

Compensation particles (BD 552845) were prepared by adding each antibody above to 100 µl of FACS buffer containing 1 drop of positive particles (~60 µl) and 1 drop of negative particles (~60 µl) to the same final concentration of antibodies. Particles were incubated in the dark at room temperature for 20 minutes then washed with 1 ml FACS buffer, centrifuged at 500 *g* for 5 minutes and resuspended in 300 µl of FACS buffer. Cells were run on a BD LSRFortessa after compensation with antibody labelled particles and analysed with FlowJo (Tree Star, Inc).

2.4 *Optn*$^{-/-}$*Nod2*$^{-/-}$ mouse generation

2.4.1 *Nod2*$^{-/-}$ mice

Nod2$^{-/-}$ mice on a C57BL/6 background, B6.129S1-*Nod2*^{tm1Flv}/J were obtained from The Jackson Laboratory and housed in SPF cages in the same animal unit as the *Optn*$^{-/-}$ mice.

2.4.2 *Optn*$^{-/-}$*Nod2*$^{-/-}$ mice

Optn$^{-/-}$*Nod2*$^{-/-}$ mice were generated by crossing *Optn*$^{-/-}$ and *Nod2*$^{-/-}$ mice to obtain *Optn*$^{-/-}$*Nod2*$^{-/-}$ and *Optn*$^{+/+}$*Nod2*$^{+/+}$ mice, which were housed in SPF cages with the other mice. Mice were genotyped using primers provided by Jackson for genotyping the *Nod2*$^{-/-}$ mice (Appendix 1). Pure breeding pairs of *Optn*$^{-/-}$*Nod2*$^{-/-}$ and *Optn*$^{+/+}$*Nod2*$^{+/+}$ mice were used to generate mice for experiments.

2.5 Antibodies and stains

2.5.1 Antibodies used in immunoblots

The following antibodies were used for MDM and THP-1 immunoblots: OPTN (Sigma HPA003360; 1:2,000), actin (Sigma A5060; 1:2,000), EEA1 (Cell Signaling #3288; 1:1,000), LAMP1 (Abcam ab24170; 1:1,000), GM130 (BD 610823; 1:250), Golgin-245 (Santa Cruz sc-102565; 1:250), GAPDH (Santa Cruz sc-51906; 1:2,000), anti-rabbit IgG-HRP (Cell Signaling #7074; 1:2,000), anti-mouse IgG-HRP (GE Healthcare NA931; 1:2,000). The following antibodies were used for BMDM immunoblots: OPTN (Abcam ab101592; 1:2,000), TNF (Abcam ab9739; 1:2,000), CHOP (Affinity BioReagents MA1-250; 1:500), GRP78/BiP (Santa Cruz sc-1051; 1:250), GRP94 (Santa Cruz sc-11402; 1:250), LC3B (Sigma L7543; 1:1,000).

2.5.2 Antibodies used in confocal microscopy

The following antibodies and stain were used for MDM confocal microscopy: GM130 (BD 610823, 1:100), OPTN (Gift from F. Buss, Cambridge, 1:100), EEA1 (BD 610456, 1:100), DAPI (Invitrogen D3571, 1:33,000), Alexa Fluor® 488-TNF/adalimumab (Abbott, 1:1,000) made with Alexa Fluor® 488 antibody labelling kit (Invitrogen A20181), Alexa Fluor® 546 anti-rabbit IgG (Invitrogen A11010; 1:1,000), Alexa Fluor® 488 anti-mouse IgG (Invitrogen A11001; 1:1000). The following antibodies were used for BMDM confocal microscopy: Alexa Fluor® 488-TNF (BD 557719, 1:100), EEA1 (Abcam ab2900; 1:100), GM130 (BD 610823; 1:100).

2.5.3 Antibodies used in flow cytometry

The following were used for flow cytometry: Compensation particles set (BD 552845), LIVE/DEAD® fixable blue dead cell stain kit (Invitrogen L23105), CD16/CD32 Fc block (eBioscience 16-0161; 1:500), F4/80 FITC (eBioscience 11-4801; 1:1,000), CD3 PE-Cy™7 (BD 560591; 1:800), CD19 PerCP-Cy™5.5 (BD 551001; 1:800), Gr1 PE (BD 553128; 1:800), Ly-6C APC (BD 560595, 1:800), CD11b-V450 (BD 560455, 1:400) CD19 PE (BD 553786; 1:400), CD45 PerCP-Cy™5.5 (BD 550994, 1:200).

2.5.4 Antibodies used in immunohistochemistry

The following were used for immunohistochemistry: Myeloperoxidase (Dako A0398; 1:1,000), normal goat serum (Sigma G9023, 1:10), Bond Polymer Refine Detection (Leica DS9800), Bond DAB Enhancer (Leica AR9432), OPTN (Sigma HPA003360; 1:100).

2.6 Reagents

2.6.1 Heat-killed *E. coli* (HkEc) stock

The fully antibiotic sensitive clinical isolate, *E. coli* NCTC 10418 was cultured by adding 1 µl glycerol stock into 10 ml LB broth (Sigma L3022) and incubated at 37 °C, 250 rpm in an Innova™ 4000 incubator shaker (New Brunswick Scientific) overnight. *E. coli* was centrifuged at 3000 *g* for 20 minutes, room temperature in a Heraeus Multifuge X1R (Thermo Scientific), washed once in 20 ml PBS, resuspended in 1 ml PBS and counted at 1:20 dilution using a Cecil BioQuest™ CE2502 spectrophotometer. The *E. coli* optical density at 600 nm (OD_{600}) of 1×10^8 bacteria/ml in PBS is 0.365. Concentration of *E. coli* in PBS was adjusted to 1×10^{10} bacteria/ml and incubated at 60 °C for 1 hour in a Grant GD100 circulating immersion bath and stored at -20 °C. Killing of *E. coli* was checked by plating 80 µl of HkEc onto LB agar plates with no antibiotics.

2.6.2 MTT cell viability assay reagents

2.6.2.1 MTT (3-[4,5-dimethylthiazol-2-yl]-2,5-diphenyl tetrozolium bromide)

0.2% MTT was made by dissolving 1 g of MTT (Sigma M2128) in 500 ml of PBS and stored at 4 °C in the dark.

2.6.2.2 MTT lysis solution

900 ml of isopropranol, 47 ml of dH_2O, 50 ml of 10% SDS and 3 ml of concentrated HCl were added together, which was kept at room temperature.

2.6.3 Buffers

2.6.3.1 DNA extraction buffer

DNA extraction buffer was made by adding 1 ml 1M Tris pH 8 (VWR 103156X), 100 µl 0.5 M EDTA (Sigma E6511), 2 ml 1M NaCl (Sigma S7653) and 50 µl 1% SDS (Sigma L3771) to 6.85 ml of dH_2O.

2.6.3.2 Laemmli sample buffer

3× Laemmli sample buffer was made by adding together 2.4 ml 1M Tris-HCl pH 6.8 (VWR), 3 ml 10% SDS (Sigma), 3 ml 100% glycerol (BDH 101186M) , 1.6 ml 2-mercaptoethanol (Sigma 63689) and 0.006 g bromophenol blue (Sigma B0126), and stored at 4 °C.

2.6.3.3 10× Transfer buffer

10× transfer buffer was made by dissolving 144 g glycine (Sigma G7126), 3.74 g SDS (Sigma L3771) and 30.25 g Tris (VWR 103156X) to 800 ml dH_2O using a magnetic stirrer then made up to 1L.

2.6.3.4 Tris-buffered saline (TBS) and TBS-Tween 0.1%

10× TBS was made by adding 800 g NaCl (Sigma), 20 g KCl (Sigma P4054) and 300 g Tris to dH_2O, pH adjusted to 7.4 using HCl and made up to 10 litres dH_2O. 1× TBS-Tween 0.1% was made by adding 5 ml Tween-20 (Sigma P1379) to 500 ml of 10× TBS, made up to 5 litres with dH_2O.

2.6.3.5 50× Tris-acetate-EDTA (TAE) buffer

484 g of Tris, 114.2 ml of glacial acetic acid and 200 ml of 0.5 M EDTA pH 8.0 was made up to 2 L of dH_2O.

2.6.3.6 FACS buffer (PBS containing 1% BSA and 0.01% azide)

5 g of bovine serum albumin (BSA)/albumin fraction V (VWR 1120180100) was added to a new bottle of 500 ml PBS pH 7.2 (Gibco 20012). 500 µl of 10% sodium azide in dH_2O (Sigma S8032) was added to the 500 ml of PBS and stored at 4 °C.

2.6.3.7 Confocal buffer (PBS containing 0.5% BSA, 0.1% saponin, 0.01% azide)

2.5 g of BSA, 0.5 g of saponin (Sigma S4521) and 500 µl of 10% azide was added to a new bottle of 500 ml PBS and stored at 4 °C.

2.6.4 Cell culture media

2.6.4.1 THP-1 cell culture media (RPMI 10% FBS, 20 mM HEPES, 100 U/ml penicillin/streptomycin, 20 µM BME)

50 ml of foetal bovine serum (Sigma F9665), 10 ml of 1 M HEPES (Sigma H0887), 5 ml of 10,000 U/ml Penicillin/Streptomycin (Gibco 15140-122), 200 µl of 50 mM 2-mercaptoethanol (Gibco 31350) were added to a new 500 ml bottle of RPMI-1640, GlutaMAX™ Supplement (Gibco 61870).

2.6.4.2 BMDM cell culture media (DMEM 10% FBS, 25 mM HEPES, 100 U/ml penicillin/streptomycin, 1 g/L D-glucose, 4 mM L-glutamine, 1 mM pyruvate)

50 ml of FBS (Sigma) and 5 ml of 10,000 U/ml Penicillin/Streptomycin (Gibco) were added to a 500 ml bottle of low-glucose Dulbecco's Modified Eagle Medium (DMEM) (Gibco 22320) and stored at 4 °C.

2.6.4.3 Thioglycollate-induced peritoneal macrophage (TiPM) cell culture media (RPMI 10% FBS, 100 U/ml penicillin/streptomycin, 20 mM HEPES)

50 ml of FBS (Sigma), 10 ml of 1 M HEPES (Gibco) and 5 ml of 10,000 U/ml Penicillin/Streptomycin (Gibco) was added to a 500 ml bottle of RPMI-1640, GlutaMAX™ Supplement (Gibco) and stored at 4 °C.

2.6.5 Bacterial culture broth

2.6.5.1 3% thioglycollate broth

30 g of thioglycollate broth (Merck 108191) was dissolved in 1 L of dH_2O and autoclaved. Sterile 3% thioglycollate was aliquoted into sterile 50 ml Falcon tubes and aged at 4 °C for 1 year prior to use.

2.6.5.2 Luria-Bertani (LB) broth and agar plates

5 g bacto-peptone (BD 211677), 2.5 g bacto-yeast extract (Oxoid LP0021), 5 g NaCl (Sigma), 7.5 g agar (Oxoid LP0011) were added to ~400 ml dH_2O, mixed with a magnetic stirrer and made up to 500 ml then autoclaved and plated. LB broth was made up as above without the agar.

2.6.6 Histology and microscopy reagents

2.6.6.1 Desalted human IgG at 50 mg/ml, 0.01% azide

Pooled human immune globulin/Vivaglobin® (CSL Behring) at 160 mg/ml was desalted through a PD-10 desalting column (GE Healthcare 17-0851-01) following manufacturer's instructions and eluted with PBS. The eluted desalted human IgG was quantified using a BCA protein assay kit (Thermo Scientific 13276818) as per manufacturer's instructions, then diluted to 50

mg/ml with PBS. Volume of human IgG was measured with a P1000 pipette and the required volume of 10% sodium azide was added to make a final concentration of 0.01% azide.

2.6.6.2 Mowiol® mountant

6 ml of glycerol, 2.4 g of Mowiol (Calbiochem 475904) and 6 ml dH_2O were added together in a 50 ml Falcon tube, vortexed and shaken for 2 hours. 12 ml of 200 mM Tris-HCl pH 8.5 was added and the mountant was incubated at 50 °C on a shaker until Mowiol fully dissolves, which took 3 hours. The mountant was filtered through a 0.45 µm filter, aliquoted and stored at -20 °C.

2.6.6.3 2.5% gum mastic in absolute ethanol

10 g of gum mastic (Sigma G0878) was dissolved in 100 ml absolute alcohol overnight. The 10% gum mastic was filtered using a Whatman #1 filter paper in a funnel. 2.5% gum mastic was made by adding 25 ml 10% gum mastic to 75 ml absolute alcohol and stored at 4 °C.

2.6.6.4 Steiner Silver reducing solution

The Steiner silver reducing solution was made by adding 60 ml of 2.5% gum mastic to 100 ml of freshly made 2% hydroquinone (Sigma 53960) in dH_2O and 0.8 ml of 1% silver nitrate (0.005% $AgNO_3$ final concentration). NB reducing solution will be milky.

2.7 Cell culture and stimulation

2.7.1 Monocyte-derived macrophages (MDM)

2.7.1.1 Isolation of monocytes and culture of MDM

100 ml of peripheral venous blood was collected from CD patients and HC in 5 U/ml heparin by adding 300 µl of 1,000 IU/ml heparin sodium (Wockhardt) to each 50 ml syringe. Peripheral blood monocytes were isolated using Lymphoprep™ (Axis-Shield) by layering 25 ml of blood onto 15 ml of Lymphoprep in 50 ml Falcon tubes. Tubes were centrifuged at 900 *g* for 30 minutes at 20 °C with the brakes off. The lymphocyte-monocyte layer at the interface of the serum at the top and the Lymphoprep in the middle was harvested and pooled into two 50 ml Falcon tubes. The cell suspension was topped up with PBS and centrifuged at 575 *g* for 5 minutes at 20 °C with the brakes on. The cells were washed two further times with PBS but centrifuged at 500 *g* and 325 *g* respectively.

The cell pellet was resuspended in 10 ml of RPMI-1640, GlutaMAX™ supplement (Gibco) containing 100 U/ml penicillin, 100 µg/ml streptomycin (PAA) and 20 mM HEPES (Sigma) and plated onto 92 mm Nunclon™ Δ coated tissue culture plates (Nunc). The cells were incubated in a tissue culture incubator at 37 °C, 5% CO_2 for 2 hours in a Heraeus BB15 incubator (Thermo Scientific) to allow for monocyte adherence induced by serum starvation. After 2 hours, the RPMI media was tipped off, cells were washed with PBS once to remove non adherent lymphocytes and fed with 10 ml of RPMI containing 10% FBS (Sigma), 100 U/ml penicillin, 100 µg/ml streptomycin and 20 mM HEPES. After 24 hours, cells were fed with a further 10 ml of RPMI containing 10% FBS and incubated for a total of 5 days to obtain adherent monocyte-derived macrophages as previously described.

2.7.1.2 Stimulation of MDM

After 5 days, MDM were washed in PBS, scraped, counted and cultured overnight in X-VIVO™ 15 medium (Lonza) at 1×10^6 cells on 35 mm × 10 mm Nunclon™ Δ coated tissue culture plates (Nunc) for RNA collection, at 2.5×10^5 cells/well in FALCON® 24-well tissue culture plates for immunoblots, at 1×10^5 cells/well in FALCON® 96-well tissue culture plates for cytokine assays or at 5×10^4 cells/coverslip in FALCON® 24-well tissue culture plates for confocal microscopy.

After 24 hours, MDM were stimulated with 1 µg/ml muramyl dipeptide (MDP) (Sigma), 4 µg/ml Pam_3CSK_4 (Alexis Biochemicals), 200 ng/ml lipopolysaccharide (LPS) (Alexis Biochemicals) or heat-killed *E. coli* (HkEc) NCTC 10418 at a multiplicity of infection (MOI) of 20 and harvested for total RNA and whole cell lysates.

2.7.2 THP-1 cells

2.7.2.1 THP-1 cell culture

THP-1 cells, an acute monocytic leukaemia cell line were maintained in RPMI/THP-1 culture media (see section 2.6 Reagents). Prior to being stimulated, THP-1 cells were passaged at 1:20 and left to grow for 3 days prior to being harvested and counted.

2.7.2.2 THP-1 cell stimulation

THP-1 cells were plated in THP-1 culture media in densities as described for MDM and stimulated with 1 µg/ml muramyl dipeptide (MDP) (Sigma), 4 µg/ml Pam_3CSK_4 (Alexis Biochemicals), 200 ng/ml lipopolysaccharide (LPS) (Alexis Biochemicals) or heat-killed *E. coli* (HkEc) NCTC 10418 at a multiplicity of infection (MOI) of 20 and harvested for total RNA and whole cell lysates.

2.7.3 Bone marrow-derived macrophages (BMDM)

2.7.3.1 Bone marrow cell harvest and culture

Naïve *Optn*$^{+/+}$ and *Optn*$^{-/-}$ mice age 9 to 12 weeks were culled with CO_2 and cervical dislocation. Their hind legs were dislocated at the hips, removed and transported in PBS on ice. The overlying muscle and tendons were cut off in a tissue culture hood, the bones cleaned briefly by dipping in 70% ethanol and kept in PBS on ice. The cleaned bones were cut at either end and the bone marrow cavity was flushed through with ice cold sterile PBS in a 10 ml syringe attached to a 26 G needle into sterile petri dishes. The bone marrow cells from both femurs and tibiae of one mouse were filtered through a sterile 70 µm nylon filter into a 50 ml Falcon tubes and centrifuged at 500 *g* for 5 minutes at 4 °C.

Red blood cells were lysed by adding 1 ml of red cell lysing solution (Sigma R7757) to the bone marrow cell pellet for 3 minutes at room temperature. Cells were washed in 30 ml of PBS and centrifuged at 500 *g* for 5 minutes at 4 °C. Bone marrow cells were resuspended in 4 ml of BMDM culture media (see section 2.6 Reagents) containing 20 ng/ml recombinant mouse M-CSF (Peprotech 315-02). 1 ml of resuspended bone marrow cells were added to each 92 mm × 17 mm Nunclon™ Δ coated tissue culture plates (Nunc) and topped up with 9 ml of BMDM culture media containing 20 ng/ml M-CSF. After 24 hours, a further 10 ml of BMDM culture media containing 20 ng/ml M-CSF was added to each plate. After 5 days, BMDM from both *Optn*$^{+/+}$ and *Optn*$^{-/-}$ mice were ~96% CD11b^{+} F4/80^{+} on flow cytometry (Figure 4.18).

2.7.3.2 BMDM cell stimulation

After 5 days, BMDM were washed in PBS, scraped, counted and cultured overnight in BMDM culture media at 1×10^{6} cells on 35 mm × 10 mm

Nunclon™ Δ coated tissue culture plates (Nunc) for RNA collection, at 5×10^5 cells/well in FALCON® 24-well tissue culture plates for immunoblots, at 1×10^5 cells/well in FALCON® 96-well tissue culture plates for cytokine assays or at 5×10^4 cells/coverslip in FALCON® 24-well tissue culture plates for confocal microscopy.

After 24 hours, BMDM were stimulated with 1 µg/ml muramyl dipeptide (MDP) (Sigma), 4 µg/ml Pam_3CSK_4 (Alexis Biochemicals), 200 ng/ml lipopolysaccharide (LPS) (Alexis Biochemicals) or heat-killed *E. coli* (HkEc) NCTC 10418 at a multiplicity of infection (MOI) of 20 and harvested for total RNA and whole cell lysates.

2.7.4 Thioglycollate induced peritoneal macrophages (TiPM)

2.7.4.1 TiPM cell induction and harvest

1ml sterile aged 3% thioglycollate broth (see section 2.6 Reagents) was injected into the peritoneum of age-matched *Optn*$^{+/+}$ and *Optn*$^{-/-}$ mice using a 26 G needle. Mice were scruffed and held supine with their heads down at 45 ° to minimise accidental organ puncture. After 5 days, mice were culled with CO_2 and cervical dislocation. Mice were laid supine and their external abdominal skin and hair was cleaned with 70% ethanol and a superficial cut in the midline lower abdominal skin was made. The hind legs and tail of the mice was firmly held down and the abdominal skin was pulled away by holding the skin where it was cut and pulling up towards the head to reveal the intact peritoneal cavity.

4 ml of cell dissociation buffer (Gibco 13151) and 1 ml of air was injected carefully into the peritoneal cavity with a 26 G needle. The peritoneal cavity was shaken by holding the head down and shaking the abdomen by its hind legs and tail to facilitate adequate cell collection from the whole cavity. The parietal peritoneum was held with forceps at the centre of the abdomen

and tented up and a small ~5 mm cut in the parietal peritoneum was made above the air pocket. Sterile plastic Pasteur pipettes were used to collect the cell dissociation buffer containing peritoneal cells from the whole peritoneal cavity including the flanks into 15 ml Falcon tubes on ice. The volume of buffer extracted was noted. Cells were centrifuged at 500 *g* for 5 minutes at 4 °C. Red blood cells were lysed by adding 1 ml of red cell lysing solution (Sigma R7757) to the peritoneal cell pellet for 3 minutes at room temperature. Cells were washed in 10 ml of PBS and centrifuged at 500 *g* for 5 minutes at 4 °C.

2.7.4.2 TiPM cell stimulation

Cells were counted and cultured overnight in TiPM culture media at 1×10^6 cells on 35 mm × 10 mm Nunclon™ Δ coated tissue culture plates (Nunc) for RNA collection, at 5×10^5 cells/well in FALCON® 24-well tissue culture plates for immunoblots, at 1×10^5 cells/well in FALCON® 96-well tissue culture plates for cytokine assays or at 5×10^4 cells/coverslip in FALCON® 24-well tissue culture plates for confocal microscopy

After 24 hours, TiPM were stimulated with 1 µg/ml muramyl dipeptide (MDP) (Sigma), 4 µg/ml Pam_3CSK_4 (Alexis Biochemicals), 200 ng/ml lipopolysaccharide (LPS) (Alexis Biochemicals) or heat-killed *E. coli* (HkEc) NCTC 10418 at a multiplicity of infection (MOI) of 20 and harvested for total RNA and whole cell lysates.

2.8 Macrophage Expression Microarray

Total RNA was harvested from unstimulated MDM and after 4 hours of stimulation with Pam_3, LPS and HkEc in Buffer RLT (Qiagen) using the RNeasy Mini Kit columns with RNase-free DNase treatment (Qiagen). Concentration of total RNA in RNase-free H_2O (Qiagen) was measured with a NanoDrop ND-1000 spectrophotometer (Thermo Scientific). Additionally,

OD_{260}/OD_{280} and OD_{260}/OD_{230} was measured, which assessed protein and solvent contamination. RNA integrity was analysed by measuring ribosomal RNA band 28S/18S ratios using high resolution electrophoresis on an Agilent Bioanalyzer (Agilent Technologies, Inc), which was >8.

500 ng of total RNA was amplified using the Illumina TotalPrep-96 RNA Amplification kit (Ambion) and normalised to 150 ng/µl. 750 ng was hybridised to Illumina Human-WG6 v3.0 Expression BeadChips (Illumina) for 16 hours at 58ºC. Beadarrays were stained with streptavidin-Cy3 (GE Healthcare) and scanned using the Beadarray reader and processed with GenomeStudio® data analysis software (Illumina).

Gene expression outlier analysis was carried out on customised software developed in collaboration with Anna Lobley and Daniel Roden (Department of Computer Science, UCL). This software identifies outlier genes by comparing gene expression in individual CD patients with the cohort of HCs using both p-value significance of the standardised deviation of CD test sample expression levels compared to the mean expression in HCs and $\log_2$ fold-change between CD test sample expression levels compared to the mean expression in HCs. The p value was set at a threshold of $p<0.005$ and a minimum fold change of 1.5 compared to the mean expression in HCs.

2.9 Quantitative reverse transcription PCR (qRT-PCR)

2.9.1 Cell preparation and conversion into cDNA

Total RNA from BMDM was collected by lysing cells in 350 µl of Buffer RLT (Qiagen) containing 10 µl of 2-mercaptoethanol (Sigma) per 1 ml Buffer RLT. The whole of the large bowel was cut into 4 segments, open longitudinally to remove faeces and weighed to ensure that each segment was <30 mg. Large bowel segments were placed in 600 µl of RNA*later* (Qiagen) and

homogenised with a TissueLyser LT (Qiagen) for 5 minutes at 50 Hz. Tubes were centrifuged at 14,000 *g* for 3 minutes at 4 °C and supernatants were transferred into fresh tubes. 600 µl of 70% ethanol was added to each tube and sample was transferred to RNeasy® Mini kit columns (Qiagen) and processed following manufacturer's instructions with no DNase digestion step.

Total RNA was converted to complementary DNA (cDNA) using the QuantiTect® Reverse Transcription Kit (Qiagen) following the manufacturer's instructions. 1 µg of total RNA was added to 2 µl of gDNA Wipeout Buffer (Qiagen), made up to 14 µl with RNase-free water and incubated for 2 minutes at 42 °C then placed on ice. 6 µl reverse transcription-mix containing 1 µl Quantiscript Reverse Transcriptase, 4 µl Quantiscript RT buffer, 5× and 1 µl RT primer mix (Qiagen) was added to each RNA sample making a total volume of 20 µl. Samples were incubated at 42 °C for 15 minutes and 95 °C for 3 minutes on a DNA Engine Tetrad 2® Peltier Thermal Cycler (Bio-Rad), made up to 100 µl with buffer TE (10 mM Tris pH 8.0, 1 mM EDTA) and stored at -20 °C.

2.9.2 qRT-PCR protocol

qRT-PCR of *Tnf, Il6, Il10* and *Cxcl1* was performed using the QuantiFast SYBR® Green PCR kit (Qiagen), in duplicate on a Mastercycler® ep *realplex* (Eppendorf) with primers created using Primer3 (Appendix 1). Stock primers at 100 µM were diluted to 3 µM i.e. 30 µl per 1 ml of RNase-free water for qRT-PCR and stored at -20 °C. The qRT-PCR reaction was made up of 12.5 µl 2× QuantiFast SYBR Green PCR Master Mix, 2.5 µl forward primer, 2.5 µl reverse primer, 2 µl cDNA and 5.5 µl RNase-free water, to a total volume of 25 µl. The final concentration in the reaction volume was 1× QuantiFast SYBR Green PCR Master Mix, 0.3 µM of each primer and ~400 ng cDNA/reaction. The PCR mix was activated at 95 °C for

15 minutes, denatured at 95 °C for 15 s and annealed/extended at 60 °C for 60 s, for a total of 40 cycles, then a melting curve was performed. The annealing temperature of 60 °C was chosen after a temperature gradient was run for each primer pair.

Normalized mean gene expression values ± SD were determined from duplicate cycle threshold (Ct) values for each gene and the housekeeping gene peptidylprolyl isomerase A (*Ppia*). Relative transcript levels were determined by the 2−ΔΔCt method [231].

2.10 Immunoblot

2.10.1 Whole cell lysate preparation

After stimulation, MDM and BMDM supernatants were removed then the adherent cells were washed once in 500 µl PBS then lysed in 200 µl Laemmli sample buffer (see section 2.6 Reagents) containing protease inhibitors (Roche 11697498001) and phosphatase inhibitors 2 & 3 (Sigma P5726 & P0044). Samples were scraped with sterile 24 cm cell scrapers (SLS 99002T), transferred into eppendorfs and pipetted up and down 10 times to break DNA then boiled at 95°C for 5 mins on an Eppendorf Thermostat plus and stored at -20 °C. Stimulated THP-1 cells were transferred into eppendorfs then centrifuged at 500 *g* for 5 minutes at 20 °C with a Beckman Coulter Microfuge 22R. Supernatants were transferred into new eppendorfs. 200 µl Laemmli sample buffer containing protease inhibitors and phosphatase inhibitors was added to wells to lyse any remaining cells then transferred to the eppendorfs to lyse the cell pellet and pipetted up and down 10 times to break DNA then boiled at 95 °C for 5 mins and stored at -20 °C.

2.10.2 Semi-dry transfer

SDS-PAGE gels were cast using the Mini-PROTEAN® System (Bio-Rad) with 30% w/v Acrylamide/ProtoFLOWGel (SLS H16996), 1.5 M Tris-HCl pH 8.8 (resolving gel), 1 M Tris-HCl pH 6.8 (stacking gel), dH_2O, 10% SDS (Sigma L3771), freshly made 10% ammonium persulphate (Sigma A7460) and TEMED (Sigma T9281) (added in the order listed with TEMED last). 10% SDS-PAGE gels were used for all experiments except for TNF and LC3 where 15% gels were cast. 10 µl of sample were loaded onto 10-well SDS-PAGE gels and run in ~700 ml of 1× transfer buffer without methanol (see section 2.6 Reagents) at 30 mA per gel for 40 minutes.

60 ml of 100% methanol was added to the remaining 300 ml of 1× transfer buffer to make a 1× transfer buffer containing 20% methanol. Hybond-P PVDF membranes (GE Healthcare/Amersham RPN303F) were cut into 9 cm × 6 cm rectangles and activated in 100 % methanol. Four sheets of 12 cm × 8 cm blotting paper were soaked in transfer buffer, layered onto a Trans-Blot® SD semi-dry transfer cell (Bio-Rad) and rolled with an empty FACS tube to remove trapped bubbles. The activated PVDF membrane was washed in transfer buffer than placed on the blotting paper. The SDS-PAGE gel was removed from its glass mould in the transfer buffer, the stacking gel was gently cut off with the edge of the glass plate and the gel was placed on top of the PVDF membrane. Four more sheets of blotting paper were layered on top of the gel and rolled to remove trapped bubbles. The transfer cell was run at 100 mA per gel for 60 minutes.

Membranes were blocked in 5% Marvel non-fat skimmed milk (Premier Foods) for 1 hour then washed 3 times in TBS-Tween. Membranes were probed with primary antibody overnight at 4°C (see section 2.5 Antibodies) then washed 3 times with TBS-Tween. Membranes were probed with secondary antibody for 1 hour at room temperature then washed 3 times

with TBS-Tween. Bound antibody was detected using 1 ml ECL Plus (Amersham) per membrane, which was made up as per manufacturer's instructions. Membranes were exposed to Hyperfilm ECL (Amersham) in a film cassette and scanned in at 300 dpi.

Band intensity was quantified and normalised to actin using ImageJ (National Institutes of Health).

2.11 Immunoprecipitation

THP-1 cells (10^7) were lysed in 50 mM HEPES pH 7.5 (Sigma), 100 mM NaCl (Sigma), 10% glycerol, 0.5% NP-40 (Sigma), 0.5% CHAPS (Sigma), protease inhibitors (Roche), phosphatase inhibitor cocktail 1, 2 (Sigma) and 300 µg/ml PMSF (Sigma) then passed through a 21G needle. Insoluble material was removed by centrifugation and the supernatant pre-cleared with protein A-agarose (Sigma) for 2 hours at 4°C. Pre-cleared supernatant was then incubated with anti-OPTN antibody (Sigma, 1:50) for 30 minutes at 4°C. Protein A-agarose was added, incubated overnight at 4°C and then washed 5 times with ice cold PBS. THP-1 supernatant was incubated with protein A-agarose overnight at 4°C and then washed 5 times with ice cold PBS and used as a negative control.

2.12 Mass spectrometry

For liquid chromatography-tandem mass spectrometry (LC-MS/MS) analysis, proteins were separated by 10% SDS-PAGE under reducing conditions. Proteins were visualized by silver-staining with ProteoSilver Plus (Sigma), bands were excised from both the OPTN-IP and control-IP gel lanes and processed for in-gel digestion and LC-MS/MS with the LTQ-Orbitrap mass spectrometer (Thermo Fisher Scientific), as previously described [232]. Raw MS files were analysed by the Mascot search engine 2.3.02 (Matrix Science) and searched against a SwissProt human database 2013_10 (containing

39,696 entries including common contaminants). Mascot search analysis parameters included: trypsin enzyme specificity, allowance for 2 missed cleavages, peptide mass tolerance of 20 ppm for precursor ions and fragment mass tolerance of 0.8 Da. Oxidation (M) was selected as a variable modification and carbamidomethyl (C) was selected as a fixed modification.

2.13 Subcellular fractionation

2.13.1 Preparation of sucrose gradients

A 50% sucrose solution containing 1 mM EDTA pH 7.4 and 5 U/ml heparin and a separate 1 mM EDTA pH 7.4 and 5 U/ml heparin were made. Nine 5% step dilutions of 50% sucrose were made (Table 2-1).

Table 2-1 Sucrose gradient composition used for subcellular fractionation.

% sucrose	Volume of 50% sucrose solution used (ml)	Volume of 1 mM EDTA pH 7.4 added (ml)
50	10	0
45	9	1
40	8	2
35	7	3
30	6	4
25	5	5
20	4	6
15	3	7
10	2	8

1 ml of each sucrose gradient was added to a 15 ml Falcon tube sequentially starting from 50% to the 15% sucrose gradient and left overnight to equilibrate at 4°C.

2.13.2 Subcellular fractionation of THP-1 cells

2×10^8 THP-1 cells were incubated in RPMI 1640 and stimulated with HkEc at a multiplicity of infection of 20 for 24 hours. THP-1 cells were harvested and made up in 10% sucrose 1 mM EDTA pH 7.4 with 5 U/ml heparin containing protease inhibitor (Roche 11697498001) then lysed on ice with a dounce homogeniser (GPE limited) and sonicated 3×5 s (MSE Soniprep 150) up to three times or until cells are visibly lysed on light microscopy. Lysed THP-1 cells were centrifuged at 750 *g* for 10 minutes at 4 °C.

The post-nuclear supernatant was layered onto the sucrose gradient and ultracentrifuged in a TST 41.14 Kontron swing-bucket rotor at 220,000 *g* for 3 hours at 4°C on a Beckman Optima™ LE-80K Ultracentrifuge with slow acceleration and deceleration. The nuclear pellet was resuspended in 50 µl 10% sucrose and stored at -80 °C. After centrifugation, 1 ml fractions were removed. The pellet was also resuspended in 50 µl 10% sucrose and all fractions were stored at -80 °C.

Fraction sucrose percentages were measured with a Bellingham + Stanley Abbe 60 Refractometer.

2.14 Lysosomal inhibition and TNF production

5×10^5 BMDM from *Optn*$^{-/-}$ and *Optn*$^{+/+}$ mice were plated in FALCON® 24-well tissue culture plates in DMEM and stimulated for 4 hours with HkEc at a MOI of 20 plus either DMEM alone, or DMEM with 2.5 µM monensin (Sigma M5273), 10 mM NH_4Cl (Sigma A4514), 100 µM chloroquine (Sigma C6628), 2.5 µM brefeldin A (Merck 203729) or 200 nM bafilomycin A (Sigma B1793).

1 µl of 5M NH_4Cl in dH_2O, 1 µl of 1.25 mM monensin in DMEM (1:80 dilution from 0.1 M monensin in methanol stock), 1 µl of 50 mM chloroquine in DMEM, 1 µl of 1.25 mM brefeldin A (1:2 dilution from 2.5 mM brefeldin A in

methanol stock) or 1 µl of 100 µM bafilomycin A in 10% DMSO stock was added to the 500 µl DMEM containing BMDM and HkEc at the start of the 4 hour experiment to obtain final concentrations above. After 4 hours, supernatants were removed and stored at -80 °C and BMDM were lysed in Laemlli buffer and immunoblotted for TNF (see section 2.10 Immunoblot).

2.15 Intraperitoneal *E. coli* infection

2.15.1 Live *E. coli* infection

The fully antibiotic sensitive clinical isolate of *E. coli* NCTC 10418 was cultured overnight in 10 ml LB broth, washed once in PBS, resuspended in 1 ml PBS and counted at 1:20 dilution using a Cecil BioQuest™ CE2502 spectrophotometer. The *E. coli* optical density at 600 nm (OD_{600}) of 1×10^8 bacteria/ml in PBS is 0.365. Nine to twelve week old *Optn*$^{-/-}$ and *Optn*$^{+/+}$ female mice were injected intraperitoneally with serially diluted *E. coli* at 1×10^8, 5×10^7, 2.5×10^7 and 1×10^7 bacteria/ml in PBS. Mice were weighed daily and tail bleed serum was collected for cytokine analysis at 48 hours. To tail bleed, mice were restrained with a plastic mouse restraint, the distal 5 mm of its tail was cut off with a blade and the tail was massaged repeatedly to collect drops of blood in an eppendorf. Eppendorfs were sat at room temperature for 3 hours to allow clotting then centrifuged to obtain serum. After 6 days, mice were culled using CO_2.

2.15.2 Killed *E. coli* infection

To assess cellular recruitment to the peritoneum, 1 ml heat-killed *E. coli* was injected into nine to twelve week old *Optn*$^{-/-}$ and *Optn*$^{+/+}$ mice at $1\text{-}5\times10^8$ HkEc/ml in PBS. Naïve and day 1 peritoneal washouts were harvested in cell dissociation buffer (Gibco) and analysed using flow cytometry (see section 2.7.4 TiPM and 2.29 Flow cytometry).

2.16 Zebrafish Study

2.16.1 *Optn* in situ hybridisation

Whole-mount in situ hybridization was carried out as previously described with *optn* target-specific probes (Appendix 1) [233]. Stained specimens were mounted in paraffin, sectioned and counterstained with Nuclear Fast Red (Vector Labs) prior to imaging with a Leica DMR compound microscope equipped with a DFC420C camera.

2.16.2 *Salmonella* immersion and injection infection

Salmonella enterica serovar Typhimurium was grown in LB broth at 37°C, 200 rpm overnight. To prepare *Salmonella* for an immersion (bath) infection, the culture was diluted 1 in 10 with DMEM, grown at 37°C, 200 rpm for a further 3 hours, washed once and resuspended in E3. Groups of 20 zebrafish larvae at 4 dpf were exposed to *Salmonella* at a final concentration of 5×10^8 CFU/ml at 28.5°C. *Salmonella* injection was carried out using a method adapted from Prajsnar et al [234]. *Salmonella* was grown as above, washed and resuspended (1:1 ratio) in PBS. Injection doses were prepared by diluting the resuspended *Salmonella* 1:100 with PBS. 1 nl of this solution (approximately 200 CFU) was microinjected into the yolk sac of anesthetized 2 dpf embryos mounted in methylcellulose. Immersion and injection doses were verified by plating onto LB agar. Embryos were recovered to E3, washed to remove excess methylcellulose and incubated for observations at 28°C. Total RNA was isolated from zebrafish embryos using Trizol (Invitrogen). cDNA was synthesized from 2 µg of total RNA with the High Capacity cDNA Reverse Transcription Kit (Applied Biosystems). qRT-PCR and primer used (Appendix 1) was as previously described [235].

2.16.3 *Optn* morpholino knockdown

Morpholinos (GeneTools, LLC) were designed to target the splice donor site after exon 1 of the *optn* gene (Appendix 1). Primers that spanned introns were used for RT-PCR of the targeted junctions (Appendix 1). Morpholinos were injected into one- to four-cell stage embryos at 1.0 pmol per embryo as previously described [236]. Embryos were then injected with *Salmonella* at 2 dpf as above and incubated for observations at 28°C.

2.17 Dextran sodium sulphate (DSS) colitis

2.17.1 DSS colitis protocol

Optn$^{+/+}$ and *Optn*$^{-/-}$ mice age 9 to 12 weeks were given 2% DSS (MW 36,000-50,000) (MP Biomedicals 160110) in their drinking water for 7 days as described [237]. The normal drinking water in the animal unit was used to make up the 2% DSS to minimise the effect of alteration in water taste on consumption of the DSS that results from autoclaving water. The DSS was changed with fresh DSS after 2 days and 5 days from the start of the experiment and was changed back to fresh drinking water in a new water bottle after 7 days (Figure 2.1).

2.17.2 DSS colitis clinical score

Mice were weighed and faeces collected daily to calculate the disease activity score (Table 2-2) and guaiac faecal occult blood test slides (immunostics, inc HS-100). At set time points, mice were culled with CO_2 and cervical dislocation and bowel and blood was harvested.

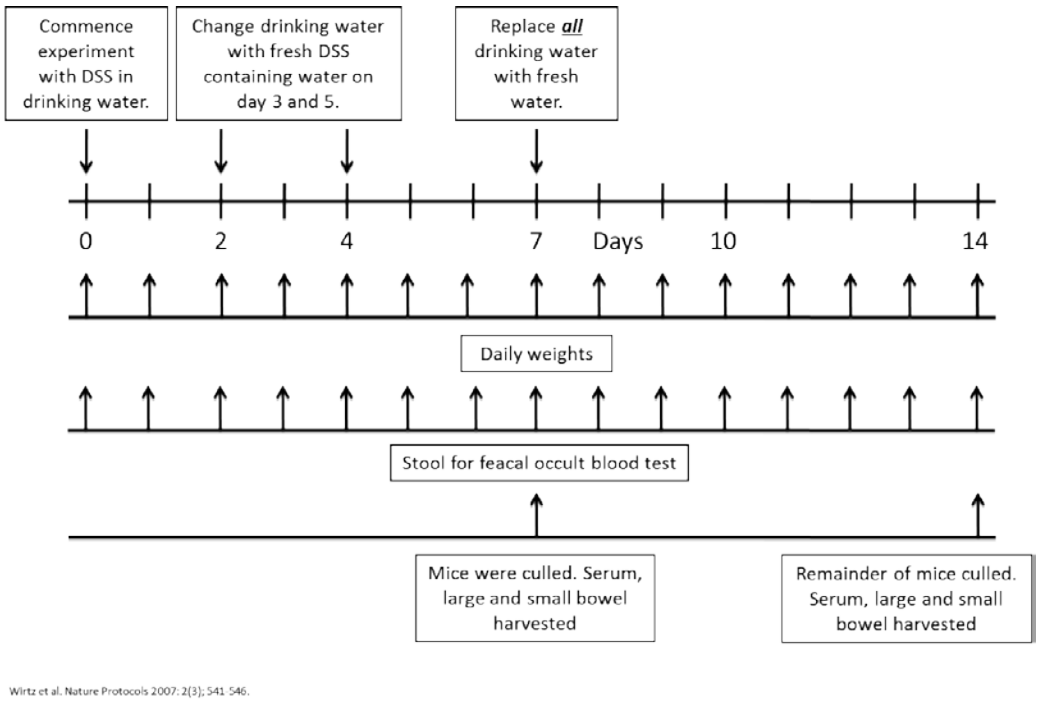

Figure 2.1 Acute DSS colitis protocol. Protocol involves 7 days of DSS in the drinking water. Adapted from Wirtz et al, 2007 [237].

Table 2-2 DSS clinical disease activity score [238].

Score	0	1	2	3	4
% Weight loss	No weight loss	1 to 5	6 to 10	10 to 20	>20
Stool consistency	Well-formed pellets		Pasty stools		Watery stools
Bleeding	No blood on hemoccult		Positive hemoccult		Gross bleeding

2.18 *Citrobacter rodentium* colitis

2.18.1 Preparation of *C. rodentium*

C. rodentium strain ICC169 was kindly provided by Gad Frankel (Division of Cell and Molecular Biology, Imperial College London, UK). *C. rodentium* was

cultured overnight by adding 1 µl glycerol stock to 10 ml LB broth medium containing 50 µg/ml nalidixic acid and incubated at 37°C 250 rpm in a shaker-incubator. *C. rodentium* was washed once in 10 ml phosphate-buffered saline (PBS), pH 7.2 then made up in 1 ml PBS per 10 ml original LB broth, pooled and counted at an optical density of 600 nm (OD_{600}), which is 0.161 for 1×10^8 bacteria/ml in PBS.

2.18.2 Induction of *C. rodentium* colitis

Nine to twelve week old *Optn*$^{-/-}$ and *Optn*$^{+/+}$ littermate female mice were orally gavaged with 200 µl of *C. rodentium* in PBS using a 1 ml syringe attached to a curved 1 inch 20G stainless steel 2 mm ball-tipped gavage needle, giving each mouse 2.5 – 4.5 x 10^9 CFU of *C. rodentium*. Mice were scruffed firmly and held head up to minimize movement that may cause oesophageal or gastric perforation.

Mice were weighed daily. Faeces collected for *C. rodentium* excretion and tail bleeds for serum cytokine analysis. After 2, 3 or 9 days, mice were culled with CO_2 and cervical dislocation and cardiac punctures for blood was performed. Large bowel was collected for histology (see section 2.20 Histology) and livers and spleens for bacterial culture.

2.18.3 Sample preparation for *C. rodentium* culture

Spleens and liver from *C. rodentium* infected mice were also harvested to check if there was a bacteraemia. Organs were homogenised in sterile 5 ml bijous containing 1 ml PBS using a 5 ml syringe plunger. 20 µl of supernatant was plated in each sector of a 4-sector 90 mm Petri Star™ dish (VWR 710-3519) containing LB agar with 50 µg/ml nalidixic acid and incubated overnight at 37 °C in a LEEC MkII dry incubator.

Fresh faeces was collected from individual mice, weighed dry then dispersed in 500 µl PBS using sterile pipette tips. The faeces was vortexed for 30 seconds then centrifuged at 500g for 30 seconds to pellet solid faeces. Serial dilutions were plated on LB agar plates as above and counted the next day.

2.19 Lamina propria cell isolation

Mice were culled with CO_2 and cervical dislocation. Large bowels were cut longitudinally and washed in ice cold PBS containing 100 U/ml penicillin, 100 µg/ml streptomycin (PAA) to remove faeces. Epithelial cells were removed by incubation of each large bowel in 20 ml of predigestion solution (HBSS (Gibco) containing 10% FBS, 100 U/ml penicillin, 100 µg/ml streptomycin and 2 mM EDTA) in 50 ml Falcon tubes at 37°C, 250 rpm for 1 hour in an Innova™ 4000 incubator shaker [239]. Epithelial cells were passed through a 70 µm filter. The remaining lamina propria tissue was cut into 1 mm pieces and washed with PBS to remove EDTA. Lamina propria tissue was incubated in 20 ml digestion solution (HBSS containing 10% FBS, 100 U/ml penicillin, 100 µg/ml streptomycin, 30 mg collagenase (Sigma C2139), 0.8 mg DNase I (Sigma DN25) and 15 mg Dispase II (Sigma D4693)) at 37°C, 250 rpm for 30 minutes, and vortexed vigorously for 20s at the start, middle and end of incubation. Lamina propria cells were passed through a 70 µm filter, washed with PBS then stained for flow cytometry (see section 2.29 Flow cytometer.)

2.20 Histology and immunohistochemistry.

2.20.1 Haematoxylin and eosin staining

Large bowel tissue and organs were fixed in 10% neutral buffered formalin (CellPath BAF-0010-10A) overnight then paraffin-embedded using a Leica TP1050 tissue processor and RA Lamb Blockmaster embedding center. Blocks were sectioned at 5 µm onto SuperFrost® Plus slides (Thermo

Scientific) using a Leica RM2235 rotary microtome. Sections were stained on a Leica ST4040 linear stainer. Sections were dewaxed through 4 xylene stations and rehydrated through 4 graded industrial methylated spirit stations then water for 1 minute per station. Sections were stained in acidified VFM Harris' haematoxylin (CellPath RBA-4205-00A) for 5 minutes, differentiated in 0.2% acid alcohol for 1 minute and stained in Eosin Y (VWR 1.15935.1000) for 4 minutes with a running tap water wash between each step. Sections were dehydrated, cleared and mounted in Pertex (Leica 3808706E).

Colitis scoring of haematoxylin and eosin stained large bowel was performed blind with the 6 parameters in Table 2-3.

2.20.2 OPTN immunohistochemistry

The OPTN antibody (Sigma) was used to performed immunohistochemistry on available UCLH archival *OPTN*^{low} bowel biopsy samples with patient consent and a healthy control small bowel. Initial antibody optimisation was performed on control small bowel tissue. Sections underwent automated dewaxing and endogenous peroxidase was blocked using 3-4% (v/v) hydrogen peroxide. After preliminary optimisation where optimal conditions were chosen based upon the criterion of background-free selective cellular labelling, the antibody was used on the *OPTN*^{low} and healthy control small bowel samples at a dilution of 1:100 with 30 minute incubation at ambient temperature following heat induced epitope retrieval for 20 minutes using an EDTA-based (pH 9.0) epitope retrieval solution. Signal visualization using the Bond Polymer Refine Detection kit (DS9800) with DAB Enhancer (AR9432) was performed on the Bond-III automated staining platform (Leica). Cell nuclei were counterstained with haematoxylin.

Table 2-3 H&E colitis scoring system.

Epithelial hyperplasia	
0	None
1	Mild hyperplasia but retaining architecture
2	Moderate hyperplasia with mild distortion
3	Severe, marked, crowding of cells
Crypt deformity/architectural distortion	
0	None
1	Mild branching/twisting/deformity
2	Moderate, affecting >50%
3	Severe, marked deformity near 100% surface due to inflammation & oedema
Ulceration	
0	None
1	Small focal erosions
2	Small ulcers/multiple erosions
3	Large/deep transmural ulcers
Variation	
0	None/no inflammation
1	Mild variability/patchy inflammation
2	Moderate/>50% inflammation
3	Severe, diffuse near 100% inflammation
Inflammatory cell infiltrate	
0	None
1	Few multifocal mononuclear cells in lamina propria
2	Several multifocal areas & neutrophils
3	Multiple transmural infiltrates/crypt abscesses
Goblet cell depletion	
0	None/normal
1	Mild/scattered depletion
2	Moderate/>50% depletion
3	Severe depletion/few visible/absent

2.20.3 Myeloperoxidase immunohistochemistry

The rabbit polyclonal anti-myeloperoxidase (MPO) antibody (Dako) was chosen for use in this study due to its reported specificity for MPO in murine tissues [240] and suitability for use with formalin-fixed paraffin-embedded

tissues. 3 µm thick sections of naïve murine large bowel as a negative control and bone marrow cells as a positive control were used for antibody optimisation on the Bond-III automated staining platform (Leica). Sections underwent automated dewaxing and endogenous peroxidase was blocked using 3-4% (v/v) hydrogen peroxide. After preliminary optimisation where optimal conditions were chosen based upon the criterion of background-free selective cellular labelling, the antibody was used on the *Citrobacter* infected large bowel samples at 1:1,000 with 30 minute incubation at ambient temperature following heat induced epitope retrieval for 20 minutes using an EDTA-based (pH 9.0) epitope retrieval solution. Prior to signal visualization using the Bond Polymer Refine Detection kit (Leica DS9800) with DAB Enhancer (Leica AR9432) a 10% block of normal goat serum (Sigma G9023) was applied at ambient temperature for 30 minutes to reduce non-specific binding of the polymer. Cell nuclei were counterstained with haematoxylin.

2.20.4 Steiner Silver stain

Slides were deparaffinised in xylene for 10 minutes then hydrated through an alcohol gradient (100%, 100%, 90%, 70%, 50%) to dH_2O at 30 s per gradient. Slides were then incubated in preheated 1% uranyl nitrate at 60˚C for 15 minutes in plastic coplin jars and rinsed in three changes of hot 60˚C dH_2O. Slides were then incubated in preheated 1% silver nitrate at 60˚C for 1.5 hours, rinsed in three changes of hot 60˚C dH_2O, two changes of room temperature 95% ethanol and 2 changes of room temperature absolute ethanol. Slides were placed in room temperature 2.5% gum mastic for 5 minutes and allowed to air dry. Slides were then incubated in reducing solution at 45˚C for 20 minutes then allowed to stand in the reducing solution at room temperature until desired degree of black staining for 1 to 2 minutes and rinsed in three changes of room temperature dH_2O. Slides were dehydrated through the alcohol gradient, cleared in xylene and mounted in DPX Mountant (Sigma 44581).

2.21 Killing assay

Cells were plated at 2.5×10^5/well in a 24-well plate in their respective culture media containing penicillin and streptomycin and incubated overnight to allow cells to adhere to plate. Cells were washed once in 1 ml PBS and incubated overnight in media with no antibiotics to allow washing out of the antibiotics. Cells were washed once in 1 ml PBS and incubated with *E. coli* in media containing no antibiotics at an MOI of 20 for 2 hours at 37 °C, 5% CO_2 to facilitate adequate phagocytosis of *E. coli*.

After 2 hours, the cells were washed once in 1 ml PBS to remove bacteria and incubated in media containing 300 µg/ml gentamicin for 1 hour to kill extracellular *E. coli*. Cells were washed once in PBS to remove gentamicin and lysed for the 1 hour time point in PBS containing 1% Triton X-100 (BDH 306324N). Remaining cells were also washed in PBS and incubated in media containing 100 µg/ml gentamicin for further time points. Neat and three 1:10 serial dilutions of lysed cells in PBS was plated on LB agar plates and bacterial CFUs were counted the next day.

2.22 Phagocytosis assay

2.22.1 Preparation of FITC-labelled HkEc

HkEc was labelled with fluorescein isothiocyanate (FITC) (Invitrogen F1906). 1×10^9 HkEc was washed three times in 20 ml then resuspended in 1 ml of 0.1 M sodium bicarbonate. 10 µl of 10 mg/ml FITC dye in DMSO was added to the HkEc and incubated at 1400 rpm, 4 °C for 30 minutes on an Eppendorf Thermomixer comfort incubator. 100 µl of 1.5 M hydroxylamine pH 8.5 (Sigma 159417) was added to terminate the reaction. HkEc was washed 3 times in PBS and stored at -20 °C. Trypan blue (Merck FN1072132) was made up at 2.5 mg/ml in dH_2O and filtered with a Nalgene 0.45µm filter

(Thermo Scientific 190-2545) to remove undissolved residue and stored at room temperature.

2.22.2 Phagocytosis of FITC-HkEc

1×10^5 cells were plated onto Corning 96-well special optics plates (Sigma CLS3720) and incubated overnight to allow cells to adhere to the bottom of the plate. 100 µl of FITC-HkEc at an MOI of 20 was added to each well. 10 µl of 2.5 mg/ml Trypan blue was added to each well to quench the FITC at different time points. Fluorescence intensity was measured at an excitation wavelength of 485 nm and read at an emission wavelength of 520 nm using a FLUOstar Omega microplate reader (BMG LABTECH).

2.23 Autophagy assay

Optn$^{+/+}$ and *Optn*$^{-/-}$ whole cell lysates from BMDM stimulated with HkEc at time points up to 24 hours were immunoblotted for LC3B (Sigma) to investigate autophagy in BMDM.

2.24 Endoplasmic reticulum stress assays

Optn$^{+/+}$ and *Optn*$^{-/-}$ BMDM stimulated with HkEc for 4 hours were assessed for the unfolded protein response and were immunoblotted for CHOP (Affinity BioReagents), GRP78/BiP (Santa Cruz) and GRP94 (Santa Cruz). Additionally, BMDM were stimulated for 4 hours with 2 µM of 10mM Thapsigargin (Sigma T9033) in DMSO, 2 µg/ml of 1 mg/ml Tunicamycin (Sigma T7765) and 200 nM Bafilomycin A (Sigma) for mRNA. Total RNA was harvested and converted to cDNA as described above. PCR was performed on cDNA samples and digested with PstI (Promega) restriction enzyme. Samples were run on a 2% high performance MetaPhor™ Agarose (Lonza 50181) gel, made as per manufacturer's instructions and run at 4 °C to separate the bands.

2.25 Subcutaneous HkEc injection

Nine to twelve week old *Optn*$^{+/+}$ and *Optn*$^{-/-}$ female mice were anaesthetised with Halothane and their backs were shaved. Serial dilutions of HkEc were made up to 1×10^{10}, 1×10^{9}, 1×10^{8}, 1×10^{7}, 1×10^{6} per ml in PBS and 100 µl was injected subcutaneously in two areas over both scapulae for a dose response experiment. Injection was performed by tenting up the skin to ensure insertion of the 26 G needle into the subcutaneous space. Mice were weighed daily and size of the injection site was measured using Vernier callipers. Skin and serum was harvested for histology. 1×10^{8} HkEc was used and injected into *Optn*$^{+/+}$ and *Optn*$^{-/-}$ mice as described above.

2.26 Confocal immunofluorescence microscopy

2.26.1 Specimen preparation and staining

Cells were plated onto methanol cleaned 13 mm diameter 0.13 mm thick pure white, hydrolytic class 1 round borosilicate glass coverslips (VWR 631-0149) at 50,000 cells/coverslip overnight. Cells were fixed in 500 µl of 4% formaldehyde for 10 minutes then washed with 1 ml of PBS. The aldehydes were quenched in 500 µl of 50 mM NH_4Cl for 10 minutes then washed with 1 ml PBS and then permeabilised in 500 µl of 0.01% Triton X-100 for 10 minutes then blocked in 500 µl of 100 µg/ml desalted human IgG (CSL Behring) in confocal buffer (see section 2.6 Reagents) for 15 minutes.

Cells were then stained with primary antibody in confocal buffer for 30 minutes. After 3 washes with 2 ml of confocal buffer per wash, cells were stained with secondary antibody and 300 nM DAPI (Invitrogen) for 30 minutes. Cells were washed 3 times with 2 ml of confocal buffer and reblocked with 500 µl of 100 µg/ml desalted human IgG for 15 minutes. Cells were then stained in second primary antibody for 30 minutes, washed 3 times and stained with secondary antibody. Cells were washed in 2 ml

confocal buffer, 2 ml dH_2O and then 1 ml of dH_2O to remove traces of PBS salts.

Coverslips were gently lifted with a straight needle probe and then gripped with a pair of sharp pointed straight dissection forceps. Slides were mounted cells facing down in 12 µl of Mowiol® (Calbiochem), dried overnight in the dark at room temperature then stored at -20ºC. 8 bit, 0.5 µm thick single or z-stack, sequential images were taken using a Leica 40×/1.15 or 63×/1.30 oil CS apochromatic objective on a Leica TCS SPE confocal microscope with LAS AF Version 2.3.6.

2.26.2 Colocalisation analysis

Colocalisation analysis was performed using ImageJ (National Institutes of Health). Individual BMDM were selected and thresholds were set for TNF, EEA1 and GM130 to visualise vesicles and the Golgi complex. The image calculator function was used with the AND operator to generate an image of colocalised pixels for each z-stack, then the histogram function was used to quantify the total number of TNF, EEA1, GM130 and colocalised pixels in each z-stack.

Vesicle colocalisation in MDM was quantified by counting the number of double positive and single positive staining vesicles using Leica's LAS AF Lite viewing program.

2.27 Electron microscopy

Cells were plated onto methanol cleaned 13 mm diameter glass coverslips at 100,000 cells/coverslip overnight then stimulated with HkEc at a MOI of 20 for 4 hours. Cells were fixed in fresh 2% paraformaldehyde/1.5% glutaraldehyde (Agar scientific) in 0.1 M sodium cacodylate buffer pH 7.3 (BDH) for 1 hour. Cells were washed in 0.1 M cacodylate buffer for 5 min

twice then post fixed in 1% osmium tetraoxide (OsO_4) (Agar Scientific)/1.5% potassium ferrocyanine ($K_4Fe(CN)_6$) (BDH) in 0.1 M cacodylate buffer pH 7.3 for 1 hour at 4°C in the dark. Cells were washed in 0.1 M cacodylate buffer, then in 1% tannic acid in 0.05 M cacodylate buffer for 5 min, a further wash in 0.1 M cacodylate buffer and finally in dH_2O for 5min. After rinsing with dH_2O, specimens were dehydrated in a graded ethanol-water series and infiltrated with Agar 100 resin. Serial 1 µm sections were cut and stained with 1% toluidine blue in dH_2O for light microscopy. At the correct position ultrathin sections were cut at 70-80 nm using a diamond knife on a Reichert ultracut microtome. Sections were collected on a 300 mesh copper grid, stained with uranyl acetate (BDH) and lead citrate (BDH) then viewed in a Joel 1010 transition electron microscope and images recorded with a Gatan Orius camera.

2.28 Cell Viability Assay

2.28.1 MTT Assay

Cells were plated at 10^5/well in a 96-well plate and stimulated with bacteria. After 4 hours, supernatants were removed and cell viability was assessed using the MTT (3-[4,5-dimethylthiazol-2-yl]-2,5-diphenyl tetrozolium bromide, tetrazolium salt) assay (Sigma). 30 µl of 2 mg/ml MTT in PBS was added to 100 µl of media/well and incubated for 4 hours at 37 °C. Media was tipped off and 100 µl of MTT lysis solution was added to each well. Absorbance was measured on a FLUOstar Omega microplate reader (BMG LABTECH) at 563 nm after complete cell lysis and formazan solubilisation occurred.

2.29 Flow cytometry

2.29.1 Cell preparation and staining

Cells (blood, bone marrow and peritoneal cells) were washed in FACS buffer (PBS containing 1% BSA, 0.01% azide), centrifuged at 500 *g* for 5 minutes at 4 °C and resuspended in 200 µl of FACS buffer containing 2.0 µg/ml anti-CD16/CD32 Fc block (eBioscience) for 20 minutes. Cells were washed in 1 ml of FACS buffer then stained in 100 µl FACS buffer containing 0.5 µg/ml CD11b V450 (BD), 0.25 µg/ml Gr1 PE (BD), 0.25 µg/ml CD3 PE-Cy™7 (BD), 0.25 µg/ml CD19 PerCP-Cy™5.5 (BD), 0.25 µg/ml Ly-6C APC (BD) and 0.5 µg/ml F4/80 FITC (eBioscience) antibodies for 30 minutes in the dark at room temperature then fixed in 1% formaldehyde in PBS for 10 minutes.

Lamina propria cells in PBS were incubated in the dark with 1 µl of the LIVE/DEAD® stain (Invitrogen) for 30 minutes following the manufacturer's instructions. Cells were washed in 1 ml of PBS then blocked in 2.0 µg/ml CD16/CD32 antibody in FACS buffer prior to staining at 0.5 µg/ml of each antibody above in combination with 1.0 µg/ml CD45 PerCP-Cy™5.5 (BD) and either 0.5 µg/ml CD19 PE (BD) or 0.5 µg/ml Gr1 PE (BD).

2.29.2 Compensation particle preparation and flow cytometry

Compensation particles (BD 552845) were prepared by adding each antibody above to 100 µl of FACS buffer containing 1 drop of positive particles (~60 µl) and 1 drop of negative particles (~60 µl) to the same final concentration of antibodies. Particles were incubated in the dark at room temperature for 20 minutes then washed with 1 ml FACS buffer, centrifuged at 500 *g* for 5 minutes and resuspended in 300 µl of FACS buffer. Cells were run on a BD LSRFortessa (blood, bone marrow and peritoneal cells) or LSR II (lamina propria cells) after compensation with antibody labelled particles and analysed with FlowJo (Tree Star, Inc).

2.30 Cytokine assay

2.30.1 ELISA and MSD® immunoassay

Cells were cultured in FALCON® 96-well tissue culture plates at 1×10^5 cells/well for cytokine secretion assays. After removal of supernatants for storage at -80 °C, cell viability was assessed using the MTT (3-[4,5-dimethylthiazol-2-yl]-2,5-diphenyl tetrozolium bromide, tetrazolium salt) assay (Sigma).

Serum TNF levels from *Optn*$^{+/+}$ and *Optn*$^{-/-}$ intraperitoneal *E. coli* infected mice were measured using the murine TNF-α ELISA kit (Peprotech 900-K54) as per manufacturer's instructions and read on a FLUOstar Omega microplate reader (BMG LABTECH) at 405 nm. TNF, IL6, IL10 and CXCL1 levels in *C. rodentium* colitis serum and BMDM supernatants from *Optn*$^{+/+}$ and *Optn*$^{-/-}$ mice were measured using the Mouse Pro-Inflammatory 7-plex Ultrasensitive plate (Meso Scale Discovery K15012C) and read on a SECTOR® Imager 6000 (Meso Scale Discovery).

2.30.2 Proteome Profiler™ Array

10^6 BMDM were stimulated with HkEc at an MOI of 20 in 6-well plates for 4 hours. Cells were lysed in cold TBS containing 0.1% NP-40 and protease inhibitors, sonicated for 3× 3 s bursts on ice and then interrogated with the Mouse Cytokine Proteome Profiler™ Array Panel A (R&D ARY006), as per manufacturer's instructions. Processed arrays were exposed to X-ray film and imaged.

2.31 Statistical analysis

All data are presented as mean ± SEM using GraphPad Prism 4.03 (GraphPad Software, Inc). Statistical significance was calculated using

paired or unpaired two-tailed Student's t-test, logrank test or Fisher's exact test. Mean differences were considered significant when $p<0.05$.

2.32 Ethics

This human study was approved by the Joint University College London (UCL)/University College London Hospitals (UCLH) Committee for the Ethics of Human Research (project numbers 02/0324) and the NHS National Research Ethics Service, London-Surrey Borders Committee (project number 10/H0806/115). Ethics committee approved consent forms were signed by all participants.

Animal studies were performed in accordance with guidelines of University College London's Biological Sciences Unit and licensed by the Animals (Scientific Procedures) Act 1986 and European Directive 2010/63/EU on the protection of animals used for scientific purposes. All mice were euthanised humanely under Schedule 1 of the Animals (Scientific Procedures) Act 1986 by CO_2 asphyxiation and confirmed with dislocation of the neck.

Chapter 3 Optineurin in macrophages of Crohn's disease patients

3.1 Introduction

Macrophages are specialised cells of the innate immune system that are equipped with a wide range of pattern recognition receptors to detect, phagocytose and kill microbes in diverse tissue locations. Others in our research group previously showed defective neutrophil accumulation in the bowel of CD patients compared to HC at sites of trauma, by quantifying neutrophils in bowel biopsy and re-biopsy at the exact same location after six hours [107]. More recently, our group found that patients with CD mounted a poorer acute inflammatory response with impaired blood flow to sites of *E. coli* injection on the forearm and delayed accumulation of radioactively labelled autologous neutrophils to the site of infection [187]. This delayed neutrophil accumulation was associated with reduced clearance of radioactively labelled killed *E. coli* from forearm of CD patients.

To investigate this impaired neutrophil recruitment, our group performed transcriptomic analysis on human monocyte-derived macrophages from CD patients and HC, with UC patients as an inflammatory disease control. We identified defective proinflammatory cytokine secretion in macrophages from CD patients but not in HC and UC patients [187]. Anti-inflammatory and chemokine levels were not different. Further analysis identified an enrichment of abnormally expressed genes associated with vesicle trafficking and cytoskeletal organisation in CD patients. Outlier analysis of macrophage gene transcription by myself and others in our group identified low macrophage expression of optineurin in seven out of 58 CD patients but none in HC or UC patients, as recently published [191].

3.2 Results

3.2.1 Low *OPTN* expression is replicated in 10% of CD patient

In order to verify the previously reported link between low *OPTN* expression and CD (batch 1) [191], an additional 47 CD patients and 33 healthy controls (HC) were recruited into a replication cohort (batch 2). Outlier analysis of macrophage gene expression in this replication cohort identified a further four CD patients with low *OPTN* (*OPTN*^{low}) expression, replicating the previously reported link (Figure 3.1).

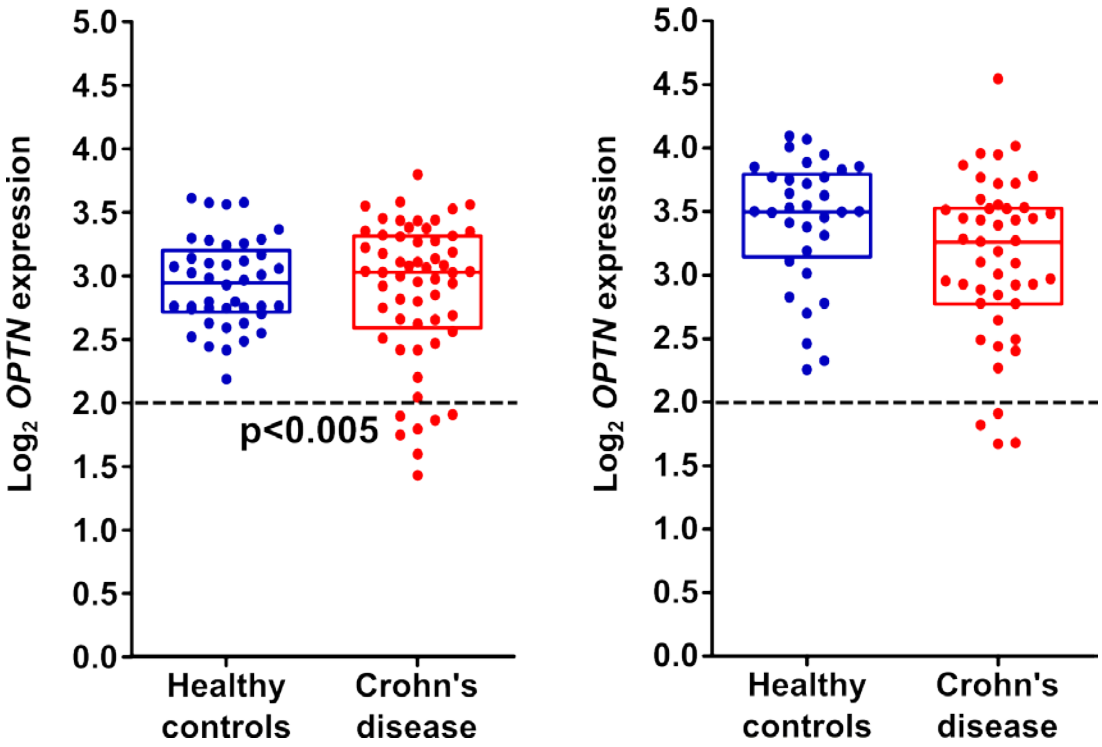

Figure 3.1 Outlier analysis of macrophage *OPTN* expression on microarray identified 11 *OPTN*^{low} CD patients. A primary cohort (left) identified seven and a subsequent replication cohort (right) identified four CD patients with low *OPTN* expression on outlier analysis. p value was set at a threshold of p<0.005 and a minimum fold change of 1.5 compared to the mean expression in HC. Data collection and analysis in the primary (left) and replication cohort (right) was performed by myself and others in our group.

To validate the microarray results and establish the level of *OPTN* under expression, qPCR was performed (Figure 3.2). Three out of four *OPTN*^{low} CD patients in the replication cohort that were available for retesting demonstrated on average a three-and-a-half fold reduction in *OPTN* transcript levels ($p<0.01$), replicating the qPCR validation in the initial seven *OPTN*^{low} CD patients identified [191]. Immunoblot of OPTN in MDM from four *OPTN*^{low} CD patients confirmed reduced OPTN protein expression compared to HC (Figure 3.3).

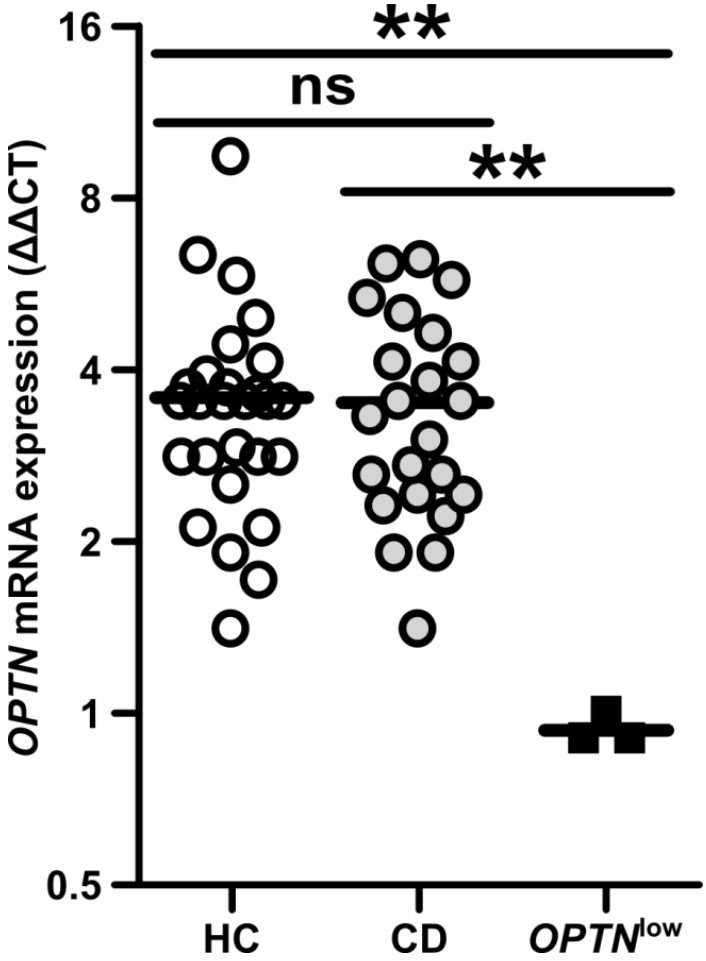

Figure 3.2 qPCR verification of OPTN expression in macrophages confirms reduced expression in three *OPTN*^{low} Crohn's disease patients. Results shown are mean ± SEM (ns, non-significant; **p<0.01; two-tailed, unpaired t test). qPCR of the three *OPTN*^{low} CD from the replication cohort was performed by myself whilst qPCR of the HC and CD patients were performed by others in our group.

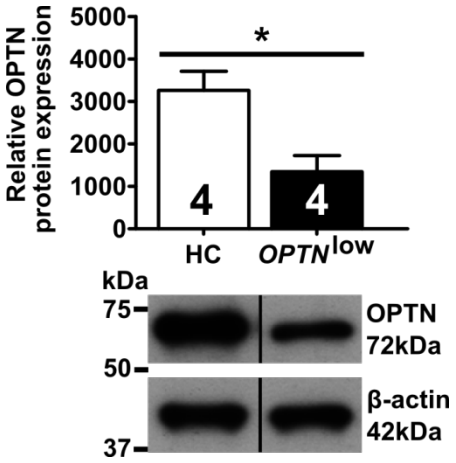

Figure 3.3 Immunoblot of OPTN confirmed low OPTN protein levels in macrophages from four *OPTN*^{low} CD patients. The OPTN protein levels were significantly lower than four HC tested. Results shown are mean ± SEM (*p<0.05; two-tailed, unpaired *t* test). All four *OPTN*^{low} CD patients and the four randomly selected HCs from our research group were all part of the primary cohort. Immunoblotting was performed by myself and others in our group.

Of the 105 CD patients in total from both cohorts, 11 (10.5%) were identified as expressing *OPTN* at a level significantly below the range found in the HC population (n=75). By contrast, patients with the other major inflammatory bowel disease (IBD) phenotype, UC (n=49), demonstrated normal *OPTN* expression (p=0.0029 and p=0.0172 for difference from HC and UC respectively) (Table 3-1).

Table 3-1 Outlier analysis of monocyte-derived macrophage gene expression identified a statistically significant cohort of *OPTN*^{low} CD patients. HC, healthy controls; CD, Crohn's disease; UC, ulcerative colitis.

Group	Batch 1		Batch 2		Combined	
	***OPTN*^{normal}**	***OPTN*^{low}**	***OPTN*^{normal}**	***OPTN*^{low}**	***OPTN*^{normal}**	***OPTN*^{low}**
HC	42	0	33	0	75	0
CD	51	7*/#	43	4	94	11**/#
UC	49	0	-	-	49	0

CD vs HC *p<0.05, **p<0.01; CD vs UC #p<0.05, Fisher's exact test

3.2.2 Low *OPTN* expression in CD shows a potential male sex bias

Having established a link with CD, demographic data, smoking status, medication and Montreal classification of Crohn's disease of all the CD patients were collected and analysed to look for any association with low *OPTN* expression. A weak association was found between low *OPTN* expression and male CD patients (p=0.011) but otherwise no association was found with age, medication or smoking status (Table 3-2 and Figure 3.4). The whole cohort of CD patients consisted of 47 males and 58 females of which 9 males and 2 females had low *OPTN* expression. These results suggest a potential sex bias in *OPTN* expression within the CD population. Separating *OPTN* expression by disease and sex revealed a lower expression in CD males compared to CD females (Figure 3.5), but the numbers were too small to come to definitive conclusions. This sex difference in the CD population was not replicated in either the HC or UC cohorts.

Phenotypically, all of the *OPTN*^{low} males had ileal involvement comprising four with ileal (L1) and five with ileocolonic (L3) disease (Table 3-3). To further investigate the role of *OPTN* in ileal disease in males, a recently published online dataset (GSE16879) was interrogated, which contains biopsy material from 6 (3M, 3F) controls and 18 (9M, 9F) CD patients both before and after infliximab anti-TNF treatment (Figure 3.6) [241]. Ileal *OPTN* expression was significantly lower in the male CD patients before treatment compared to male controls (p=0.006) and female CD patients (p=0.004). Interestingly, female CD patients demonstrated no reduction in *OPTN* in the terminal ileum compared to female controls and infliximab treatment had minimal effect on the expression of *OPTN* in both sexes (Figure 3.7). Further work is needed to confirm an association between reduced *OPTN* expression and male CD patients.

Table 3-2 Demographic data for healthy controls, Crohn's disease patients and 11 *OPTN*^{low} CD patients show a potential enrichment of males.

		Healthy controls	Crohn's disease	*OPTN*^{low}	p-value$^{\#}$
n=		75	94	11	
Gender, *n* (M:F)		40:35	38:56	9:2	**0.011**
Mean age ± standard deviation		39.7 ± 11.6	39.3 ± 13.8	45.3 ± 17.0	0.185
Age range		22 - 69	20 - 70	23 - 65	
Smokers, *n* (%)			11 (12.1)	2 (18.2)	0.629
Non smokers			80 (87.9)	9 (81.8)	
Medication, *n* (%)					
	Nil		23 (24.5)	2 (18.2)	1.000
	Budesonide/Prednisolone 5mg		1 (1.1)	1 (9.1)	0.200
	5-aminosalicylates		52 (55.3)	4 (36.4)	0.340
	Immunomodulators		26 (27.7)	4 (36.4)	0.506
	Anti-TNF		11 (11.7)	1 (9.1)	1.000
Montreal classification for Crohn's disease, *n* (%)					
Age onset	A1: ≤16		19 (20.2)	3 (27.3)	0.695
	A2: 17 - 40		62 (66.0)	5 (45.4)	0.200
	A3: >40		13 (13.8)	3 (27.3)	0.367
Location	L1: ileal		29 (30.9)	5 (45.5)	0.329
	L2: colonic		22 (23.4)	1 (9.0)	0.449
	L3: ileocolonic		41 (43.6)	5 (45.5)	1.000
	L4: upper GI		10 (10.6)*	1 (9.0)†	1.000
Behaviour	B1: non-stricturing, non-penetrating		52 (55.3)	4 (36.4)	0.340
	B2: stricturing		23 (24.5)	5 (45.5)	0.158
	B3: penetrating		27 (28.7)	6 (54.5)	0.096
	p: perianal		24 (25.5)	4 (36.4)	0.479

$^{\#}$p-values shown are comparisons between *OPTN*^{low} and Crohn's disease

*Two patients have purely upper GI disease; †patient also has lower GI disease

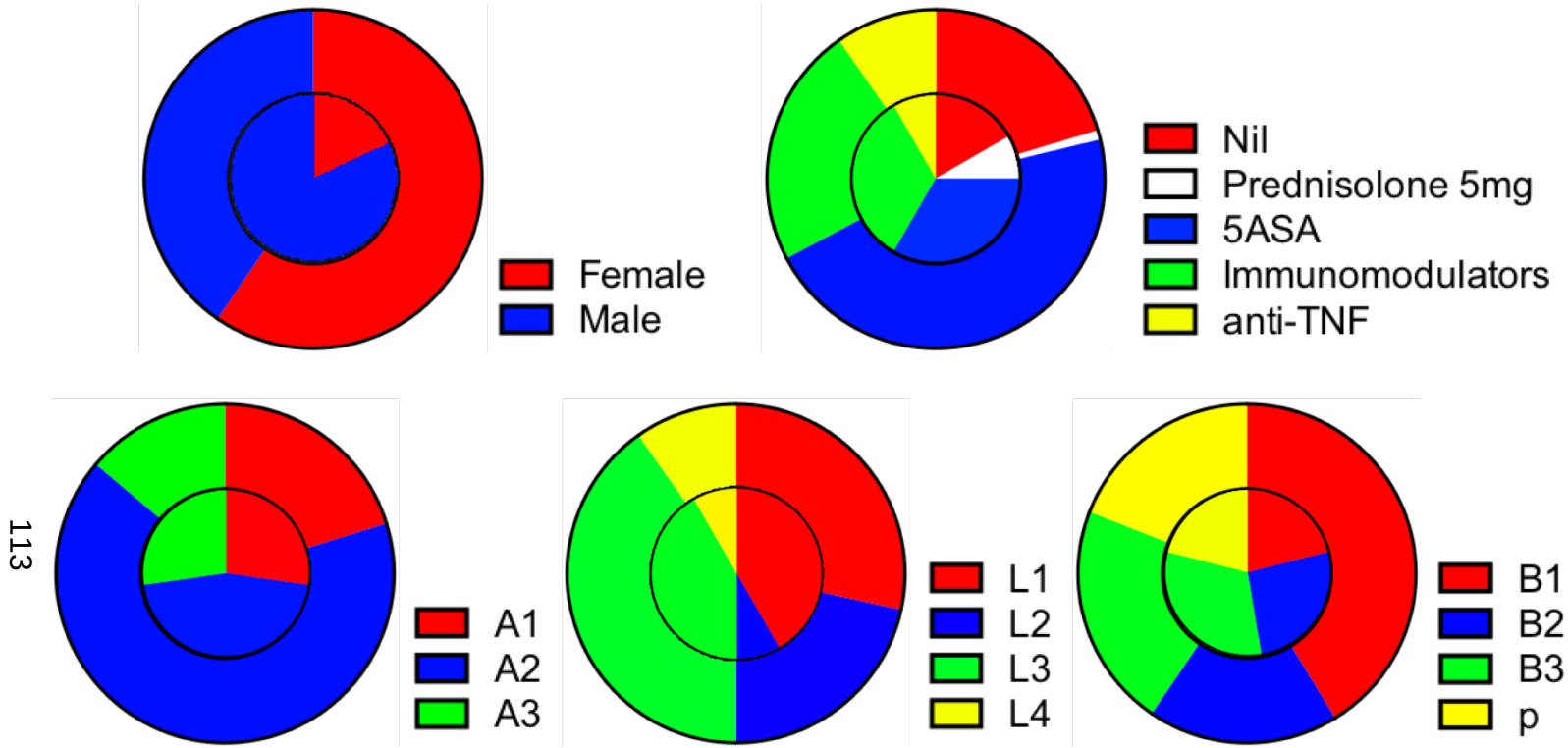

Figure 3.4 Crohn's disease and *OPTN*^{low} patients by sex, medication and Montreal classification. ***Outer*** donut charts represents the 94 CD patients whilst the ***inner*** pie chart represents the 11 *OPTN*^{low} CD patients. Charts depict proportion by sex (top left), active medication (top right), Montreal classification for CD parameter for age of disease onset (bottom left), location (bottom middle) and behaviour of disease (bottom right).

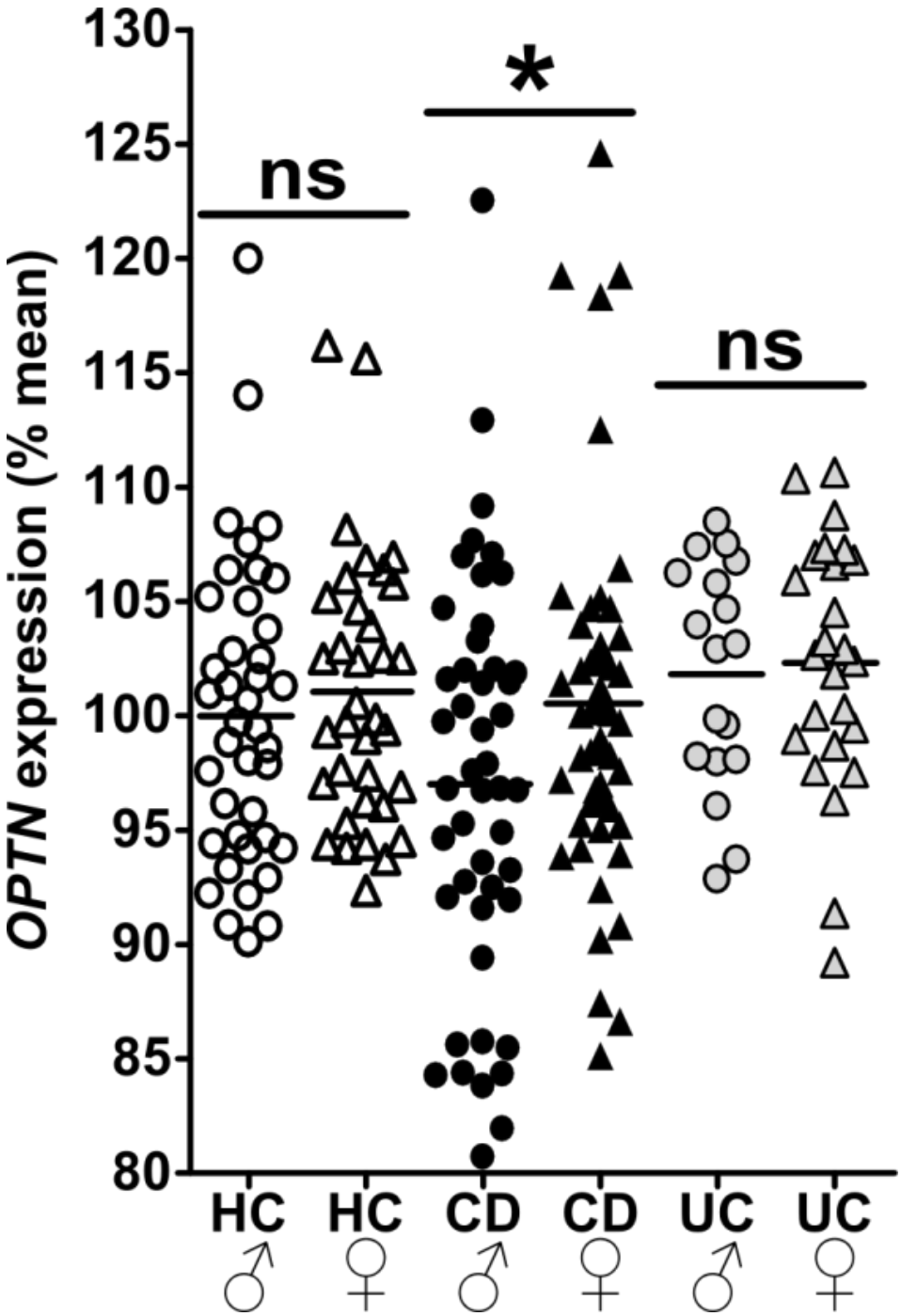

Figure 3.5 *OPTN* expression in macrophages was significantly lower in male CD patients compared to female CD patients. Results shown are mean ± SEM (ns, non-significant; *p<0.05; two-tailed, unpaired *t* test). *OPTN* expression was calculated as a % mean of all HC for each cohort.

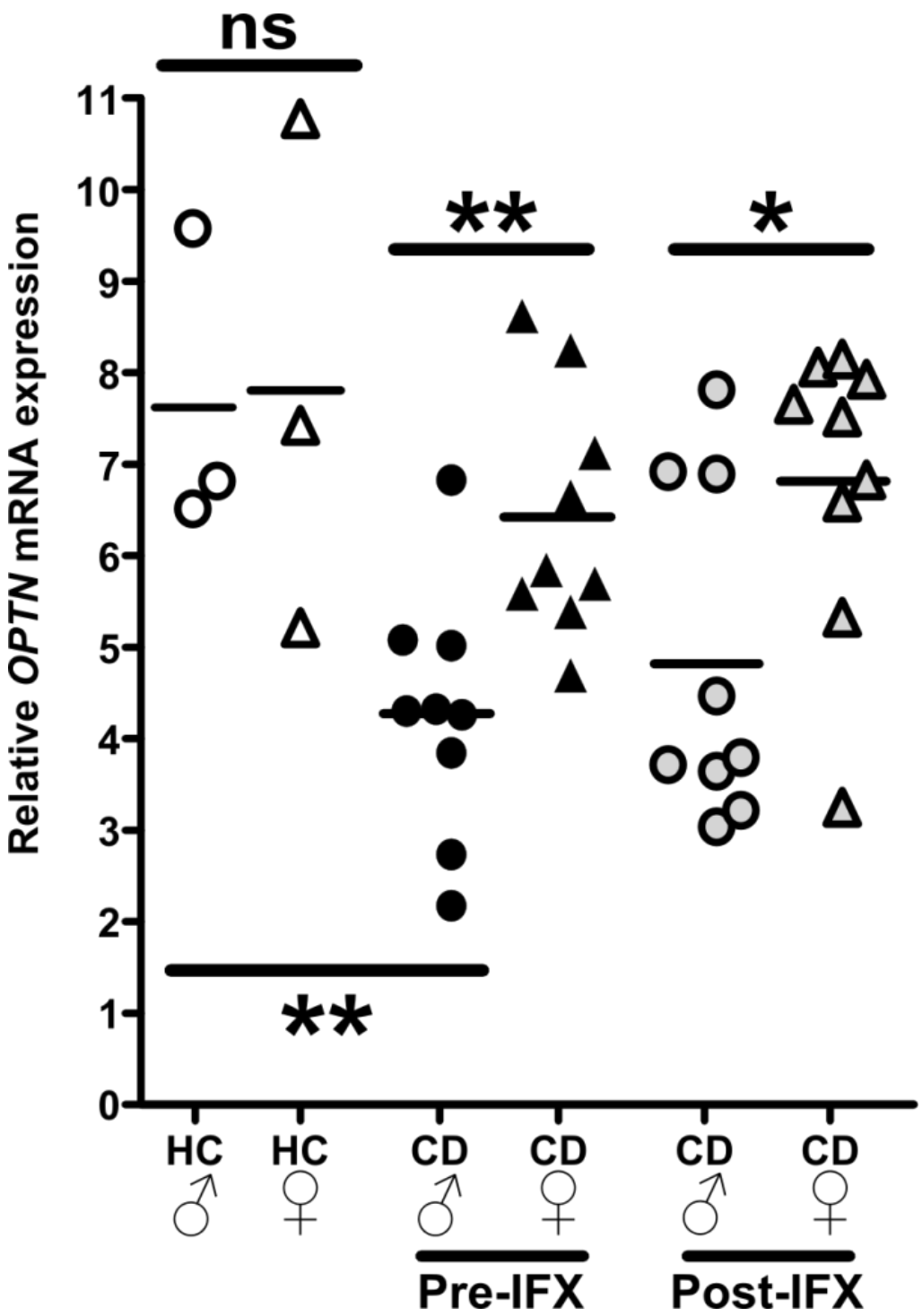

Figure 3.6 *OPTN* expression in the ileum was significantly lower in male CD patients compared to controls and female CD patients. The lower *OPTN* levels were minimally altered with infliximab anti-TNF treatment. Data from GSE 16879, de Bruyn *et al*. 2014. Results shown are mean ± SEM (*p<0.05 and **p<0.01; two-tailed, unpaired and paired *t* test).

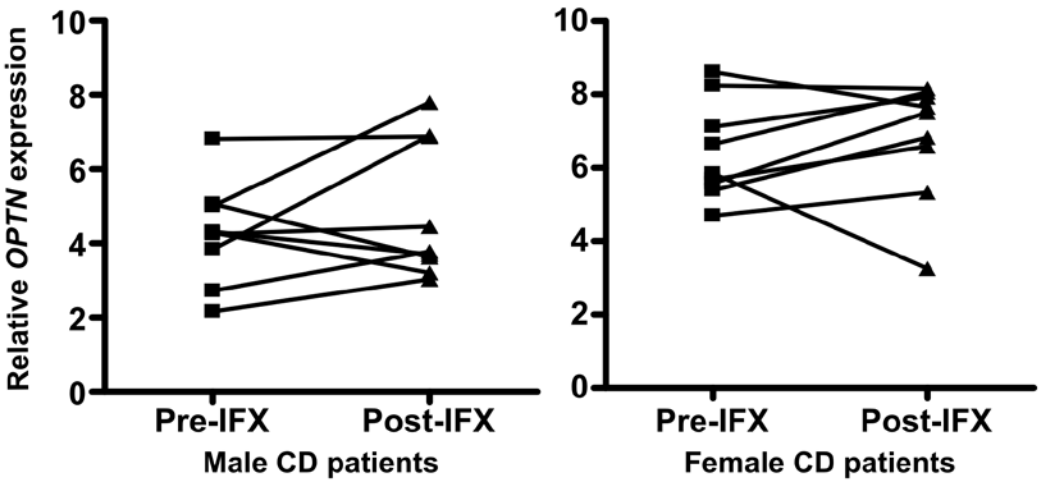

Figure 3.7 *OPTN* expression in the ileum is variably affected by IFX treatment. Data from GSE 16879, de Bruyn *et al.* 2014.

Table 3-3 Demographic data, Montreal classification of Crohn's disease, drug treatment and smoking status in the 11 *OPTN*^{low} CD patients show an enrichment of ileal involved disease.

	Age	Sex	Montreal classification			Treatment	Smoking status
			Age onset	Location	Behaviour	(when MDM grown)	
1	23	M	A1 (10)	L3	B2 + B3p	Azathioprine, Adalimumab	Non smoker
2	23	M	A1 (11)	L1	B2 + B3p	Methotrexate	Non smoker
3	26	M	A1 (13)	L1 + L4	B1	5-aminosalicylate	Non smoker
4	34	M	A2 (29)	L3	B1	5-aminosalicylate	Non smoker
5	36	M	A2 (21)	L3	B2 + B3p	Nil	Non smoker
6	50	M	A2 (20)	L1	B2	Azathioprine	Non smoker
7	58	M	A3 (42)	L3	B3p	Methotrexate	Non smoker
8	60	M	A2 (23)	L1	B3	Prednisolone 5mg	Non smoker
9	61	F	A2 (40)	L1	B2 + B3	Nil	Smoker
10	62	F	A3 (60)	L2	B1	5-aminosalicylate	Non smoker
11	65	M	A3 (52)	L3	B1	5-aminosalicylate	Smoker

3.2.3 OPTN expression is associated with inheritance of a minor SNP

To investigate the deficient *OPTN* expression identified in this subset of CD patients, all exons, exon-flanking regions and 2 kilobase regions up and downstream of the *OPTN* gene was sequenced in seven *OPTN*^{low} CD patients [191]. None of the commonly published glaucoma and amyotrophic lateral sclerosis variants were identified in these seven *OPTN*^{low} CD patients. However, five of the *OPTN*^{low} CD patients were homozygous and two were heterozygous for the rs12415716 minor allele that is located in the intronic region downstream of the last exon. To determine if the haplotype was associated with macrophage *OPTN* expression, 66 HCs and 76 CD patients including the newly identified *OPTN*^{low} CD patients from our microarray cohort were genotyped for the rs12415716 single nucleotide polymorphism (SNP). Low *OPTN* expression in macrophages, was found to be associated with inheritance of the minor allele at rs12415716 (Figure 3.8), which was exaggerated by CD.

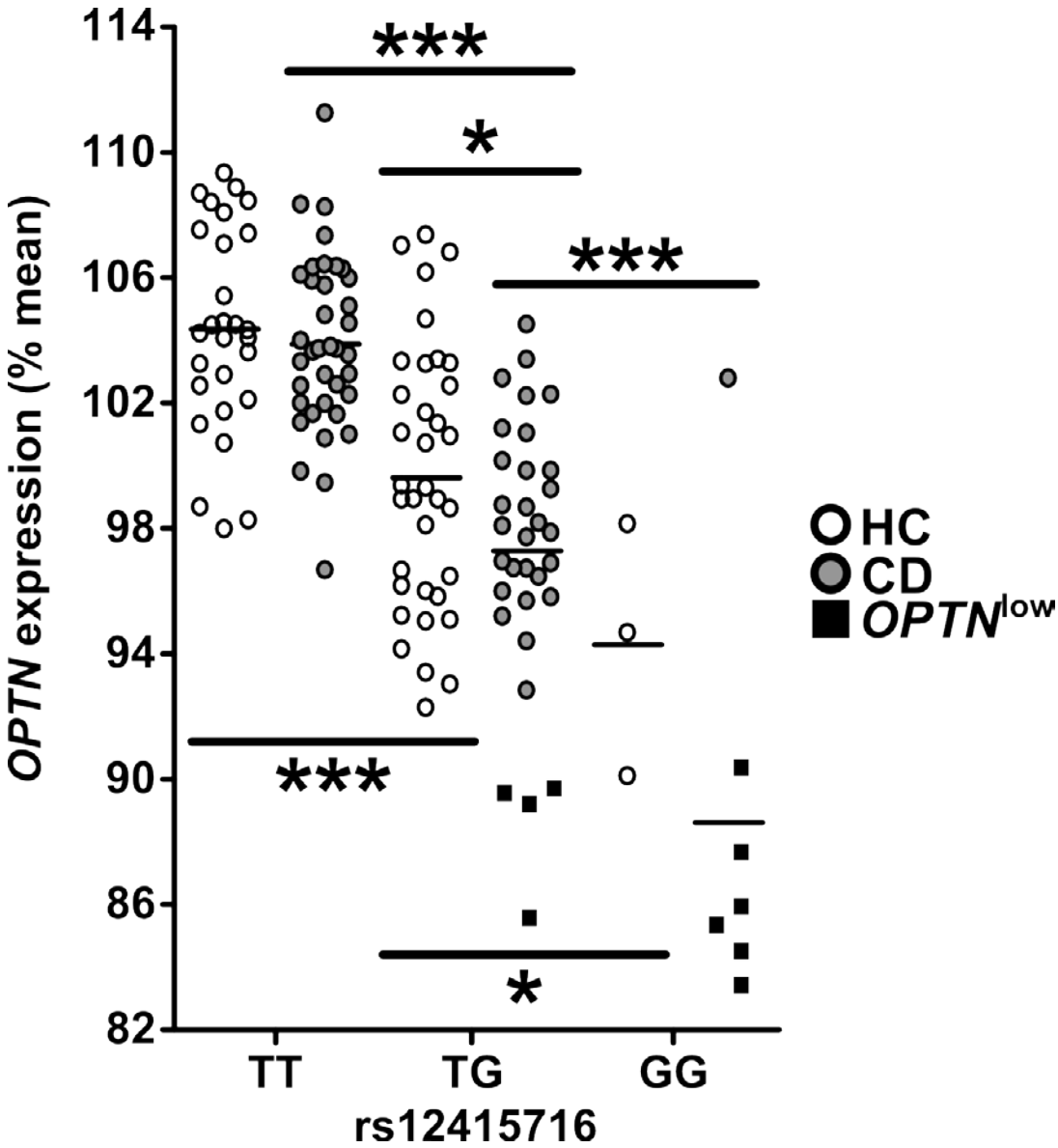

Figure 3.8 Low *OPTN* expression is driven by inheritance of the minor SNP at rs12415716, which is exaggerated by CD. Results shown are mean ± SEM (*p<0.05, **p<0.01 and ***p<0.001; two-tailed, unpaired *t* test).

3.2.4 OPTN is expressed in monocytes, lymphocytes and macrophages but not neutrophils

In order to ascertain which cells types express OPTN, we isolated peripheral blood monocytes, lymphocytes, neutrophils and monocyte-derived macrophages (MDM) (Figure 3.9). Immunoblotting demonstrated that OPTN is expressed in monocytes, lymphocytes and MDM but not neutrophils in both a HC and *OPTN*^{low} individual.

Ileal biopsies from four *OPTN*^{low} CD patients were stained for OPTN protein expression and compared against control small bowel (Figure 3.10). All *OPTN*^{low} patients tested demonstrated lower levels of OPTN expression in the lamina propria tissue-resident cells.

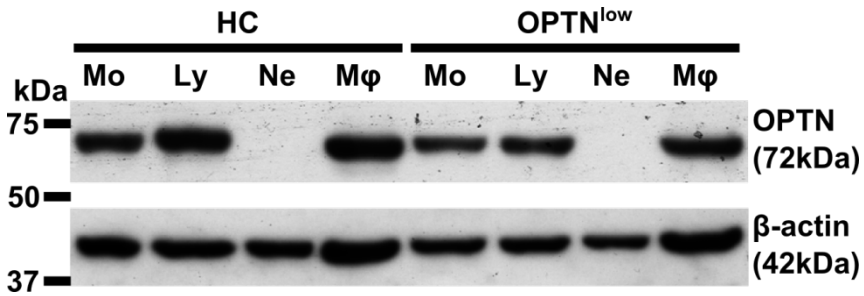

Figure 3.9 Immunoblot of OPTN showing that OPTN is expressed in human monocytes, lymphocytes and macrophages but not in neutrophils. The immunoblot also shows reduced OPTN expression in the monocytes, lymphocytes and macrophages of an *OPTN*^{low} individual compared to the healthy control. Mo, monocytes; Ly, lymphocytes; Mφ, macrophages; Ne, neutrophils.

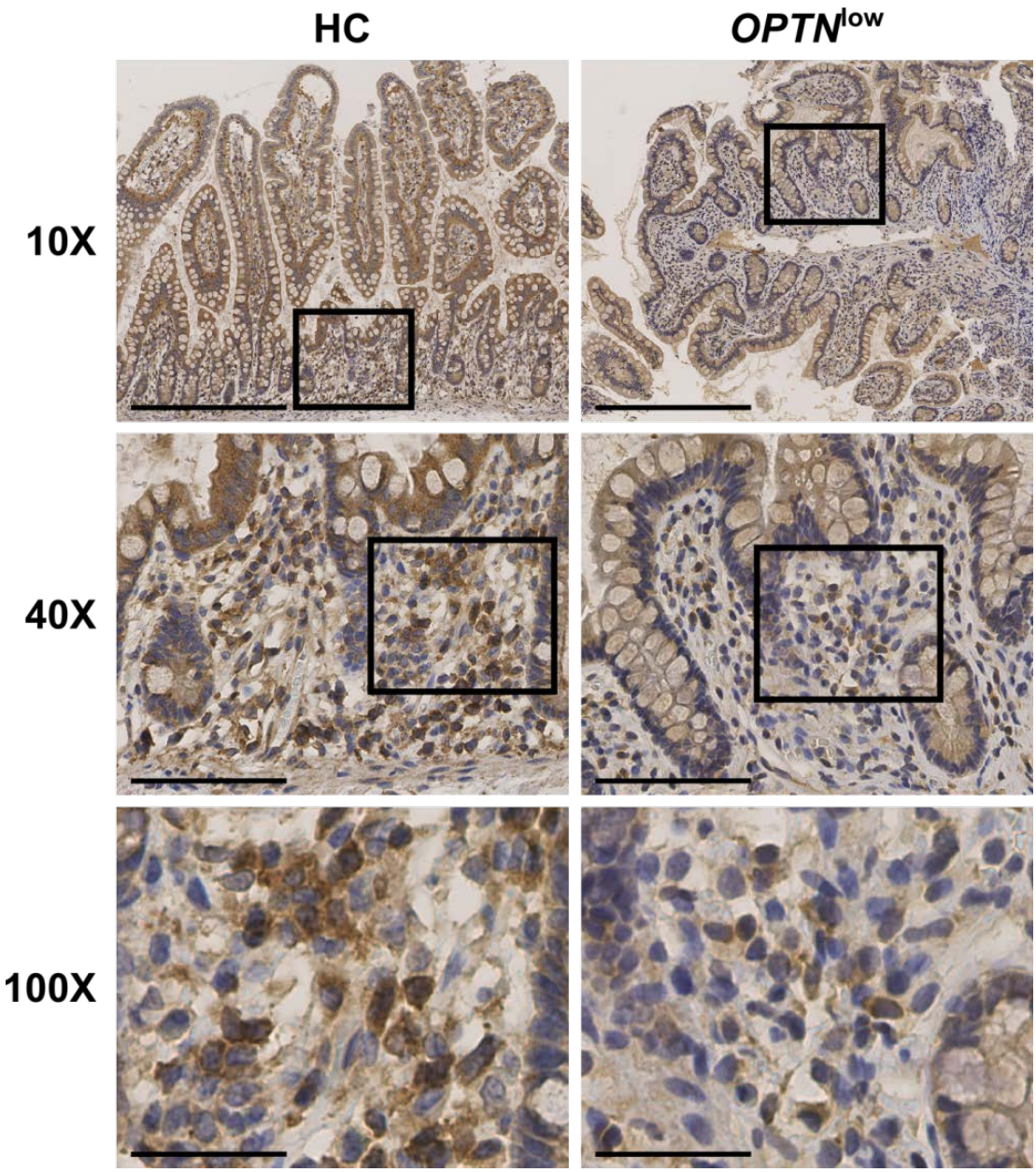

Figure 3.10 OPTN immunohistochemistry in the small bowel shows weaker staining in the lamina propria cells of an *OPTN*^{low} CD patient compared to a healthy control. (Upper panels 10× magnification, scale bar 400 µm; middle 40×, 100 µm; lower 100×, 40 µm). Staining was performed by UCL-Advanced Diagnostics.

3.3 Discussion

In this chapter, microarray transcriptomic profiling of human MDM from patients with CD, HC and UC patients as an inflammatory disease control was performed to investigate the phenotype of impaired proinflammatory cytokine secretion and defective neutrophil recruitment in CD. The first cohort investigated identified significantly reduced *OPTN* expression in around 10% of CD patients but none amongst HC or patients with UC [191]. This second replication cohort reproduced our earlier findings and out of 105 CD patients in total, 11 (10.5%) had low MDM *OPTN* expression but none in the 75 HC or 49 UC patients recruited.

The same microarray outlier analysis in MDM also identified reduced expression of ADAM-like, decysin 1 (*ADAMDEC1*), an ADAMs related metalloprotease in around 10% CD patients. Absence of ADAMDEC1 results in exaggerated DSS and *Citrobacter* colitis in experimental mice, further verifying the outlier analysis employed to identify genes of significance in CD macrophages that render increased susceptibility to colitis [242]. This work is the subject of another PhD.

OPTN was not identified in GWAS of CD. This is because GWAS works on a common disease, common variant hypothesis that may fail to identify rarer variants of stronger effect [134]. This is sited as a potential reason why only 23% of the heritability of CD has been identified through GWAS [99]. For example, there were no GWAS loci identified in X-linked inhibitor of apoptosis protein (*XIAP*), which has been shown to be a risk factor for CD and supports an immunodeficient pathogenesis in CD [243]. Alternatively, the association of OPTN with CD may be limited to macrophages requiring a transcriptomic approach to identifying the association.

Nine out of eleven of the *OPTN*^{low} CD patients were males. Separation of *OPTN* expression in MDM according to sex in HC, CD and UC patients revealed significantly lower *OPTN* expression in males compared to females in CD (Figure 3.5). The sex bias is not seen in HC and UC patients. The male bias in low *OPTN* expression is statistically significant but limited by small numbers, hence definitive conclusions cannot be made without further replication, larger numbers or functional corroboration. At this point, it is not clear what is causing this male bias and sex-influence on *OPTN* expression but may be due to linkage of the associated SNP with sex-linked or sex-limited genes.

There was also an association between low *OPTN* expression and ileal involvement in CD (Table 3-2). Ten out of eleven (~91%) of the *OPTN*^{low} CD patients has ileal involved CD with only one female patient having pure colonic CD. This is in contrast to widely published data on the distribution of CD with upto a third having pure colonic disease and only two-thirds with ileal involvement [5]. The terminal ileum is the commonest site for CD and represents the area of greatest transition between the relatively sterile jejunum and the bacteria dense caecum, which may be exposed to refluxed bacteria from the caecum through the ileocaecal valve. The association of *OPTN* expression and ileal involved CD mirrors the association of NOD2 inheritance with ileal CD and highlights the important association of bacterial response genes and by extrapolation intraluminal bacteria with ileal inflammation [244]. It is therefore plausible that low *OPTN* expression causing an abnormal bacterial response may predispose an individual to bacteria driven colitis.

Interrogation of a recently published online dataset (GSE16879) [241] found that *OPTN* expression from ileal biopsies was significantly lower in male CD patients compared to male HC and females with CD (Figure 3.6). This verifies our finding of reduced *OPTN* expression in CD patients and the potential male bias. It also implicates the ileum as a site of potential

importance in the association of low *OPTN* expression and CD. The use of the anti-TNF IFX only marginally altered *OPTN* expression, which suggests that IFX is unlikely to be affecting the expression of *OPTN* in our cohort. What remains unclear from this data is whether CD disease activity may be driving down the expression of *OPTN* in the ileum since there was little difference in ileal inflammation and *OPTN* remained unchanged before and after IFX treatment in this cohort of patients with active CD. By contrast, patients that were recruited to our study had quiescent CD.

There was no significant difference in age, smoking status, drug treatment, age of onset or behaviour of CD in the *OPTN*^{low} cohort. There may be a trend towards more aggressive disease with a greater proportion of *OPTN*^{low} CD patients with stricturing and fistulating disease. However, the small numbers of *OPTN*^{low} CD patients is again a limiting factor in identifying any association between disease behaviour and *OPTN* expression.

Although none of the widely published variants associated with glaucoma and ALS were identified (Figure 1.7), an expression quantitative trait locus (eQTL) was found at SNP position rs12415716, which lies in an intronic region downstream of the last *OPTN* exon. Inheritance of the minor allele, with an allele frequency of 0.18 was associated with reduced *OPTN* expression. Gene expression and hence eQTL analysis is highly tissue specific. eQTL analysis using Genevar (GENe Expression VARiation) software [245] also identified rs17512962 as a proxy SNP in linkage disequilibrium with rs12415716, which is in eQTL with *OPTN* expression in fibroblasts [246]. The rs17512962 interaction with *OPTN* expression was more recently replicated in peripheral blood [247].

Up to 88% of disease associated SNPs are intergenic (43%) or intronic (45%) [248]. This SNP is unlikely to be the sole cause of impaired *OPTN* expression as the minor allele is necessary but not sufficient to fully account for the altered expression, since the expression of *OPTN* influenced

by inheritance of this minor allele was exaggerated in CD patients. It is likely that this SNP is in linkage disequilibrium with other yet unidentified variant or variants that either individually or collectively reduce *OPTN* expression in CD. The penetrance of this minor allele in *OPTN* expression is incomplete, which is unsurprising since the penetrance of the most strongly associated gene with CD, NOD2 is only 4.9% in homozygotes/compound heterozygotes [249].

MDM, monocytes, neutrophils and lymphocytes were isolated to investigate the expression of OPTN in these various leukocytes cells types. Interestingly, while OPTN was expressed in monocytes, lymphocytes and macrophages, OPTN was undetectable in neutrophils by immunoblotting. It is unclear why OPTN is not expressed in neutrophils since autophagic processes and cytokine secretion have been reported in neutrophils [250, 251]. It is possible that neutrophils have evolved such efficient killing mechanisms that autophagy of ubiquitinated cytosolic bacteria via autophagosomes are redundant and autophagy merely serves the purpose of recycling organelles in neutrophils. Additionally, TNF is not secreted by neutrophils [251] and cytokines that are secreted by neutrophils occurs independent of OPTN.

Immunohistochemistry for OPTN in small bowel specimens from HC and *OPTN*^{low} CD patients revealed reduced staining for OPTN In lamina propria cells in the *OPTN*^{low} CD patients. Costaining with macrophage or B cell markers was not performed due to limited biopsy specimens but the OPTN staining lamina propria cells were morphological identical to macrophages and B cells according to our GI Histopathologist. Whilst this is by no means conclusive in proving that the lamina propria macrophages have reduced OPTN levels in the *OPTN*^{low} CD patient small bowel specimens, the sections were all treated simultaneously under the same conditions and concentration of antibodies that verifies the reduced *OPTN* expression reported in ileal biopsies [241]. What remains unclear despite these two pieces of evidence is

the contribution of CD itself to the expression of *OPTN* in the ileum as discussed above.

Whilst these findings are noteworthy, the association between altered *OPTN* expression and CD is incomplete without the further functional studies in the next few chapters that link the role of OPTN with the CD phenotype of impaired neutrophil recruitment and severe colitis.

Chapter 4 Intracellular location and function of optineurin in macrophages

4.1 Introduction

Low *OPTN* expression in MDM was identified in 10% of CD patients, as demonstrated in Chapter 3. OPTN was a good candidate for further investigation in CD due to its role in post-Golgi protein trafficking and autophagy. However, most published work on OPTN was in non-immune cells including work on autophagy, in HeLa cells [125].

OPTN's role in protein trafficking is via its role as an intracytoplasmic adaptor protein that forms complexes with Rab8, myosin VI and HTT. OPTN and myosin VI together were localised to the Golgi complex and were shown to have a role in maintaining the structure of the Golgi in HeLa cells [201]. Additionally, OPTN in complex with myosin VI and Rab8 has a role in post-Golgi membrane trafficking since OPTN RNAi resulted in reduced transport from the Golgi to the plasma membrane in nonpolarised HeLa cells and to the basolateral domain in polarised MDCK kidney epithelial cells [203]. OPTN and myosin VI depletion was also found to reduce secretory vesicle fusion events at the plasma membrane in HeLa cells [205]. OPTN was also colocalised with huntingtin (HTT) to the Golgi complex in rat striatal cells [206]. RNAi of wildtype *Htt* resulted in impaired post-Golgi trafficking to lysosomes, which was dependent on the expression of wildtype Rab8 and OPTN and resulted in the accumulation of the lysosome bound mannose-6-phosphate receptor at the TGN and reduced lysosomal function in proteolysis.

The LC3-interacting region (LIR) in OPTN (Figure 1.7) was mapped to amino acids 169 to 209 [125]. Phosphorylation of OPTN within the LIR at serine-177 by TANK binding kinase 1 (TBK1) enhanced binding of OPTN to

LC3 and autophagic clearance of ubiquitin-coated cytosolic *Salmonella enterica*. Conversely, OPTN with ubiquitin and LC3 binding domain mutations as well as silencing of OPTN or TBK1 resulted in impaired *Salmonella* autophagy and intracellular bacterial proliferation.

Here I investigate the intracellular location and role of OPTN in macrophages in the context of inflammation and bacterial infection.

4.2 Results

4.2.1 Intracellular location of OPTN in human monocytes and macrophages

Previous studies have localised OPTN to multiple intracellular locations [201, 205]. Subcellular fractionation was performed on HkEc stimulated THP-1 cells to determine the intracellular location of OPTN (Figure 4.1). The majority of OPTN was localised to the cytoplasmic fractions, 1 to 3 and also to a lesser extent, the Golgi enriched fraction 5. There was minimal overlap between OPTN and LAMP1 positive fractions, which suggest that OPTN is not localised to lysosomal vesicles.

Immunoprecipitation (IP) of OPTN was performed on THP-1 cells, verified by immunoblotting (Figure 4.2) and co-precipitated proteins were identified using shotgun proteomics (Table 4-1). The strongest signal in the OPTN IP associated with the myosin complex was the unconventional myosin 18A (MYO18A), which has been shown to apply a tensile force to the trans-Golgi membrane, participating in the process of vesicle budding in anterograde trafficking [252]. Additionally, OPTN's binding partner myosin VI was also pulled down in the IP.

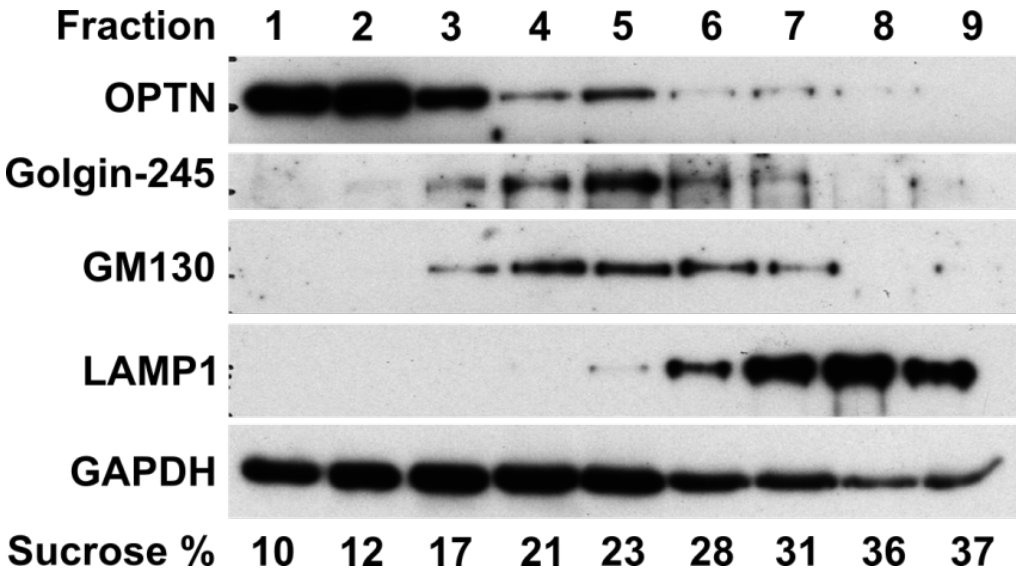

Figure 4.1 Subcellular fractionation of HkEc stimulated THP-1 cells show OPTN localised to the cytoplasm and fractions containing Golgi membranes but not lysosomes. Immunoblots for the Golgi markers golgin-245 and GM130, LAMP1, OPTN and GAPDH on sucrose density gradient separated subcellular fractions show that OPTN is in the cytoplasmic (fractions 1 to 3) and Golgi fractions (fraction 5) but not in LAMP1 vesicle fractions (fractions 6 to 9) in THP-1 cells.

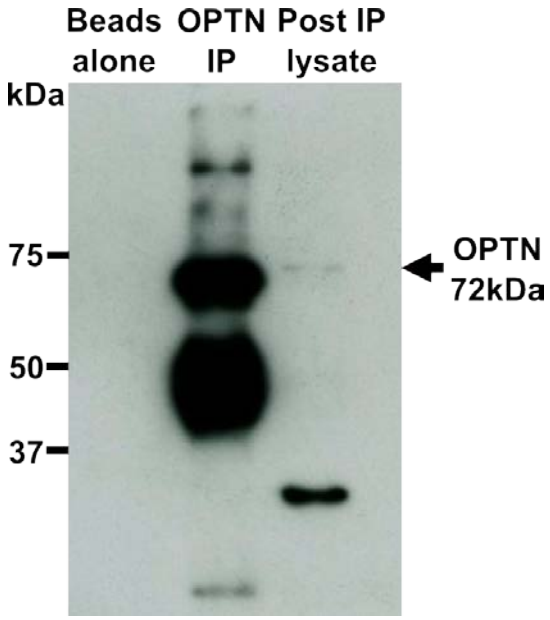

Figure 4.2 Immunoblot of OPTN after immunoprecipitation confirms successful pull down of OPTN. Immunoblot of OPTN on OPTN IP sample confirms the pull down of OPTN with minimal OPTN staining in the post IP lysate and the absence of OPTN in the beads alone control.

Table 4-1 Proteins identified in the OPTN IP on mass spectrometry localise OPTN to the Golgi*.

Protein	Symbol	Mascot Protein	Mascot Expect Value	Peptides Identified	Protein Coverage %
Complement C4-B	C4B	1240	3.70E-120	22	18.4
Isoform 2 of Unconventional myosin-XVIIIa	MYO18A	1182	2.50E-114	20	18.6
Isoform 2 of Unconventional myosin-Ic	MYO1C	924	1.50E-88	17	27
Isoform 2 of Fibrinogen alpha chain	FGA	854	1.70E-81	15	32.1
Isoform 2 of Optineurin	OPTN	822	2.60E-78	14	32.7
High affinity immunoglobulin gamma Fc receptor I	FCGR1A	625	1.30E-58	11	28.9
Actin, cytoplasmic 2	ACTG1	633	1.80E-59	10	41.9
Isoform 2 of Myosin-10	MYH10	601	3.10E-56	10	5.7
Structural maintenance of chromosomes protein 4	SMC4	597	8.00E-56	10	11.3
Apolipoprotein B-100	APOB	428	5.70E-39	10	2.9
Isoform 6 of Unconventional myosin-VI	MYO6	546	9.70E-51	9	10.1
Isoform 2 of Myosin-14	MYH14	538	6.30E-50	9	4.5
Isoform Beta-1 of DNA topoisomerase 2-beta	TOP2B	401	3.50E-36	8	6.3
Complement factor H	CFH	389	4.80E-35	8	8.9
Valine--tRNA ligase	VARS	453	2.00E-41	6	8.5
Protein S100-A8	S100A8	311	2.90E-27	6	49.5
Isoform 2 of Programmed cell death 6-interacting protein	PDCD6IP	302	2.30E-26	6	8.4
Isoform 2 of Clusterin	CLU	300	4.20E-26	6	15.8
Protein-glutamine gamma-glutamyltransferase K	TGM1	277	8.50E-24	6	10.2
Isoform 1 of Protein POF1B	POF1B	260	4.50E-22	6	11.4
Unconventional myosin-If	MYO1F	333	2.10E-29	5	6.3
Protein S100-A9	S100A9	317	8.30E-28	5	51.8
Isoform 2 of Caprin-1	CAPRIN1	298	6.20E-26	5	8.4
Pentatricopeptide repeat domain-containing protein 3, mitochondrial	PTCD3	297	8.80E-26	5	9.1
Engulfment and cell motility protein 1	ELMO1	294	1.60E-25	5	11.1
Caspase-14	CASP14	285	1.40E-24	5	21.9
Coatomer subunit delta	ARCN1	257	8.50E-22	5	14.1
Isoform 2 of Protein flightless-1 homolog	FLII	255	1.20E-21	5	7.4
Structural maintenance of chromosomes protein 3	SMC3	249	5.40E-21	5	7.1
DNA replication licensing factor MCM4	MCM4	245	1.10E-20	5	8

*Only proteins that have been identified with five or more peptides, which are not found in the control sample are included.

Table 4-2 Gene Ontology analysis of proteins identified in the OPTN IP shows association with intracellular vesicles and the cytoskeleton.

GO Term	Go Term Name	Count	%	p value	Benjamini	Genes
GO:0016459	myosin complex	6	20.0	0.00000018	0.00003065	MYO6, MYO1C, MYO1F, MYH14, MYO18A, MYH10
GO:0015629	actin cytoskeleton	7	23.3	0.00001328	0.00115430	ACTG1, MYO6, MYO1C, MYO1F, MYH14, MYO18A, MYH10
GO:0043232	intracellular non-membrane-bounded organelle	16	53.3	0.00003096	0.00179392	MYO6, MYO1C, S100A9, MYO1F, MCM4, SMC3, SMC4, ELMO1 ACTG1, TGM1, FLII, MYH14, PDCD6IP, TOP2B, MYO18A, MYH10
GO:0043228	non-membrane-bounded organelle	16	53.3	0.00003096	0.00179392	MYO6, MYO1C, S100A9, MYO1F, MCM4, SMC3, SMC4, ELMO1, ACTG1, TGM1, FLII, MYH14, PDCD6IP, TOP2B, MYO18A, MYH10
GO:0005856	cytoskeleton	12	40.0	0.00003727	0.00162012	ACTG1, MYO6, MYO1C, TGM1, FLII, MYO1F, MYH14, PDCD6IP, MYO18A, SMC3, MYH10, ELMO1
GO:0016461	unconventional myosin complex	3	10.0	0.00008303	0.00288549	MYO6, MYO1C, MYO1F
GO:0031941	filamentous actin	3	10.0	0.00041103	0.01185145	MYO6, MYO1C, MYO1F
GO:0044430	cytoskeletal part	9	30.0	0.00042766	0.01057625	MYO6, MYO1C, FLII, MYO1F, MYH14, PDCD6IP, MYO18A, SMC3, MYH10
GO:0044433	cytoplasmic vesicle part	5	16.7	0.00051546	0.01115140	APOB, MYO6, FGA, ARCN1, CLU
GO:0016023	cytoplasmic membrane-bounded vesicle	7	23.3	0.00068045	0.01307366	APOB, MYO6, FGA, ARCN1, CLU, PDCD6IP, OPTN
GO:0031988	membrane-bounded vesicle	7	23.3	0.00080607	0.01393329	APOB, MYO6, FGA, ARCN1, CLU, PDCD6IP, OPTN
GO:0031410	cytoplasmic vesicle	7	23.3	0.00152299	0.02382103	APOB, MYO6, FGA, ARCN1, CLU, PDCD6IP, OPTN
GO:0031982	vesicle	7	23.3	0.00189513	0.02713060	APOB, MYO6, FGA, ARCN1, CLU, PDCD6IP, OPTN
GO:0043233	organelle lumen	11	36.7	0.00200579	0.02651576	APOB, MYO6, MYO1C, FGA, CLU, S100A9, FLII, TOP2B, MYO18A, MCM4, SMC3
GO:0031974	membrane-enclosed lumen	11	36.7	0.00233124	0.02859114	APOB, MYO6, MYO1C, FGA, CLU, S100A9, FLII, TOP2B, MYO18A, MCM4, SMC3
GO:0005884	actin filament	3	10.0	0.00310731	0.03545710	MYO6, MYO1C, MYO1F
GO:0005938	cell cortex	4	13.3	0.00313077	0.03352562	ACTG1, MYO6, MYO1F, MYH10
GO:0031983	vesicle lumen	3	10.0	0.00389765	0.03918319	APOB, FGA, CLU

Proteins that were co-precipitated with OPTN were subjected to Gene Ontology (GO) analysis (Table 4-2). GO analysis resulted in the identification of GO-terms primarily associated with intracellular vesicles, organelles and the cytoskeleton, in keeping with known functions of OPTN.

In order to confirm the subcellular localisation of OPTN, confocal microscopy was performed on HkEc stimulated MDM. HkEc stimulated MDM were fixed and co-stained for OPTN and the Golgi marker, GM130 (Figure 4.3). There was evidence of a strong overlap between OPTN and GM130 confirming the Golgi localisation of OPTN in stimulated MDM. OPTN positive staining was also present within the cytoplasm of MDM.

4.2.2 OPTN and TNF in human monocytes and macrophages

RNAi of OPTN in THP-1 cells was shown to result in reduced TNF and IL6 secretion [191]. Therefore, it was important to investigate whether TNF and OPTN are co-localised in the cell. Confocal images of HkEc stimulated MDM clearly demonstrate a high degree of overlap between OPTN and TNF within the Golgi complex (Figure 4.4 and Figure 4.5). A number of vesicles stained positively for TNF or OPTN in MDM after stimulation, but only 12% of TNF positive vesicles also stained positively for OPTN (Figure 4.7).

Previous studies have shown that TNF is trafficked from the Golgi complex to the plasma membrane through an endosomal pathway in murine RAW293 macrophages [171]. Human MDM were also found to traffic TNF predominantly through the endosomal pathway (Figure 4.6 and Figure 4.7). We calculated that 70% of TNF positive vesicles also expressed the endosomal marker, early endosome antigen 1 (EEA1) demonstrating that human and mouse macrophages secrete TNF along a similar pathway.

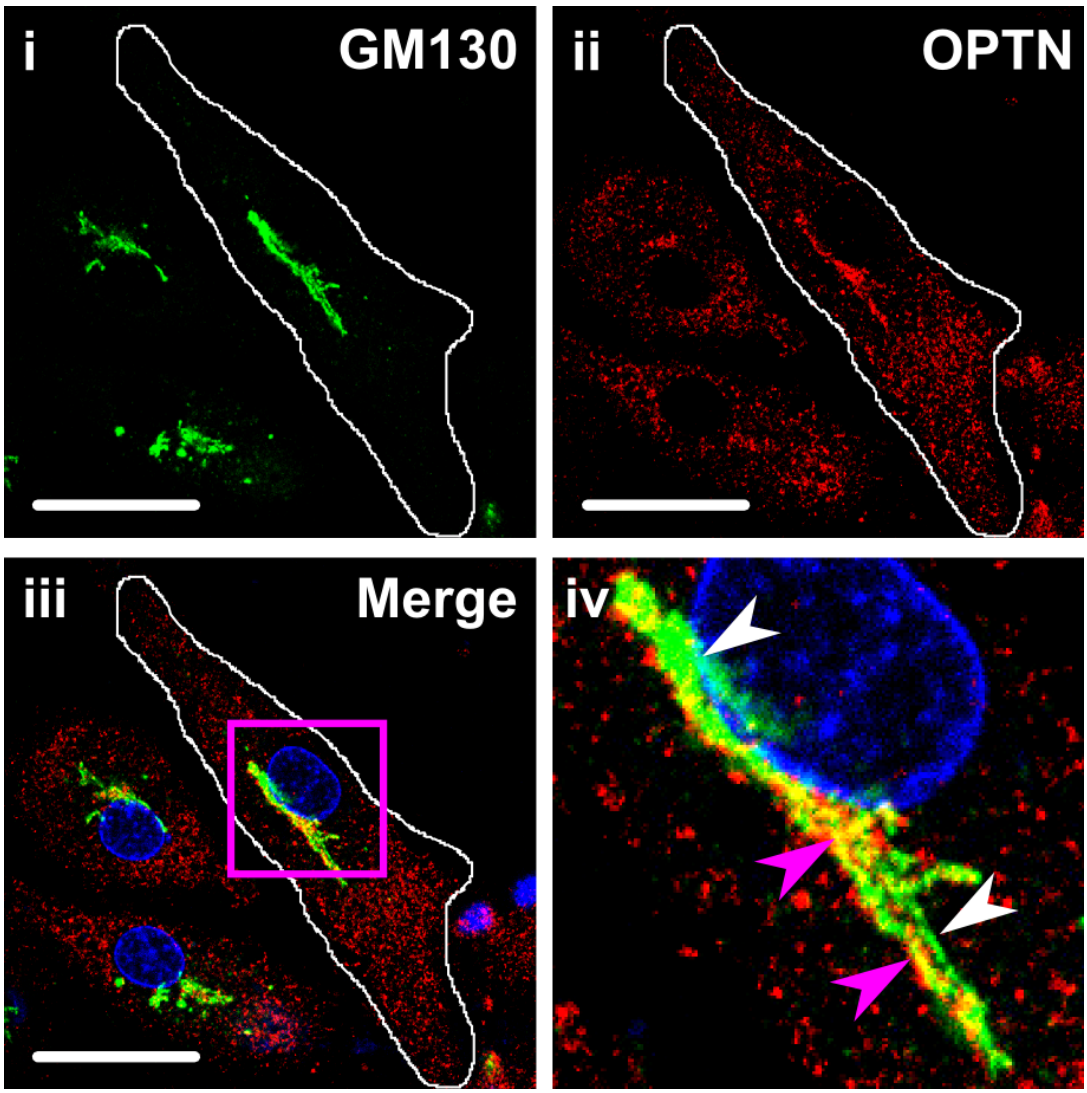

Figure 4.3 Confocal microscopy in monocyte-derived macrophages show colocalisation of OPTN with GM130 in the Golgi complex. MDM (white outline) show colocalisation of OPTN (ii) with GM130 (i) in the Golgi complex, next to the DAPI stained nucleus in blue (iii). Single stained GM130 Golgi complex (white arrows) and double stained OPTN and GM130 (pink arrows) are visible in the enlarged area of the pink box (iv) (image i, ii, iii at 63×, scale bar 20 µm).

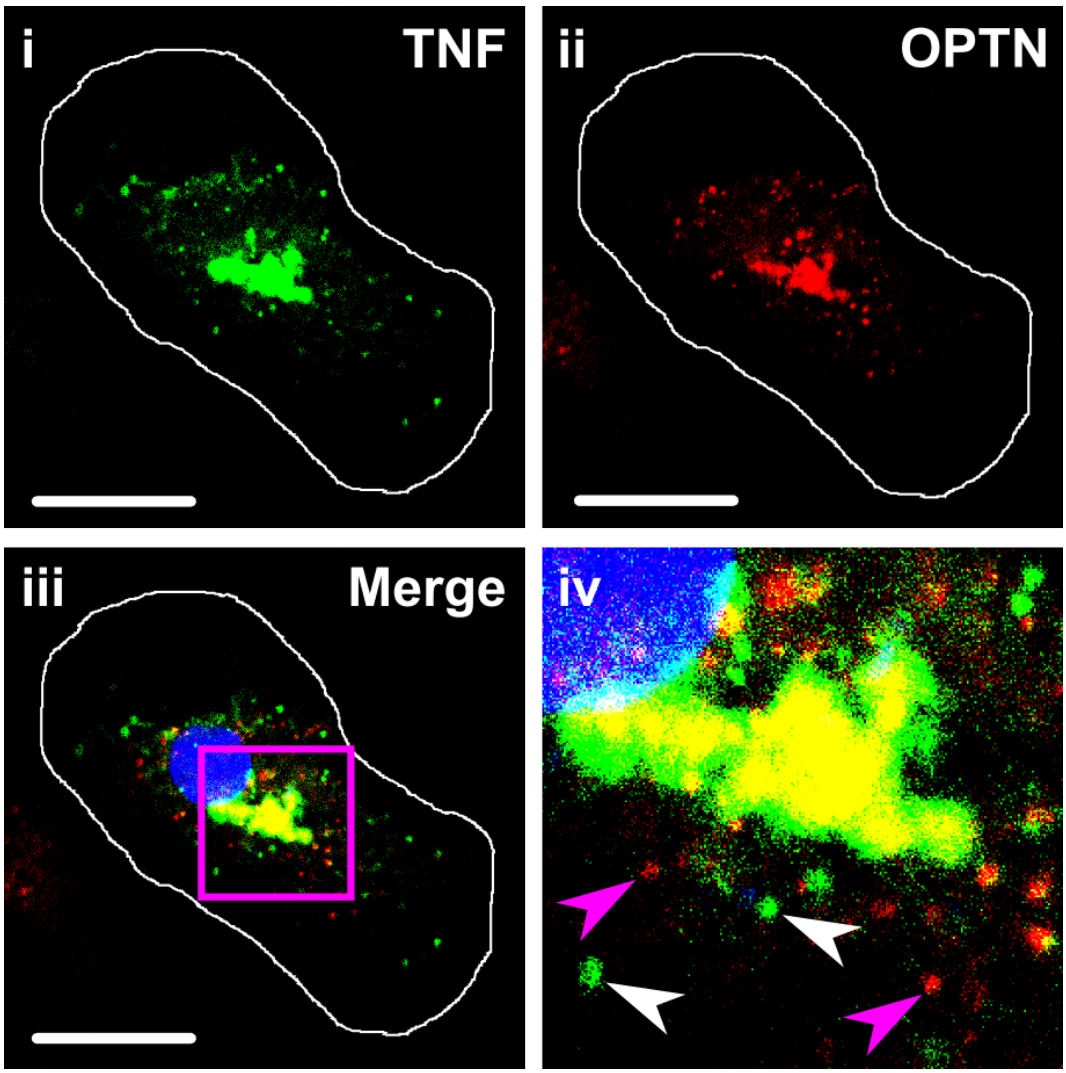

Figure 4.4 Confocal microscopy in monocyte-derived macrophages show colocalisation of OPTN with TNF in the Golgi complex. MDM (white outline) show colocalisation of OPTN (ii) with TNF (i) in the Golgi complex, next to the DAPI stained nucleus in blue (iii). Single stained OPTN vesicles (pink arrows) and TNF vesicles (white arrows) are visible in the enlarged area of the pink box (iv) (image i, ii, iii at 63×, scale bar 20 μm).

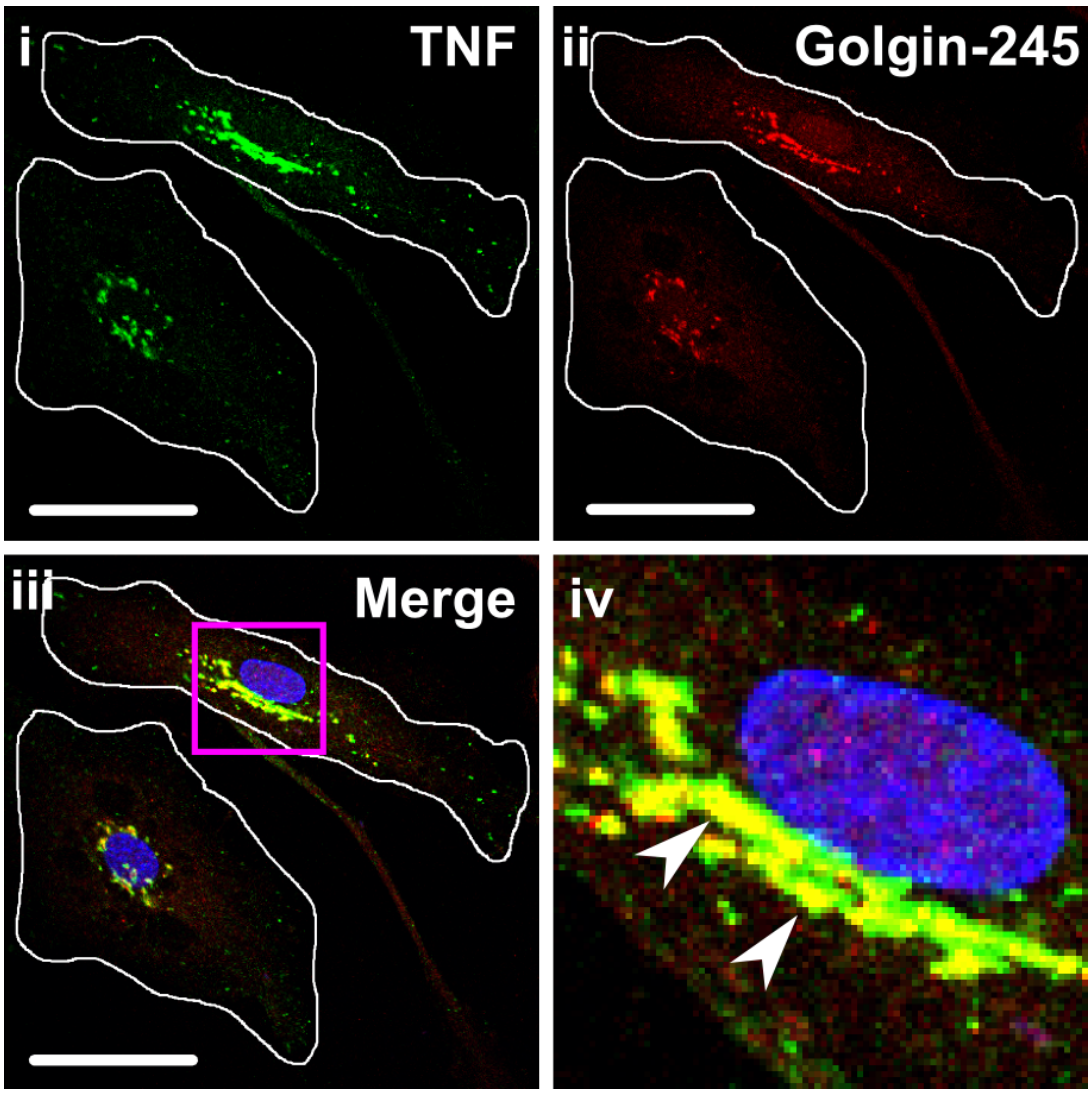

Figure 4.5 Confocal microscopy in monocyte-derived macrophages show colocalisation of the *trans*-Golgi marker Golgin-245 with TNF. MDM (white outline) show colocalisation of the *trans*-Golgi marker Golgin-245/p230 (ii) with TNF (i), next to DAPI stained nucleus in blue (iii). Double positive Golgin-245 and TNF staining (white arrows) in enlarged area of the pink box (iv) are shown (image i, ii, iii at 63×, scale bar 20 µm).

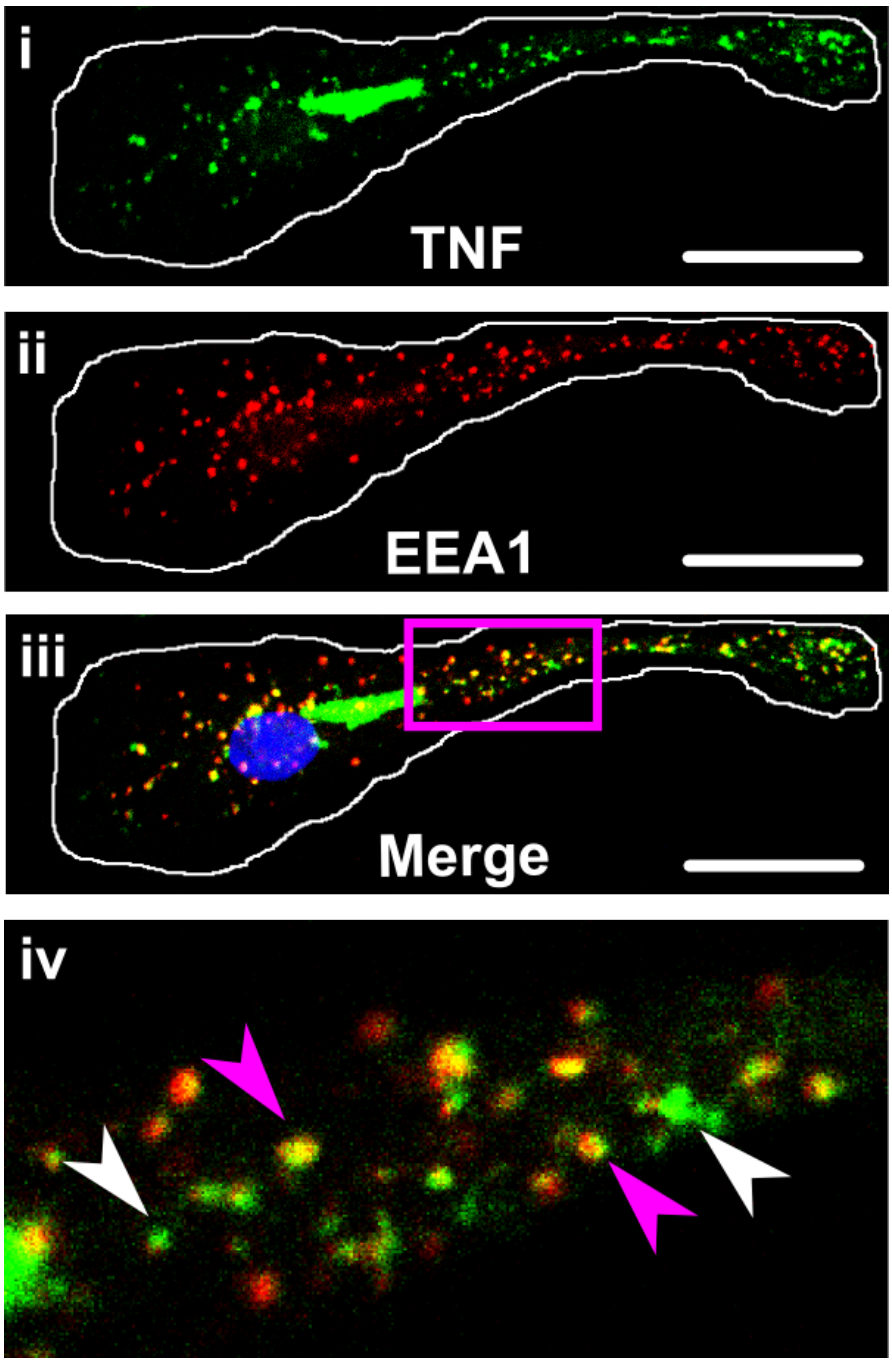

Figure 4.6 Confocal microscopy in monocyte-derived macrophages show colocalisation of TNF and early endosome antigen 1. MDM (white outline) show colocalisation of TNF (i) and early endosome antigen 1 (EEA1) (ii) in peripheral vesicles. Double positive vesicles (pink arrows) and single positive TNF vesicles (white arrows) in enlarged area of the pink box (iv) are shown (image i, ii, iii at 63×, scale bar 20 µm).

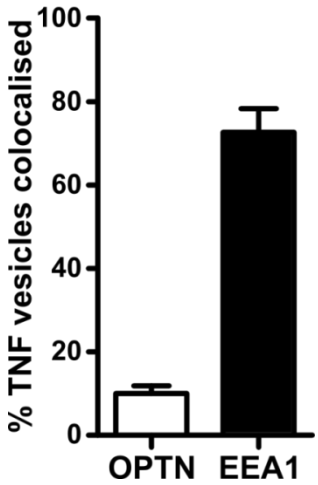

Figure 4.7 TNF is predominantly trafficked in EEA1$^+$ endosomes. Quantification of colocalisation in TNF vesicles shows that only ~12% of TNF vesicles contain colocalised OPTN whereas ~70% TNF vesicles colocalise with EEA1 (n=8-16 cells/person, 2 persons performed).

4.2.3 OPTN is upregulated on bacterial stimulation

OPTN was upregulated at both the transcriptional and protein levels in MDM after stimulation with bacteria and microbial ligands (Figure 4.8 and Figure 4.9). Gram negative heat-killed *E. coli* (HkEc) and lipopolysaccharide (LPS) were the most potent inducers of OPTN transcription and resulted in the highest levels of intracellular protein whereas the Toll-like receptor 2 (TLR2) ligand, $Pam_{3,}$ and NOD2 ligand, muramyl dipeptide (MDP) were less potent inducers.

OPTN was similarly upregulated at the protein level in THP-1 cells after stimulation with bacteria and microbial ligands (Figure 4.10). HkEc and LPS again resulted in the most statistically significant increase in OPTN in contrast to Pam_3 and MDP. The upregulation of OPTN is fastest with HkEc then Pam_3 and MDP and continues to rise till 24 hours (Figure 4.11).

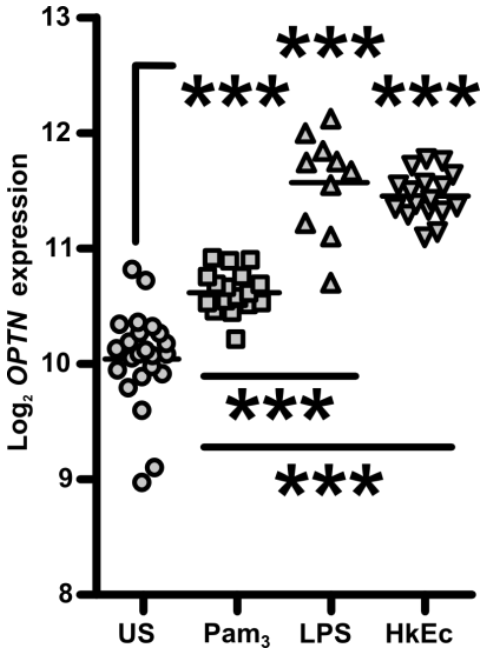

Figure 4.8 *OPTN* gene transcription in MDM is significantly upregulated after HkEc, TLR2 and TLR4 stimulation with Pam_3 and LPS. Gene transcription was measured at four hours. Results shown are mean ± SEM; n=10-23/group, over 2 independent experiments (***p<0.001; two-tailed, paired *t* test).

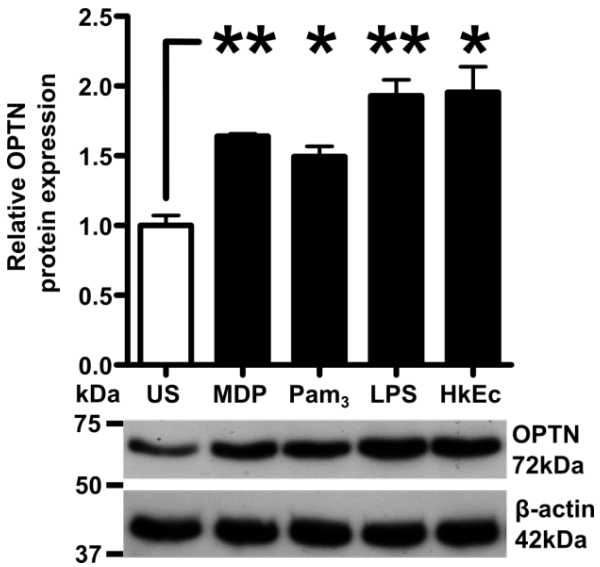

Figure 4.9 OPTN protein expression in MDM are also significantly upregulated after HkEc, TLR2, TLR4 and NOD2 stimulation with MDP. Protein expression was measured at 24 hours. Results shown are mean ± SEM, all immunoblots are normalised to actin; n=4, over 4 independent experiments (*p<0.05 and **p<0.01; two-tailed, paired *t* test).

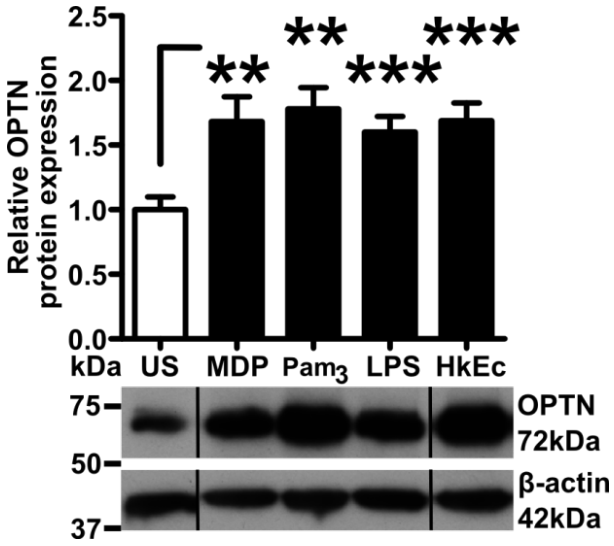

Figure 4.10 OPTN protein expression in THP-1 (human acute monocytic leukaemia) cells is upregulated after HkEc, TLR2, TLR4 and NOD2 stimulation with Pam_3, LPS and MDP. Protein expression was measured at 24 hours. Results shown are mean ± SEM, all immunoblots are normalised to actin; n=5, over 5 independent experiments (**p<0.01 and ***p<0.001; two-tailed, paired *t* test).

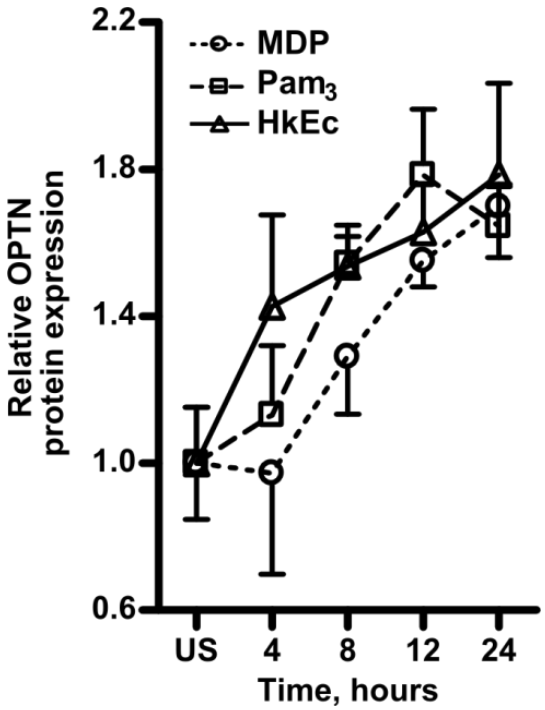

Figure 4.11 Upregulation of OPTN protein expression in THP-1 cells occurs with MDP and Pam_3 stimulation but is fastest with HkEc stimulation. Results shown are mean ± SEM, all immunoblots are normalised to actin; n=3/group, over 3 independent experiments.

4.2.4 *Optn*$^{-/-}$ mouse generation and charaterisation

To investigate the effect of deleting the OPTN gene on inflammation and cytokine secretion *in vivo*, *Optn*$^{-/-}$ mice that had been generated on a C57BL/6 background by insertion of a promoter-driven Neo targeting cassette upstream of exon 3 were studied (Figure 4.12) [230]. To exclude off-target effects of the Neo cassette, qRT-PCR of *Mcm10* and *Ccdc3* that flank *Optn* on chromosome 2 was performed in bone marrow-derived macrophages (BMDM), which demonstrated no difference in expression between *Optn*$^{+/+}$ and *Optn*$^{-/-}$ cells (Figure 4.13).

Genotyping of *Optn*$^{+/+}$ and *Optn*$^{-/-}$ mice was performed on ear clip genomic DNA (Figure 4.14), using recommended primers (Figure 4.12 and Appendix 1). RT-PCR of *Optn*$^{-/-}$ macrophage total RNA identified a 115 bp larger amplicon compared to *Optn*$^{+/+}$ cells (Figure 4.15). Sequencing of this *Optn*-SA amplicon identified a 115 bp splice acceptor (SA) insert between exon 2 and 3, which causes a frameshift and multiple predicted premature termination codons (Figure 4.16).

Flow cytometry of peripheral blood (Figure 4.17) and bone marrow cells (Figure 4.18) from *Optn*$^{+/+}$ and *Optn*$^{-/-}$ mice did not show a difference in the percentage of CD19^{+} B cells, CD3^{+} T cells, CD11b^{+} Gr1^{+} neutrophils and CD11b^{+} Ly6C^{+} monocytes. Additionally, naïve *Optn*$^{+/+}$ and *Optn*$^{-/-}$ organs such as large and small bowel, spleen, bone marrow, thymus, stomach, liver, kidney, heart and brain were reviewed by a Histopathologist (see Acknowledgements) and not found to be histologically different on H&E staining (Figure 4.19).

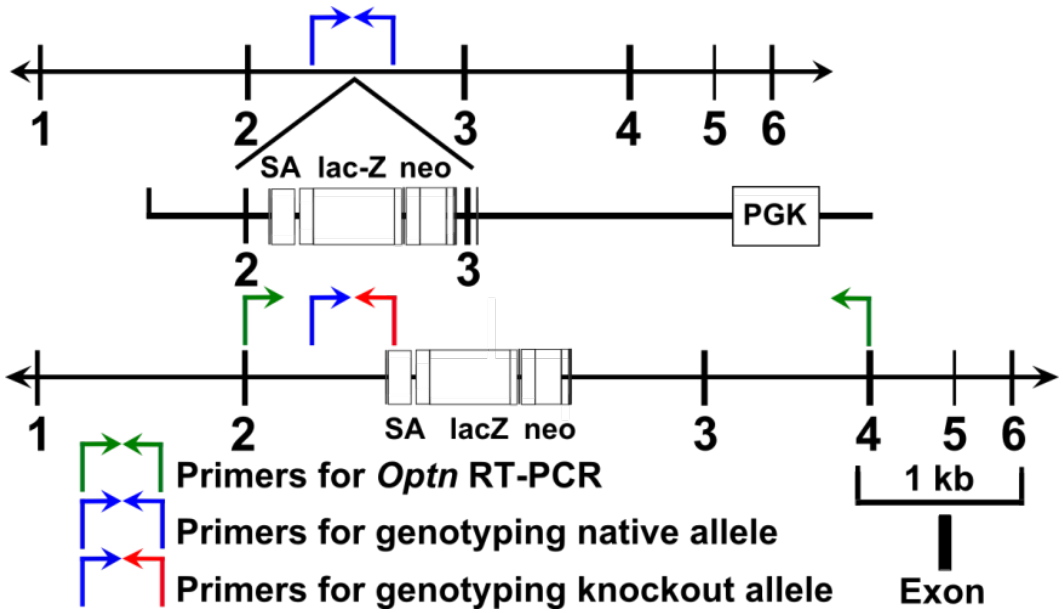

Figure 4.12 Generation of *Optn*$^{-/-}$ mice. The exon-intron layout of the murine *Optn* gene on chromosome 2, structure of the L1/L2 human β-actin promoter driven neoR targeting cassette with a PGK backbone and the *Optn* locus after homologous recombination. Positions of primers used for genotyping and RT-PCR are depicted (widths of exons, introns and targeting cassette are proportional to sequence length). Data from Wellcome Trust Sanger Institute.

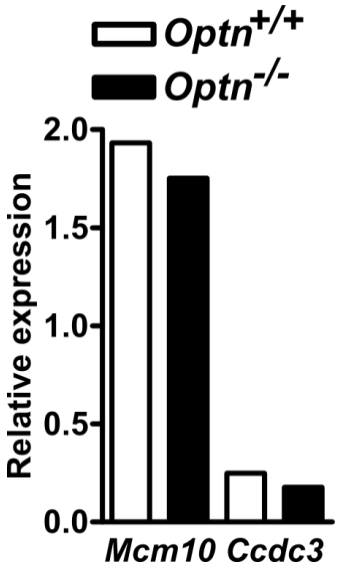

Figure 4.13 qRT-PCR of *Mcm10* and *Ccdc3* that flank *Optn* on chromosome 2 show no difference in expression between *Optn*$^{+/+}$ and *Optn*$^{-/-}$ mice. qRT-PCR on total RNA was performed on BMDM stimulated with HkEc for four hours.

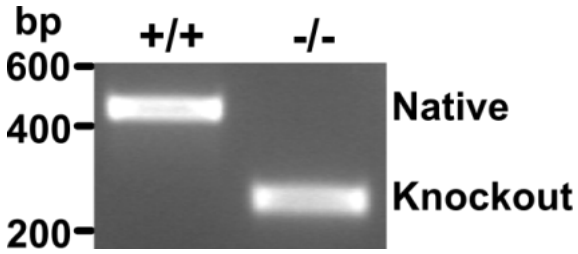

Figure 4.14 Genotyping of *Optn*$^{+/+}$ and *Optn*$^{-/-}$ mice. Genotyping was performed by PCR of gDNA isolated from ear clips amplified with *Optn* gene-specific primers, producing a 238 bp knockout amplicon and a 435 bp native amplicon.

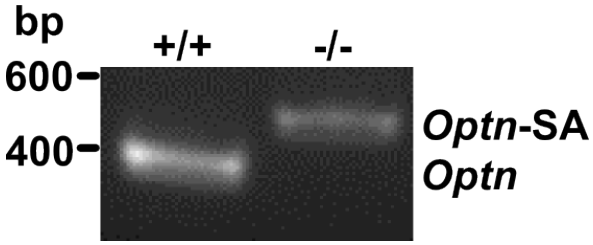

Figure 4.15 RT-PCR of *Optn* in *Optn*$^{+/+}$ and *Optn*$^{-/-}$ bone marrow-derived macrophages. RT-PCR produced a 115 bp larger *Optn*-SA amplicon from the *Optn*$^{-/-}$ mouse, which was absent in the *Optn*$^{+/+}$ mouse.

GGACAGCCCTTGTGAGACCCCAGGAAATGGACCCTCCAATATGGTT
CACCCCAGCCTGGACACATTCACCCCTGAGGAGCTGCTGCAGCAA
ATGAAGGAACTCCTGGTTGAGAACCACCAGCTGAAAGGTCCCAGGT
CCCGAAAACCAAAGAAGAAGAACCCTAACAAAGAGGACAAGCGGC
CTCGCACAGCCTTCACTGCTGAGCAGCTCCAGAGGCTCAAGGCTG
AGTTTCAGACCAACAGAAGCCATGAAGCTAAATAATCAAGCTATGAA
AGGGCGATTTGAGGAGCTGTCCGCCTGGACAGAGAAGCAGAAGGA
AGAGCGCCTGTTGTTTGAGATGCAAAGCAAAGAGGTTAAGGAGCGC
CTTAAGGCCCTGACTCATGAAAATGAGAGGCTGAAGGAAGAGCTTG
GAAAATTCAAAGAGAAATCAGAAAAGCCATTGGAAGACCTCAC

D S P C E T P G N G P S N M V H P S L D T F T P E E L L Q Q M K E L
L V E N H Q L K G P R S R K P K K K N P N K E D K R P R T A F T A E
Q L Q R L K A E F Q T N R S H E A K **Stop** S S Y E R A I **Stop** G A V R
L D R E A E G R A P V V **Stop** D A K Q R G **Stop** G A P **Stop** G P D S
Stop K **Stop** E A E G R A W K I Q R E I R K A I G R P H

Figure 4.16 Sequencing of the *Optn*-SA amplicon from *Optn*$^{-/-}$ macrophages identified a 115 bp splice acceptor (SA) insert between exon 2 and 3. The SA insert results in multiple premature termination codons. Sequence is shown above, amino acid translation below; exon 2 in yellow, SA insert in green and exon 3 in pink.

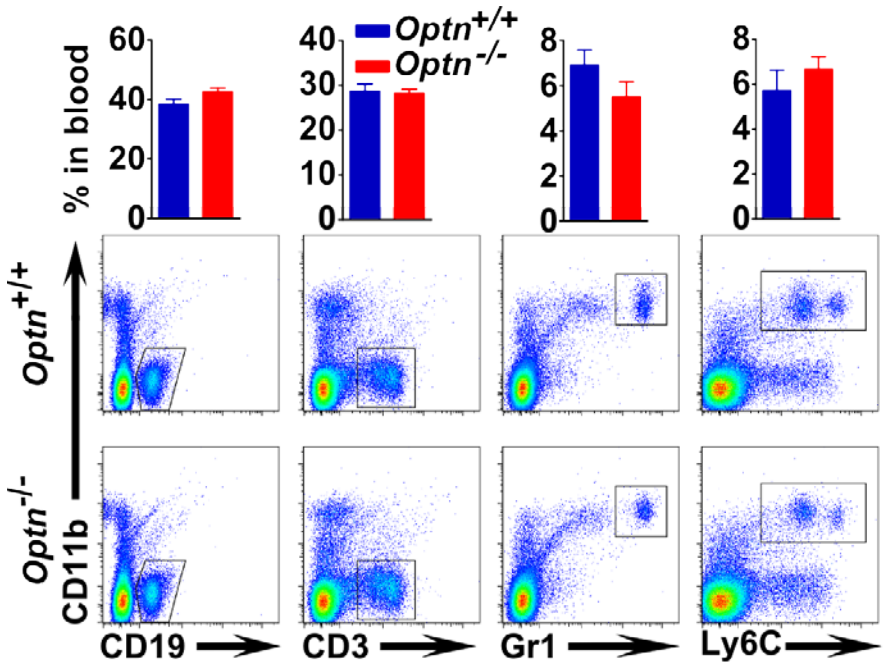

Figure 4.17 Flow cytometry of naïve *Optn*$^{+/+}$ and *Optn*$^{-/-}$ peripheral blood showed no difference in the percentage of CD19^{+} B cells, CD3^{+} T cells, Gr1^{+} neutrophils or Ly6C^{+} monocytes. Results shown are mean ± SEM; n=14-25 mice/genotype, over 4 independent experiments (two-tailed, unpaired *t* test).

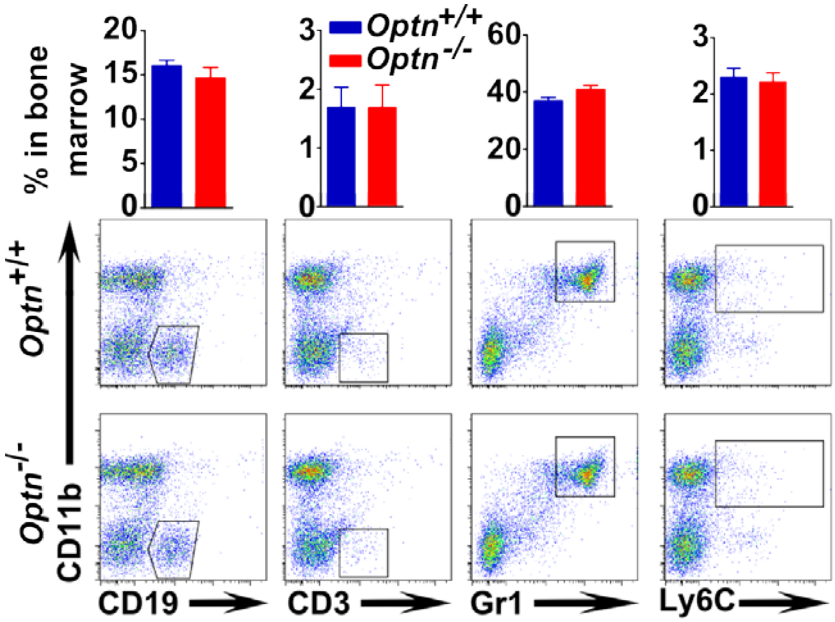

Figure 4.18 Flow cytometry of naïve *Optn*$^{+/+}$ and *Optn*$^{-/-}$ bone marrow cells showed no difference in the percentage of CD19^{+} B cells, CD3^{+} T cells, Gr1^{+} neutrophils or Ly6C^{+} monocytes. Results shown are mean ± SEM; n=7 mice/genotype, over 3 independent experiments (two-tailed, unpaired *t* test).

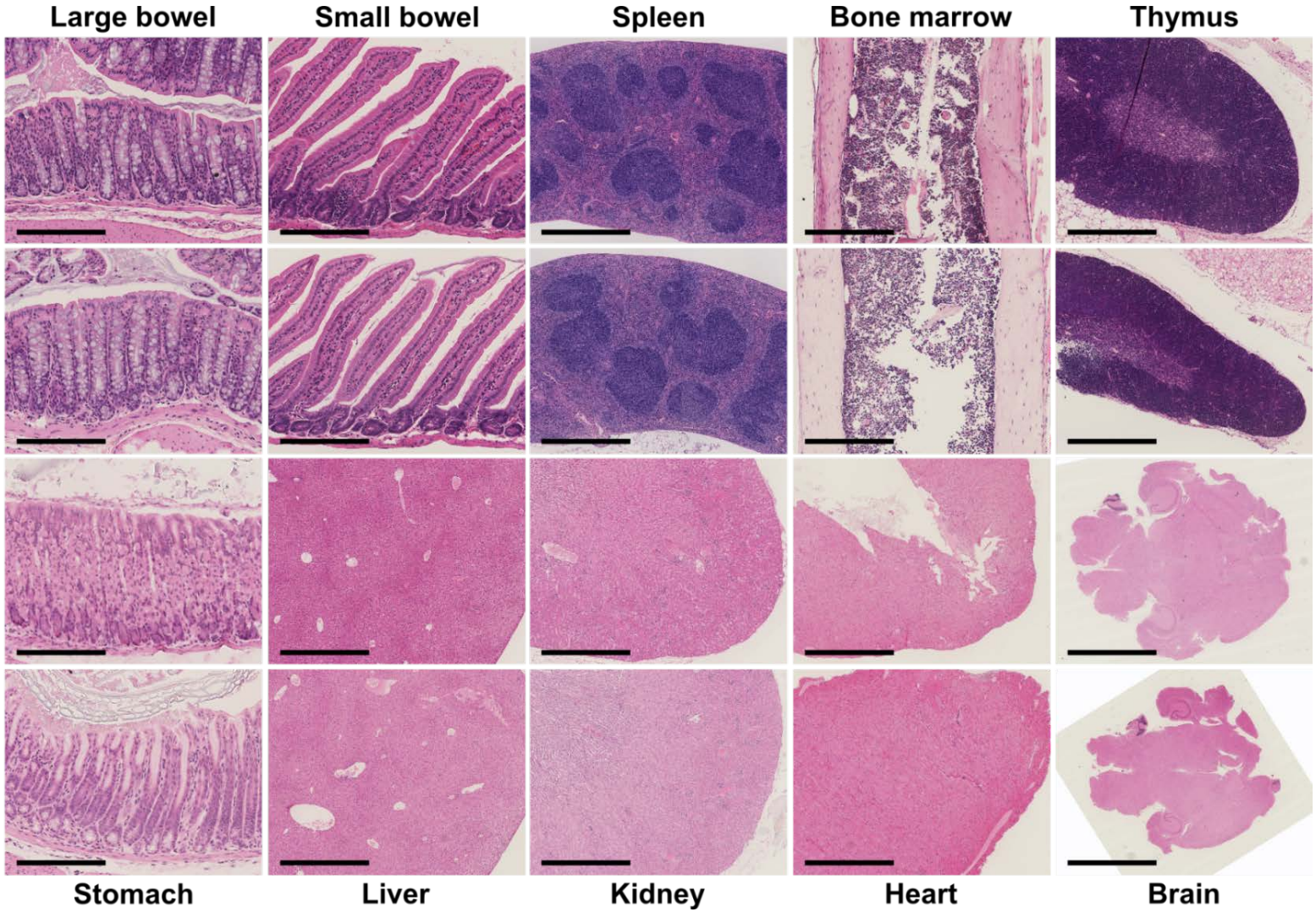
Large bowel
Small bowel
Spleen
Bone marrow
Thymus
Optn+/+
Optn-/-
Optn+/+
Optn-/-
Stomach
Liver
Kidney
Heart
Brain

Figure 4.19 Naïve *Optn*$^{+/+}$ and *Optn*$^{-/-}$ organs were not histologically different on H&E staining. Magnification and scale bar of large bowel 20× 200 µm, small bowel 20× 200 µm, spleen 5× 800 µm, bone marrow 15× 250 µm, thymus 10× 400 µm, stomach 20× 200 µm, liver 5× 800 µm, kidney 5× 800 µm, heart 5× 800 µm and brain 1× 4 mm.

4.2.5 Thioglycollate-induced peritoneal macrophages

Thioglycollate-induced peritoneal macrophages (TiPM) were collected and stimulated with MDP, Pam_3 and HkEc for 24 hours (Figure 4.20). Immunoblot of OPTN in TiPM whole cell lysates confirmed the lack of the OPTN protein in *Optn*$^{-/-}$ cells (Figure 4.20).

As has previously been shown with human MDM (Figure 4.8), HkEc was the most potent inducer of OPTN, which resulted in a significant increase in intracellular OPTN relative to unstimulated TiPM compared to Pam_3 and MDP, which only caused a two-fold increase (Figure 4.20).

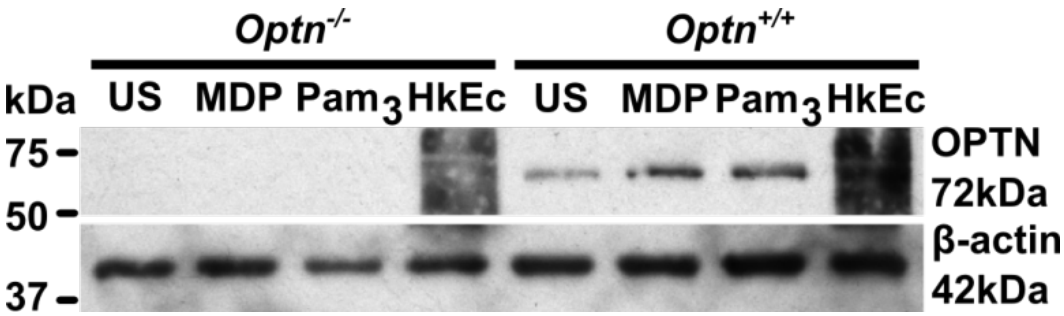

Figure 4.20 OPTN protein is absent in *Optn*$^{-/-}$ thioglycollate-induced peritoneal macrophages and upregulated in *Optn*$^{+/+}$ cells on stimulation with MDP, Pam_3 and HkEc. Immunoblot of OPTN in *Optn*$^{+/+}$ and *Optn*$^{-/-}$ TiPM, shown with β-actin loading control.

In view of the previous finding of decreased proinflammatory TNF secretion from *OPTN* siRNA knockdown THP-1 cells [191], a dose response and time course stimulation of *Optn*$^{+/+}$ and *Optn*$^{-/-}$ TiPM with bacteria and microbial ligands was performed (Figure 4.21). As expected, increasing

doses of Pam_3, LPS and HkEc resulted in increasing secretion of TNF from TiPM but there was no difference between *Optn*$^{+/+}$ and *Optn*$^{-/-}$ cells at all doses tested. Over time, stimulation with Pam_3, LPS and HkEc resulted in rapid release of TNF from TiPM by four hours reaching maximal secretion by eight hours with LPS and HkEc, but a slower rise to a maximum at 24 hours with Pam_3 but no difference between *Optn*$^{+/+}$ and *Optn*$^{-/-}$ cells were found. These kinetic findings of TNF release in TiPM are similar to what was previously seen in human MDM.

OPTN has been shown to play a role in the autophagic clearance of *Salmonella* in HeLa cells [125]. To exclude the possibility that the lack of a difference in TNF secretion could be due to alterations in uptake and handling of *E. coli* in *Optn*$^{-/-}$ TiPM, phagocytosis and killing experiments were performed (Figure 4.22). Phagocytosis of FITC-labelled HkEc resulted in the gradual increase of intracellular fluorescence in TiPM at 1, 3 and 24 hours but was not different between *Optn*$^{+/+}$ and *Optn*$^{-/-}$ cells. Similarly, killing of intracellular *E. coli* by TiPM after three hours of bacterial incubation was no different between *Optn*$^{+/+}$ and *Optn*$^{-/-}$ cells.

OPTN was previously reported to be involved with myosin VI in the maintenance of Golgi structure [201]. To investigate the effect of OPTN deficiency on the Golgi complex, electron microscopy of naïve and HkEc stimulated TiPM was done (Figure 4.23). Multiple large vacuoles were found within *Optn*$^{+/+}$ and *Optn*$^{-/-}$ TiPM that likely contain phagocytosed thioglycollate. The ER and Golgi complex structures within these TiPM were no different between *Optn*$^{+/+}$ and *Optn*$^{-/-}$ cells but the effects of these large vacuoles on cellular function and vesicle trafficking is uncertain despite retaining its ability to phagocytose HkEc.

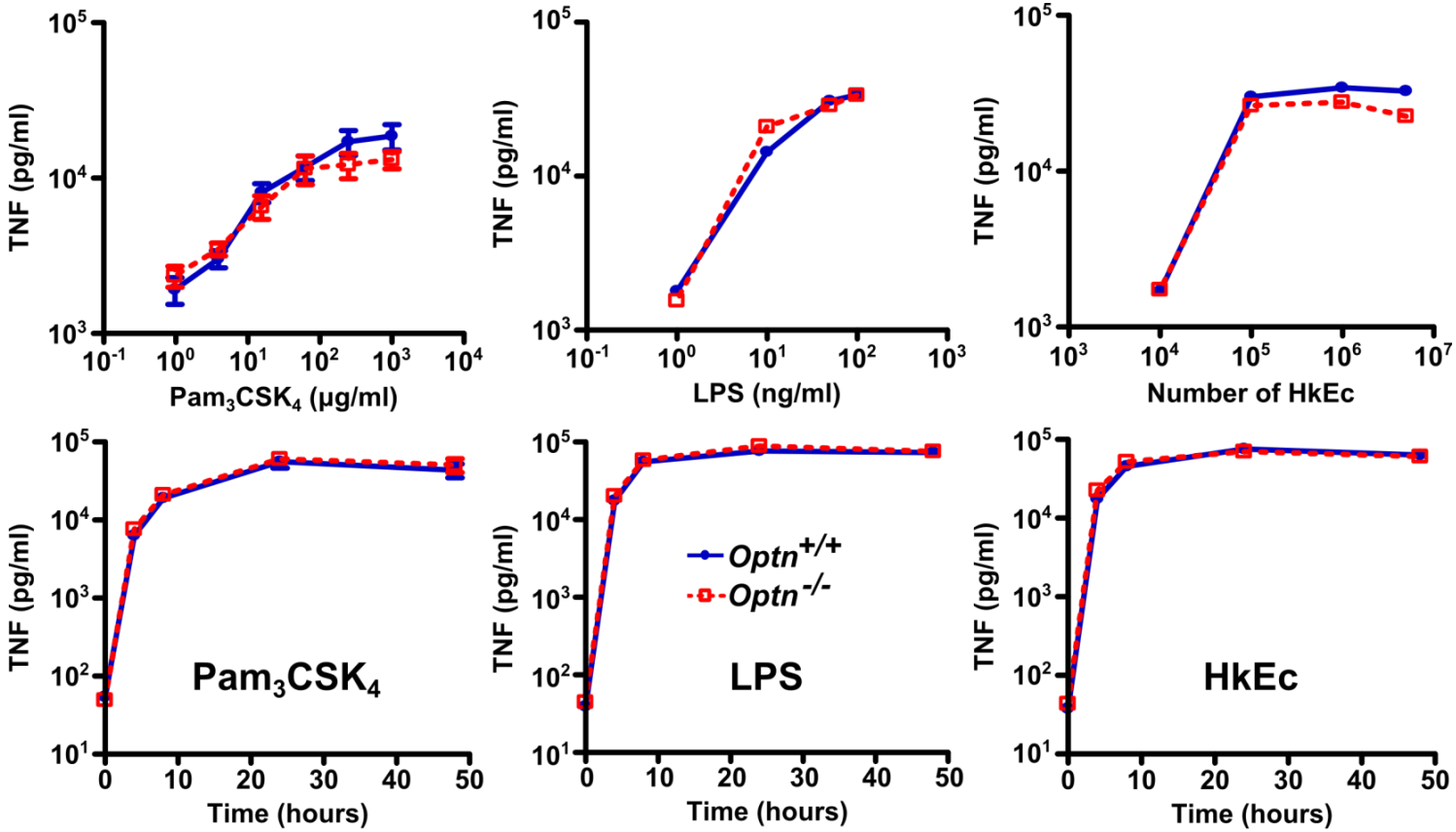

Figure 4.21 TNF secretion from stimulated *Optn*$^{+/+}$ and *Optn*$^{-/-}$ thioglycollate-induced peritoneal macrophages was no different. Dose response (above) and time course (below) curves in TiPM stimulated with Pam_3CSK_4, lipopolysaccharide (LPS) and heat-killed *E. coli* (HkEc) are shown. Results shown are mean ± SEM (two-tailed, unpaired *t* test).

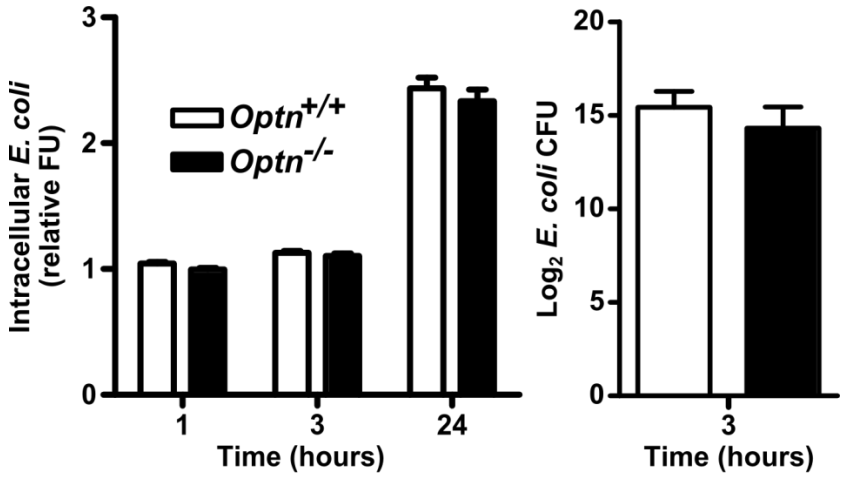

Figure 4.22 Thioglycollate-induced peritoneal macrophage phagocytosis and killing of *E. coli* was not different between *Optn*$^{+/+}$ and *Optn*$^{-/-}$ mice. Phagocytosis of FITC-labelled HkEc (left) and killing of *E. coli* (right) are shown. Results shown are mean ± SEM; n=12-13 and n=14-15 mice/genotype for phagocytosis and killing, over 6 independent experiments (two-tailed, unpaired *t* test).

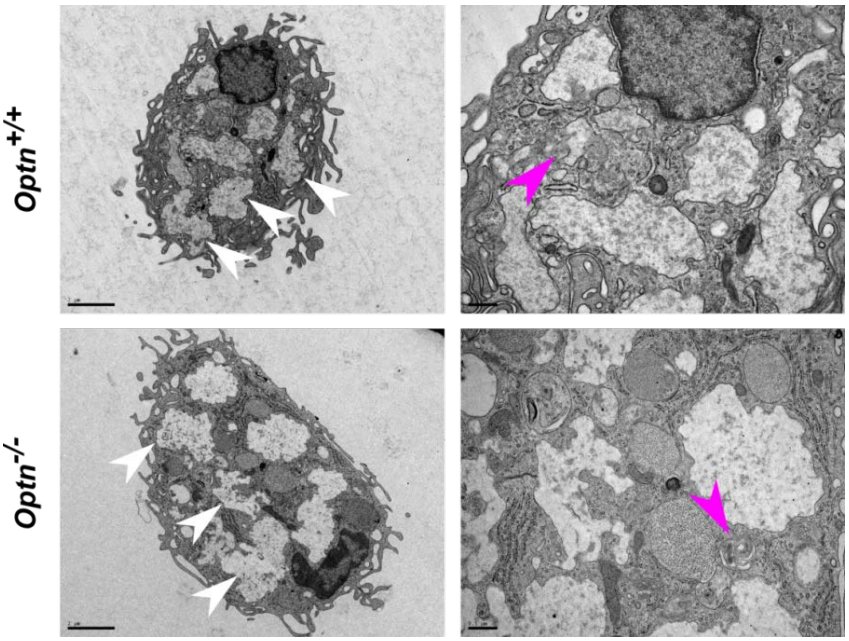

Figure 4.23 Thioglycollate-induced peritoneal macrophages were found to have multiple vacuoles on electron microscopy. The TiPM contained multiple vacuoles (white arrows, left) that are presumed to contain thioglycollate (8,000×, scale bar 2 µm). Macrophages were still able to phagocytose *E. coli*, visible at higher magnification (pink arrows, right) (20,000×, scale bar 1 µm). Slides prepared by Mr Mark Turmaine, UCL Biosciences.

4.2.6 Bone marrow-derived macrophages

In view of the discovery of multiple large vacuoles in TiPM and the potential of these vacuoles interfering with vesicle trafficking, bone marrow-derived macrophages (BMDM) were studied. Culture of bone marrow cells for five days with M-CSF resulted in a 96% to 97% enriched population of adherent $CD11b^+$ $F4/80^+$ macrophages in both *Optn*$^{+/+}$ and *Optn*$^{-/-}$ mice (Figure 4.24).

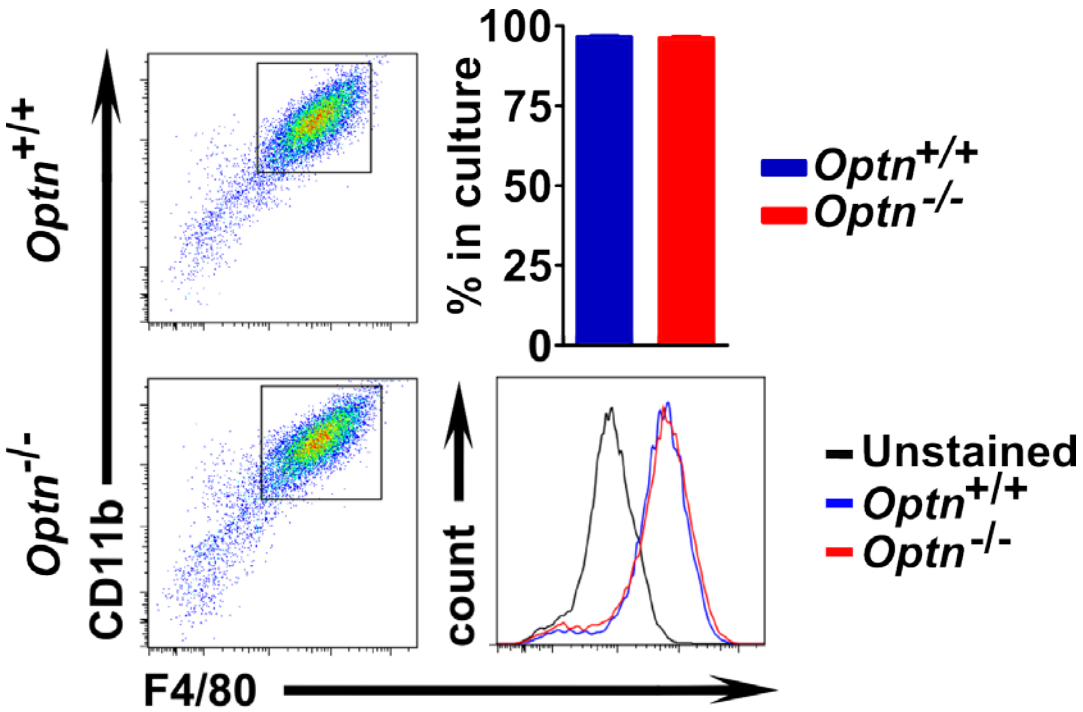

Figure 4.24 Bone marrow cells after 5 days of culture with M-CSF produce equal numbers of $CD11b^+F4/80^+$ macrophages in *Optn*$^{-/-}$ and *Optn*$^{+/+}$ mice. Flow cytometry analysis show that the populations are 96-97% enriched for $CD11b^+F4/80^+$ macrophages in culture. Representative flow cytometry plots shown (n=2 mice/genotype, over 2 independent experiments).

Transmission electron microscopy (TEM) of HkEc stimulated *Optn*$^{+/+}$ and *Optn*$^{-/-}$ BMDM did not show any of the large vacuoles found in TiPMs (Figure 4.25). Similar to TiPM, HkEc within phagosomes were visible in both *Optn*$^{+/+}$ and *Optn*$^{-/-}$ cells.

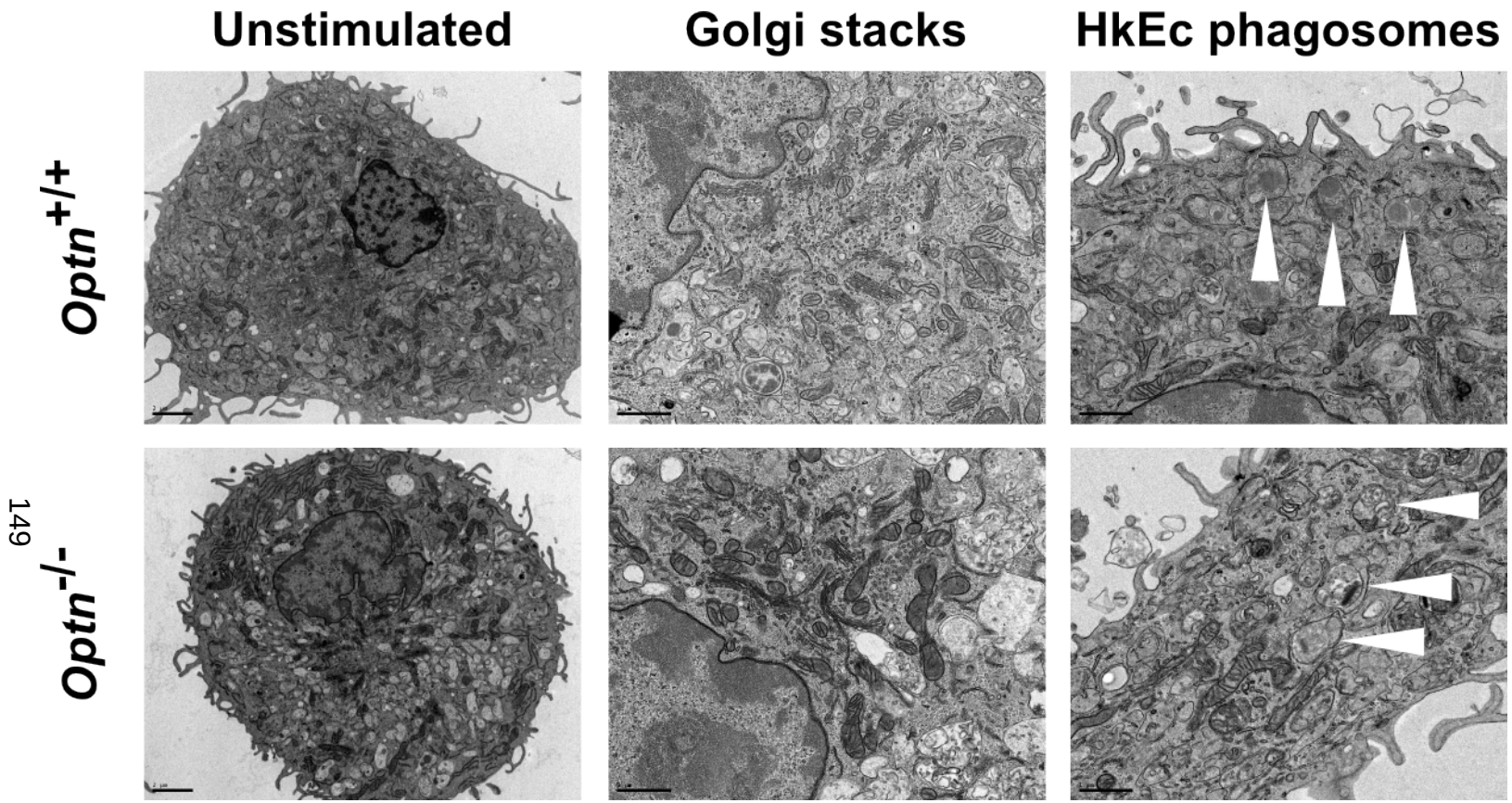

Figure 4.25 Transmission electron microscopy of HkEc stimulated *Optn*$^{-/-}$ and *Optn*$^{+/+}$ bone marrow derived macrophages. Unstimulated BMDM (8,000×, scale bar 2 µm) and HkEc fed BMDM (20,000×, scale bar 1 µm) did not show any large vacuoles that were seen in TiPMs. Phagosomes containing HkEc (arrowheads) were visible in equal numbers in both *Optn*$^{-/-}$ and *Optn*$^{+/+}$ macrophages (20,000×, scale bar 1 µm). Slides prepared by Mr Mark Turmaine, UCL Biosciences.

Phagocytosis of FITC-labelled HkEc showed an expected rise in intracellular fluorescence with bacterial uptake at 1, 4 and 24 hours, which was not statistically different between *Optn*$^{+/+}$ and *Optn*$^{-/-}$ BMDM at each time point (Figure 4.26). Killing of live E. coli was also not significantly different between BMDM genotypes after 3 hours of bacterial incubation.

In view of the role of OPTN in autophagy, the induction of autophagy in the *Optn*$^{-/-}$ BMDM was assessed. Baseline autophagic flux was investigated using bafilomycin A, the vacuolar-type H^+-ATPase (V-ATPase) inhibitor that blocks fusion of autophagosomes with lysosomes. Immunoblot for LC3 in *Optn*$^{+/+}$ and *Optn*$^{-/-}$ BMDM stimulated with bafilomycin A demonstrated an equal upregulation in the autophagosome-bound LC3-II in both genotypes indicating a normal baseline autophagic flux occurs in the absence of OPTN (Figure 4.27).

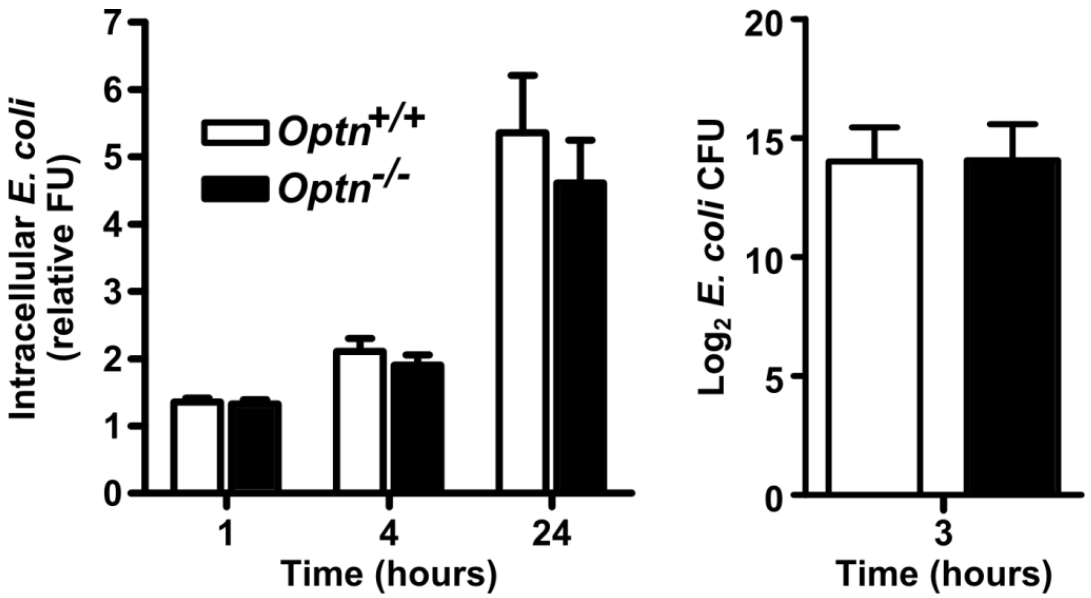

Figure 4.26 Bone marrow-derived macrophage phagocytosis and killing of *E. coli* was not different between *Optn*$^{+/+}$ and *Optn*$^{-/-}$ mice. Phagocytosis of FITC-labelled HkEc (left) and killing of *E. coli* (right) are shown. Results shown are mean ± SEM, n=5 and n=3 mice/genotype for phagocytosis and killing over 3 independent experiments (two-tailed, unpaired *t* test).

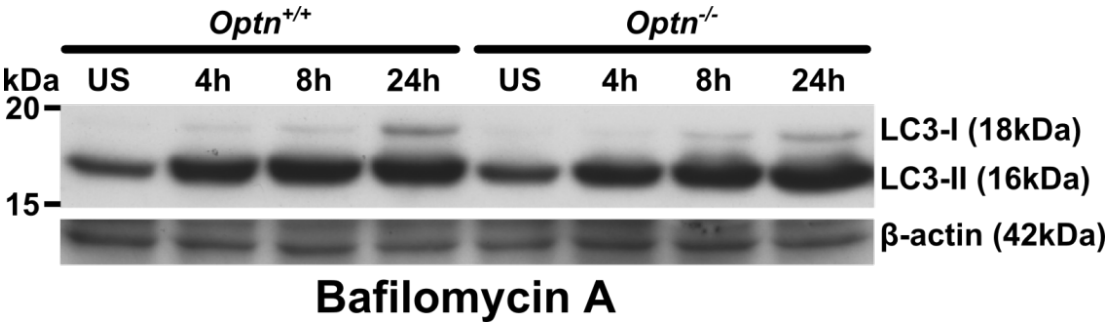

Figure 4.27 Basal autophagic flux in *Optn*$^{+/+}$ and *Optn*$^{-/-}$ bone marrow derived macrophages is not different. Immunoblot of LC3 in bafilomycin A treated *Optn*$^{+/+}$ and *Optn*$^{-/-}$ BMDM shows no difference in the accumulation of LC3-II, shown with β-actin loading control. Bafilomycin A, a V-ATPase inhibitor blocks fusion of autophagosome with lysosomes and hence LC3-II degradation.

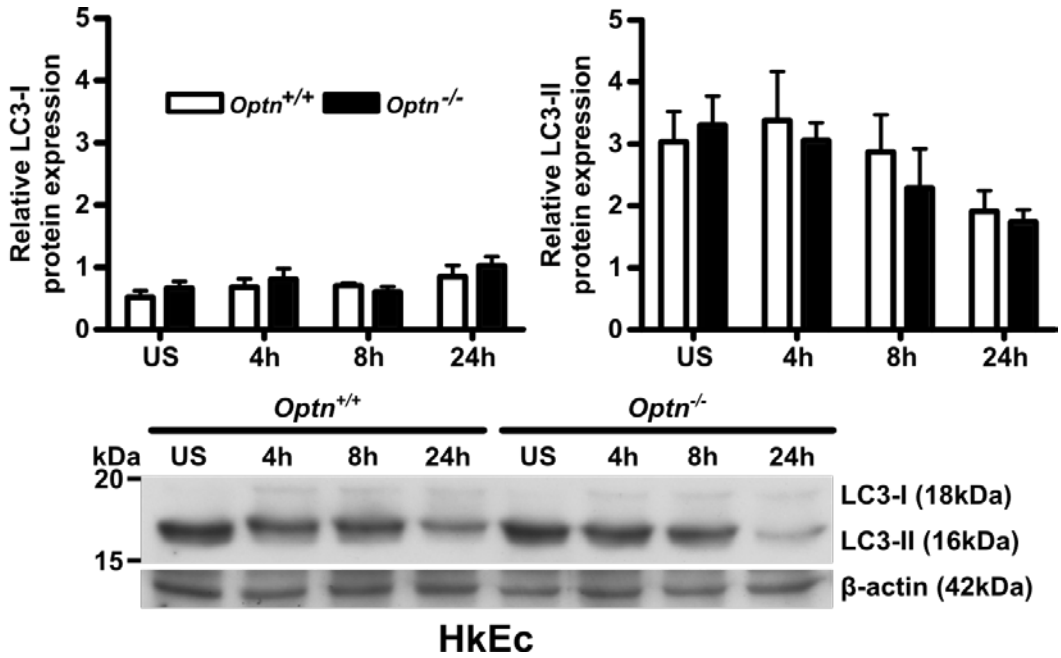

Figure 4.28 Induction of autophagy in *Optn*$^{+/+}$ and *Optn*$^{-/-}$ bone marrow derived macrophages by heat-killed *E. coli* was no different. Immunoblot for LC3-I and LC3-II in HkEc stimulated BMDM showed an equal rise then gradual fall in autophagosome-bound LC3-II in *Optn*$^{+/+}$ and *Optn*$^{-/-}$ BMDM but minimal change in cytoplasmic LC3-I. Results shown are mean ± SEM, all immunoblots are normalised to actin, n=6 mice/genotype, over 6 independent experiments (two-tailed, paired *t* test).

The induction of autophagy by HkEc was also investigated in BMDM (Figure 4.28). *Optn*$^{+/+}$ and *Optn*$^{-/-}$ BMDM were exposed to HkEc at a multiplicity of infection (MOI) of 20 to look at LC3-II induction at various time points. The LC3-II autophagosome-bound LC3 was marginally higher at four hours but subsequently decreased thereafter to 24 hours. There was no difference in LC3-II levels between *Optn*$^{+/+}$ and *Optn*$^{-/-}$ cells, and cytoplasmic LC-I levels remained low and unaltered through that 24 hours period.

OPTN siRNA knockdown resulted in reduced proinflammatory TNF and IL6 release from human MDM, hence the effect of the lack of OPTN was investigated [191]. Similar to the *OPTN* siRNA knockdown experiments, secretion of the proinflammatory cytokines TNF and IL6 was significantly reduced in *Optn*$^{-/-}$ BMDM compared to *Optn*$^{+/+}$ cells (Figure 4.29). By contrast, anti-inflammatory cytokine IL10 and chemokine CXCL1 was elevated in the OPTN deficient BMDM. To investigate if this was related to abnormal gene transcription, qRT-PCR was performed to quantify the expression of *Tnf, Il6, Il10* and *Cxcl1* in HkEc stimulated HkEc. Similar to our previous findings in human MDM, gene transcription was equal between *Optn*$^{+/+}$ and *Optn*$^{-/-}$ BMDM (Figure 4.29).

To ensure that this cytokine defect was not due to differences in cell death, cell viability in the HkEc stimulated *Optn*$^{+/+}$ and *Optn*$^{-/-}$ BMDM was evaluated using the MTT assay (Figure 4.30). In this assay the MTT salt, 3-[4,5-dimethylthiazol-2-yl]-2,5-diphenyl tetrozolium bromide, is taken up by viable cells and reduced into insoluble purple formazan that is colorimetrically measured. Purple formazan formation as a measure of cell viability in HkEc stimulated *Optn*$^{+/+}$ and *Optn*$^{-/-}$ BMDM rose at four hours, peaked at eight hours but was lower at 24 hours. However, there was no difference between *Optn*$^{+/+}$ and *Optn*$^{-/-}$ BMDM at all time points measured.

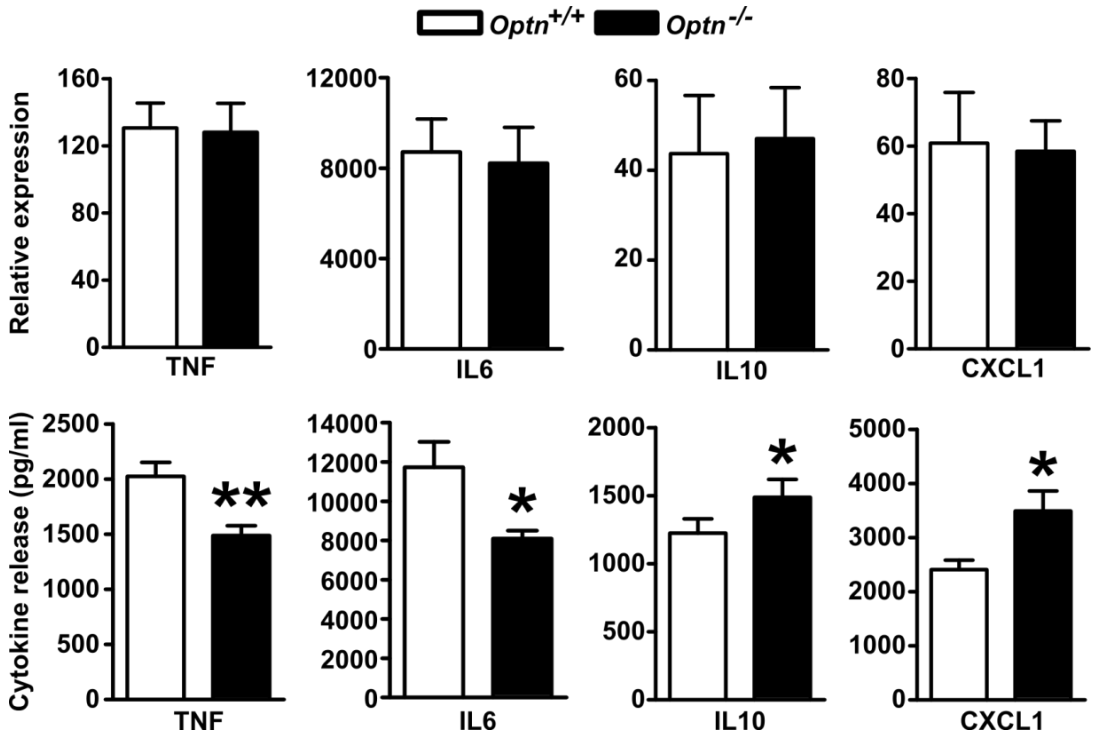

Figure 4.29 Stimulation of bone marrow derived macrophages with heat-killed *E. coli* resulted in equal cytokine gene transcription but significantly lower secretion of proinflammatory TNF and IL6 and higher IL10 and CXCL1 in *Optn*$^{-/-}$ cells. Upper panel shows gene transcription whilst the lower panel shows cytokine secretion. Results shown are mean ± SEM; n=5 mice/genotype, over 5 independent experiments (*p<0.05, and **p<0.01; two-tailed, unpaired *t* test).

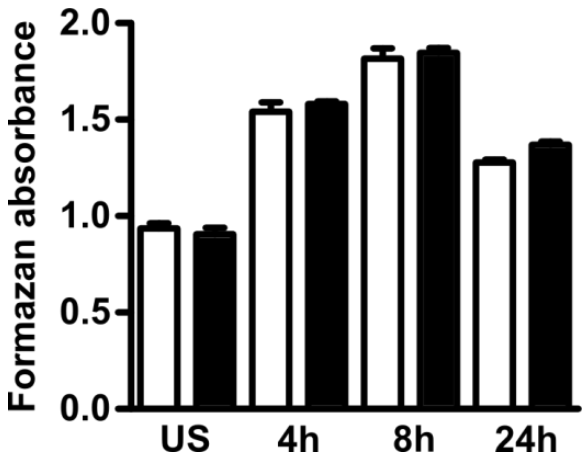

Figure 4.30 Cell viability of HkEc stimulated *Optn*$^{+/+}$ and *Optn*$^{-/-}$ bone marrow-derived macrophage was not different. Cell viability assay was measured using the MTT assay. Results shown are mean ± SEM, n=2 mice/genotype (two-tailed, unpaired *t* test).

In light of the normal cell viability, ER stress in the HkEc stimulated BMDM was assessed to investigate if in the absence of OPTN and potential cytokine mistrafficking, unfolded proteins may accumulate and result in diminished proinflammatory cytokine secretion. The unfolded protein response (UPR) is a highly conserved cellular stress response to the presence of misfolded proteins in the endoplasmic reticulum and the aim of the UPR is to stop protein translation, degrade the misfolded proteins and upregulate chaperone molecules that fold proteins.

To study ER stress in the HkEc stimulated BMDM, whole cell lysates were immunoblotted for two of the ER stress molecular chaperones, glucose-regulated protein, 78kDa (GRP78) that is also known as binding immunoglobulin protein (BiP), glucose-regulated protein, 94kDa (GRP94) and CCAAT-enhancer binding protein homologous protein (CHOP). GRP78 and GRP94 are upregulated in ER stress and functions as a molecular chaperone and inducer of further ER stress pathways whilst CHOP drives a pro-apoptotic signal in ER stress at the mitochondria. Immunoblot of GRP94, GRP78 and CHOP did not reveal a difference in induction of these proteins over time between the *Optn*$^{+/+}$ and *Optn*$^{-/-}$ BMDM (Figure 4.31).

Additionally, *Xbp1* splicing is associated with induction of ER stress. RT-PCR of total RNA from BMDM stimulated with HkEc and the ER stress inducers tunicamycin, thapsigargin and bafilomycin A which are then restriction enzyme digested did not reveal a difference in concentration of spliced *Xbp1* transcripts between *Optn*$^{+/+}$ and *Optn*$^{-/-}$ BMDM (Figure 4.32). Collectively, this indicates that ER stress was not different between BMDM of each genotype.

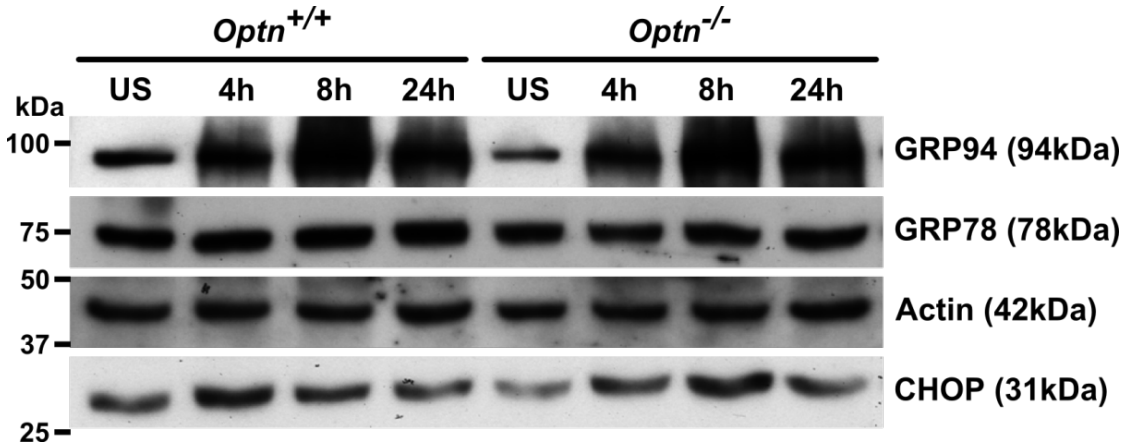

Figure 4.31 ER stress protein induction in *Optn*$^{+/+}$ and *Optn*$^{-/-}$ bone marrow derived macrophages stimulated with HkEc was not different over time. Immunoblot of ER stress proteins GRP94, GRP78/BiP and CHOP in a HkEc stimulated BMDM time course did not show a difference in ER stress between *Optn*$^{+/+}$ and *Optn*$^{-/-}$ cells, shown with β-actin loading control.

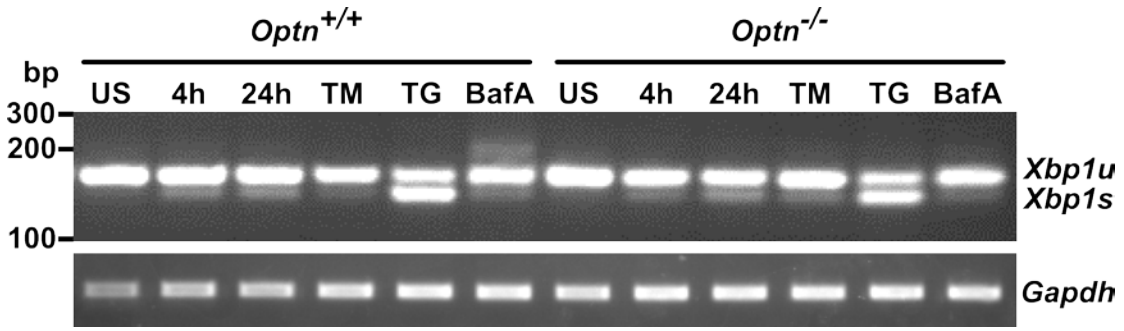

Figure 4.32 *Xbp1* splicing as a marker of ER stress in *Optn*$^{+/+}$ and *Optn*$^{-/-}$ bone marrow-derived macrophages stimulated with HkEc was not different over time. Metaphor™ agarose gel electrophoresis of PstI digested *Xbp1* RT-PCR of BMDM stimulated for four hours and 24 hours of HkEc, four hours of tunicamycin (TM), thapsigargin (TG) or bafilomycin A (BafA) demonstrated no difference in *Xbp1* splicing. US, unstimulated.

To investigate if the reduced intracellular TNF was due to defective protein translation in *Optn*$^{-/-}$ BMDM, brefeldin A, a potent inhibitor of protein transport from the endoplasmic reticulum to the Golgi was used. Intracellular TNF has previously been shown to exist as a membrane bound 26-kDa precursor and a 17-kDa secreted form [161]. Stimulation of BMDM with HkEc in the presence of brefeldin A resulted in elevation of the 26-kDa precursor TNF and loss of the 17-kDa secreted form to similar levels in both *Optn*$^{+/+}$ and *Optn*$^{-/-}$ BMDM (Figure 4.33) demonstrating that TNF is translated normally in the absence of OPTN.

By contrast, the inclusion of bafilomycin A, an inhibitor of vacuolar type H^+-ATPase that blocks fusion between autophagosome and lysosomes produced a greater increase in intracellular levels of the 17-kDa secreted form ($p=0.041$) in the *Optn*$^{-/-}$ compared with *Optn*$^{+/+}$ BMDM (Figure 4.33). There was no difference in the 26-kDa precursor TNF form, indicating that in the absence of OPTN, a greater proportion of the secreted form of TNF is trafficked through a bafilomycin A sensitive intracellular compartment in BMDM.

Inhibition of lysosomal proteases has been shown to increase intracellular cytokine levels in HkEc stimulated human MDM [187]. Therefore, the role of the lysosome in intracellular TNF trafficking was investigated with the inclusion of monensin, chloroquine and NH_4Cl in mouse BMDM. Chloroquine and NH_4Cl partition into acidic compartments and elevate the lysosomal pH, whereas monensin is a proton ionophore with similar but more potent effects [253-255]. In HkEc-stimulated BMDM, all three inhibitors of lysosomal degradation increased intracellular levels of TNF to equal levels in *Optn*$^{-/-}$ and *Optn*$^{+/+}$ cells when compared with HkEc stimulation alone (Figure 4.34), indicating that a greater proportion of intracellular TNF is directed to lysosomal degradation in the absence of OPTN.

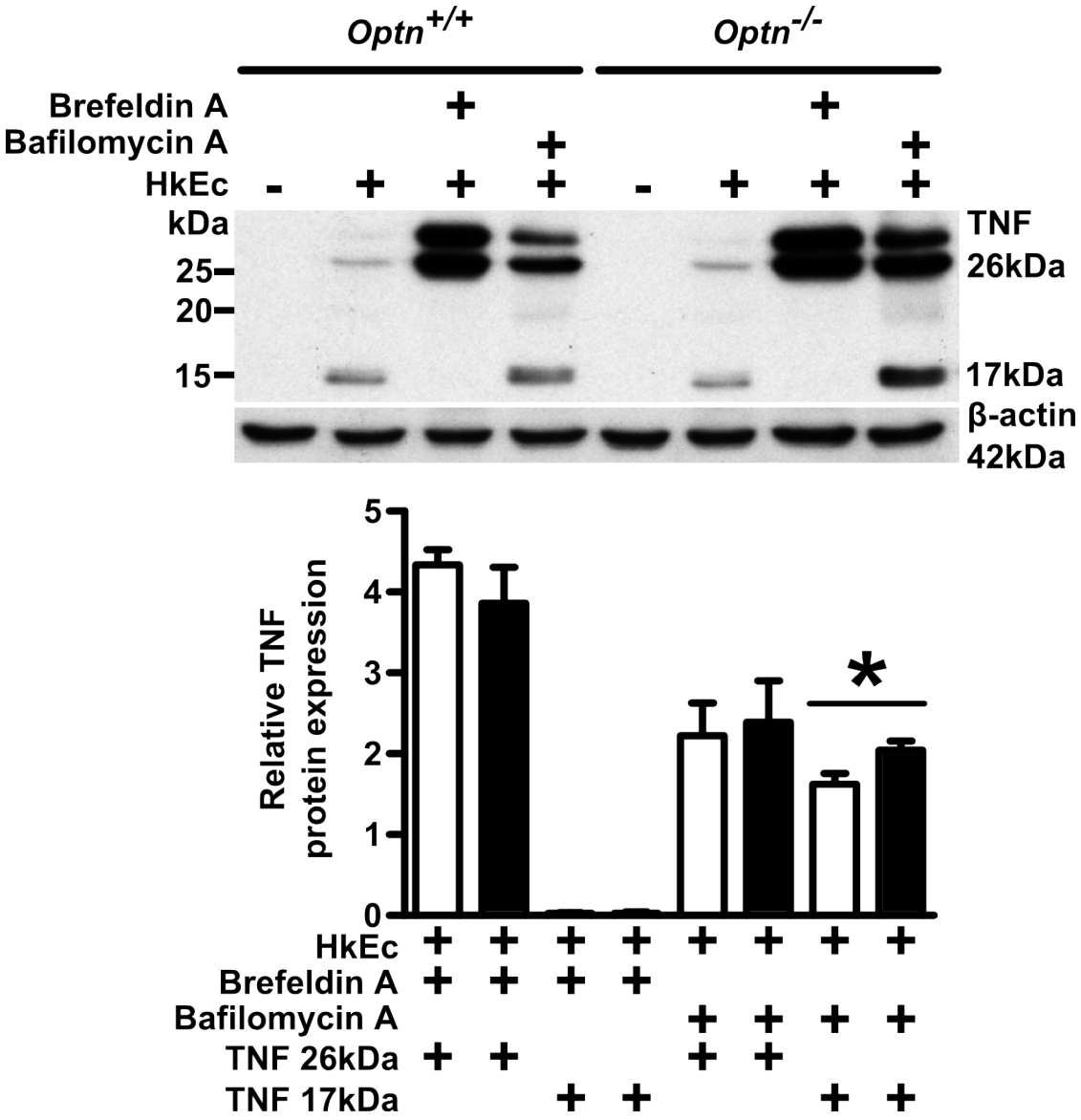

Figure 4.33 Brefeldin A results in undetectable levels of 17kDa secreted TNF but bafilomycin A results in significantly higher levels of 17kDa secreted TNF in *Optn*$^{-/-}$ BMDM. Representative immunoblot of TNF (above) with β-actin loading control and quantification of 26kDa precursor and 17kDa secreted TNF (below). Results shown are mean ± SEM, all immunoblots are normalised to actin; n=3-5 mice/genotype over 3-5 independent experiments (*p<0.05; two-tailed, unpaired *t* test).

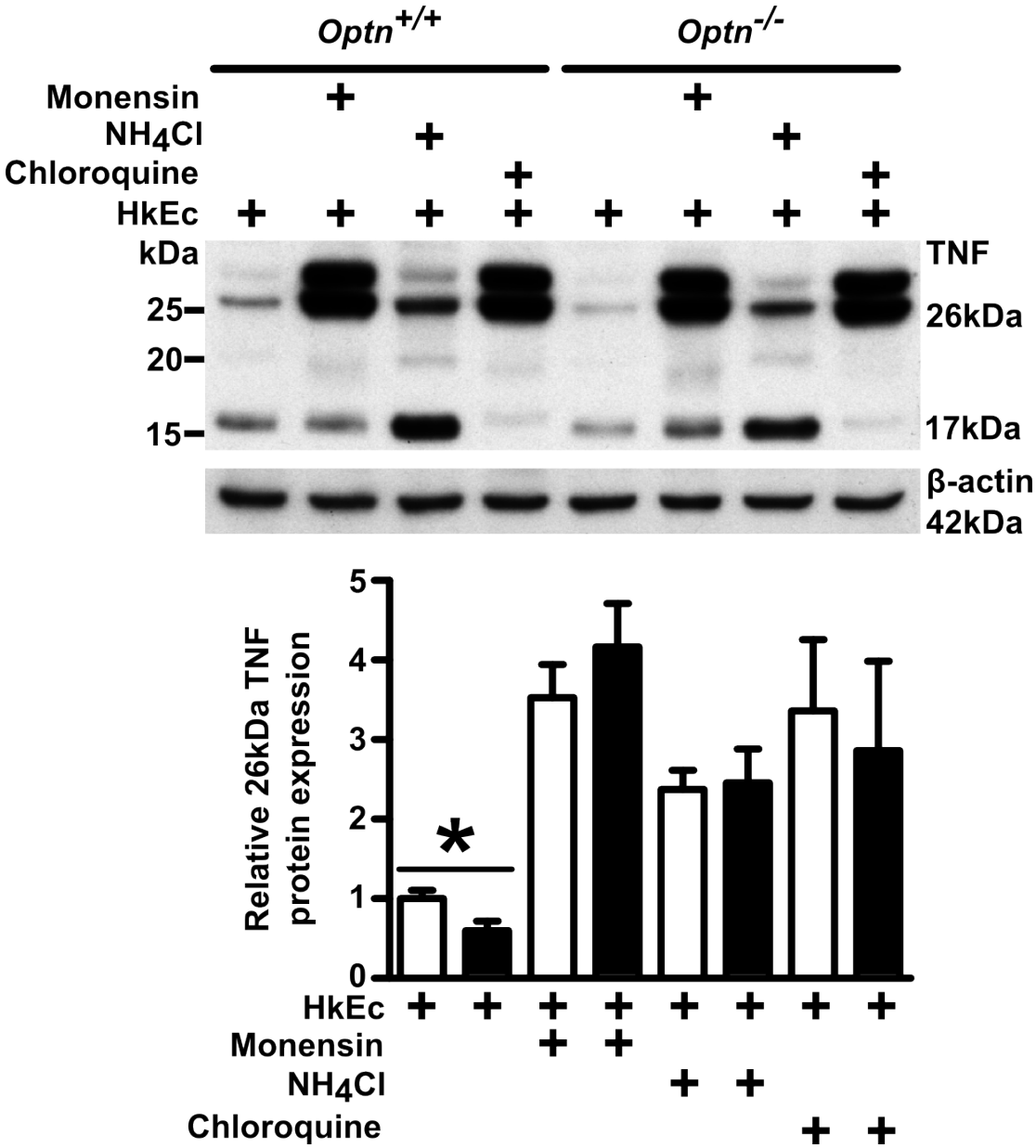

Figure 4.34 The TNF secretory defect is associated with significantly less intracellular 26kDa precursor TNF on immunoblot, which is normalised to wildtype levels on addition of lysosomal function inhibitors monensin, NH_4Cl and chloroquine. Representative immunoblot of TNF (above) showing 26kDa precursor TNF band and 17kDa secreted TNF band with β-actin loading control and quantification of TNF immunoblot (below). Results shown are mean ± SEM, all immunoblots are normalised to actin; n=3-8 mice/genotype over 4 independent experiments (*$p<0.05$; two-tailed, unpaired *t* test).

TNF trafficking in macrophages has been shown to occur via the endosomal compartment [162, 171]. Confocal immunofluorescence microscopy was used to investigate TNF trafficking in BMDM, which demonstrated reduced levels of intracellular TNF (Figure 4.35 and Figure 4.36) and replicated the immunoblot findings above (Figure 4.34). Additionally, significantly less colocalisation of TNF positive vesicles with EEA1 in *Optn*$^{-/-}$ BMDM was found (Figure 4.35). Similar to human MDM, TNF in BMDM were present in vesicles but also colocalised with the pan-Golgi marker GM130 (Figure 4.36).

The previous OPTN siRNA knockdown in HkEc stimulated THP-1 cells resulted in reduced TNF and IL6 release [191]. To investigate if any other cytokines were altered, a cytokine profiler array was used to measure intracellular cytokine levels in HkEc stimulated BMDM. *Optn*$^{-/-}$ BMDM had lower intracellular IL6 levels but higher CXCL13, IL16 and TIMP-1 levels. The significance of these findings would require further study.

The cytokine release defect in BMDM is specific to the lack of OPTN since there was no defect in TNF release in the absence of OPTN's binding partner myosin VI. *Myo6*$^{+/+}$ and *Myo6*$^{-/-}$ BMDM stimulated with Pam_3, LPS and HkEc did not secrete different levels of TNF (Figure 4.38).

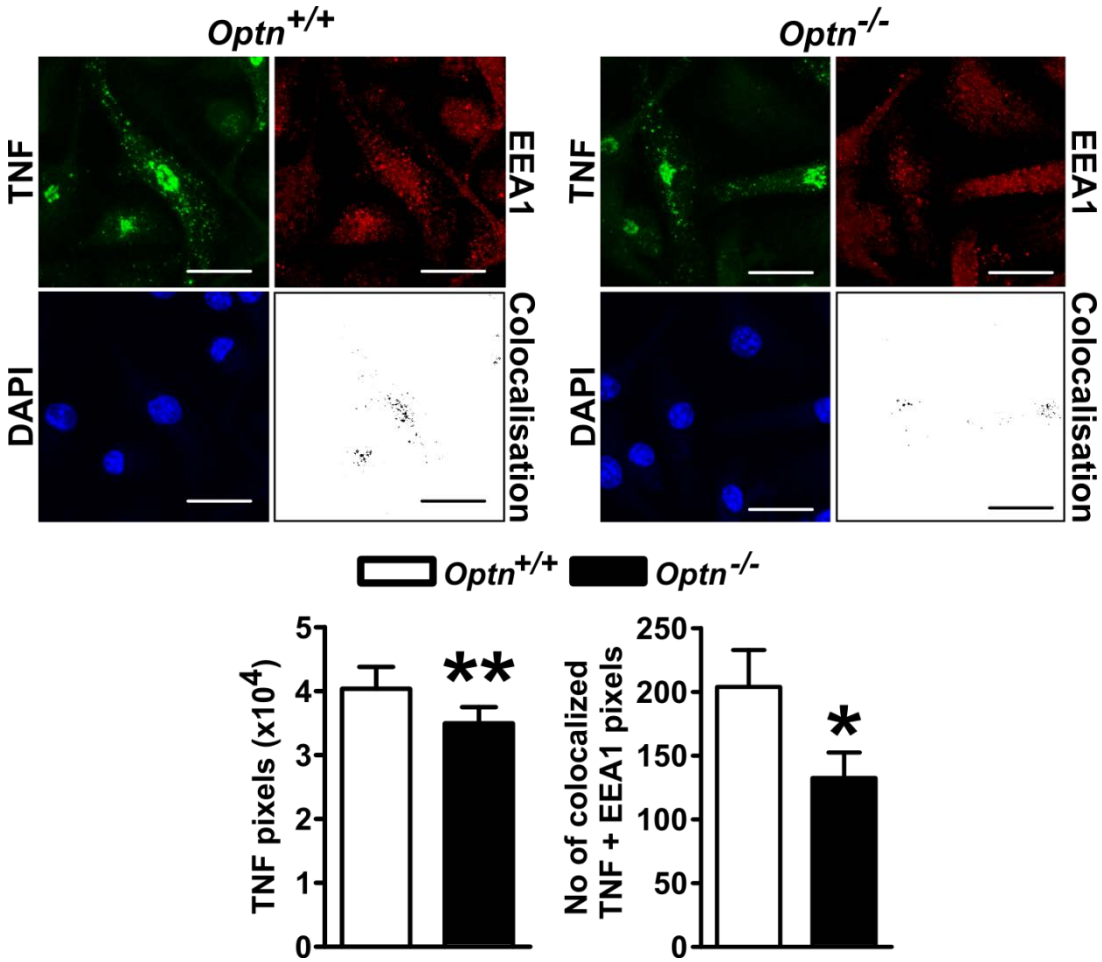

Figure 4.35 Confocal microscopy in HkEc stimulated *Optn*$^{+/+}$ and *Optn*$^{-/-}$ bone marrow derived macrophages show decreased colocalisation of TNF with early endosome antigen 1 in *Optn*$^{-/-}$ cells. Quantification showed significantly less intracellular TNF and colocalisation of TNF with EEA1 in *Optn*$^{-/-}$ BMDM (images at 63×, scale bar 20 µm; n=63-66 cells/genotype, over 2 independent experiments; results shown are mean ± SEM; *p<0.05, and **p<0.01; two-tailed, unpaired *t* test).

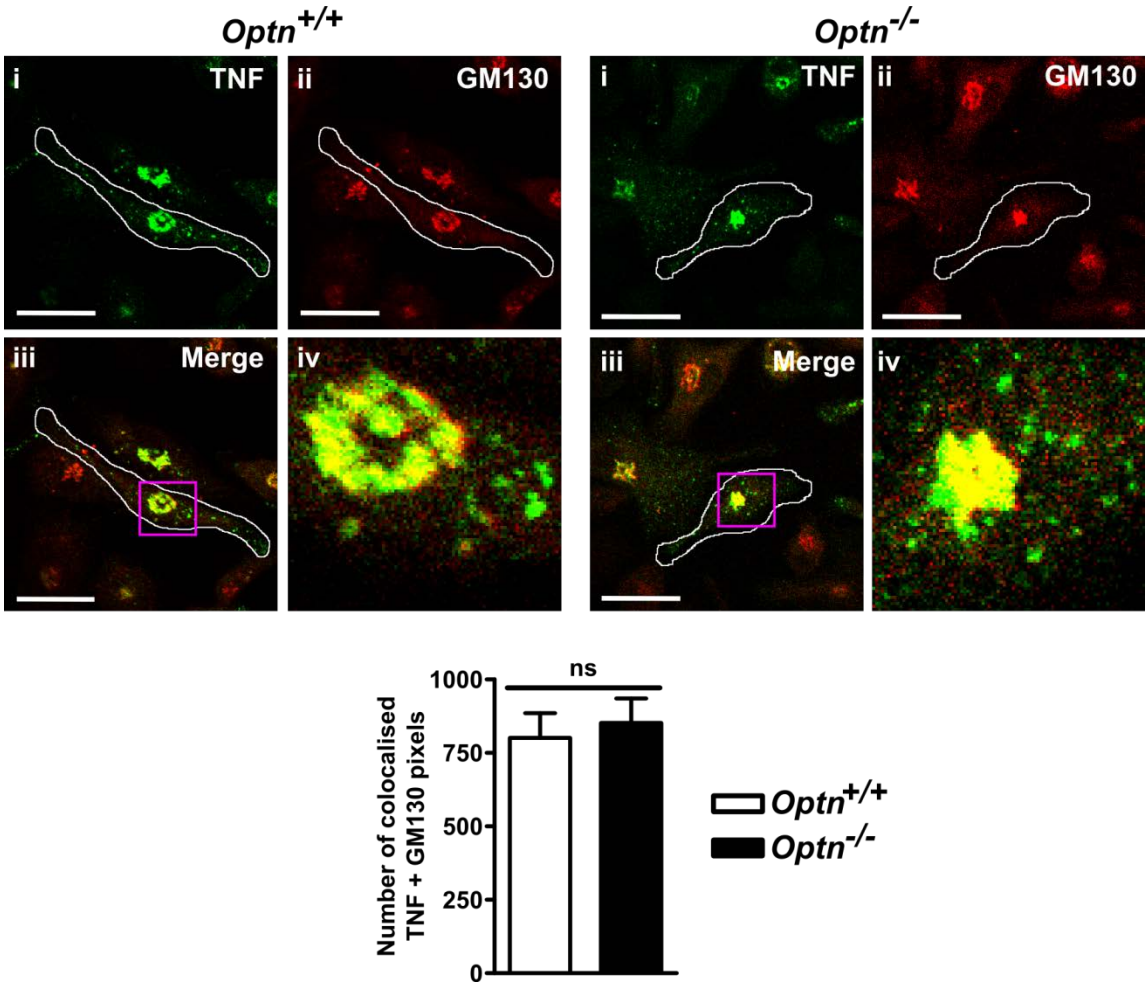

Figure 4.36 Confocal microscopy in HkEc stimulated *Optn*$^{+/+}$ and *Optn*$^{-/-}$ bone marrow derived macrophages show equal colocalisation of TNF with the Golgi marker GM130. Quantification showed no difference in colocalisation of TNF (i) with the Golgi marker GM130 (ii) in *Optn*$^{-/-}$ and *Optn*$^{+/+}$ BMDM (white outline) (image i, ii, iii at 63×, scale bar 20 µm; n= 35 cells/genotype; ns, non-significant; results shown are mean ± SEM, two-tailed, unpaired *t* test).

+											+
CXCL13	C5a	G-CSF	GM-CSF	CCL1	CCL11	sICAM-1	IFN-γ	IL-1α	IL-1β	IL-1ra	IL-2
IL-3	IL-4	IL-5	IL-6	IL-7	IL-10	IL-13	IL-12p70	IL16	IL-17	IL-23	IL-27
CXCL10	CXCL11	CXCL1	M-CSF	CCL2	CCL12	CXCL9	CCL3	CCL4	CXCL12	CCL5	CXCL12
CCL17	TIMP-1	TNF-α	TREM-1								
+											-

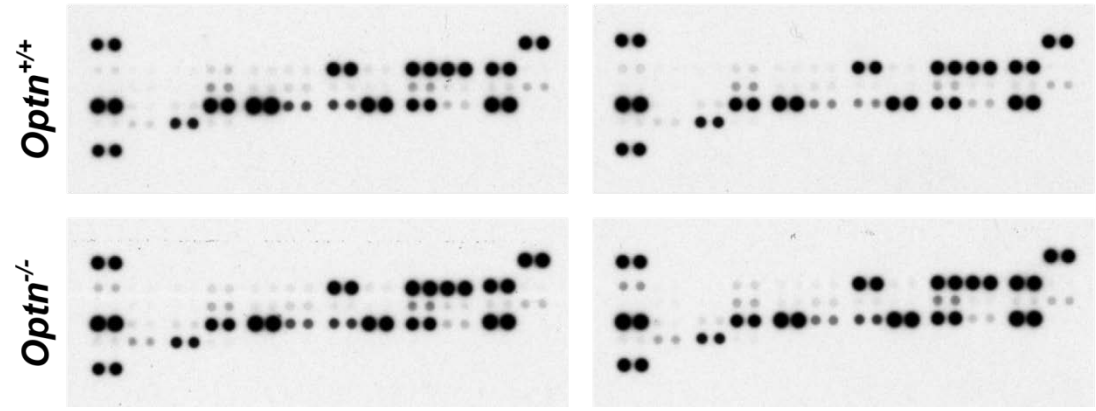

Figure 4.37 Stimulation of *Optn*$^{+/+}$ and *Optn*$^{-/-}$ bone marrow-derived macrophages with HkEc resulted in reduced levels of intracellular IL6 and elevated levels of CXCL13, IL16 and TIMP1 in *Optn*$^{-/-}$ cells. Intracellular cytokine levels were measured in HkEc stimulated *Optn*$^{+/+}$ and *Optn*$^{-/-}$ BMDM at four hours using a cytokine proteome profiler array. The cytokine array map (above) and cytokine array profiles (below) are shown (n=2 mice/genotype).

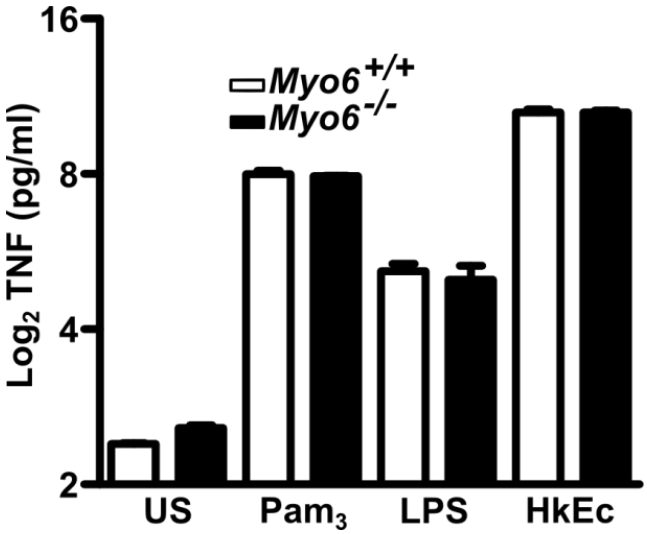

Figure 4.38 TNF secretion in *Myo6*$^{+/+}$ and *Myo6*$^{-/-}$ bone marrow-derived macrophages stimulated with Pam_3, LPS and HkEc for four hours was not different (n=2 mice/genotype). Experiments were performed by Dr Andrew Smith.

4.3 Discussion

In the previous chapter, low *OPTN* expression was discovered in MDM from CD patients but not in HC or UC patients. This low *OPTN* expression was associated with inheritance of a minor allele in a SNP downstream of the last *OPTN* exon.

In this chapter, the intracellular function of OPTN in macrophages was further elucidated. Subcellular fractionation of HkEc stimulated THP-1 cells and subsequent immunoblotting localised OPTN to the cytoplasmic and Golgi membrane containing but not lysosomal fractions. This is not surprising since OPTN has been widely shown to localise to the Golgi complex in other cell types [201]. Notably, OPTN is not localised to lysosomes, which we had previously showed to be the target of misdirected proinflammatory cytokines in human CD MDM. THP-1 cells are monocytic cells and not macrophages and as such may not truly reflect the subcellular localisation of proteins in macrophages. However, bacteria or LPS-stimulated THP-1 cells, become adherent and take on a ‘macrophage-like’ phenotype, which have been shown to be comparable to MDM functionally and in its expression of activation markers [256].

For decades, all tissue resident macrophages were widely accepted as originating from circulating blood monocytes [151]. More recently, fate mapping studies in mice have shown that brain macrophages/microglial cells originate from yolk sac macrophages that are set down during development and undergo clonal expansion during inflammation that is independent of circulating monocytes whilst skin macrophages/Langerhans cells are derived from yolk sac and foetal liver derived monocytes [154, 155]. Importantly, lamina propria macrophages have been shown to originate from recruited $Ly6C^+$ peripheral monocytes during inflammation [153, 257, 258]. As such, ‘THP-1 macrophages’ and MDM should be representative of lamina propria macrophages in view of its monocytic origins.

To confirm OPTN's binding partners, IP of OPTN and shotgun proteomics of immunoprecipitated proteins was performed in THP-1 cells. This identified known binding partners of OPTN such as myosin VI and myosin 18A, which localised OPTN to the Golgi complex. Gene ontology analysis of co-precipitated proteins with OPTN identified vesicles, organelles and the cytoskeleton as key roles for these proteins. This verified the antibody that was used but also the localisation of OPTN to the Golgi complex demonstrated with subcellular fractionation. This focused attention on the Golgi complex as the place where OPTN likely functions in MDM. Although mass spectrometry allows good global protein identification, peptides from different proteins may share similar fragmentation spectra or when alternatively spliced may result in misidentification of proteins. This was minimised by setting the threshold of identification of proteins at 5 peptides. However, the identification of myosin VI and 18A as well as gene ontology analysis provides good evidence of successful shotgun proteomics.

Others in our research group previously showed that CD was associated with the phenotype of reduced proinflammatory TNF secretion from macrophages that results in impaired neutrophil recruitment and bacterial clearance [187]. TNF is secreted via endosomes in mouse RAW264.7 macrophages [171]. Confocal microscopy in MDM localised TNF to OPTN at the Golgi complex but not in peripheral vesicles where TNF localises to endosomes. These findings strengthen the subcellular localisation of OPTN to the Golgi complex in macrophages but also suggest a role for OPTN in the trafficking of TNF at the Golgi complex in contrast to peripheral vesicles or the plasma membrane. These findings are limited by the permeabilisation of macrophages prior to confocal staining that diminishes the staining of OPTN in the cytoplasm that was seen in subcellular fractionation. However, the localisation of OPTN to the Golgi has been widely seen in other non-immune cells and has been shown to be similar in human macrophages for the first time here.

OPTN expression was significantly upregulated when MDM were exposed to HkEc, the TLR ligands LPS and Pam_3 as well as the NOD2-ligand MDP. *OPTN* gene and protein induction was not equal between different stimuli and also between MDM and THP-1 cells. LPS and HkEc were the strongest or most significant stimulus of OPTN in MDM and THP-1 cells in contrast to Pam_3 and MDP. The rise in OPTN protein expression was fastest with HkEc in contrast to Pam_3 and MDP in THP-1 cells but resulted in comparable levels at 24 hours. Kinetic studies of OPTN expression in MDM was not performed due to limited numbers that are obtained from cell culture. OPTN protein stimulation in MDM was lower with Pam_3 and MDP in contrast to HkEc and LPS at 24 hours. This difference at 24 hours is possibly due to actual differences in stimulation of OPTN in MDM since the kinetics of OPTN induction in MDM is likely identical to THP-1 cells in view of the similarities between MDM and THP-1 cells when activated. However, this cannot be conclusively proven without actual kinetic studies into OPTN induction in MDM.

An additional consideration is what the baseline levels of OPTN may be in tissue resident macrophages in healthy bowel and CD. Lamina propria macrophages are potentially exposed to higher levels of intraluminal TLR and NLR ligands but conversely may be strongly influence by anti-inflammatory factors in their immediate environment. Functional studies remain difficult due to the extensive digestion required in the extraction process of lamina propria macrophages but is a potential avenue to explore coupled with FACS sorting. An alternative is to perform intravital studies in mice.

To investigate the role of OPTN in macrophages, a knockout mouse was obtained. The $Optn^{-/-}$ compared to their $Optn^{+/+}$ littermates exhibited normal litter sizes, lived a normal lifespan, did not develop spontaneous colitis and did not show gross differences in organ histology or percentage of B cells, T cells, neutrophils and monocytes in the peripheral blood and bone

marrow. This was not surprising since *NOD2*, the strongest associated gene with CD when knocked out, the *Nod2*$^{-/-}$ mouse does not develop a spontaneous colitis or phenotype. This supports our understanding of CD as a syndrome where different defects of modest effect for example impaired bacterial handling with *OPTN* or defective autophagy with *ATG16L1* result in a similar phenotype of colitis, namely CD.

Peritoneal macrophages are often used as a source of macrophages due to accessibility and ease of harvest. Naïve peritoneal macrophages can be harvested from the peritoneum but to increase the numbers harvested a sterile inflammation is set up using sterile thioglycollate broth that results in an early neutrophil then late macrophage migration into the peritoneal cavity as first described by Gallily *et al* in 1964 as a modification of Barski's method [259, 260]. Similar to human macrophages, OPTN is upregulated in mouse peritoneal macrophages upon stimulation with HkEc, Pam_3 and MDP. TNF release in peritoneal macrophages showed a dose dependent increase in keeping with what we previously found in human macrophages, which occurs early with the greatest rise at 4 hours that plateaus at 8 hours to 24 hours. Importantly OPTN deficiency did not affect TNF release in peritoneal macrophages.

Macrophage phagocytosis and killing also did not reveal any difference between wildtype and knockout cells. This was surprising since, it was hypothesised that since OPTN was involved in autophagy of bacteria its absence might result in defective killing. However, autophagic mechanisms involved in intracellular bacterial killing are thought to be switched on to bacteria such as *Salmonella* that escape the phagosome that are then engulfed in double membrane autophagosomes [125]. As such, the lack of difference may be due to the *E. coli* used, which are readily killed in phagosomes. However, a previous study has shown that thioglycollate induction itself can result in defective bacterial killing in peritoneal macrophages [261]. Electron microscopy of the peritoneal macrophages

found multiple large vacuoles that may result from phagocytosis of the thioglycollate broth. The presence of multiple large vacuoles may potentially affect the normal trafficking of cytokines and phagocytosis of bacteria, abolishing any difference due to the absence of OPTN.

In order to circumvent the problem of preactivation in the thioglycollate induced peritoneal macrophages, M-CSF induced bone marrow derived macrophages were obtained, which are more immature and quiescent [262]. Electron microscopy of unstimulated and HkEc fed BMDM did not show any of the large vacuoles seen in TiPM and the presence of HkEc phagosome in *Optn*$^{-/-}$ and *Optn*$^{+/+}$ cells. Previously, other groups have reported that knockdown of OPTN resulted in fragmentation of the Golgi complex in HeLa cells [201]. In view of the thin sections obtained and the arrangement of the Golgi complex, Golgi fragmentation is difficult to identify on electron microscopy. However, Golgi complex staining on confocal microscopy did not show obvious fragmentation of the Golgi in *Optn*$^{-/-}$ BMDM compared to wildtype cells. This raises the question that the fragmentation seen in HeLa cells with OPTN RNAi is either cell specific to HeLa cells or was a result of non-specific effects of the siRNA used on the Golgi or other proteins required for maintenance of the Golgi complex structure.

Phagocytosis and killing of *E. coli* was no different between *Optn*$^{-/-}$ and *Optn*$^{+/+}$ BMDM. The lack of a difference in the knockout cells despite use of BMDM would suggest that the thioglycollate vacuoles did not affect the physiological functions of phagocytosis or killing in these cells. Additionally, it would be surprising to find a difference in phagocytosis in the absence of OPTN when subcellular fractionation and confocal microscopy did not localise it to lysosomes or the plasma membrane in macrophages where phagosomes are formed. The argument against a defect in killing in the absence of OPTN is likely because *E. coli* is readily killed by phagosomes in macrophages independent of autophagosomes and OPTN.

Basal autophagic flux as measured by accumulation of autophagosomal LC3-II in *Optn*$^{+/+}$ and *Optn*$^{-/-}$ BMDM was not different. This is not surprising since OPTN has been shown to function as an adaptor in selective autophagy that binds to ubiquitinated bacteria and brings them to the autophagosome (Figure 1.3). OPTN has not been shown to play a role in the formation of the LC3-II bound double membrane autophagosome. When BMDM were stimulated with HkEc, there was a small rise then gradual fall in autophagosomal LC3-II levels, dropping below baseline levels, stable levels of cytoplasmic LC3-I and crucially, no difference in LC3-I or LC3-II levels in wildtype or knockout cells. This lack of difference indicates that the breakdown of HkEc in phagosomes within macrophages is not dependent on OPTN, which is unsurprising. A shortcoming of this experiment is the use of killed versus live *E. coli* since OPTN and autophagy may only be important when live bacteria escape the phagosome. Therefore, live *Salmonella* that escapes the phagosome may be a better bacteria to use.

However, HkEc stimulation of BMDM resulted in significantly lower levels of secreted proinflammatory TNF and IL6, with significantly higher levels of anti-inflammatory IL10 and the neutrophil chemokine CXCL1. Similar to CD macrophages, this defective proinflammatory cytokine secretion was occurring at the protein level since *Tnf, Il6, Il10* and *Cxcl1* gene transcription was not statistically different. This defect was also not due to differences in cell viability measured using the MTT assay.

The defect in cytokine secretion was initially postulated to be due to an abnormal unfolded protein response or endoplasmic reticulum (ER) stress, which has been associated with CD [263-265]. Immunoblot for various ER stress molecular chaperones such as GRP78, GRP94 and CHOP as well as *Xbp1* splicing all did not show increased ER stress in *Optn*$^{-/-}$ BMDM exposed to HkEc suggesting that ER stress was not accounting for the defect in TNF and IL6 release.

Our group previously found that CD macrophages secreted lower levels of proinflammatory TNF due to misdirected trafficking to lysosomes for destruction. Similarly, when *Optn*$^{-/-}$ BMDM were stimulated with HkEc in the presence of lysosomal function inhibitors, intracellular TNF levels normalised to wildtype levels. This indicates that adequate amounts of TNF are synthesised by the BMDM but are misdirected and destroyed in lysosomes. By contrast, stimulation of *Optn*$^{-/-}$ BMDM with HkEc in the presence of bafilomycin A, the autophagy inhibitor TNF levels rose significantly higher than in the wildtype mice indicating that in the absence of OPTN, TNF is degraded via a bafilomycin A dependent pathway.

In contrast to the signalling pathways of cytokine gene transcription, much less is known about the complex network of cytokine trafficking within cells and particularly macrophages. Work in mouse macrophage cell lines have begun to shed light on the complex pathways of cytokine vesicle trafficking particularly TNF. Both TNF and IL6 have been found to share a similar pathway via recycling endosomes where they then are secreted via different pathways to the extracellular space [171]. Although OPTN has previously been postulated to have a role in vesicle fusion at the plasma membrane, confocal microscopy in macrophages did not show staining at the plasma membrane and the fact that IL6 and TNF are trafficked separately to the plasma membrane but both have reduced secreted levels would argue against a role for OPTN at the plasma membrane in macrophage cytokine secretion.

To investigate if the defective cytokine secretion was due to fusion defects at the plasma membrane or more proximal in the vesicle pathway at the Golgi complex, confocal microscopy of TNF and early endosome antigen 1 (EEA1) was performed that showed reduced colocalisation of TNF with EEA1 in *Optn*$^{-/-}$ BMDM. This suggests that the defect in *Optn*$^{-/-}$ BMDM lies proximally at the Golgi complex since there was significantly less TNF

staining, less colocalisation with EEA1 but no difference in TNF at the Golgi complex.

In addition to the defective TNF and IL6 secretion, IL10, CXCL1, CXCL13, IL16 and TIMP1 were secreted at higher levels in *Optn*$^{-/-}$ compared to *Optn*$^{+/+}$ BMDM. The fact that some cytokines were secreted at higher levels in the *Optn*$^{-/-}$ BMDM adds validity to the findings of reduced TNF and IL6 secretion and suggests that the defective secretion was genuine and not simply due to poorly viable cells. Little is known about cytokine trafficking within cells beyond TNF, IL6 and IL10, which is secreted via a different pathway that will make clarifying the trafficking pathways more difficult for CXCL1, CXCL13, IL16 and TIMP1.

Finally, there was no difference in TNF release between HkEc stimulated *MyoVI*$^{-/-}$ BMDM compared to wildtype BMDM. This suggests that the defect in cytokine processing for secretion is specific to OPTN deficiency occurring during packaging of cytokines at the Golgi complex and not during trafficking of vesicles since myosin VI links vesicles to actin via OPTN. The lack of difference in TNF release in *MyoVI*$^{-/-}$ BMDM also suggests that TNF traffics via myosin VI independent pathways.

Chapter 5 Animal Models of Inflammation

5.1 Introduction

Animal use in scientific research can be traced back to the 17th Century with William Harvey's use of animals to study the blood circulation. However, it was the thalidomide tragedy that resulted in a rapid rise in the use of animals initially to test drug toxicity then later to develop animal models of human disease to better treat and understand disease pathophysiology.

Murine models of intestinal inflammation have provided invaluable insights into the pathophysiological processes that underlie CD and UC. No animal model can fully replicate human CD and UC. Two different induced colitis models were chosen, the first being the *Citrobacter rodentium* model of colitis [266], due to the similar effects of *Citrobacter* infection in mice bowel as enteropathic *E. coli* in humans and the association of *E. coli* with CD as discussed earlier [81]. The second model was the dextran sodium sulphate (DSS) chemical induced model of colitis due to its induction of a more UC-like superficial colitis.

Citrobacter infection in the GI tract results in formation of attaching and effacing (A/E) lesions, which are characterised by the attachment of *Citrobacter* to the intestinal epithelium, effacement of the brush border microvilli and formation of pedestals between the bacteria and epithelial cells [266]. Disruption of the epithelial barrier occurs via the translocation of bacterial effectors into epithelial cells using *Citrobacter*'s type 3 secretion system (T3SS), resulting in the dissemination of bacteria into the lamina propria and recruitment of neutrophils into the bowel and clearance of *Citrobacter* [267].

The mechanism of action of DSS in inducing colitis is not entirely clear. However, DSS is widely believed to be directly cytotoxic to colonic epithelial

cells and result in the breakdown of epithelial integrity [268]. This allows intraluminal bacteria to invade into the normally sterile lamina propria layer.

5.2 Results

5.2.1 Zebrafish model of *Salmonella* infection

To determine the importance of OPTN in antibacterial response across species, we utilised a zebrafish infection model involving *Salmonella enterica* [269]. *Optn* expression was localised to the intestinal bulb, brain and eye in both embryonic and larval stages of development (Figure 5.1). As previously shown in humans (Figure 4.8 and Figure 4.9) and mice (Figure 4.20) *optn* expression was elevated after bacterial stimulation with *Salmonella* via both an oral (immersion) infection and direct injection of bacteria into the yolk sac of embryos 2 days post fertilisation (dpf) (Figure 5.2).

Figure 5.1 *In situ* hybridisation of *optn* in zebrafish embryos and larvae reveal expression in the brain/eyes and the intestinal bulb. Images are of the embryo (i) and larvae (ii) with arrows pointing at the brain/eyes (blue) and the intestinal bulb (red). Experiments were performed by Dr Stefan Oehlers and Professor Philip Crosier, University of Auckland.

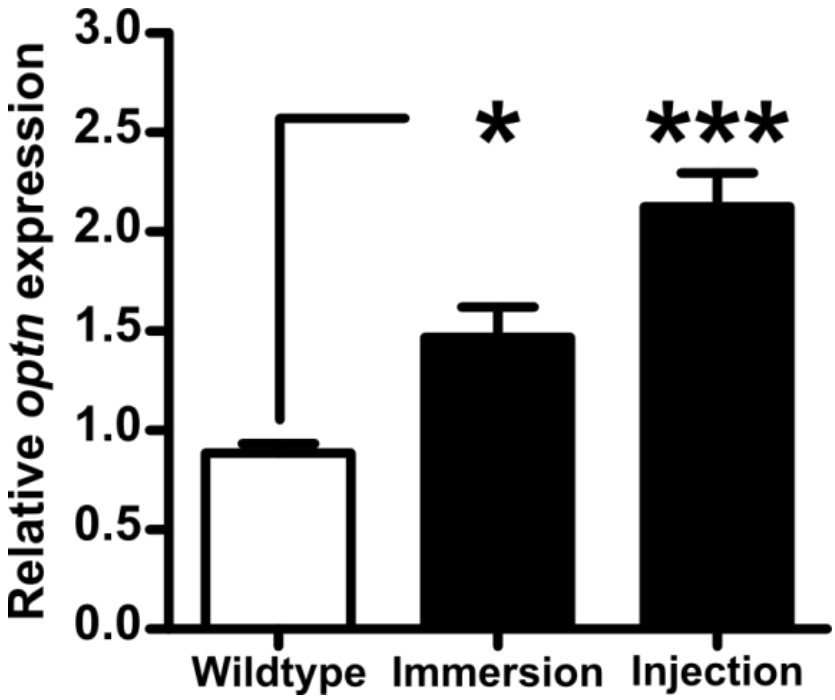

Figure 5.2 Zebrafish *optn* expression is significantly increased both in (bath) immersion and injection infection of *Salmonella* at 24 hours. Results shown are mean ± SEM; n=16-19 zebrafish/group (*p<0.05 and ***p<0.001; two-tailed, unpaired *t* test). Experiments were performed by Dr Stefan Oehlers and Professor Philip Crosier, University of Auckland.

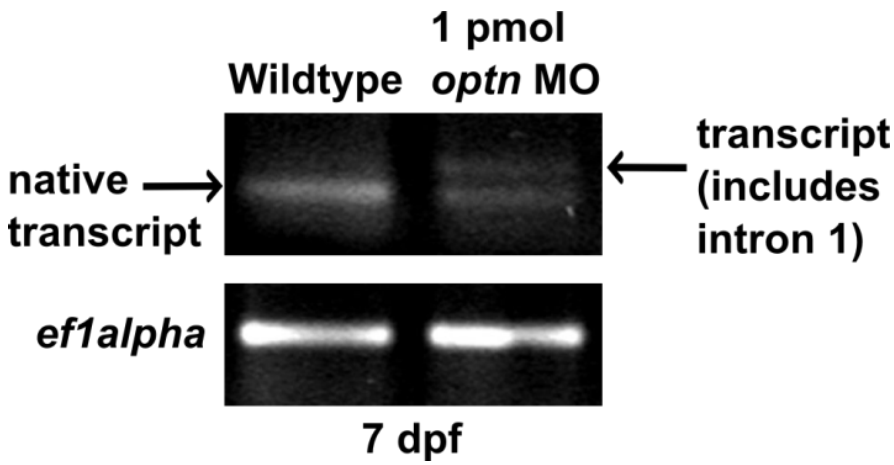

Figure 5.3 *Optn* knockdown in zebrafish was achieved by retention of *optn* intron 1 using an *optn* morpholino. RT-PCR of wildtype and *optn* knockdown in zebrafish at 7 days post fertilisation (dpf), by retention of *optn* intron 1 using 1 pmol of an *optn* morpholino (MO) that targets the intron 1/exon 2 junction, shown with *ef1alpha* loading control. Experiments were performed by Dr Stefan Oehlers and Professor Philip Crosier, University of Auckland.

To study the functional consequence of Optn deficiency in zebrafish antibacterial responses, *optn*-specific morpholinos (MO) were used (Figure 5.3). *Optn* knockdown resulted in an increased susceptibility to *Salmonella* infection compared to wildtype fish, and those treated with control morpholinos (Figure 5.4).

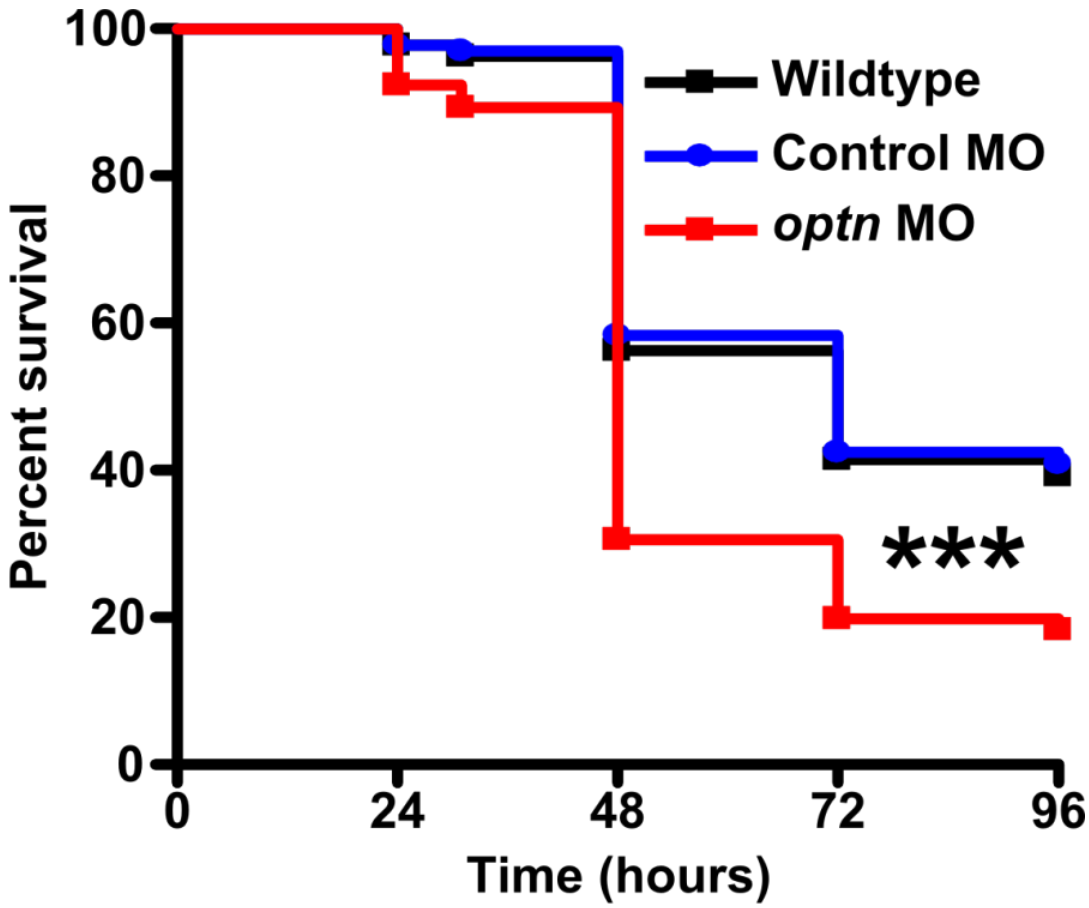

Figure 5.4 *Optn* knockdown resulted in significantly greater mortality compared to controls in zebrafish injected with *Salmonella.* Results shown are mean; n=104–119 zebrafish/group over 2 independent experiments (***p<0.001, logrank test). Experiments were performed by Dr Stefan Oehlers and Professor Philip Crosier, University of Auckland.

5.2.2 Mouse model of subcutaneous *E. coli* infection

To determine the importance of OPTN in host antibacterial response, models of infection were employed in two evolutionarily divergent species, zebrafish and mice (Figure 1.6). To exclude a baseline difference in growth and weight, naïve 9 to 12 week old *Optn*$^{+/+}$ and *Optn*$^{-/-}$ mice were fed standard chow, housed in specified pathogen free (SPF) cages and weighed daily. The *Optn*$^{+/+}$ and *Optn*$^{-/-}$ mice did not show a difference in weight over a two-week monitoring period (Figure 5.5).

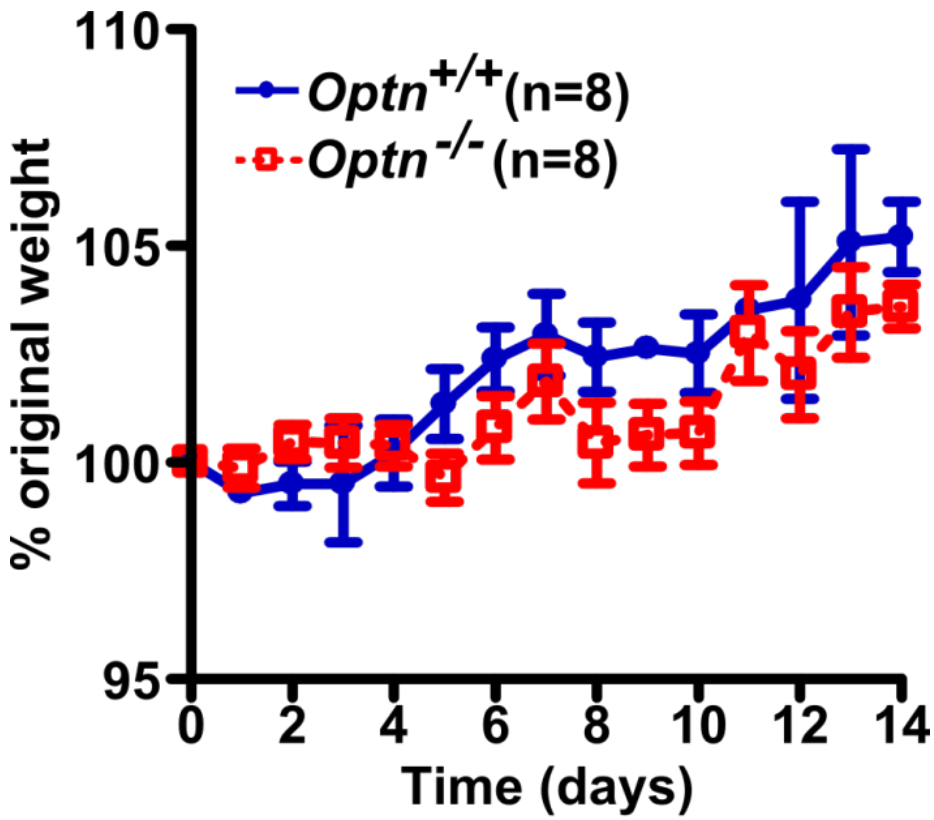

Figure 5.5 There was no difference in the weight gain of naïve *Optn*$^{+/+}$ and *Optn*$^{-/-}$ mice. Mice were fed regular chow, housed under similar conditions and weighed daily over a 14 day period of monitoring. Results are mean ± SEM; n=8 mice/genotype (two-tailed, unpaired *t* test).

Initial dose response experiments showed that increasing the dose of subcutaneous HkEc resulted in increasing weight loss in C57BL/6 wildtype mice (Figure 5.6). The local acute inflammatory response in the skin resulted in the formation of nodules that were larger with increasing dose of HkEc (Figure 5.6). The highest dose of 10^9 HkEc resulted in ulceration of the nodules but not the lower doses of 10^8 (Figure 5.7) and below (not shown). The ulcerated nodules in mice injected with 10^9 HkEc were associated with significant inflammatory cell infiltration at day 9 with epithelialisation of the ulcer in contrast to skin injected with 10^7 HkEc (Figure 5.8). *Optn*$^{+/+}$ and *Optn*$^{-/-}$ mice injected with 10^8 HkEc subcutaneously did not show a difference in weight loss or nodule size over the first six days (Figure 5.9).

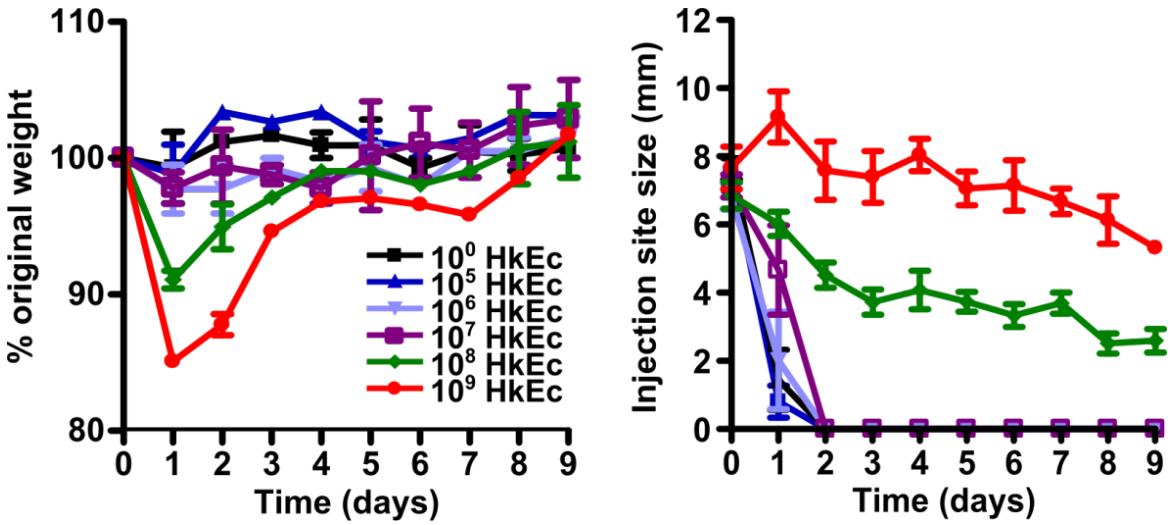

Figure 5.6 Subcutaneous HkEc back injection causes greater weight loss and larger injection site size at higher doses of HkEc. Dose response experiments shows that higher concentrations of HkEc causes greater weight loss at day one to two post injection (left) with larger injection site sizes (right). Results shown are mean ± SEM, n=2 mice/dose with 2 injection sites/mouse.

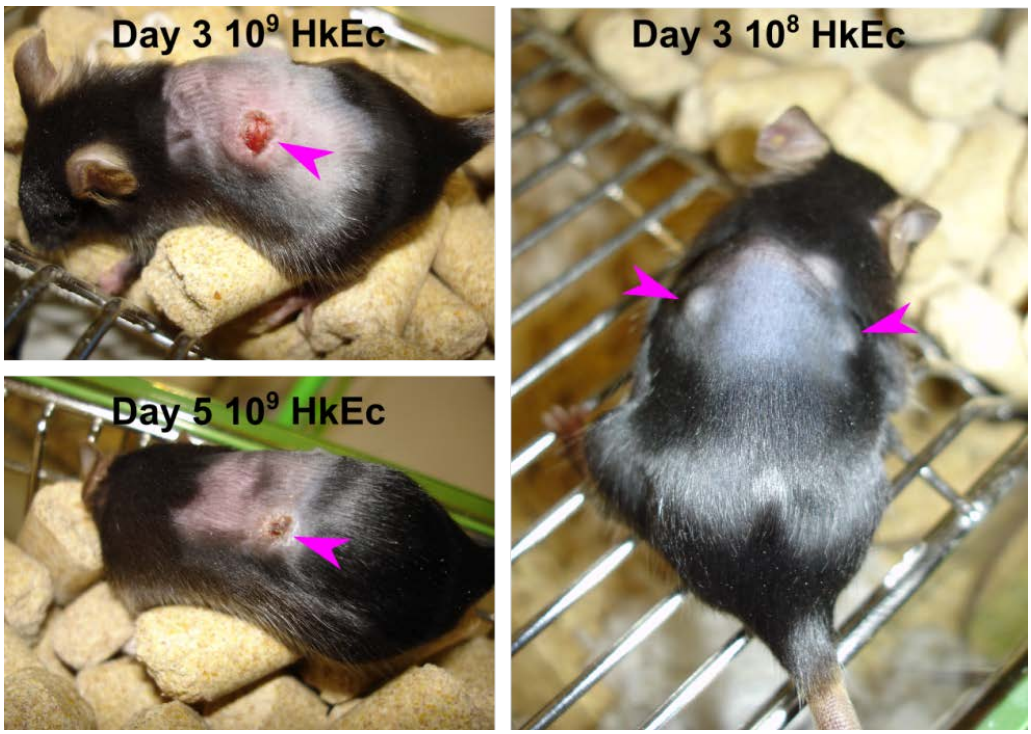

Figure 5.7 Subcutaneous HkEc back injection creates nodules that only ulcerate at 10^9 bacteria. Images show that at the highest dose of HkEc (10^9) mice developed nodules with ulceration at day 3 (pink arrow, top left), which at day 5 has begun to heal (pink arrow, bottom left). Mice injected with a lower dose (10^8) develop nodules but no ulceration (pink arrows, right).

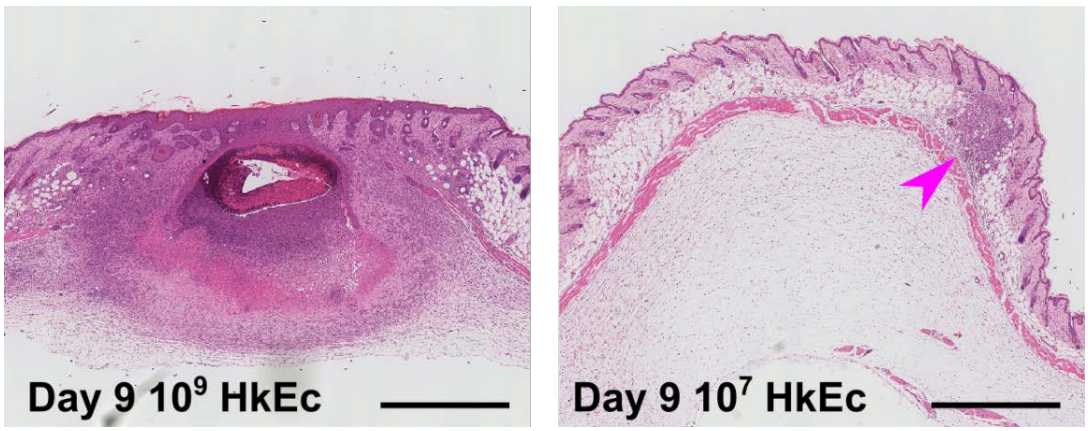

Figure 5.8 Subcutaneous HkEc back injection causes a large inflammatory cell infiltrate at 10^9 but not at 10^7 bacteria. H&E staining of skin injection sites shows a healing ulcer at day 9 in the highest (10^9 HkEc) injected dose (left) with a large inflammatory cell infiltration, in contrast to skin injected with a lower dose (10^7 HkEc) with minimal inflammatory cell infiltration (pink arrow, right) by day 9. Magnification 2.5×, scale bar 1 mm.

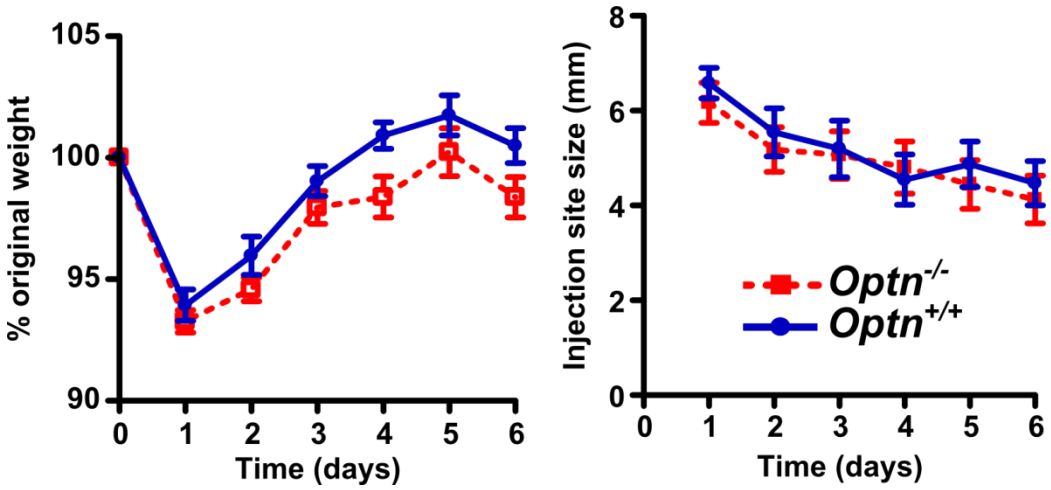

Figure 5.9 Subcutaneous HkEc back injection in *Optn*$^{+/+}$ and *Optn*$^{-/-}$ mice did not show a difference in weight loss or injection site size. *Optn*$^{+/+}$ and *Optn*$^{-/-}$ mice were injected with 10^8 HkEc and monitored over a six day period. Results shown are mean ± SEM, n= 18-21 mice/genotype over 3 independent experiments (two-tailed, unpaired *t* test).

5.2.3 Mouse model of intraperitoneal *E. coli* infection

When peritonitis was induced in mice with live *E. coli* there was a dose dependent increase in the mortality of both *Optn*$^{+/+}$ and *Optn*$^{-/-}$ mice (Figure 5.10) but the *Optn*$^{-/-}$ mice appeared to be slightly more susceptible to *E. coli* inoculation. Compatible with the observed reduction of the release of TNF from cultured macrophages, the levels of TNF in the circulation were lower in *Optn*$^{-/-}$ mice (Figure 5.10).

The numbers of macrophages and neutrophils in the naïve peritoneum of *Optn*$^{+/+}$ and *Optn*$^{-/-}$ mice were not different (Figure 5.11). 24 hours after the induction of an *E. coli* peritonitis, there was a significant reduction in the number of CD11b$^+$ F4/80$^+$ macrophages in the peritoneal washout, in both *Optn*$^{+/+}$ and *Optn*$^{-/-}$ mice, with no significant differences between them. By contrast, Gr1$^+$ neutrophil numbers were significantly increased at 24 hours after the induction of peritonitis but the elevation in *Optn*$^{+/+}$ animals was significantly greater than in *Optn*$^{-/-}$ mice (p=0.007) (Figure 5.11). Representative FACS plots are shown with percentage Gr1$^+$ cells.

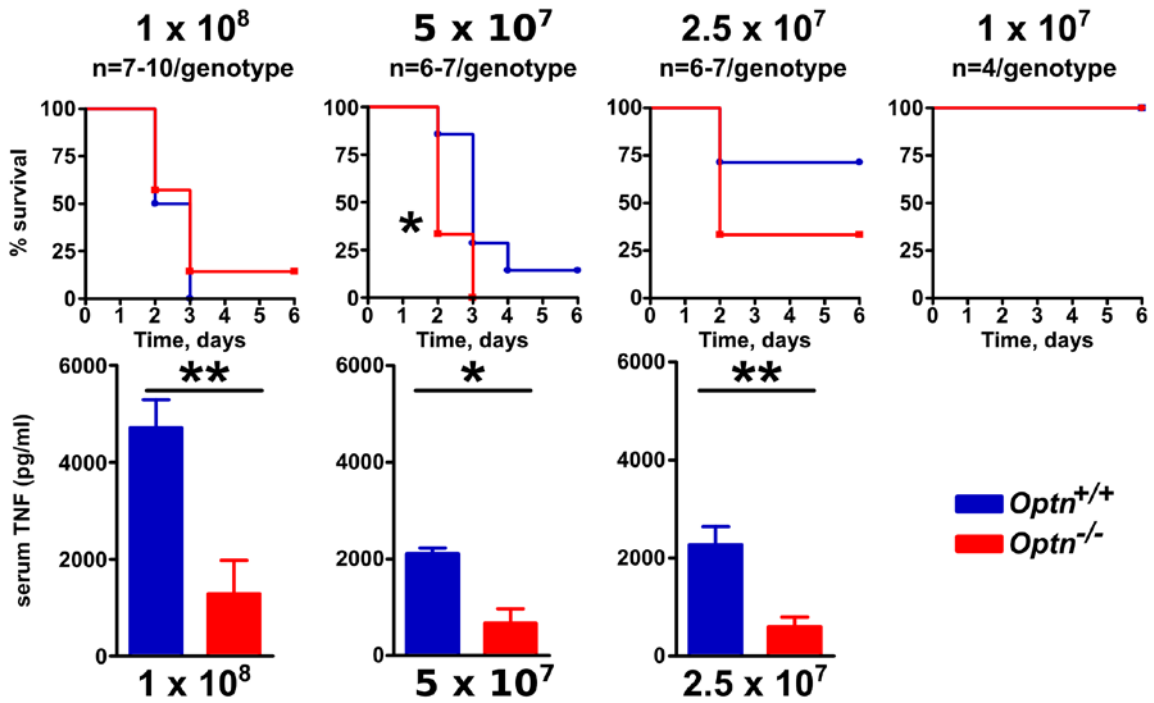

Figure 5.10 Live intraperitoneal *E. coli* caused greater mortality in *Optn*$^{-/-}$ mice with significantly lower levels of serum TNF. Mortality in *Optn*$^{+/+}$ and *Optn*$^{-/-}$ mice increased with higher doses of bacteria but was significantly greater in *Optn*$^{-/-}$ mice at 5×10^7 *E. coli*. There was significantly less serum TNF in the *Optn*$^{-/-}$ mice at three different doses. Results shown are mean ± SEM; n=4-10 mice/genotype, over 4 independent experiments (*p<0.05, **p<0.01; two-tailed, unpaired *t* or logrank test).

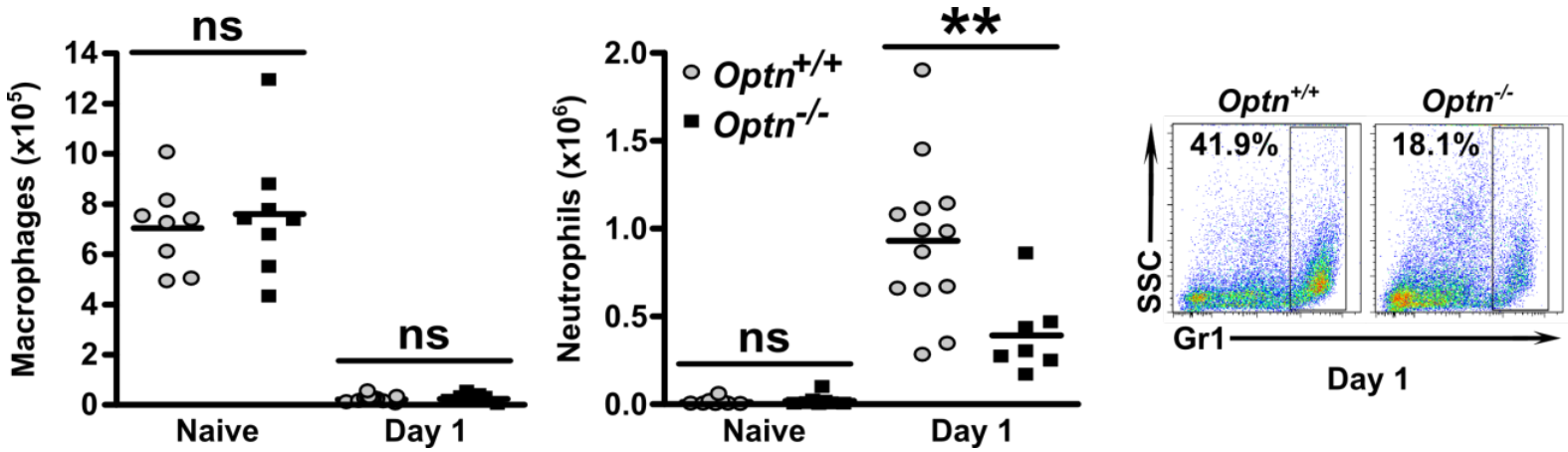

Figure 5.11 Intraperitoneal *E. coli* injection resulted in robust recruitment of neutrophils to the peritoneum that was significantly impaired in *Optn*$^{-/-}$ mice. Peritoneal washouts after *E. coli* injection revealed no statistically significant difference (ns) in CD11b^{+} F4/80^{+} macrophages or Gr1^{+} neutrophils in the naïve peritoneum and one day after E. coli injection. By contrast, there was significantly less Gr1^{+} neutrophils recruited ($p<0.01$) to the *Optn*$^{-/-}$ peritoneum at day one. Representative flow cytometry plots with percentage of Gr1^{+} neutrophils at day one are shown. Results shown are mean (**$p<0.01$; two-tailed, unpaired *t* test).

5.2.4 Mouse model of *Citrobacter rodentium* colitis

To investigate the antibacterial role of OPTN in the bowel, a *Citrobacter rodentium* bacteria induced colitis model was used. Following inoculation with *Citrobacter*, the *Optn*$^{-/-}$ mice demonstrated increased susceptibility in the first two days after *Citrobacter* inoculation, as evidenced by significantly greater weight loss (Figure 5.12) and increased mortality (Figure 5.12). This increased susceptibility in the *Optn*$^{-/-}$ mice was not due to a difference in faecal *Citrobacter* levels (Figure 5.13) and *Citrobacter* was seen to invade the normally sterile large bowel crypts in both *Optn*$^{+/+}$ and *Optn*$^{-/-}$ mice (Figure 5.14).

Citrobacter inoculation resulted in increased serum levels of TNF, IL6 and CXCL1 in both *Optn*$^{+/+}$ and *Optn*$^{-/-}$ mice at day 2 as compared with naïve animals (Figure 5.15). In the *Optn*$^{+/+}$ mice, there was a further increase in the levels of IL6 and CXCL1 at day 9 whereas the level of TNF remained similar to that on day 2. *Optn*$^{-/-}$ mice released equivalent levels of CXCL1 at day 2 but demonstrated a less pronounced increase in TNF and IL6 in comparison to wildtype animals. By day 9 post *Citrobacter* inoculation, TNF, IL6 and CXCL1 were all significantly lower in *Optn*$^{-/-}$ compared to *Optn*$^{+/+}$ mice. The rise in serum IL6 and CXCL1 between day 2 and day 9 seen in *Optn*$^{+/+}$ mice was not evident in *Optn*$^{-/-}$ animals.

Tnf and *Cxcl1* gene expression in the large bowel was elevated at day 2 compared to naïve animals in *Optn*$^{+/+}$ mice and further increased at day 9 (Figure 5.16). In contrast to the diminished serum TNF and CXCL1 levels, *Tnf* and *Cxcl1* expression in the *Optn*$^{-/-}$ mice was not statistically different compared to *Optn*$^{+/+}$ mice at day 2 and day 9. By contrast, *Il6* expression at day 2 and day 9 was unchanged compared to naïve mice.

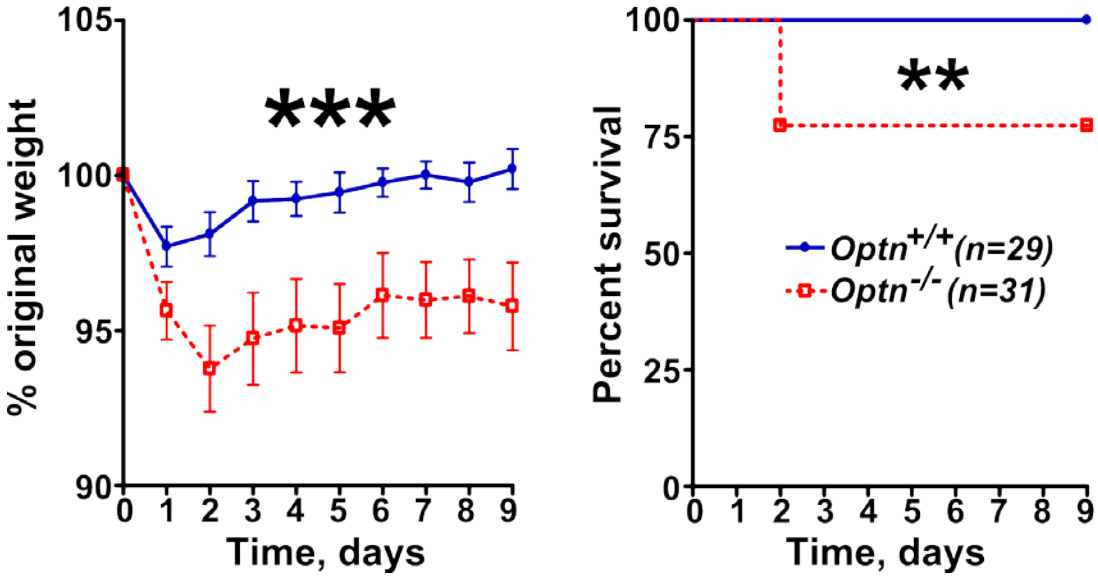

Figure 5.12 *Citrobacter rodentium* induced colitis causes significantly more weight loss and mortality in *Optn*$^{-/-}$ mice compared to *Optn*$^{+/+}$ mice. Results shown are mean ± SEM; n=29–31 mice/genotype over 5 independent experiments (**p<0.01 and ***p<0.001; two-tailed, unpaired *t* test and logrank test).

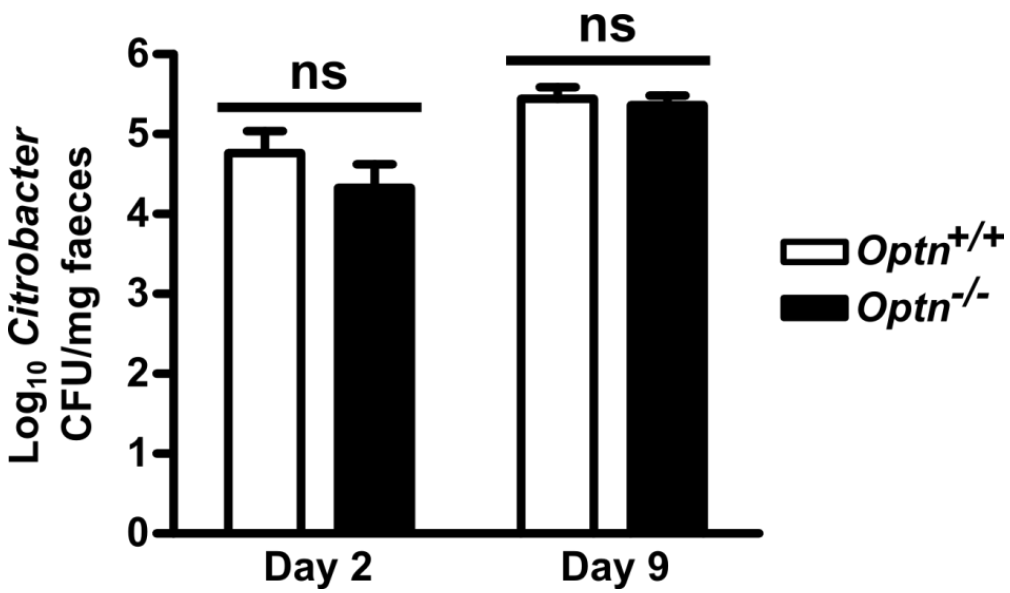

Figure 5.13 *Citrobacter rodentium* levels in the faeces at day 2 and 9 were no different between *Optn*$^{+/+}$ and *Optn*$^{-/-}$ mice. Results shown are mean ± SEM, n=10-26 mice/genotype, over 3 independent experiments (ns, non-significant; two-tailed, unpaired *t* test).

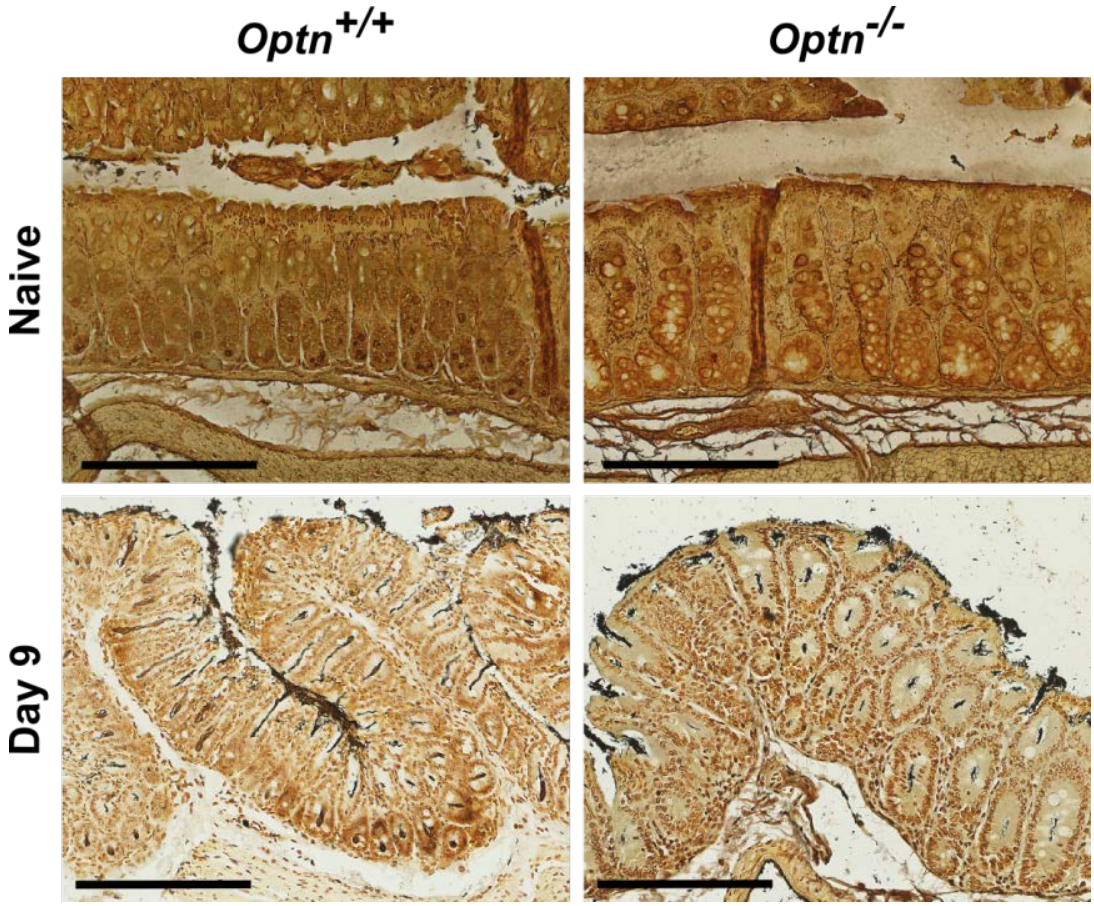

Figure 5.14 Steiner silver staining of bacteria in the large bowel showed the absence of bacteria in the large bowel crypts of naïve mice but the abundance of infiltrating *Citrobacter rodentium* in the crypts of *Optn*$^{+/+}$ and *Optn*$^{-/-}$ large bowels. Representative Steiner silver images shown, 20× magnification, scale bar 200 µm. *Citrobacter rodentium* is stained black.

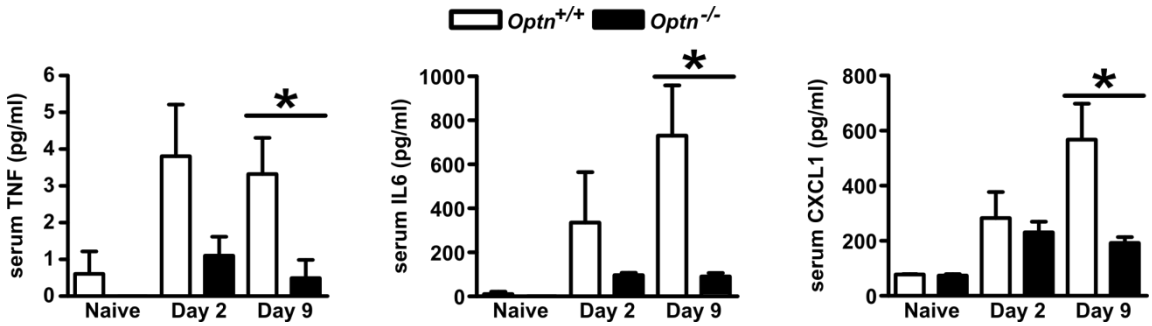

Figure 5.15 *Citrobacter* colitis resulted in lower levels of serum TNF and IL6 at day 2 and 9 but only at day 9 for CXCL1 in *Optn*$^{-/-}$ mice. There was no difference in serum TNF, IL6 or CXCL1 in naïve mice and at day 2 for CXCL1 between *Optn*$^{-/-}$ and *Optn*$^{+/+}$ mice. Results shown are mean ± SEM, n=5 mice/group (*p<0.05; two-tailed, unpaired *t* test).

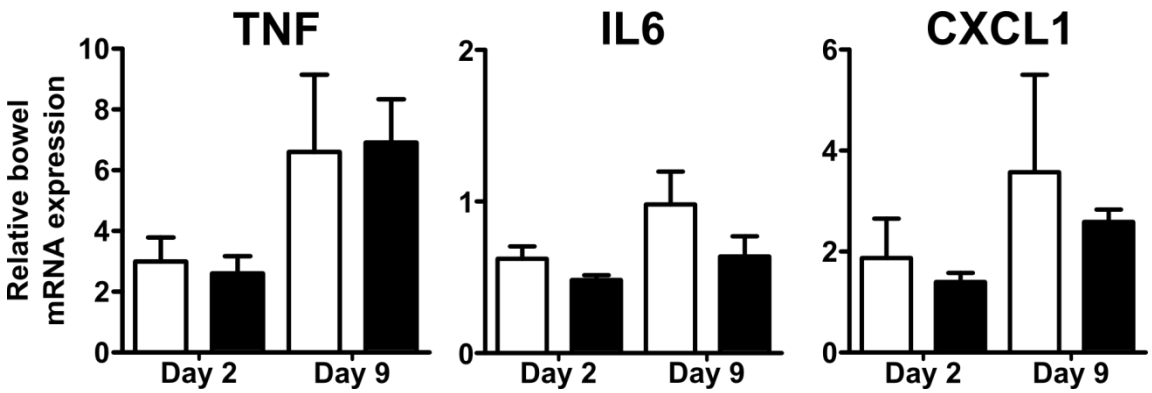

Figure 5.16 qRT-PCR of large bowel TNF, IL6 and CXCL1 gene expression at day 2 and 9 of *Citrobacter* colitis was no different between *Optn*$^{+/+}$ and *Optn*$^{-/-}$ mice. Results shown are mean ± SEM, relative to naive wildtype bowel expression, n=5 mice/genotype (two-tailed, unpaired *t* test).

Naive colons of *Optn*$^{+/+}$ and *Optn*$^{-/-}$ mice were histologically indistinguishable, with no evidence of inflammation (Figure 5.17). However, 9 days after *Citrobacter* infection, both groups of mice had developed a colitis (Figure 5.17), but the colitis score was significantly higher in the *Optn*$^{-/-}$ mice, with evidence of greater inflammatory cell infiltration, crypt elongation, mucosal disruption and loss of goblet cells in *Optn*$^{-/-}$ compared to *Optn*$^{+/+}$ bowel.

To investigate the cellular composition of the inflammatory milieu, we performed flow cytometry of cells recovered from whole colonic tissue. Naïve tissue contained equivalent numbers of CD11b^{+} F4/80^{+} macrophages, CD19^{+} B cells, CD3^{+} T cells and CD11b^{+} Gr1^{+} neutrophils in both *Optn*$^{+/+}$ and *Optn*$^{-/-}$ mice (Figure 5.18). Three days after infection with *Citrobacter*, there was a significant increase in neutrophil numbers within the *Optn*$^{+/+}$ and *Optn*$^{-/-}$ colons. This early recruitment of neutrophils was significantly lower in *Optn*$^{-/-}$ mice ($p=0.024$) and the numbers subsequently equalized by day 9. There were no changes in the numbers of macrophages or T cells at day 3, but by day 9 both cell populations had significantly increased. By contrast, B cells were unchanged throughout the inflammatory episode.

This early defective recruitment of neutrophils in the *Optn*$^{-/-}$ mice during a *Citrobacter* colitis was visualised using immunohistochemistry of myeloperoxidase as a marker for neutrophils in the large bowel (Figure 5.19). There were minimal neutrophils in the naïve large bowel but a significant number of neutrophils at day 9 of *Citrobacter* colitis in *Optn*$^{+/+}$ and *Optn*$^{-/-}$ mice. By contrast, at day 2 there were less neutrophils in the *Optn*$^{-/-}$ compared to the *Optn*$^{+/+}$ large bowel.

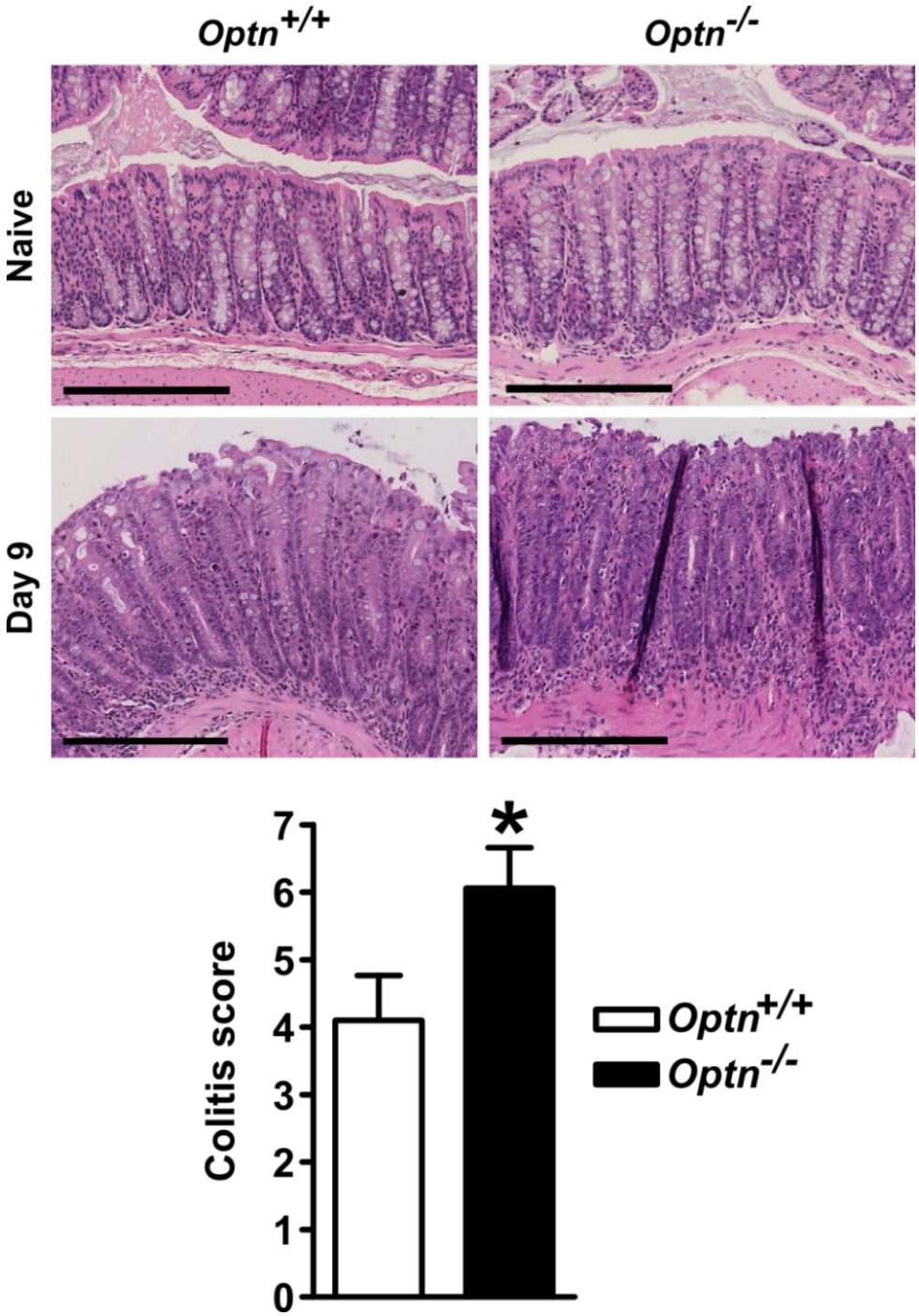

Figure 5.17 *Citrobacter rodentium* cause a significantly worse large bowel colitis at day 9 in *Optn*$^{-/-}$ mice. Naïve *Optn*$^{+/+}$ and *Optn*$^{-/-}$ mice do not develop a spontaneous colitis but developed a colitis by day 9 (representative H&E images shown above, 20× magnification, scale bar 200 µm). Blinded colitis scoring (below) revealed a significantly worse colitis in the *Optn*$^{-/-}$ mice at day 9. Results shown are mean ± SEM, n=17-20 mice/genotype, over 2 independent experiments (*p<0.05; two-tailed, unpaired *t* test).

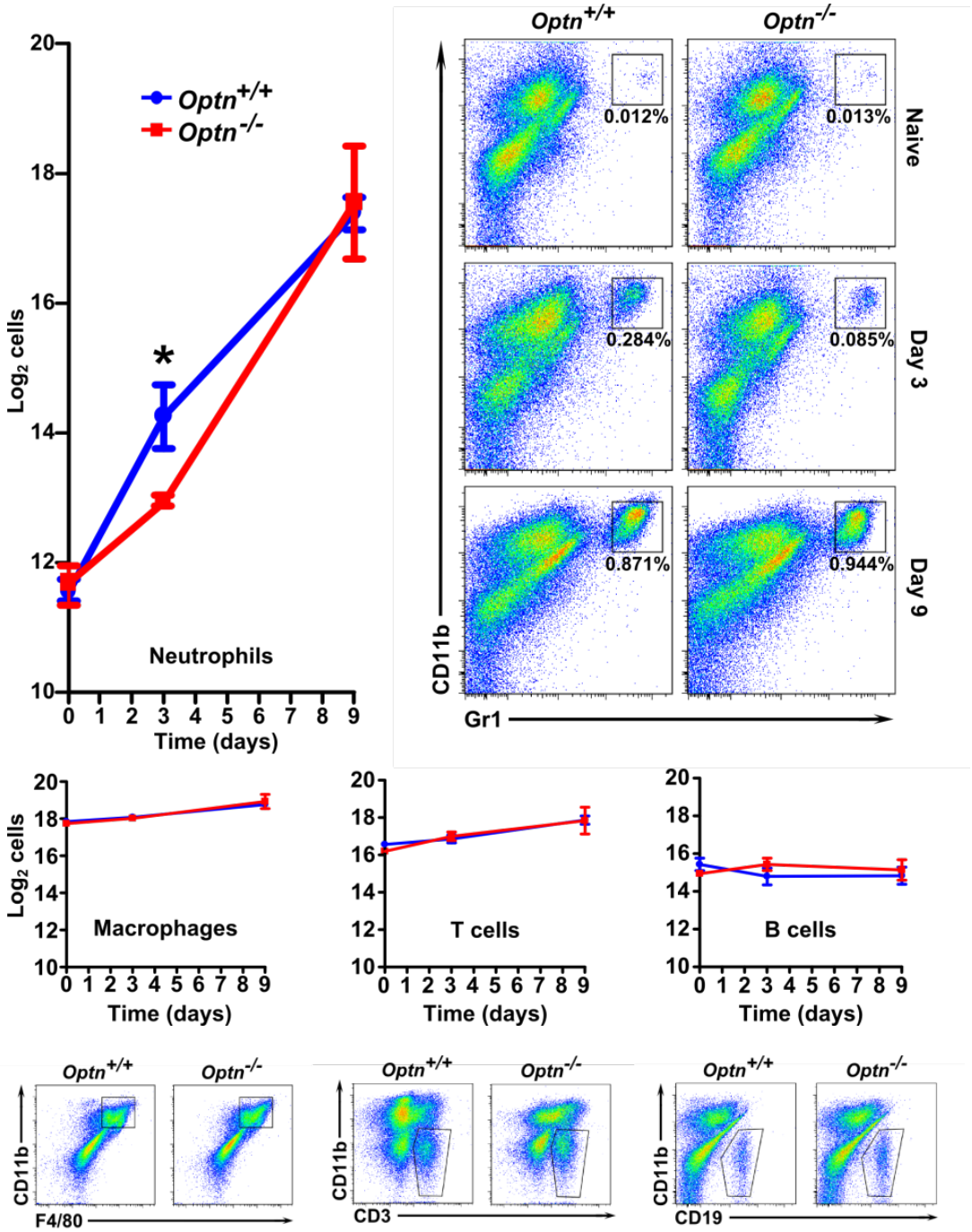

Figure 5.18 *Citrobacter rodentium* infection resulted in robust recruitment of neutrophils to the bowel that was significantly impaired in *Optn*$^{-/-}$ mice. Representative flow cytometry plots at day 3 are shown. Results shown are mean ± SEM, n=10-11 mice/genotype over 3 independent experiments (*p<0.05; two-tailed, unpaired *t* test).

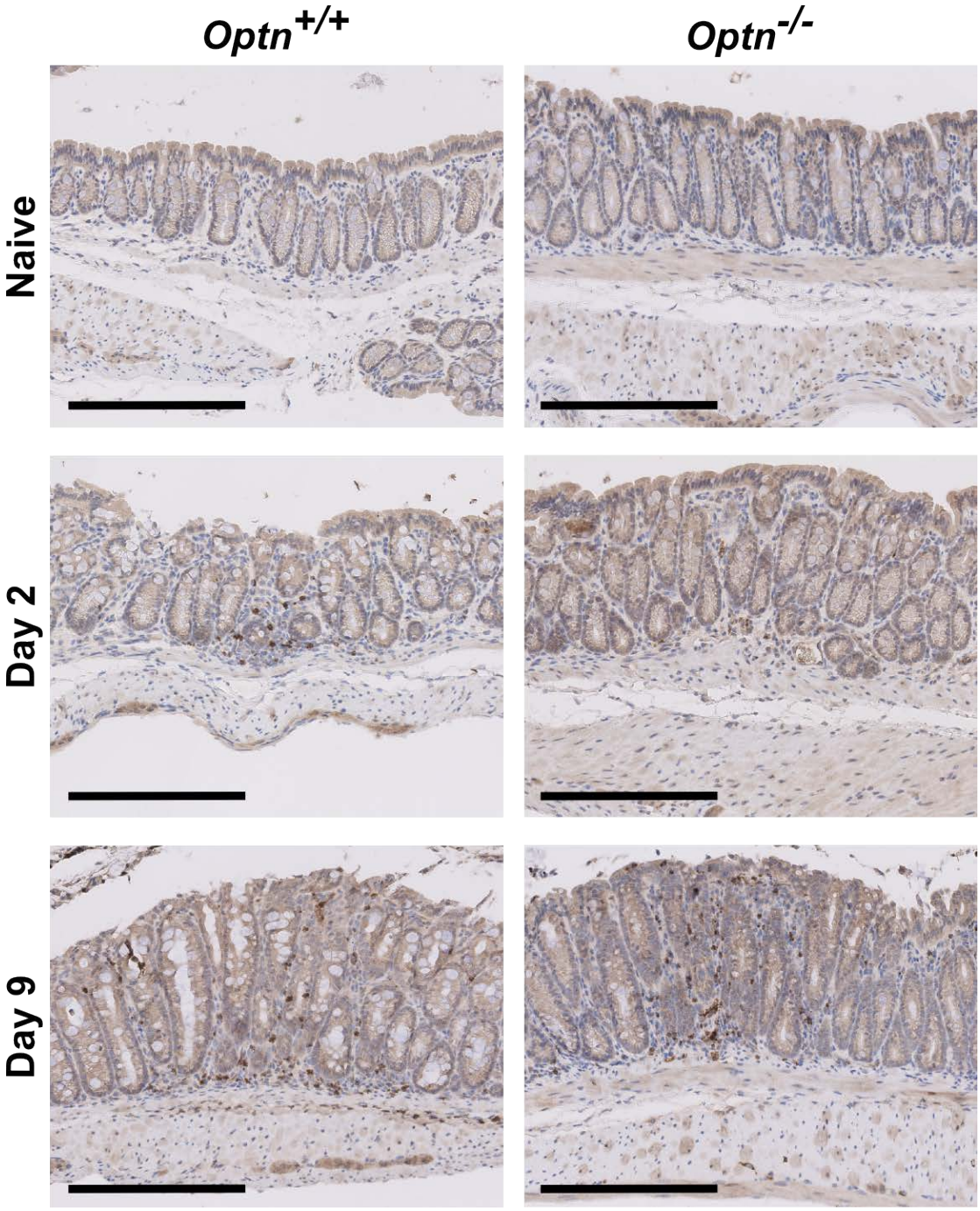

Figure 5.19 Immunohistochemistry staining of myeloperoxidase for neutrophils shows an early defective recruitment of neutrophils in the *Optn*$^{-/-}$ bowel during a *Citrobacter* infection. Representative histology images are shown, magnification 20×, scale bar 200 µm, n=5-10 mice/genotype. Slides prepared by UCL-Advanced Diagnostics.

To investigate the effect of being both NOD2 and OPTN deficient, *Optn*$^{-/-}$*Nod2*$^{-/-}$ double knockout mice were generated from *Optn*$^{-/-}$ and *Nod2*$^{-/-}$ mice together with *Optn*$^{+/+}$*Nod2*$^{+/+}$ mice. *Citrobacter rodentium* colitis induced in *Optn*$^{+/+}$*Nod2*$^{+/+}$ and *Nod2*$^{-/-}$ mice showed minimal weight loss (Figure 5.20). By contrast, *Optn*$^{-/-}$*Nod2*$^{-/-}$ double knockout mice showed more weight loss akin to *Optn*$^{-/-}$ mice but this was not statistically significant compared to the *Optn*$^{+/+}$*Nod2*$^{+/+}$ and *Nod2*$^{-/-}$ mice. Survival in the *Optn*$^{-/-}$*Nod2*$^{-/-}$ and *Nod2*$^{-/-}$ mice were not significantly different compared to the *Optn*$^{+/+}$*Nod2*$^{+/+}$ mice.

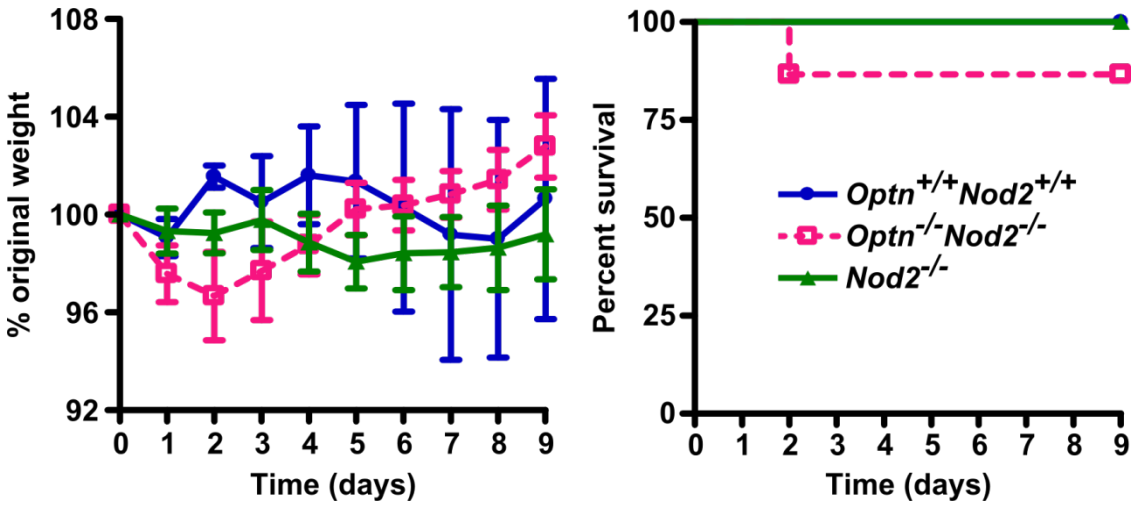

Figure 5.20 *Citrobacter* colitis in *Nod2*$^{-/-}$, *Optn*$^{-/-}$*Nod2*$^{-/-}$ and *Optn*$^{+/+}$*Nod2*$^{+/+}$ mice did not show any significant survival difference. Results shown are mean ± SEM, n=3-13 mice/genotype over 3 independent experiments (two-tailed, unpaired *t* and logrank test).

5.2.5 Mouse model of acute DSS colitis

An acute 2% dextran sodium sulphate (DSS) colitis was used to investigate the role of the gut microflora in activating mucosal immunity in the absence of OPTN. In contrast to a *Citrobacter* colitis that is induced by a single pathogenic organism, a DSS colitis results in stripping of the epithelium and exposure of the *Optn*$^{-/-}$ large bowel to the whole gut microflora.

A 2% acute DSS colitis was chosen since it caused a maximal weight loss of 15% original weight in the majority of C57BL/6 wildtype mice, which was the cut off for culling of mice on the animal project license (Figure 5.21). By contrast, the higher doses of 3% and 5% DSS resulted in maximal weight loss of more than 15% and spontaneous death in a number of mice.

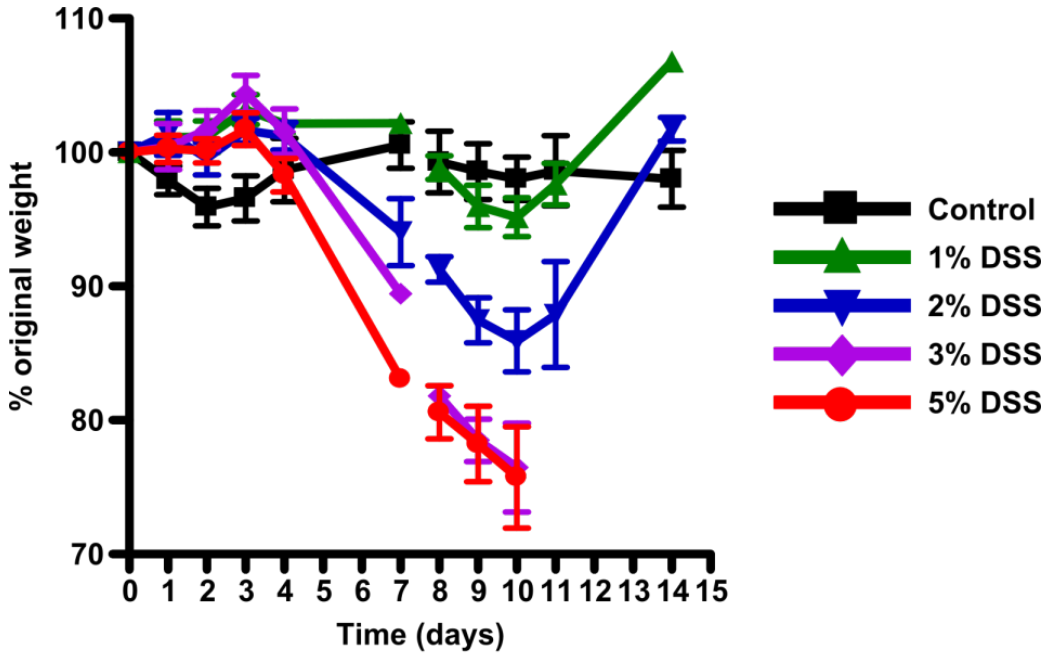

Figure 5.21 Acute dextran sodium sulphate (DSS) colitis dose response curves shows increasing weight loss with higher doses of DSS. Results are mean ± SEM, n=5 mice/group.

The acute DSS experiment was performed with 2% DSS in the drinking water of mice for the first seven days with monitoring over a total of three weeks. The 2% DSS did not show a difference in weight loss or survival in the *Optn*$^{+/+}$ and *Optn*$^{-/-}$ mice (Figure 5.22). Additionally, clinical severity scores that encompassed weight loss, the presence of blood in the faeces and the severity of diarrhoea was not statistically different between *Optn*$^{+/+}$ and *Optn*$^{-/-}$ mice (Figure 5.23). The onset of blood in the faeces on faecal occult blood testing was also not different between the genotypes (Figure 5.23).

Histological assessment at the peak of the colitis at day 7 and during the recovery phase of the colitis at day 14 did not reveal a difference in blinded colitis scores between *Optn*$^{+/+}$ and *Optn*$^{-/-}$ mice (Figure 5.24). Unblinded review of histological specimens identified areas of reepithelialisation at day 14 but not at day 7 (Figure 5.24). Large bowel lengths measured in naïve mice were not significantly different between *Optn*$^{+/+}$ and *Optn*$^{-/-}$ mice (Figure 5.25). During the 2% DSS colitis, large bowel length at day 7 was significantly shorter than naïve mice ($p=0.035$), but not at day 14 compared to naïve mice. Large bowel length at day 21 was significantly longer than day 14, 7 and naïve mice. However, large bowel lengths between *Optn*$^{+/+}$ and *Optn*$^{-/-}$ mice at day 7, 14 and 21 were not statistically different.

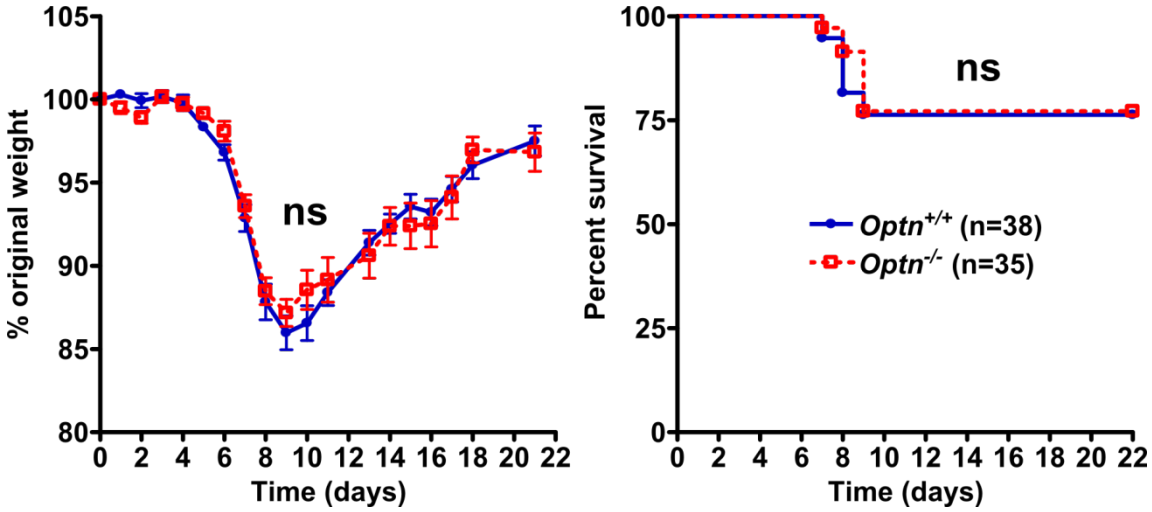

Figure 5.22 Acute 2% DSS colitis results in similar weight loss and mortality in *Optn*$^{-/-}$ and *Optn*$^{+/+}$ mice. Results shown are mean ± SEM, n=35-38 mice/genotype, over 3 independent experiments (ns, not significant; two-tailed, unpaired *t* test and logrank test).

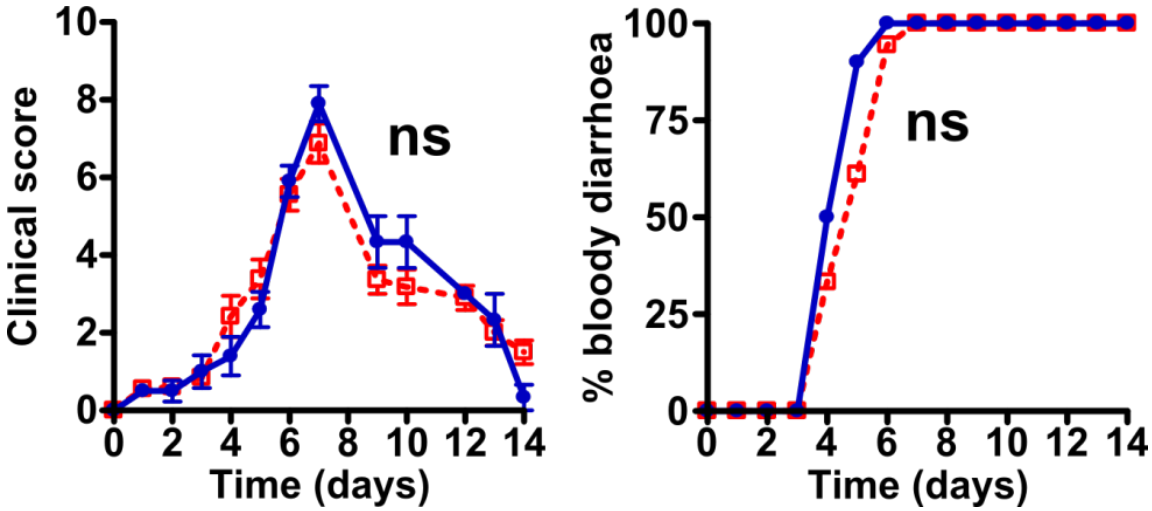

Figure 5.23 Acute 2% DSS colitis did not cause a significant difference in clinical scores or onset of blood in the faeces between *Optn*$^{-/-}$ and *Optn*$^{+/+}$ mice. Clinical score (left) and % mice with bloody diarrhoea (right) are shown. Results shown are mean ± SEM, n=10-20 mice/genotype, over 3 independent experiments (ns, not significant; two-tailed, unpaired *t* test).

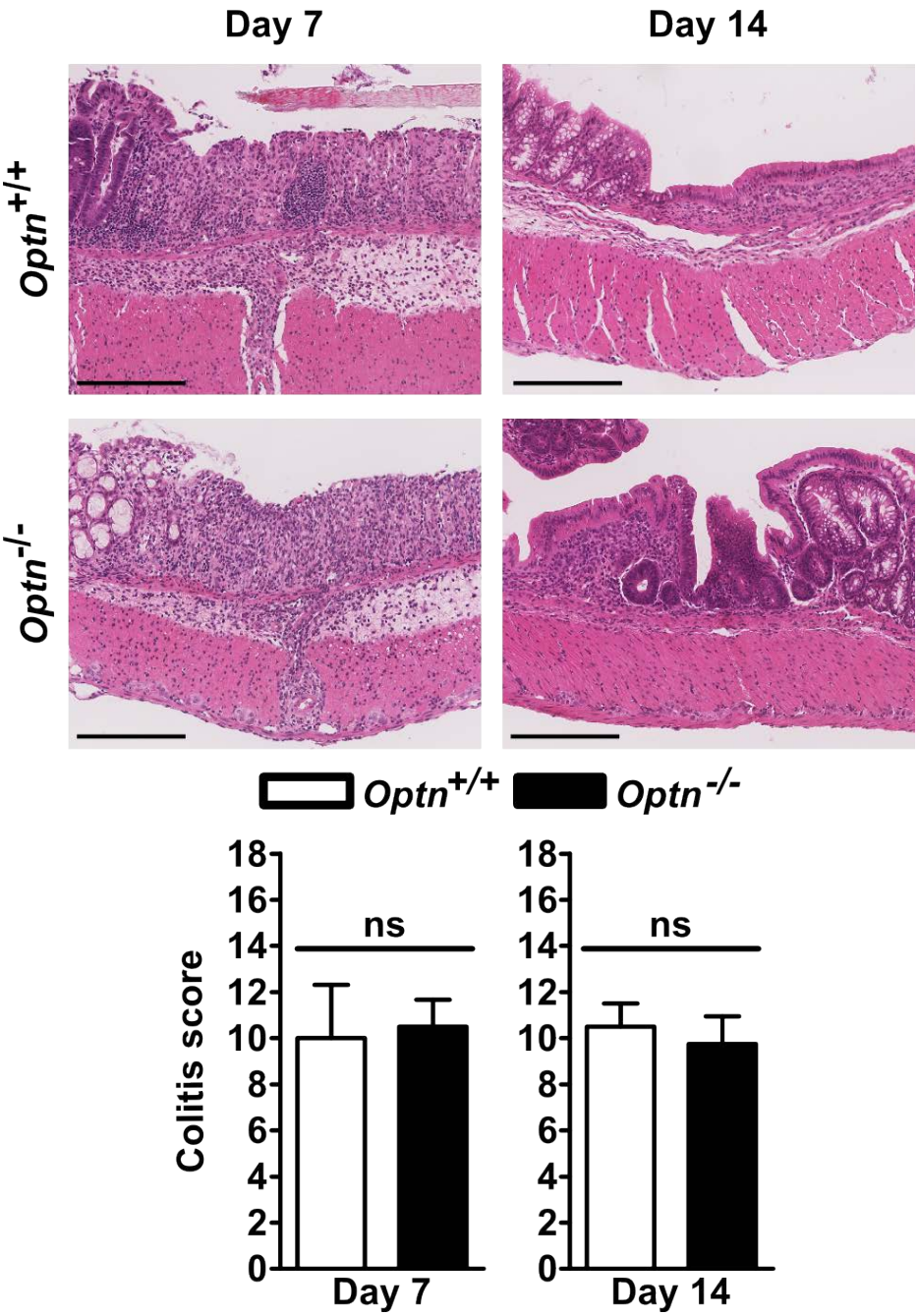

Figure 5.24 An equally severe colitis was induced by 2% DSS in *Optn*$^{-/-}$ and *Optn*$^{+/+}$ mice. Representative H&E stain of acute 2% DSS colitis in the large bowel (above) of *Optn*$^{-/-}$ and *Optn*$^{+/+}$ mice. At day 7 there is widespread mucosal destruction, oedema and inflammatory cell infiltration. At day 14, there is re-epithelialisation of the mucosa. Blinded scoring at day 7 and 14 (below) did not reveal a significant difference in large bowel colitis scores in *Optn*$^{-/-}$ and *Optn*$^{+/+}$ mice. Results shown are mean ± SEM, magnification 15×, scale bar 200 µm, n=3-5 mice/genotype (ns, not significant; two-tailed, unpaired *t* test).

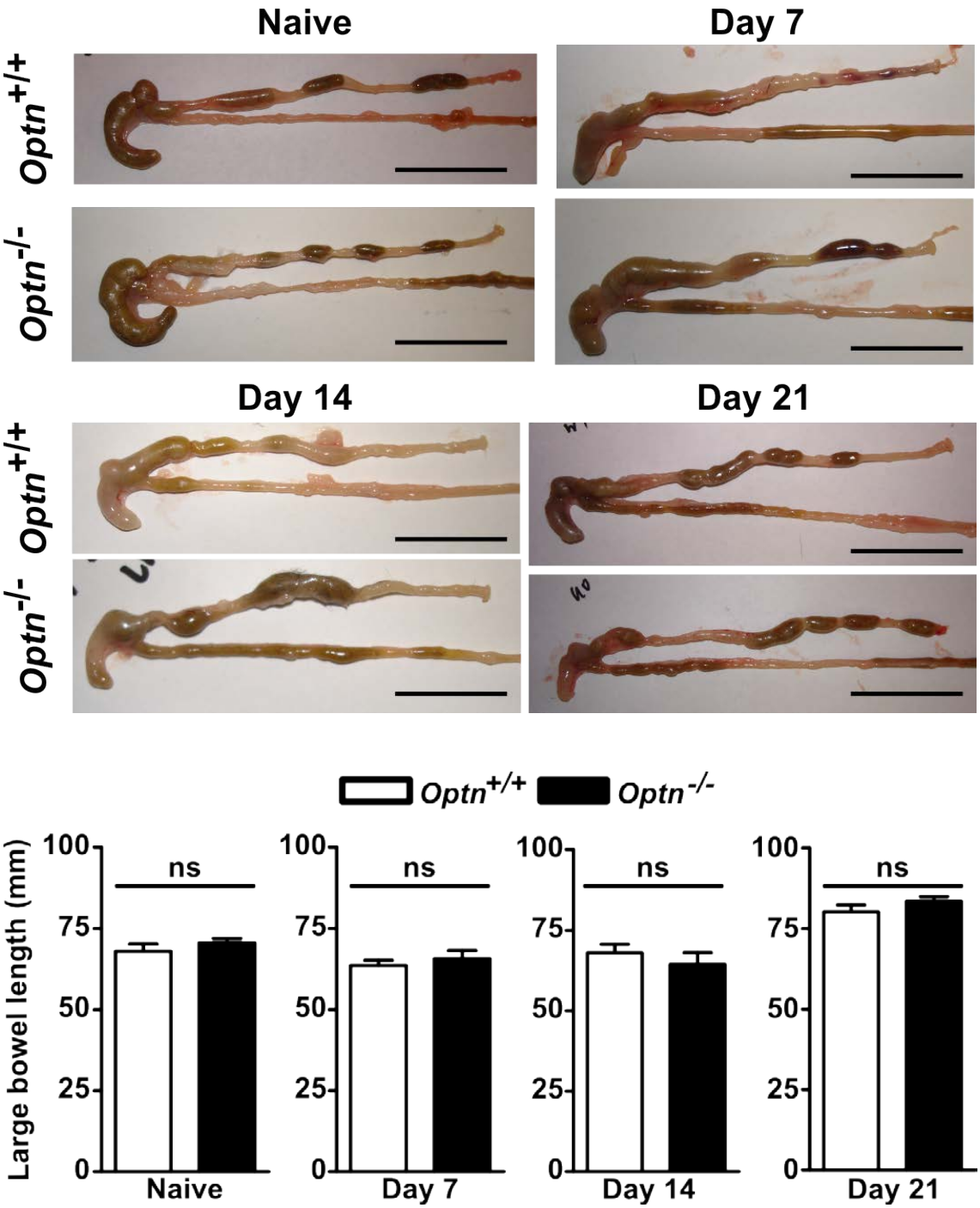

Figure 5.25 There is no difference in large bowel length between naive *Optn*$^{-/-}$ and *Optn*$^{+/+}$ mice or at day 7, 14 and 21 of an acute 2% DSS colitis. Representative images of *Optn*$^{-/-}$ and *Optn*$^{+/+}$ large bowel in naïve, day 7, 14 and 21 of DSS are shown (scale bar 20 mm). Results shown are mean ± SEM, n=4-10 mice/genotype (ns, not significant; two-tailed, unpaired *t* test).

Again, to investigate the effect of being both NOD2 and OPTN deficient, *Optn*$^{-/-}$*Nod2*$^{-/-}$ double knockout mice were compared with *Optn*$^{+/+}$*Nod2*$^{+/+}$ mice. Acute 2% DSS colitis induced in *Optn*$^{-/-}$*Nod2*$^{-/-}$, *Nod2*$^{-/-}$ and *Optn*$^{+/+}$*Nod2*$^{+/+}$ mice showed similar weight loss to 80% original weight in all three genotypes that were not statistically different between genotypes (Figure 5.26). However, the *Nod2*$^{-/-}$ mice did show a slightly slower recovery of weight (green line) compared to the *Optn*$^{-/-}$*Nod2*$^{-/-}$ and *Optn*$^{+/+}$*Nod2*$^{+/+}$ mice that was not significantly different. Survival in the *Optn*$^{-/-}$*Nod2*$^{-/-}$, *Nod2*$^{-/-}$ and *Optn*$^{+/+}$*Nod2*$^{+/+}$ mice were also not significantly different between genotypes.

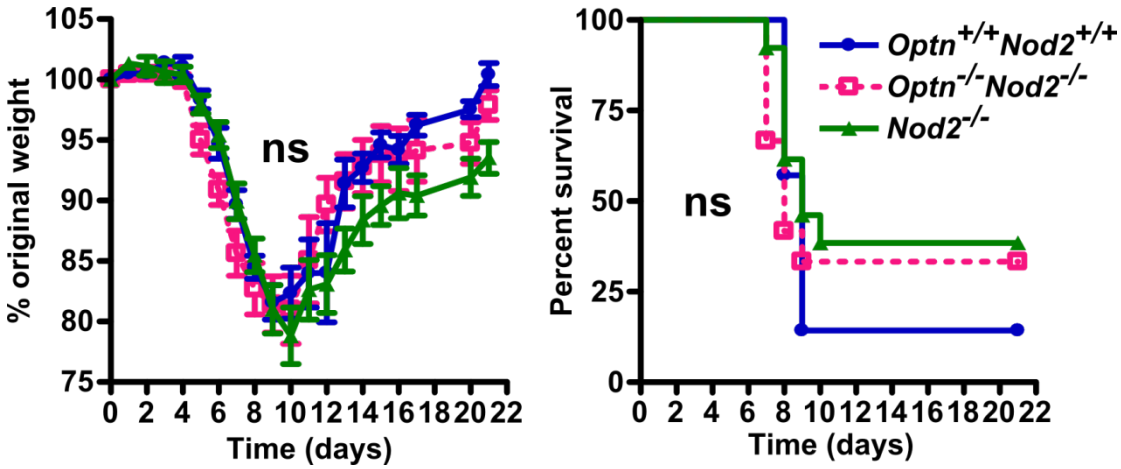

Figure 5.26 Acute 2% DSS colitis results in similar weight loss and mortality in *Optn*$^{-/-}$*Nod2*$^{-/-}$, *Optn*$^{+/+}$*Nod2*$^{+/+}$ and *Nod2*$^{-/-}$ mice. Results shown are mean ± SEM, n=7-13 mice/genotype, over 3 independent experiments (ns, not significant; two-tailed, unpaired *t* test and logrank test).

5.2.6 Mouse model of chronic DSS colitis

To assess if the slower recovery from a colitis in the *Nod2*$^{-/-}$ mice was important and had a bearing on further episodes of colitis in the *Nod2*$^{-/-}$ mice as well as the *Optn*$^{-/-}$, *Optn*$^{-/-}$*Nod2*$^{-/-}$ and *Optn*$^{+/+}$ mice, a chronic 2% DSS colitis was performed.

Mice were exposed to 7 days of 2% DSS then exposed to 2% DSS for a further 7 days after 14 days of recovery. The initial colitis proved to be protective and as a result the 2nd exposure to DSS only resulted in minimal weight loss (Figure 5.27). Extending the recovery to 28 days after the 2nd exposure to DSS resulted in similar weight loss in the 3rd exposure of DSS as experienced in the 1st exposure.

Weight loss in the *Optn*$^{-/-}$*Nod2*$^{-/-}$ mice was similar compared to the *Optn*$^{+/+}$ mice but the *Nod2*$^{-/-}$ mice exhibited significantly reduced weight during the recovery phase after the 1st exposure to DSS, which did not fully recover thereafter in the 2nd and 3rd exposure periods.

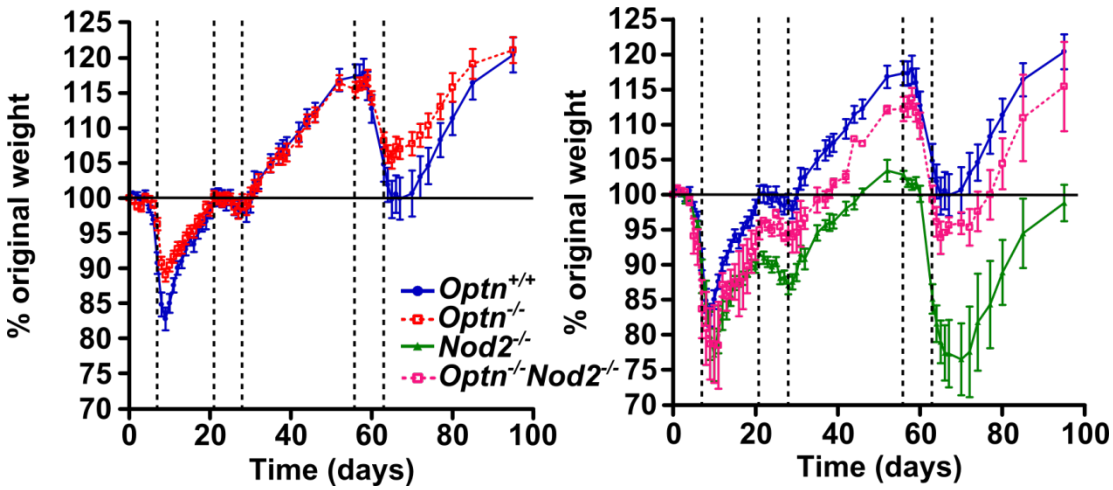

Figure 5.27 Chronic 2% DSS colitis did not cause a difference in weight loss of *Optn*$^{+/+}$, *Optn*$^{-/-}$, *Nod2*$^{-/-}$ and *Optn*$^{-/-}$*Nod2*$^{-/-}$ mice but may cause a difference in weight recovery in *Nod2*$^{-/-}$ mice. Chronic 2% DSS was performed with DSS given at day 0 to 7, 21 to 28 and 56 to 63 (dotted vertical lines). Recovery from DSS to 100% original weight (horizontal solid line) was slowest in the *Nod2*$^{-/-}$ mice whilst the *Optn*$^{-/-}$*Nod2*$^{-/-}$ was intermediate compared to *Optn*$^{+/+}$ mice. Results shown are mean ± SEM, n=5-15 mice/genotype.

5.3 Discussion

In Chapter 3, low OPTN expression in macrophages from CD patients was identified and was associated with inheritance of a minor allele in a SNP downstream of the last OPTN exon. In Chapter 4, OPTN was localised to the Golgi complex in macrophages, and the absence of OPTN was associated with reduced proinflammatory TNF and IL6 secretion due to mistrafficking via a bafilomycin A dependent pathway to lysosomes. In this chapter, in vivo studies were performed to look at the effect of OPTN knockdown or knockout on bacterial handling and specifically colitis.

In situ hybridisation in zebrafish embryos and larvae localised *optn* to the brain, eyes and intestinal bulb (Figure 5.1), which was upregulated when zebrafish were infected with *Salmonella* (Figure 5.2). Additionally, *Salmonella* infection resulted in significantly higher mortality in *optn* knockdown zebrafish compared to wildtype and control morpholino knockdown (Figure 5.3). This suggests that OPTN is localised to the gut and has an evolutionarily conserved function in bacterial handling and survival even in zebrafish, which are an evolutionarily divergent species from humans.

A recently published paper found that zebrafish injected with OPTN-specific translation blocking morpholinos resulted in a curved tail phenotype similar to zebrafish overexpression SOD1 G93A, an ALS associated variant [270]. There was no report of a curved tail phenotype in the zebrafish with the morpholino used, but a review of the literature in zebrafish identified different genetic knockdowns or treatments in zebrafish that resulted in curved tails [271-273]. This suggests that the reported curved tail phenotype seen with OPTN knockdown may be a non-specific outcome of morpholino use rather than specifically related to OPTN gene knockdown.

To investigate if the absence of OPTN results in an innate immune defect, HkEc was injected subcutaneously, which resulted in an acute inflammatory response that was dose dependent but weight and injection site size was not different between *Optn*$^{+/+}$ and *Optn*$^{-/-}$ mice. The study was limited by variability in the measurement of the injection site size as well as a lack of an established method to digest down the inflammatory skin site to assess cellular recruitment or local cytokine release.

An intraperitoneal injection of *E. coli* was performed which allowed for assessment of mortality, serum cytokine levels as well as cellular recruitment to the peritoneal cavity. Notably, the phenotype of impaired TNF release and defective neutrophil recruitment in CD patients was replicated here in the *Optn*$^{-/-}$ mice. Live intraperitoneal *E. coli* resulted in greater mortality in the *Optn*$^{-/-}$ mice with increasing doses of *E. coli* except in the highest dose tested likely due to overwhelming sepsis in both the wildtype and knockout mice. Serum TNF levels increased with higher levels of *E. coli* used in the wildtype mice, which also rose in the *Optn*$^{-/-}$ mice but was consistently lower compared to wildtypes.

Intraperitoneal CD11b^{+} F4/80^{+} macrophages were no different in the naïve peritoneum and on day 1 after intraperitoneal *E. coli* inoculation. Macrophage numbers were lower on day 1 due to activation and adherence of macrophages to the peritoneum resulting in a reduction in macrophages from the intraperitoneal washout [274, 275]. Neutrophils are recruited to the peritoneal cavity as seen in wildtype mice [274] but importantly there was early defective neutrophil recruitment at day 1 in the *Optn*$^{-/-}$ peritoneal cavity. The defective neutrophil recruitment may be related to the impaired TNF secretion that has resulted in a defective intraperitoneal neutrophil recruitment and subsequent increased mortality in the *Optn*$^{-/-}$ mice.

The discovery of an OPTN deficiency in CD focussed attention on the role of OPTN in the development of colitis. *Citrobacter rodentium* is an

enteropathic bacteria that results in colitis in mice in a similar way to enteropathogenic *E. coli*. *Optn*$^{-/-}$ mice experienced greater weight loss and higher mortality in a *Citrobacter* colitis. This occurred despite similar levels of faecal *Citrobacter* and invasion into the normally sterile crypts in both wildtype and knockout mice. This occurred in the presence of reduced levels of serum proinflammatory TNF, IL6 and CXCL1 in the *Optn*$^{-/-}$ mice with no difference in *Tnf*, *Il6* and *Cxcl1* gene expression in the large bowel. The *Optn*$^{-/-}$ mice experienced a greater colitis later at day 9, with an early defective recruitment of neutrophils to the large bowel at day 3.

NOD2 is the strongest genetic risk factor for developing CD. *Nod2*$^{-/-}$ mice were previously found to have impaired intestinal clearance of *Citrobacter* with reduced CCL2 production and monocyte recruitment [276]. To see if the absence of Nod2 would result in an additive susceptibility to a bacterial colitis, we generated *Optn*$^{-/-}$*Nod2*$^{-/-}$ double knockouts. The *Nod2*$^{-/-}$ mouse did not show a drop in weight and the *Optn*$^{-/-}$*Nod2*$^{-/-}$ resulted in an early weight loss that was not statistically significant, diminishing the effect of the absence of OPTN.

The dextran sodium sulphate (DSS) model of colitis is a commonly used model of chemical induced colitis that results in DSS induced cytotoxicity of the bowel epithelium that resembles human ulcerative colitis [268, 277]. An acute 2% DSS colitis did not result in a difference in weight loss, mortality, clinical score or the onset of bloody diarrhoea in the *Optn*$^{-/-}$ and *Optn*$^{+/+}$ mice. Additionally there was no difference in large bowel length or colitis score at the peak of colitis on day 7 or during the resolution phase of the colitis on day 14 between wildtype and OPTN deficient mice. This is not surprising since OPTN deficiency was not identified in UC patients but exclusively in CD patients and as such *Optn*$^{-/-}$ mice would not be expected to suffer a more severe ‘UC-type’ colitis. We hypothesise that the lack of difference is due to mucosal exposure to colonising microflora in both the wildtype and knockout bowel that is independent of OPTN in contrast to the invasion of *Citrobacter*

rodentium that is OPTN dependent and results in an exaggerated bacteria induced colitis.

Nod2$^{-/-}$ mice did not experience increased weight loss or mortality in the acute 2% DSS colitis compared to wildtype mice but did show reduced recovery of weight that did not reach statistical significance (Figure 5.26). By contrast, *Optn*$^{-/-}$*Nod2*$^{-/-}$ double knockout mice experience weight loss that was indistinguishable from wildtype mice. Initial studies did not show an increased susceptibility to an acute DSS colitis in *Nod2*$^{-/-}$ mice [278] but later studies have shown increased susceptibility in *Nod2*$^{-/-}$ mice [279, 280]. It is not clear why these differences in response exist, possible explanations include the small numbers of mice used in some of the experiments, differences in gut microflora in different animal units or subtle genetic differences that exist among inbred C57BL/6 mice [281].

When *Nod2*$^{-/-}$ mice were subject to repeated exposure to DSS in a chronic DSS model of colitis, *Nod2*$^{-/-}$ mice were slow to regain weight with repeated exposure to DSS in contrast to *Optn*$^{-/-}$*Nod2*$^{-/-}$ and *Optn*$^{-/-}$ mice that were no different from wildtype mice (Figure 5.27). Whilst inheritance of NOD2 variants is associated with an increased risk of CD, it has protective effects in UC [100]. It is therefore not surprising that the absence of NOD2 results in a defect in a UC-like model of colitis. The impaired recovery in weight with each subsequent DSS insult likely renders mice incapable of an adequate responds to further insults that may provide insights into the pathogenesis of UC. This interesting discovery warrants further investigation.

Chapter 6 General Discussion

6.1 Summary of investigations conducted and novel findings

CD is a complex, multifaceted disease that predominantly manifests in the GI tract with patchy transmural inflammation and granulomas. We previously showed that CD is characterised by impaired neutrophil recruitment and defective bacterial clearance from sites of inoculation [107]. The phenotype of CD was associated with decreased proinflammatory TNF cytokine release from macrophages of CD patients when stimulated with HkEc [187]. Differential gene expression analysis in CD macrophages on microarray identified genes involved in vesicle trafficking. This defective TNF secretion by CD macrophages on bacterial stimulation has been replicated by others [282, 283].

6.2 Discussion of findings, implications and study limitations

The cause of defective cytokine secretion in CD is still elusive. To identify potential candidate genes involved in defective cytokine secretion we analysed the transcriptome of macrophages. The identification of reduced OPTN expression in approximately a tenth of our CD patients provided evidence that it may play a role in the cytokine secretion defect observed, underpinned by its established role in vesicle trafficking and secretion [201, 204].

Our initial studies demonstrated that upon depletion of OPTN using siRNA knockdown, proinflammatory cytokine secretion was reduced [191]. We have now expanded these initial findings and identified a major *in vivo* role for OPTN in the inflammatory response in the bowel. The loss of OPTN in knockout mice and diminished levels in CD patients did not result in complete loss of cytokine secretion, pointing to redundancy in the regulation of these secretory pathways. However, partial impairment of the secretion of

proinflammatory cytokines may be pathologically relevant when the host is exposed to a large quantity of bacteria requiring an immediate, robust inflammatory response.

This type of defect is highly relevant in the case of CD where we have previously demonstrated a dose dependent immune deficiency in these individuals [187, 284]. A breach in the mucosal wall could result in the exposure of the underlying tissue to an enormous bacterial challenge, which will need rapid containment and clearance. This may be particularly relevant in the terminal ileum where there is the greatest transition from a relatively low level of bacteria in the small bowel to the caecum where this is a high concentration of bacteria. Ten out of eleven of our *OPTN*^{low} CD patients had ileal involvement of their CD. Reduced OPTN expression, inheritance of NOD2, ATG16L1 variants or congenital monogenic innate immunodeficiencies will impact directly on the efficiency of this response, failure of which could result in inadequate clearance of foreign material and the development of chronic inflammation.

The role of OPTN in intracellular trafficking in non-immune cells has been well characterised. OPTN has been shown to localise to the Golgi complex and play an important role in vesicle trafficking through the formation of macromolecular complexes, which include numerous binding partners such as Rab8, HTT and myosin VI. The role and composition of the OPTN containing complex in vesicle trafficking is only partially elucidated. Previous studies have provided evidence of a role in protein sorting within the Golgi complex and trafficking to the plasma membrane [201]. Replacement of OPTN's binding partner HTT with a 111Q polyglutamine mutant resulted in reduced localization of OPTN to the Golgi complex and impaired post-Golgi trafficking in striatal cells [206]. Depletion of OPTN with siRNA in HeLa cells also resulted in dramatically reduced exocytosis.

However, these studies did not look at the role of OPTN in the context of bacterial or TLR stimulation that is relevant in the context of CD. More recently, a mouse in which wild-type OPTN was replaced by the polyubiquitin binding-defective OPTN mutant, demonstrated an abrogated response to LPS in BMDM due to impaired activation of TANK-binding kinase 1 [200]. This was associated with defective interferon-β release but TNF and IL6 secretion was described as normal in these mice [213]. This is in contrast to our findings of defective cytokine secretion, which indicates that TNF and IL6 secretion is partially dependent on the expression of OPTN but independent of its ability to bind ubiquitin in BMDM.

Cytokine trafficking in macrophages is complex and only partially understood. Previous work has shown that TNF and IL6 share a common pathway of secretion from the trans-Golgi network to endosomes where they are then dynamically segregated [162, 171]. In contrast, IL10 is secreted via both endosome-dependent and independent pathways [172]. Others have also shown that OPTN only minimally colocalises to the endosomal compartment [214]. BMDM that lack OPTN demonstrate a reduced overlap between TNF and the endosomal compartment. These findings would indicate that the role of OPTN in the defective release of TNF and IL6 in BMDM lies in its role in sorting proteins for transport at the Golgi complex.

Inclusion of a range of protein trafficking inhibitors results in increasing the level of TNF within the cells. The reduction in secreted protein coupled with the generation of equivalent levels of intracellular protein after bacterial stimulation provides evidence to support our previous findings in CD patients of cytokine mistrafficking. Inclusion of bafilomycin A an inhibitor of vacuolar H^+-ATPases (V-ATPases), results in a greater intracellular build-up of the 17 kDa secreted form of TNF in OPTN deficient BMDM than wildtypes. These findings suggest that in the absence of OPTN a greater proportion of TNF is trafficked through a V-ATPase dependent compartment and degraded instead of being released at the plasma membrane (Figure 6.1). It has also

been demonstrated that OPTN can function at the plasma membrane and facilitate the final fusion event of vesicle trafficking. We cannot completely rule out a role for OPTN at the plasma membrane in BMDM, but our results suggest that it does not play a major role in TNF secretion. In fibroblasts, knocking down OPTN, which is required for the final step in the vesicle plasma membrane fusion results in a dramatic increase in the number of docked vesicles at the cell surface. This causes a build-up of vesicle cargo protein within these cells. BMDM devoid of OPTN demonstrate no such build-up at the plasma membrane or within the cell, which argues against the same process occurring in these cells.

Reduced TNF and IL6 release was shown to coincide with defective neutrophil recruitment after bacterial induced inflammation in both the bowel and peritoneum of OPTN deficient mice. In both inflammatory models an increased systemic response was recorded and this contributed to an increased colitis and greater mortality. Alterations in cytokine levels can have profound effects on the outcome of infections and inflammatory episodes. Previous studies have demonstrated an elevation in inflammation resulting from a deficiency in TNF expression [285]. TNF knockout mice are more susceptible to bacterial infection and generate a more severe colitis than control mice [286, 287].

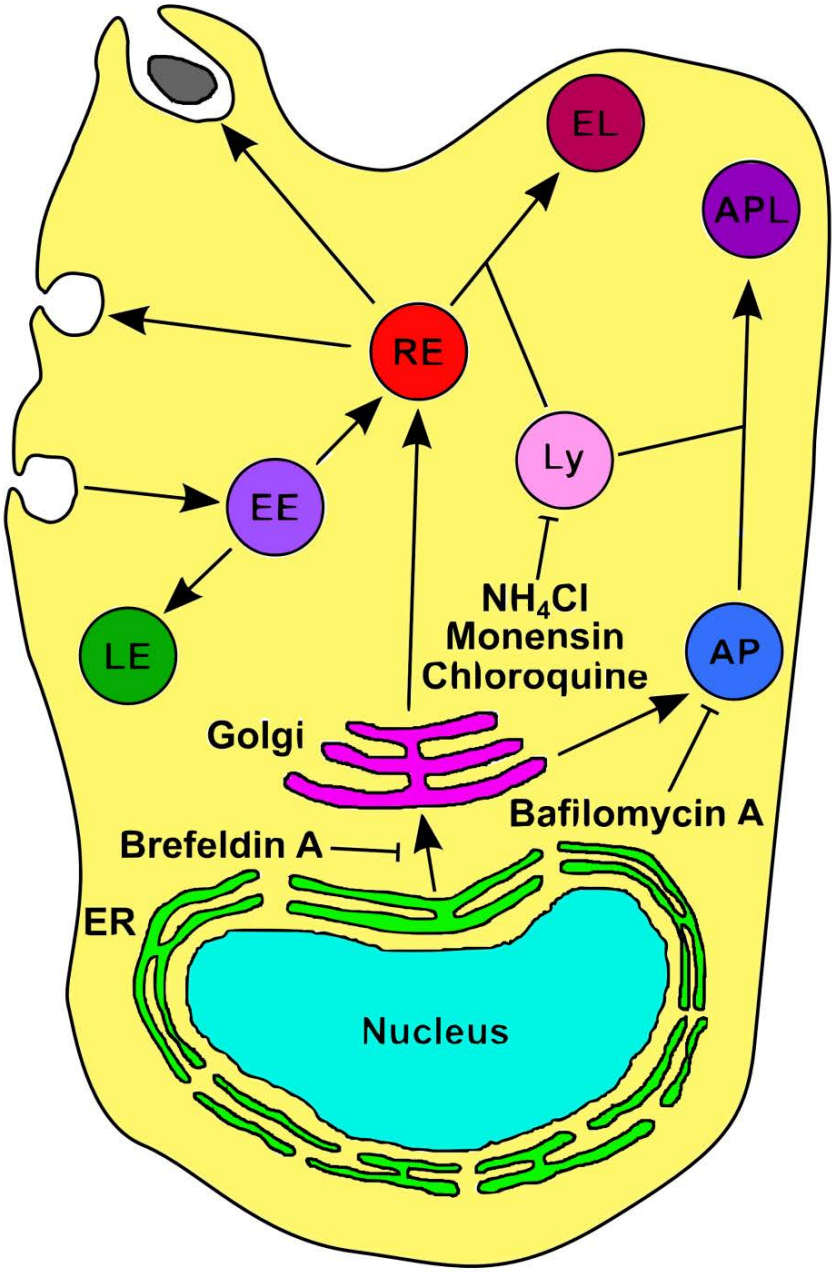

Figure 6.1 TNF trafficking in macrophages. TNF is packaged at the Golgi apparatus by OPTN to be secreted via the recycling endosome. The absence of OPTN results in degradation of TNF via a bafilomycin A dependent pathway involving lysosomes. As a result, inhibition of lysosomal function results in normalisation of TNF whilst bafilomycin A results in significantly higher TNF levels in the *Optn*$^{-/-}$ compared to *Optn*$^{+/+}$ macrophage. AP, autophagosome; APL, autophagolysosome; Ly, lysosome; EE, early endosome; LE, late endosome; RE, recycling endosome; EL, endolysosome.

Additionally, patients with ankylosing spondylitis and juvenile arthritis treated with etanercept, a fusion protein made up of the TNF-receptor II extracellular domain fused with the Fc fragment of IgG_1 were reported to develop CD [53-61]. The association of etanercept with CD is not seen with the other anti-TNF agents infliximab and adalimumab. This difference may be explained by infliximab's apoptotic action (via binding to transmembrane TNF) on T cells, which etanercept lacks in contrast to binding and neutralisation of soluble TNF [62]. These findings provide evidence that TNF has a protective role in the acute phase of an inflammatory response and the release of suboptimal TNF levels could result in the development of chronic inflammation.

Noteworthy is the lack of a difference in weight loss or mortality in the mice treated with DSS. We hypothesise that the lack of an effect may be related to the fact that DSS mimics a more UC type colitis that starts distally in the large bowel whereas the *Citrobacter* model more closely mimics a proximal colitis as the inoculated bacteria transitions from the small bowel to the caecum and large bowel. Additionally, the difference may be explained by an invasion of the bowel with a single pathogen that is in the mouse akin to enteroinvasive *E. coli* is to humans, which resembles CD more and that the chemically induced stripping and subsequent exposure of the gut mucosa to all the resident gut flora does not require OPTN in immune cells.

6.3 Future directions

The work presented in this thesis has highlighted further experiments and new exciting areas for future research, such as:

- Further human work, in the eleven *OPTN*^{low} CD patients such as staining of bowel tissue for macrophage, B and T cell markers to characterise the lamina propria cells with low OPTN expression, to look at proinflammatory cytokine secretion from these *OPTN*^{low} MDM

on HkEc stimulation, *in vivo* neutrophil recruitment, bacterial clearance studies and *OPTN* expression in bowel biopsies especially the ileum.

- An interesting study may be to identify families that express low *OPTN* and inherit the associated SNP to see if ileal and colonic OPTN expression is attenuated especially family members who may not yet have CD but have altered OPTN levels, to look at proinflammatory cytokine secretion in their MDM.
- To study autophagy using *Salmonella* in *Optn*$^{-/-}$ BMDM to see if there is a defect in the induction of autophagy when BMDM are infected with *Salmonella* that evade phagosomes and autophagy is required.
- Bone marrow transfer experiments in the *Citrobacter* colitis model to see if the neutrophil recruitment defect can be reproduced in wildtype mice grafted with *Optn*$^{-/-}$ bone marrow cells and if defective neutrophil recruitment can be reversed in *Optn*$^{-/-}$ mice grafted with wildtype bone marrow.
- Alternatively, to see if the defect in neutrophil recruitment is due to reduced proinflammatory TNF secretion, administration of TNF to the *Optn*$^{-/-}$ mice infected with *Citrobacter* may then reverse the defective neutrophil recruitment. However, these experiments may be limited by incorrect doses and mode of TNF administration used.
- To investigate if there are differences in the gut microflora of *Optn*$^{+/+}$ and *Optn*$^{-/-}$ mice that may account for the differences in response to *Citrobacter* infection and whether co-housing mice may alter the response to *Citrobacter*.

6.4 Conclusion

The present results demonstrate a role for OPTN in macrophage cytokine secretion, neutrophil recruitment to sites of bacterial infection and bowel inflammation *in vivo*. Bacterial exposure upregulates OPTN expression in human and murine macrophages, which is associated with the secretion of

proinflammatory cytokines and subsequent recruitment of neutrophils into inflamed tissue. OPTN deficiency results in increased susceptibility to bacterial infection and the development of exaggerated inflammation in the bowel. The phenotype identified in mice mirrors our findings in CD patients, reinforcing the suggestion that the reduced expression of OPTN could play an important role in the development of bowel inflammation in humans.

References

1. Baumgart, D.C. and S.R. Carding, *Inflammatory bowel disease: cause and immunobiology.* Lancet, 2007. **369**(9573): p. 1627-40.

2. Abraham, C. and J.H. Cho, *Inflammatory bowel disease.* N Engl J Med, 2009. **361**(21): p. 2066-78.

3. Baumgart, D.C. and W.J. Sandborn, *Crohn's disease.* Lancet, 2012. **380**(9853): p. 1590-605.

4. Baumgart, D.C. and W.J. Sandborn, *Inflammatory bowel disease: clinical aspects and established and evolving therapies.* Lancet, 2007. **369**(9573): p. 1641-57.

5. Thia, K.T., et al., *Risk factors associated with progression to intestinal complications of Crohn's disease in a population-based cohort.* Gastroenterology, 2010. **139**(4): p. 1147-55.

6. Peyrin-Biroulet, L., et al., *The natural history of adult Crohn's disease in population-based cohorts.* Am J Gastroenterol, 2010. **105**(2): p. 289-97.

7. Louis, E., et al., *Behaviour of Crohn's disease according to the Vienna classification: changing pattern over the course of the disease.* Gut, 2001. **49**(6): p. 777-82.

8. Loftus, E.V., Jr., P. Schoenfeld, and W.J. Sandborn, *The epidemiology and natural history of Crohn's disease in population-based patient cohorts from North America: a systematic review.* Aliment Pharmacol Ther, 2002. **16**(1): p. 51-60.

9. Jess, T., et al., *Survival and cause specific mortality in patients with inflammatory bowel disease: a long term outcome study in Olmsted County, Minnesota, 1940-2004.* Gut, 2006. **55**(9): p. 1248-54.

10. Hovde, O., et al., *Mortality and causes of death in Crohn's disease: results from 20 years of follow-up in the IBSEN study.* Gut, 2014. **63**(5): p. 771-5.

11. Sjoberg, D., et al., *Incidence and natural history of ulcerative colitis in the Uppsala Region of Sweden 2005-2009 - results from the IBD cohort of the Uppsala Region (ICURE).* J Crohns Colitis, 2013. **7**(9): p. e351-7.

12. Danese, S. and C. Fiocchi, *Ulcerative colitis.* N Engl J Med, 2011. **365**(18): p. 1713-25.

13. Solberg, I.C., et al., *Clinical course during the first 10 years of ulcerative colitis: results from a population-based inception cohort (IBSEN Study).* Scand J Gastroenterol, 2009. **44**(4): p. 431-40.

14. Langholz, E., et al., *Changes in extent of ulcerative colitis: a study on the course and prognostic factors.* Scand J Gastroenterol, 1996. **31**(3): p. 260-6.

15. Moeeni, V. and A.S. Day, *Impact of Inflammatory Bowel Disease upon Growth in Children and Adolescents.* ISRN Pediatr, 2011. **2011**: p. 365712.

16. Busch, K., et al., *Sick leave and disability pension in inflammatory bowel disease: A systematic review.* J Crohns Colitis, 2014.

17. Ananthakrishnan, A.N., E.L. McGinley, and D.G. Binion, *Inflammatory bowel disease in the elderly is associated with worse outcomes: a national study of hospitalizations.* Inflamm Bowel Dis, 2009. **15**(2): p. 182-9.

18. Burisch, J., et al., *The burden of inflammatory bowel disease in Europe.* J Crohns Colitis, 2013. **7**(4): p. 322-37.

19. Kappelman, M.D., et al., *Direct health care costs of Crohn's disease and ulcerative colitis in US children and adults.* Gastroenterology, 2008. **135**(6): p. 1907-13.

20. Rocchi, A., et al., *Inflammatory bowel disease: a Canadian burden of illness review.* Can J Gastroenterol, 2012. **26**(11): p. 811-7.

21. Bassi, A., et al., *Cost of illness of inflammatory bowel disease in the UK: a single centre retrospective study.* Gut, 2004. **53**(10): p. 1471-8.

22. Hay, J.W. and A.R. Hay, *Inflammatory bowel disease: costs-of-illness.* J Clin Gastroenterol, 1992. **14**(4): p. 309-17.

23. Yu, A.P., et al., *The costs of Crohn's disease in the United States and other Western countries: a systematic review.* Curr Med Res Opin, 2008. **24**(2): p. 319-28.

24. Cohen, R.D., et al., *Systematic review: the costs of ulcerative colitis in Western countries.* Aliment Pharmacol Ther, 2010. **31**(7): p. 693-707.

25. Ng, S.C., et al., *Incidence and Phenotype of Inflammatory Bowel Disease, Based on Results from the Asia-Pacific Crohn's and Colitis Epidemiology Study.* Gastroenterology, 2013.

26. Molodecky, N.A., et al., *Increasing incidence and prevalence of the inflammatory bowel diseases with time, based on systematic review.* Gastroenterology, 2012. **142**(1): p. 46-54 e42; quiz e30.

27. Ng, S.C., et al., *Geographical variability and environmental risk factors in inflammatory bowel disease.* Gut, 2013. **62**(4): p. 630-49.

28. Logan, R.F., *Inflammatory bowel disease incidence: up, down or unchanged?* Gut, 1998. **42**(3): p. 309-11.

29. Niriella, M.A., et al., *Prevalence of inflammatory bowel disease in two districts of Sri Lanka: a hospital based survey.* BMC Gastroenterol, 2010. **10**: p. 32.

30. Edwards, C.N., et al., *Inflammatory bowel disease: incidence, prevalence, and disease characteristics in Barbados, West Indies.* Inflamm Bowel Dis, 2008. **14**(10): p. 1419-24.

31. Sobrero, M.J., et al., *Prevalence of Inflammatory Bowel Disease in a University Hospital Health Maintenance Organization.* Gastroenterology, 2009. **136**(5): p. A361-A362.

32. Sood, A., et al., *Incidence and prevalence of ulcerative colitis in Punjab, North India.* Gut, 2003. **52**(11): p. 1587-90.

33. Tan, Y.M. and K.L. Goh, *Ulcerative colitis in a multiracial Asian country: racial differences and clinical presentation among Malaysian patients.* World J Gastroenterol, 2005. **11**(37): p. 5859-62.

34. Mahid, S.S., et al., *Smoking and inflammatory bowel disease: a meta-analysis.* Mayo Clin Proc, 2006. **81**(11): p. 1462-71.

35. Stampfli, M.R. and G.P. Anderson, *How cigarette smoke skews immune responses to promote infection, lung disease and cancer.* Nat Rev Immunol, 2009. **9**(5): p. 377-84.

36. Wilson, P.J.E., *The Young Pretender.* BMJ, 1961. **2**(5261): p. 1226-1226.

37. Hou, J.K., B. Abraham, and H. El-Serag, *Dietary intake and risk of developing inflammatory bowel disease: a systematic review of the literature.* Am J Gastroenterol, 2011. **106**(4): p. 563-73.

38. Andersen, V., et al., *Diet and risk of inflammatory bowel disease.* Dig Liver Dis, 2012. **44**(3): p. 185-94.

39. Lochs, H., et al., *ESPEN Guidelines on Enteral Nutrition: Gastroenterology.* Clin Nutr, 2006. **25**(2): p. 260-74.

40. O'Morain, C., et al., *Elemental diet in acute Crohn's disease.* Arch Dis Child, 1983. **58**(1): p. 44-7.

41. Sanderson, I.R., et al., *Remission induced by an elemental diet in small bowel Crohn's disease.* Arch Dis Child, 1987. **62**(2): p. 123-7.

42. Papadopoulou, A., et al., *Remission following an elemental diet or prednisolone in Crohn's disease.* Acta Paediatr, 1995. **84**(1): p. 79-83.

43. Zachos, M., M. Tondeur, and A.M. Griffiths, *Enteral nutritional therapy for induction of remission in Crohn's disease.* Cochrane Database Syst Rev, 2007(1): p. CD000542.

44. Nielsen, O.H., H.W. Verspaget, and J. Elmgreen, *Inhibition of intestinal macrophage chemotaxis to leukotriene B4 by sulphasalazine, olsalazine, and 5-aminosalicylic acid.* Aliment Pharmacol Ther, 1988. **2**(3): p. 203-11.

45. Hanauer, S.B. and U. Stromberg, *Oral Pentasa in the treatment of active Crohn's disease: A meta-analysis of double-blind, placebo-controlled trials.* Clin Gastroenterol Hepatol, 2004. **2**(5): p. 379-88.

46. Truelove, S.C. and L.J. Witts, *Cortisone in ulcerative colitis; final report on a therapeutic trial.* Br Med J, 1955. **2**(4947): p. 1041-8.

47. Benchimol, E.I., et al., *Traditional corticosteroids for induction of remission in Crohn's disease.* Cochrane Database Syst Rev, 2008(2): p. CD006792.

48. Knight, P., B.J. Campbell, and J.M. Rhodes, *Azathioprine and 6-Thioguanine but Not 6-Mercaptopurine Inhibit Intra-Macrophage Replication of Crohn's Disease Escherichia Coli.* Gut, 2011. **60**.

49. ten Hove, T., et al., *Infliximab treatment induces apoptosis of lamina propria T lymphocytes in Crohn's disease.* Gut, 2002. **50**(2): p. 206-11.

50. Lugering, A., et al., *Infliximab induces apoptosis in monocytes from patients with chronic active Crohn's disease by using a caspase-dependent pathway.* Gastroenterology, 2001. **121**(5): p. 1145-57.

51. Rutgeerts, P., et al., *Infliximab for induction and maintenance therapy for ulcerative colitis.* N Engl J Med, 2005. **353**(23): p. 2462-76.

52. Hanauer, S.B., et al., *Maintenance infliximab for Crohn's disease: the ACCENT I randomised trial.* Lancet, 2002. **359**(9317): p. 1541-9.

53. Ruemmele, F.M., et al., *Development of Crohn disease during anti-TNF-alpha therapy in a child with juvenile idiopathic arthritis.* J Pediatr Gastroenterol Nutr, 2004. **39**(2): p. 203-6.

54. Song, I.H., et al., *New onset of Crohn's disease during treatment of active ankylosing spondylitis with etanercept.* J Rheumatol, 2008. **35**(3): p. 532-6.

55. Yazisiz, V., et al., *Development of Crohn's disease following anti-tumour necrosis factor therapy (etanercept).* Colorectal Dis, 2008. **10**(9): p. 953-4.

56. Haraoui, B. and M. Krelenbaum, *Emergence of Crohn's disease during treatment with the anti-tumor necrosis factor agent etanercept for ankylosing spondylitis: possible mechanisms of action.* Semin Arthritis Rheum, 2009. **39**(3): p. 176-81.

57. Mrabet, D., et al., *[Onset of Crohn's disease induced by etanercept therapy: a case report].* Rev Med Liege, 2012. **67**(12): p. 619-22.

58. Freeman, H.J., *Colitis associated with biological agents.* World J Gastroenterol, 2012. **18**(16): p. 1871-4.

59. Dallocchio, A., et al., *Occurrence of inflammatory bowel disease during treatment of juvenile idiopathic arthritis with etanercept: a French retrospective study.* Rheumatology (Oxford), 2010. **49**(9): p. 1694-8.

60. Fouache, D., et al., *Paradoxical adverse events of anti-tumour necrosis factor therapy for spondyloarthropathies: a retrospective study.* Rheumatology (Oxford), 2009. **48**(7): p. 761-4.

61. Gerloni, V., et al., *Focus on adverse events of tumour necrosis factor alpha blockade in juvenile idiopathic arthritis in an open monocentric long-term prospective study of 163 patients.* Ann Rheum Dis, 2008. **67**(8): p. 1145-52.

62. Mitoma, H., et al., *Infliximab induces potent anti-inflammatory responses by outside-to-inside signals through transmembrane TNF-alpha.* Gastroenterology, 2005. **128**(2): p. 376-92.

63. Morgagni, G., *Jo. Baptistae Morgagni P.P.P.P. De sedibus, et causis morborum per anatomen indagatis, libri quinque : dissectiones, et animadversiones, nunc primum editas, complectuntur propemodum innumeras, medicis, chirurgis, anatomicis profuturas : multiplex praefixus est index rerum, & nominum accuratissimus*. Edito secunda / ed. 1765, Patavii: Sumptibus Remondinianis.

64. Morgagni, G.B., *The seats and causes of diseases investigated by anatomy; in five books, containing a great variety of dissections, with remarks*. 1960, New York,: Published under the auspices of the New York Academy of Medicine by Hafner Pub. Co.

65. Crohn, B.B., L. Ginzburg, and G.D. Oppenheimer, *Regional ileitis. A pathological and clinical entity.* JAMA, 1932. **99**(16): p. 1323-1329.

66. Fielding, J.F., *Crohn's disease and Dalziel's syndrome. A history.* J Clin Gastroenterol, 1988. **10**(3): p. 279-85.

67. Korzenik, J.R., *Past and current theories of etiology of IBD: toothpaste, worms, and refrigerators.* J Clin Gastroenterol, 2005. **39**(4 Suppl 2): p. S59-65.

68. Simon, G.L. and S.L. Gorbach, *Intestinal flora in health and disease.* Gastroenterology, 1984. **86**(1): p. 174-93.

69. Khan, K.J., et al., *Antibiotic therapy in inflammatory bowel disease: a systematic review and meta-analysis.* Am J Gastroenterol, 2011. **106**(4): p. 661-73.

70. Harper, P.H., et al., *Role of the faecal stream in the maintenance of Crohn's colitis.* Gut, 1985. **26**(3): p. 279-84.

71. Dalziel, T.K., *Chronic interstitial enteritis.* British Medical Journal, 1913. **1913**: p. 1068-1070.

72. Van Kruiningen, H.J., *Lack of support for a common etiology in Johne's disease of animals and Crohn's disease in humans.* Inflammatory Bowel Diseases, 1999. **5**(3): p. 183-191.

73. Ellingson, J.L., et al., *Absence of Mycobacterium avium subspecies paratuberculosis components from Crohn's disease intestinal biopsy tissues.* Clin Med Res, 2003. **1**(3): p. 217-26.

74. Selby, W., et al., *Two-year combination antibiotic therapy with clarithromycin, rifabutin, and clofazimine for Crohn's disease.* Gastroenterology, 2007. **132**(7): p. 2313-9.

75. Darfeuille-Michaud, A., et al., *High prevalence of adherent-invasive Escherichia coli associated with ileal mucosa in Crohn's disease.* Gastroenterology, 2004. **127**(2): p. 412-21.

76. Barnich, N., et al., *Regulatory and functional co-operation of flagella and type 1 pili in adhesive and invasive abilities of AIEC strain LF82 isolated from a patient with Crohn's disease.* Mol Microbiol, 2003. **48**(3): p. 781-94.

77. Barnich, N., et al., *CEACAM6 acts as a receptor for adherent-invasive E. coli, supporting ileal mucosa colonization in Crohn disease.* J Clin Invest, 2007. **117**(6): p. 1566-74.

78. Carvalho, F.A., et al., *Crohn's disease adherent-invasive Escherichia coli colonize and induce strong gut inflammation in transgenic mice expressing human CEACAM.* J Exp Med, 2009. **206**(10): p. 2179-89.

79. Chassaing, B., et al., *Crohn disease--associated adherent-invasive E. coli bacteria target mouse and human Peyer's patches via long polar fimbriae.* J Clin Invest, 2011. **121**(3): p. 966-75.

80. Glasser, A.L., et al., *Adherent invasive Escherichia coli strains from patients with Crohn's disease survive and replicate within macrophages without inducing host cell death.* Infect Immun, 2001. **69**(9): p. 5529-37.

81. Ryan, P., et al., *Bacterial DNA within granulomas of patients with Crohn's disease--detection by laser capture microdissection and PCR.* Am J Gastroenterol, 2004. **99**(8): p. 1539-43.

82. Manichanh, C., et al., *The gut microbiota in IBD.* Nature reviews. Gastroenterology & hepatology, 2012. **9**(10): p. 599-608.

83. Knights, D., K.G. Lassen, and R.J. Xavier, *Advances in inflammatory bowel disease pathogenesis: linking host genetics and the microbiome.* Gut, 2013. **62**(10): p. 1505-10.

84. Ott, S.J., et al., *Reduction in diversity of the colonic mucosa associated bacterial microflora in patients with active inflammatory bowel disease.* Gut, 2004. **53**(5): p. 685-93.

85. Manichanh, C., et al., *Reduced diversity of faecal microbiota in Crohn's disease revealed by a metagenomic approach.* Gut, 2006. **55**(2): p. 205-11.

86. Willing, B.P., et al., *A pyrosequencing study in twins shows that gastrointestinal microbial profiles vary with inflammatory bowel disease phenotypes.* Gastroenterology, 2010. **139**(6): p. 1844-1854 e1.

87. Sokol, H., et al., *Faecalibacterium prausnitzii is an anti-inflammatory commensal bacterium identified by gut microbiota analysis of Crohn disease patients.* Proc Natl Acad Sci U S A, 2008. **105**(43): p. 16731-6.

88. De Filippo, C., et al., *Impact of diet in shaping gut microbiota revealed by a comparative study in children from Europe and rural Africa.* Proc Natl Acad Sci U S A, 2010. **107**(33): p. 14691-6.

89. Orholm, M., et al., *Familial occurrence of inflammatory bowel disease.* N Engl J Med, 1991. **324**(2): p. 84-8.

90. Peeters, M., et al., *Familial aggregation in Crohn's disease: increased age-adjusted risk and concordance in clinical characteristics.* Gastroenterology, 1996. **111**(3): p. 597-603.

91. Yang, H., et al., *Familial empirical risks for inflammatory bowel disease: differences between Jews and non-Jews.* Gut, 1993. **34**(4): p. 517-24.

92. Halfvarson, J., et al., *Inflammatory bowel disease in a Swedish twin cohort: a long-term follow-up of concordance and clinical characteristics.* Gastroenterology, 2003. **124**(7): p. 1767-73.

93. Orholm, M., et al., *Concordance of inflammatory bowel disease among Danish twins. Results of a nationwide study.* Scand J Gastroenterol, 2000. **35**(10): p. 1075-81.

94. Tysk, C., et al., *Ulcerative colitis and Crohn's disease in an unselected population of monozygotic and dizygotic twins. A study of heritability and the influence of smoking.* Gut, 1988. **29**(7): p. 990-6.

95. Thompson, N.P., et al., *Genetics versus environment in inflammatory bowel disease: results of a British twin study.* BMJ, 1996. **312**(7023): p. 95-6.

96. Spehlmann, M.E., et al., *Epidemiology of inflammatory bowel disease in a German twin cohort: results of a nationwide study.* Inflamm Bowel Dis, 2008. **14**(7): p. 968-76.

97. Ogura, Y., et al., *A frameshift mutation in NOD2 associated with susceptibility to Crohn's disease.* Nature, 2001. **411**(6837): p. 603-6.

98. Hugot, J.P., et al., *Association of NOD2 leucine-rich repeat variants with susceptibility to Crohn's disease.* Nature, 2001. **411**(6837): p. 599-603.

99. Franke, A., et al., *Genome-wide meta-analysis increases to 71 the number of confirmed Crohn's disease susceptibility loci.* Nat Genet, 2010. **42**(12): p. 1118-25.

100. Jostins, L., et al., *Host-microbe interactions have shaped the genetic architecture of inflammatory bowel disease.* Nature, 2012. **491**(7422): p. 119-24.

101. Casanova, J.L. and L. Abel, *Revisiting Crohn's disease as a primary immunodeficiency of macrophages.* J Exp Med, 2009. **206**(9): p. 1839-43.

102. Rioux, J.D., et al., *Genome-wide association study identifies new susceptibility loci for Crohn disease and implicates autophagy in disease pathogenesis.* Nat Genet, 2007. **39**(5): p. 596-604.

103. Barnich, N., et al., *Membrane recruitment of NOD2 in intestinal epithelial cells is essential for nuclear factor-{kappa}B activation in muramyl dipeptide recognition.* J Cell Biol, 2005. **170**(1): p. 21-6.

104. Ogura, Y., et al., *Genetic variation and activity of mouse Nod2, a susceptibility gene for Crohn's disease.* Genomics, 2003. **81**(4): p. 369-77.

105. Philpott, D.J., et al., *NOD proteins: regulators of inflammation in health and disease.* Nat Rev Immunol, 2014. **14**(1): p. 9-23.

106. van Heel, D.A., et al., *Muramyl dipeptide and toll-like receptor sensitivity in NOD2-associated Crohn's disease.* Lancet, 2005. **365**(9473): p. 1794-6.

107. Marks, D.J., et al., *Defective acute inflammation in Crohn's disease: a clinical investigation.* Lancet, 2006. **367**(9511): p. 668-78.

108. Inohara, N., et al., *Host recognition of bacterial muramyl dipeptide mediated through NOD2. Implications for Crohn's disease.* J Biol Chem, 2003. **278**(8): p. 5509-12.

109. Girardin, S.E., et al., *Nod2 is a general sensor of peptidoglycan through muramyl dipeptide (MDP) detection.* J Biol Chem, 2003. **278**(11): p. 8869-72.

110. Economou, M., et al., *Differential effects of NOD2 variants on Crohn's disease risk and phenotype in diverse populations: a metaanalysis.* Am J Gastroenterol, 2004. **99**(12): p. 2393-404.

111. Watanabe, T., et al., *NOD2 is a negative regulator of Toll-like receptor 2-mediated T helper type 1 responses.* Nat Immunol, 2004. **5**(8): p. 800-8.

112. Noguchi, E., et al., *A Crohn's disease-associated NOD2 mutation suppresses transcription of human IL10 by inhibiting activity of the*

nuclear ribonucleoprotein hnRNP-A1. Nat Immunol, 2009. **10**(5): p. 471-9.

113. Wehkamp, J., et al., *NOD2 (CARD15) mutations in Crohn's disease are associated with diminished mucosal alpha-defensin expression.* Gut, 2004. **53**(11): p. 1658-64.

114. Voss, E., et al., *NOD2/CARD15 mediates induction of the antimicrobial peptide human beta-defensin-2.* J Biol Chem, 2006. **281**(4): p. 2005-11.

115. D'Inca, R., et al., *Increased intestinal permeability and NOD2 variants in familial and sporadic Crohn's disease.* Aliment Pharmacol Ther, 2006. **23**(10): p. 1455-61.

116. Russell, R.K., et al., *Genotype-phenotype analysis in childhood-onset Crohn's disease: NOD2/CARD15 variants consistently predict phenotypic characteristics of severe disease.* Inflamm Bowel Dis, 2005. **11**(11): p. 955-64.

117. Laghi, L., et al., *Carriage of CARD15 variants and smoking as risk factors for resective surgery in patients with Crohn's ileal disease.* Aliment Pharmacol Ther, 2005. **22**(6): p. 557-64.

118. Hugot, J.P., et al., *Prevalence of CARD15/NOD2 mutations in Caucasian healthy people.* Am J Gastroenterol, 2007. **102**(6): p. 1259-67.

119. Hampe, J., et al., *A genome-wide association scan of nonsynonymous SNPs identifies a susceptibility variant for Crohn disease in ATG16L1.* Nat Genet, 2007. **39**(2): p. 207-11.

120. Prescott, N.J., et al., *A nonsynonymous SNP in ATG16L1 predisposes to ileal Crohn's disease and is independent of CARD15 and IBD5.* Gastroenterology, 2007. **132**(5): p. 1665-71.

121. Cotterill, L., et al., *Replication and meta-analysis of 13,000 cases defines the risk for interleukin-23 receptor and autophagy-related 16-like 1 variants in Crohn's disease.* Can J Gastroenterol, 2010. **24**(5): p. 297-302.

122. Levine, B., N. Mizushima, and H.W. Virgin, *Autophagy in immunity and inflammation.* Nature, 2011. **469**(7330): p. 323-35.

123. Klionsky, D.J., et al., *Guidelines for the use and interpretation of assays for monitoring autophagy.* Autophagy, 2012. **8**(4): p. 445-544.

124. Tumbarello, D.A., et al., *Autophagy receptors link myosin VI to autophagosomes to mediate Tom1-dependent autophagosome maturation and fusion with the lysosome.* Nature cell biology, 2012. **14**(10): p. 1024-35.

125. Wild, P., et al., *Phosphorylation of the Autophagy Receptor Optineurin Restricts Salmonella Growth.* Science, 2011.

126. Sanjuan, M.A., et al., *Toll-like receptor signalling in macrophages links the autophagy pathway to phagocytosis.* Nature, 2007. **450**(7173): p. 1253-7.

127. Kuballa, P., et al., *Impaired autophagy of an intracellular pathogen induced by a Crohn's disease associated ATG16L1 variant.* PLoS One, 2008. **3**(10): p. e3391.

128. Saitoh, T., et al., *Loss of the autophagy protein Atg16L1 enhances endotoxin-induced IL-1beta production.* Nature, 2008. **456**(7219): p. 264-8.

129. Cadwell, K., et al., *A key role for autophagy and the autophagy gene Atg16l1 in mouse and human intestinal Paneth cells.* Nature, 2008. **456**(7219): p. 259-63.

130. Cadwell, K., et al., *Virus-plus-susceptibility gene interaction determines Crohn's disease gene Atg16L1 phenotypes in intestine.* Cell, 2010. **141**(7): p. 1135-45.

131. Cooney, R., et al., *NOD2 stimulation induces autophagy in dendritic cells influencing bacterial handling and antigen presentation.* Nat Med, 2010. **16**(1): p. 90-7.

132. Plantinga, T.S., et al., *Crohn's disease-associated ATG16L1 polymorphism modulates pro-inflammatory cytokine responses selectively upon activation of NOD2.* Gut, 2011. **60**(9): p. 1229-35.

133. Iles, M.M., *What can genome-wide association studies tell us about the genetics of common disease?* PLoS Genet, 2008. **4**(2): p. e33.

134. Manolio, T.A., et al., *Finding the missing heritability of complex diseases.* Nature, 2009. **461**(7265): p. 747-53.

135. Celsus, A.C., *De medicina*. 1478, Florence,: Nicolaus Laurentii, Alamanus. 196 leaves (the last blank).

136. Kaufmann, S.H., *Immunology's foundation: the 100-year anniversary of the Nobel Prize to Paul Ehrlich and Elie Metchnikoff.* Nat Immunol, 2008. **9**(7): p. 705-12.

137. Davies, L.C., et al., *Tissue-resident macrophages.* Nat Immunol, 2013. **14**(10): p. 986-95.

138. Hoebe, K., et al., *Identification of Lps2 as a key transducer of MyD88-independent TIR signalling.* Nature, 2003. **424**(6950): p. 743-8.

139. Hoffmann, J.A., *The immune response of Drosophila.* Nature, 2003. **426**(6962): p. 33-8.

140. Medzhitov, R., *Toll-like receptors and innate immunity.* Nat Rev Immunol, 2001. **1**(2): p. 135-45.

141. Ivashkiv, L.B. and L.T. Donlin, *Regulation of type I interferon responses.* Nat Rev Immunol, 2014. **14**(1): p. 36-49.

142. Wagner, J.G. and R.A. Roth, *Neutrophil migration mechanisms, with an emphasis on the pulmonary vasculature.* Pharmacol Rev, 2000. **52**(3): p. 349-74.

143. Fournier, B.M. and C.A. Parkos, *The role of neutrophils during intestinal inflammation.* Mucosal Immunol, 2012. **5**(4): p. 354-66.

144. Cross, A.R. and A.W. Segal, *The NADPH oxidase of professional phagocytes--prototype of the NOX electron transport chain systems.* Biochim Biophys Acta, 2004. **1657**(1): p. 1-22.

145. Borregaard, N., O.E. Sorensen, and K. Theilgaard-Monch, *Neutrophil granules: a library of innate immunity proteins.* Trends Immunol, 2007. **28**(8): p. 340-5.

146. Kuhl, A.A., et al., *Aggravation of different types of experimental colitis by depletion or adhesion blockade of neutrophils.* Gastroenterology, 2007. **133**(6): p. 1882-92.

147. Nemoto, Y., et al., *Negative feedback regulation of colitogenic CD4+ T cells by increased granulopoiesis.* Inflamm Bowel Dis, 2008. **14**(11): p. 1491-503.

148. Zhang, R., et al., *Up-regulation of Gr1+CD11b+ population in spleen of dextran sulfate sodium administered mice works to repair colitis.* Inflamm Allergy Drug Targets, 2011. **10**(1): p. 39-46.

149. Shea-Donohue, T., et al., *Mice deficient in the CXCR2 ligand, CXCL1 (KC/GRO-alpha), exhibit increased susceptibility to dextran sodium sulfate (DSS)-induced colitis.* Innate Immun, 2008. **14**(2): p. 117-24.

150. Qualls, J.E., et al., *Suppression of experimental colitis by intestinal mononuclear phagocytes.* J Leukoc Biol, 2006. **80**(4): p. 802-15.

151. van Furth, R. and Z.A. Cohn, *The origin and kinetics of mononuclear phagocytes.* J Exp Med, 1968. **128**(3): p. 415-35.

152. Yona, S., et al., *Fate mapping reveals origins and dynamics of monocytes and tissue macrophages under homeostasis.* Immunity, 2013. **38**(1): p. 79-91.

153. Varol, C., et al., *Monocytes give rise to mucosal, but not splenic, conventional dendritic cells.* J Exp Med, 2007. **204**(1): p. 171-80.

154. Ginhoux, F. and S. Jung, *Monocytes and macrophages: developmental pathways and tissue homeostasis.* Nat Rev Immunol, 2014. **14**(6): p. 392-404.

155. Geissmann, F., et al., *Development of monocytes, macrophages, and dendritic cells.* Science, 2010. **327**(5966): p. 656-61.

156. Rees, A.J., *Monocyte and macrophage biology: an overview.* Semin Nephrol, 2010. **30**(3): p. 216-33.

157. Gordon, S. and P.R. Taylor, *Monocyte and macrophage heterogeneity.* Nature reviews. Immunology, 2005. **5**(12): p. 953-64.

158. Stow, J.L. and R.Z. Murray, *Intracellular trafficking and secretion of inflammatory cytokines.* Cytokine & growth factor reviews, 2013. **24**(3): p. 227-39.

159. Carballo, E., W.S. Lai, and P.J. Blackshear, *Feedback inhibition of macrophage tumor necrosis factor-alpha production by tristetraprolin.* Science, 1998. **281**(5379): p. 1001-5.

160. Han, J., T. Brown, and B. Beutler, *Endotoxin-responsive sequences control cachectin/tumor necrosis factor biosynthesis at the translational level.* J Exp Med, 1990. **171**(2): p. 465-75.

161. Shurety, W., et al., *Localization and post-Golgi trafficking of tumor necrosis factor-alpha in macrophages.* Journal of interferon & cytokine research : the official journal of the International Society for Interferon and Cytokine Research, 2000. **20**(4): p. 427-38.

162. Murray, R.Z., et al., *A role for the phagosome in cytokine secretion.* Science, 2005. **310**(5753): p. 1492-5.

163. Lieu, Z.Z., et al., *A trans-Golgi network golgin is required for the regulated secretion of TNF in activated macrophages in vivo.* Proceedings of the National Academy of Sciences of the United States of America, 2008. **105**(9): p. 3351-6.

164. Micaroni, M., et al., *Rab6a/a' are important Golgi regulators of pro-inflammatory TNF secretion in macrophages.* PLoS One, 2013. **8**(2): p. e57034.

165. Low, P.C., et al., *Phosphoinositide 3-kinase delta regulates membrane fission of Golgi carriers for selective cytokine secretion.* J Cell Biol, 2010. **190**(6): p. 1053-65.

166. De Matteis, M.A. and A. Luini, *Exiting the Golgi complex.* Nat Rev Mol Cell Biol, 2008. **9**(4): p. 273-84.

167. Murray, R.Z., et al., *Syntaxin 6 and Vti1b form a novel SNARE complex, which is up-regulated in activated macrophages to facilitate exocytosis of tumor necrosis Factor-alpha.* J Biol Chem, 2005. **280**(11): p. 10478-83.

168. Pagan, J.K., et al., *The t-SNARE syntaxin 4 is regulated during macrophage activation to function in membrane traffic and cytokine secretion.* Curr Biol, 2003. **13**(2): p. 156-60.

169. Kay, J.G., et al., *Cytokine secretion via cholesterol-rich lipid raft-associated SNAREs at the phagocytic cup.* J Biol Chem, 2006. **281**(17): p. 11949-54.

170. Tellier, E., et al., *The shedding activity of ADAM17 is sequestered in lipid rafts.* Exp Cell Res, 2006. **312**(20): p. 3969-80.

171. Manderson, A.P., et al., *Subcompartments of the macrophage recycling endosome direct the differential secretion of IL-6 and TNFalpha.* J Cell Biol, 2007. **178**(1): p. 57-69.

172. Stanley, A.C., et al., *Recycling endosome-dependent and -independent mechanisms for IL-10 secretion in LPS-activated macrophages.* Journal of leukocyte biology, 2012. **92**(6): p. 1227-39.

173. Barthel, C., et al., *A distinct pattern of disease-associated single nucleotide polymorphisms in IBD risk genes in a family with Crohn's disease.* Eur J Gastroenterol Hepatol, 2014. **26**(7): p. 803-6.

174. Morgan, A.R., et al., *Genetic variation within TLR10 is associated with Crohn's disease in a New Zealand population.* Hum Immunol, 2012. **73**(4): p. 416-20.

175. Franchimont, D., et al., *Deficient host-bacteria interactions in inflammatory bowel disease? The toll-like receptor (TLR)-4 Asp299gly polymorphism is associated with Crohn's disease and ulcerative colitis.* Gut, 2004. **53**(7): p. 987-92.

176. Torok, H.P., et al., *Crohn's disease is associated with a toll-like receptor-9 polymorphism.* Gastroenterology, 2004. **127**(1): p. 365-6.

177. Klein, W., et al., *A polymorphism in the CD14 gene is associated with Crohn disease.* Scand J Gastroenterol, 2002. **37**(2): p. 189-91.

178. D'Agata, I.D., et al., *Leucocyte adhesion deficiency presenting as a chronic ileocolitis.* Gut, 1996. **39**(4): p. 605-8.

179. Hazzan, D., et al., *Crohn's-like colitis, enterocolitis and perianal disease in Hermansky-Pudlak syndrome.* Colorectal Dis, 2006. **8**(7): p. 539-43.

180. Ishii, E., et al., *Chediak-Higashi syndrome with intestinal complication. Report of a case.* J Clin Gastroenterol, 1987. **9**(5): p. 556-8.

181. Huang, A., F. Abbasakoor, and C.J. Vaizey, *Gastrointestinal manifestations of chronic granulomatous disease.* Colorectal Dis, 2006. **8**(8): p. 637-44.

182. Ament, M.E. and H.D. Ochs, *Gastrointestinal manifestations of chronic granulomatous disease.* N Engl J Med, 1973. **288**(8): p. 382-7.

183. Dieckgraefe, B.K., et al., *Association of glycogen storage disease 1b and Crohn disease: results of a North American survey.* Eur J Pediatr, 2002. **161 Suppl 1**: p. S88-92.

184. Couper, R., J. Kapelushnik, and A.M. Griffiths, *Neutrophil dysfunction in glycogen storage disease Ib: association with Crohn's-like colitis.* Gastroenterology, 1991. **100**(2): p. 549-54.

185. Marks, D.J., et al., *Inflammatory bowel disease in CGD reproduces the clinicopathological features of Crohn's disease.* Am J Gastroenterol, 2009. **104**(1): p. 117-24.

186. Rahman, F.Z., et al., *Phagocyte dysfunction and inflammatory bowel disease.* Inflamm Bowel Dis, 2008. **14**(10): p. 1443-52.

187. Smith, A.M., et al., *Disordered macrophage cytokine secretion underlies impaired acute inflammation and bacterial clearance in Crohn's disease.* J Exp Med, 2009. **206**(9): p. 1883-97.

188. Sewell, G.W., et al., *Defective tumor necrosis factor release from Crohn's disease macrophages in response to toll-like receptor activation: Relationship to phenotype and genome-wide association susceptibility loci.* Inflamm Bowel Dis, 2012.

189. Roden, D.L., et al., *ZODET: software for the identification, analysis and visualisation of outlier genes in microarray expression data.* PLoS One, 2014. **9**(1): p. e81123.

190. Tomlins, S.A., et al., *Recurrent fusion of TMPRSS2 and ETS transcription factor genes in prostate cancer.* Science, 2005. **310**(5748): p. 644-8.

191. Smith, A., et al., *Disruption of macrophage pro-inflammatory cytokine release in Crohn's disease is associated with reduced optineurin expression in a subset of patients.* Immunology, 2014.

192. Sewell, G.W., D.J. Marks, and A.W. Segal, *The immunopathogenesis of Crohn's disease: a three-stage model.* Curr Opin Immunol, 2009. **21**(5): p. 506-13.

193. Li, Y., J. Kang, and M.S. Horwitz, *Interaction of an adenovirus E3 14.7-kilodalton protein with a novel tumor necrosis factor alpha-inducible cellular protein containing leucine zipper domains.* Mol Cell Biol, 1998. **18**(3): p. 1601-10.

194. Rezaie, T., et al., *Adult-onset primary open-angle glaucoma caused by mutations in optineurin.* Science, 2002. **295**(5557): p. 1077-9.

195. Ying, H. and B.Y. Yue, *Cellular and molecular biology of optineurin.* Int Rev Cell Mol Biol, 2012. **294**: p. 223-58.

196. Rezaie, T. and M. Sarfarazi, *Molecular cloning, genomic structure, and protein characterization of mouse optineurin.* Genomics, 2005. **85**(1): p. 131-8.

197. Kachaner, D., et al., *Toward an integrative view of Optineurin functions.* Cell cycle, 2012. **11**(15): p. 2808-18.

198. Sudhakar, C., et al., *NF-kappaB mediates tumor necrosis factor alpha-induced expression of optineurin, a negative regulator of NF-kappaB.* PLoS One, 2009. **4**(4): p. e5114.

199. Rezaie, T., et al., *Molecular cloning and expression profiling of optineurin in the rhesus monkey.* Invest Ophthalmol Vis Sci, 2005. **46**(7): p. 2404-10.

200. Gleason, C.E., et al., *Polyubiquitin binding to optineurin is required for optimal activation of TANK-binding kinase 1 and production of interferon beta.* The Journal of biological chemistry, 2011. **286**(41): p. 35663-74.

201. Sahlender, D.A., et al., *Optineurin links myosin VI to the Golgi complex and is involved in Golgi organization and exocytosis.* J Cell Biol, 2005. **169**(2): p. 285-95.

202. Hattula, K. and J. Peranen, *FIP-2, a coiled-coil protein, links Huntingtin to Rab8 and modulates cellular morphogenesis.* Curr Biol, 2000. **10**(24): p. 1603-6.

203. Au, J.S., et al., *Myosin VI is required for sorting of AP-1B-dependent cargo to the basolateral domain in polarized MDCK cells.* J Cell Biol, 2007. **177**(1): p. 103-14.

204. Chibalina, M.V., et al., *Myosin VI and optineurin are required for polarized EGFR delivery and directed migration.* Traffic, 2010. **11**(10): p. 1290-303.

205. Bond, L.M., et al., *Myosin VI and its binding partner optineurin are involved in secretory vesicle fusion at the plasma membrane.* Mol Biol Cell, 2011. **22**(1): p. 54-65.

206. del Toro, D., et al., *Mutant huntingtin impairs post-Golgi trafficking to lysosomes by delocalizing optineurin/Rab8 complex from the Golgi apparatus.* Mol Biol Cell, 2009. **20**(5): p. 1478-92.

207. Caviston, J.P., et al., *Huntingtin coordinates the dynein-mediated dynamic positioning of endosomes and lysosomes.* Molecular biology of the cell, 2011. **22**(4): p. 478-92.

208. Nagabhushana, A., et al., *Regulation of endocytic trafficking of transferrin receptor by optineurin and its impairment by a glaucoma-associated mutant.* BMC Cell Biol, 2010. **11**: p. 4.

209. Park, B., et al., *Impairment of protein trafficking upon overexpression and mutation of optineurin.* PLoS One, 2010. **5**(7): p. e11547.

210. Sippl, C., et al., *Depletion of optineurin in RGC-5 cells derived from retinal neurons causes apoptosis and reduces the secretion of neurotrophins.* Experimental eye research, 2011. **93**(5): p. 669-80.

211. Shen, X., et al., *Processing of optineurin in neuronal cells.* J Biol Chem, 2011. **286**(5): p. 3618-29.

212. Morton, S., et al., *Enhanced binding of TBK1 by an optineurin mutant that causes a familial form of primary open angle glaucoma.* FEBS Lett, 2008. **582**(6): p. 997-1002.

213. Munitic, I., et al., *Optineurin insufficiency impairs IRF3 but not NF-kappaB activation in immune cells.* Journal of immunology, 2013. **191**(12): p. 6231-40.

214. Mankouri, J., et al., *Optineurin negatively regulates the induction of IFNbeta in response to RNA virus infection.* PLoS Pathog, 2010. **6**(2): p. e1000778.

215. Maruyama, H., et al., *Mutations of optineurin in amyotrophic lateral sclerosis.* Nature, 2010. **465**(7295): p. 223-6.

216. Ito, H., et al., *Optineurin is co-localized with FUS in basophilic inclusions of ALS with FUS mutation and in basophilic inclusion body disease.* Acta Neuropathol, 2011. **121**(4): p. 555-7.

217. Sakaguchi, T., et al., *Optineurin with amyotrophic lateral sclerosis-related mutations abrogates inhibition of interferon regulatory factor-3 activation.* Neurosci Lett, 2011. **505**(3): p. 279-81.

218. Del Bo, R., et al., *Novel optineurin mutations in patients with familial and sporadic amyotrophic lateral sclerosis.* J Neurol Neurosurg Psychiatry, 2011.

219. Tumer, Z., et al., *Novel heterozygous nonsense mutation of the OPTN gene segregating in a Danish family with ALS.* Neurobiol Aging, 2012. **33**(1): p. 208 e1-5.

220. Millecamps, S., et al., *Screening of OPTN in French familial amyotrophic lateral sclerosis.* Neurobiol Aging, 2011. **32**(3): p. 557 e11-3.

221. Solski, J.A., et al., *Mutation analysis of the optineurin gene in familial amyotrophic lateral sclerosis.* Neurobiol Aging, 2012. **33**(1): p. 210 e9-10.

222. Belzil, V.V., et al., *Analysis of OPTN as a causative gene for amyotrophic lateral sclerosis.* Neurobiol Aging, 2011. **32**(3): p. 555 e13-4.

223. Chi, Z.L., et al., *Overexpression of optineurin E50K disrupts Rab8 interaction and leads to a progressive retinal degeneration in mice.* Hum Mol Genet, 2010. **19**(13): p. 2606-15.

224. De Marco, N., et al., *Optineurin increases cell survival and translocates to the nucleus in a Rab8-dependent manner upon an apoptotic stimulus.* J Biol Chem, 2006. **281**(23): p. 16147-56.

225. Albagha, O.M., et al., *Genome-wide association study identifies variants at CSF1, OPTN and TNFRSF11A as genetic risk factors for Paget's disease of bone.* Nat Genet, 2010. **42**(6): p. 520-4.

226. Michou, L., et al., *Genetic association study of UCMA/GRP and OPTN genes (PDB6 locus) with Paget's disease of bone.* Bone, 2012. **51**(4): p. 720-8.

227. Lucas, G.J., et al., *Identification of a major locus for Paget's disease on chromosome 10p13 in families of British descent.* J Bone Miner Res, 2008. **23**(1): p. 58-63.

228. Satsangi, J., et al., *The Montreal classification of inflammatory bowel disease: controversies, consensus, and implications.* Gut, 2006. **55**(6): p. 749-53.

229. Harvey, R.F. and M.J. Bradshaw, *Measuring Crohn's disease activity.* Lancet, 1980. **1**(8178): p. 1134-5.

230. Skarnes, W.C., et al., *A conditional knockout resource for the genome-wide study of mouse gene function.* Nature, 2011. **474**(7351): p. 337-42.

231. Livak, K.J. and T.D. Schmittgen, *Analysis of relative gene expression data using real-time quantitative PCR and the 2(-Delta Delta C(T)) Method.* Methods, 2001. **25**(4): p. 402-8.

232. Mulvey, C.M., et al., *Subcellular proteomics reveals a role for nucleo-cytoplasmic trafficking at the DNA replication origin activation checkpoint.* J Proteome Res, 2013. **12**(3): p. 1436-53.

233. Oehlers, S.H., et al., *Expression of zebrafish cxcl8 (interleukin-8) and its receptors during development and in response to immune stimulation.* Dev Comp Immunol, 2010. **34**(3): p. 352-9.

234. Prajsnar, T.K., et al., *A novel vertebrate model of Staphylococcus aureus infection reveals phagocyte-dependent resistance of zebrafish to non-host specialized pathogens.* Cell Microbiol, 2008. **10**(11): p. 2312-25.

235. Oehlers, S.H., et al., *Topographical distribution of antimicrobial genes in the zebrafish intestine.* Dev Comp Immunol, 2011. **35**(3): p. 385-91.

236. Nasevicius, A. and S.C. Ekker, *Effective targeted gene 'knockdown' in zebrafish.* Nat Genet, 2000. **26**(2): p. 216-20.

237. Wirtz, S., et al., *Chemically induced mouse models of intestinal inflammation.* Nat Protoc, 2007. **2**(3): p. 541-6.

238. Cooper, H.S., et al., *Clinicopathologic study of dextran sulfate sodium experimental murine colitis.* Lab Invest, 1993. **69**(2): p. 238-49.

239. Weigmann, B., et al., *Isolation and subsequent analysis of murine lamina propria mononuclear cells from colonic tissue.* Nat Protoc, 2007. **2**(10): p. 2307-11.

240. Ward, J.M., et al., *Immunohistochemical markers for the rodent immune system.* Toxicol Pathol, 2006. **34**(5): p. 616-30.

241. de Bruyn, M., et al., *Infliximab restores the dysfunctional matrix remodeling protein and growth factor gene expression in patients with inflammatory bowel disease.* Inflamm Bowel Dis, 2014. **20**(2): p. 339-52.

242. O'shea, N.R., et al., *Adamdec1: A Novel Molecule Linked to Crohn's Disease, Is Associated with an Increased Susceptibility to Citrobacter Rodentium Colitis in the Knock out Mouse.* Gut, 2013. **62**: p. A8-A9.

243. Zeissig, Y., et al., *XIAP variants in male Crohn's disease.* Gut, 2014.

244. Cuthbert, A.P., et al., *The contribution of NOD2 gene mutations to the risk and site of disease in inflammatory bowel disease.* Gastroenterology, 2002. **122**(4): p. 867-74.

245. Yang, T.P., et al., *Genevar: a database and Java application for the analysis and visualization of SNP-gene associations in eQTL studies.* Bioinformatics, 2010. **26**(19): p. 2474-6.

246. Nica, A.C., et al., *The architecture of gene regulatory variation across multiple human tissues: the MuTHER study.* PLoS genetics, 2011. **7**(2): p. e1002003.

247. Hemani, G., et al., *Detection and replication of epistasis influencing transcription in humans.* Nature, 2014. **508**(7495): p. 249-53.

248. Hindorff, L.A., et al., *Potential etiologic and functional implications of genome-wide association loci for human diseases and traits.* Proc Natl Acad Sci U S A, 2009. **106**(23): p. 9362-7.

249. Brant, S.R., et al., *A population-based case-control study of CARD15 and other risk factors in Crohn's disease and ulcerative colitis.* Am J Gastroenterol, 2007. **102**(2): p. 313-23.

250. Mitroulis, I., et al., *Regulation of the autophagic machinery in human neutrophils.* Eur J Immunol, 2010. **40**(5): p. 1461-72.

251. Altstaedt, J., H. Kirchner, and L. Rink, *Cytokine production of neutrophils is limited to interleukin-8.* Immunology, 1996. **89**(4): p. 563-8.

252. Dippold, H.C., et al., *GOLPH3 bridges phosphatidylinositol-4-phosphate and actomyosin to stretch and shape the Golgi to promote budding.* Cell, 2009. **139**(2): p. 337-51.

253. Mollenhauer, H.H., D.J. Morre, and L.D. Rowe, *Alteration of intracellular traffic by monensin; mechanism, specificity and relationship to toxicity.* Biochim Biophys Acta, 1990. **1031**(2): p. 225-46.

254. Homewood, C.A., et al., *Lysosomes, pH and the anti-malarial action of chloroquine.* Nature, 1972. **235**(5332): p. 50-2.

255. Seglen, P.O., *Inhibitors of lysosomal function.* Methods Enzymol, 1983. **96**: p. 737-64.

256. Chanput, W., J.J. Mes, and H.J. Wichers, *THP-1 cell line: An in vitro cell model for immune modulation approach.* Int Immunopharmacol, 2014.

257. Varol, C., et al., *Intestinal lamina propria dendritic cell subsets have different origin and functions.* Immunity, 2009. **31**(3): p. 502-12.

258. Bogunovic, M., et al., *Origin of the lamina propria dendritic cell network.* Immunity, 2009. **31**(3): p. 513-25.

259. Gallily, R., A. Warwick, and F.B. Bang, *Effect of Cortisone of Genetic Resistance to Mouse Hepatitis Virus in Vivo and in Vitro.* Proc Natl Acad Sci U S A, 1964. **51**: p. 1158-64.

260. Barski, G., G. Messore, and P. Lepine, *[Artificial peritoneal exudate, source of cells for virus culture in vitro].* Ann Inst Pasteur (Paris), 1955. **89**(3): p. 366-71.

261. Leijh, P.C., et al., *Effect of thioglycolate on phagocytic and microbicidal activities of peritoneal macrophages.* Infect Immun, 1984. **46**(2): p. 448-52.

262. Wang, C., et al., *Characterization of murine macrophages from bone marrow, spleen and peritoneum.* BMC Immunol, 2013. **14**: p. 6.

263. Kaser, A., T.E. Adolph, and R.S. Blumberg, *The unfolded protein response and gastrointestinal disease.* Seminars in immunopathology, 2013. **35**(3): p. 307-19.

264. Kaser, A. and R.S. Blumberg, *Autophagy, microbial sensing, endoplasmic reticulum stress, and epithelial function in inflammatory bowel disease.* Gastroenterology, 2011. **140**(6): p. 1738-47.

265. Kaser, A., et al., *XBP1 links ER stress to intestinal inflammation and confers genetic risk for human inflammatory bowel disease.* Cell, 2008. **134**(5): p. 743-56.

266. Collins, J.W., et al., *Citrobacter rodentium: infection, inflammation and the microbiota.* Nat Rev Microbiol, 2014.

267. Lebeis, S.L., et al., *TLR signaling mediated by MyD88 is required for a protective innate immune response by neutrophils to Citrobacter rodentium.* J Immunol, 2007. **179**(1): p. 566-77.

268. Ni, J., S.F. Chen, and D. Hollander, *Effects of dextran sulphate sodium on intestinal epithelial cells and intestinal lymphocytes.* Gut, 1996. **39**(2): p. 234-41.

269. Oehlers, S.H., et al., *The inflammatory bowel disease (IBD) susceptibility genes NOD1 and NOD2 have conserved anti-bacterial roles in zebrafish.* Dis Model Mech, 2011. **4**(6): p. 832-41.

270. Korac, J., et al., *Ubiquitin-independent function of optineurin in autophagic clearance of protein aggregates.* J Cell Sci, 2013. **126**(Pt 2): p. 580-92.

271. Kinna, G., et al., *Knockdown of zebrafish crim1 results in a bent tail phenotype with defects in somite and vascular development.* Mech Dev, 2006. **123**(4): p. 277-87.

272. Brand, M., et al., *Mutations affecting development of the midline and general body shape during zebrafish embryogenesis.* Development, 1996. **123**: p. 129-42.

273. Mitchison, H.M., et al., *Mutations in axonemal dynein assembly factor DNAAF3 cause primary ciliary dyskinesia.* Nat Genet, 2012. **44**(4): p. 381-9, S1-2.

274. Jenkins, S.J., et al., *Local macrophage proliferation, rather than recruitment from the blood, is a signature of TH2 inflammation.* Science, 2011. **332**(6035): p. 1284-8.

275. Ghosn, E.E., et al., *Two physically, functionally, and developmentally distinct peritoneal macrophage subsets.* Proc Natl Acad Sci U S A, 2010. **107**(6): p. 2568-73.

276. Kim, Y.G., et al., *The Nod2 sensor promotes intestinal pathogen eradication via the chemokine CCL2-dependent recruitment of inflammatory monocytes.* Immunity, 2011. **34**(5): p. 769-80.

277. Ohkusa, T., *[Production of experimental ulcerative colitis in hamsters by dextran sulfate sodium and changes in intestinal microflora].* Nihon Shokakibyo Gakkai Zasshi, 1985. **82**(5): p. 1327-36.

278. Kobayashi, K.S., et al., *Nod2-dependent regulation of innate and adaptive immunity in the intestinal tract.* Science, 2005. **307**(5710): p. 731-4.

279. Watanabe, T., et al., *Muramyl dipeptide activation of nucleotide-binding oligomerization domain 2 protects mice from experimental colitis.* J Clin Invest, 2008. **118**(2): p. 545-59.

280. Couturier-Maillard, A., et al., *NOD2-mediated dysbiosis predisposes mice to transmissible colitis and colorectal cancer.* J Clin Invest, 2013. **123**(2): p. 700-11.

281. Zurita, E., et al., *Genetic polymorphisms among C57BL/6 mouse inbred strains.* Transgenic Res, 2011. **20**(3): p. 481-9.

282. Karaiskos, C., et al., *Defective Macrophage Function in Crohn's Disease: Role of Alternatively Activated Macrophages in Inflammation.* Gut, 2011. **60**.

283. Campos, N., et al., *Macrophages from IBD patients exhibit defective tumour necrosis factor-alpha secretion but otherwise normal or augmented pro-inflammatory responses to infection.* Immunobiology, 2011. **216**(8): p. 961-70.

284. Farthing, M.J., *Bugs and the gut: an unstable marriage.* Best Pract Res Clin Gastroenterol, 2004. **18**(2): p. 233-9.

285. Marino, M.W., et al., *Characterization of tumor necrosis factor-deficient mice.* Proc Natl Acad Sci U S A, 1997. **94**(15): p. 8093-8.

286. Xu, Y., N.H. Hunt, and S. Bao, *The correlation between proinflammatory cytokines, MAdCAM-1 and cellular infiltration in the inflamed colon from TNF-alpha gene knockout mice.* Immunol Cell Biol, 2007. **85**(8): p. 633-9.

287. Naito, Y., et al., *Enhanced intestinal inflammation induced by dextran sulfate sodium in tumor necrosis factor-alpha deficient mice.* J Gastroenterol Hepatol, 2003. **18**(5): p. 560-9.

Image References

Figure 1a. *Burrill B. Crohn* [photo]. From: http://en.wikipedia.org/wiki/Burrill_Bernard_Crohn (accessed 25/07/2014).

Figure 1b. *Terminal ileum with Crohn's disease* [photo of pathology specimen]. Segal, A. W. (2009).

Figure 1c. *Severe Crohn's disease in the sigmoid colon* [photo]. From: http://www.gastrolab.fi/images/a146.jpg (accessed 25/07/2014).

Figure 1d. *Small bowel follow through from a patient with a history of Crohn's disease* [radiographic image]. From: Patel, P., M. Ormanoski, and K.M. Hoadley, *Magnetic Resonance Enterography Findings in Crohn's disease in the Pediatric Population and Correlation with Fluoroscopic and Multidetector Computed Tomographic Techniques.* J Clin Imaging Sci, 2011. **1**: p. 41.

Figure 1e. *Crohn's disease in the colon showing granuloma* [photo]. From: http://commons.wikimedia.org/wiki/File:Crohn%27s_disease_-_colon__high_mag.jpg (accessed 25/07/2014)

Figure 1f. *Composite image of corticosterone, adalimumab, mesalazine and azathioprine* [chemical structures]. From: http://en.wikipedia.org/wiki/Corticosteroid#mediaviewer/File:Corticosterone.svg; Keystone, E.C. and C.F. Ware, *Tumor necrosis factor and anti-tumor necrosis factor therapies.* J Rheumatol Suppl, 2010. **85**: p. 27-39; http://en.wikipedia.org/wiki/Mesalazine#mediaviewer/File:Mesalazine_structure.svg;http://en.wikipedia.org/wiki/Azathioprine#mediaviewer/File:Azathioprine3Dan.gif (accessed 25/07/2014).

Figure 1g. *Montreal classification of Crohn's disease* [table]. From: Satsangi, J., et al., *The Montreal classification of inflammatory bowel disease: controversies, consensus, and implications.* Gut, 2006. **55**(6): p. 749-53.

Figure 1h. *Montreal classification of Crohn's disease* [figure]. From: http://researchonmedical.com/2013/07/10-guidelines-about-diet-modification-and-nutritional-management-in-crohn-disease/ (accessed 25/07/2014).

Figure 1i. *Uveitis in Crohn's disease* [photo]. Segal, A. W. (2009).

Figure 1j. *Pyoderma gangrenosum on the leg of a patient with Crohn's disease* [photo]. From: http://en.wikipedia.org/wiki/Pyoderma_gangrenosum (accessed 25/07/2014).

Figure 1k. *STIR sequence image in the coronal plane from a 14-year old boy showing sacroiliitis* [MRI image]. From: Tse, S.M. and R.M. Laxer, *New advances in juvenile spondyloarthritis.* Nat Rev Rheumatol, 2012. **8**(5): p. 269-79.

Figure 1l. *Superficial and irregular oral ulceration on the tongue* [photo]. From:http://www.scielo.br/scielo.php?pid=S180759322007000600018&script=sci_arttext (accessed 25/07/2014).

Appendix 1 Primers, probes and morpholinos used

Mouse primers used

Gene	Primer pair	Primer sequence	Size (bp)
Mouse genotyping primers			
Wildtype *Optn*	Optn_47570 F	5'-ACCACACGATGGCTCACAAC-3'	435
	Optn_47570 R	5'-GTGTCTCAAAACAACAAATTCTCCC-3'	
Mutant *Optn*	Optn_47570 F	5'-ACCACACGATGGCTCACAAC-3'	238
	CAS_R1_Term x	5'-TCGTGGTATCGTTATGCGCC-3'	
Wildtype *Nod2*	oIMR4112 F	5'-ACAGAGATGCCGACACCATACTG-3'	370
	oIMR4113 R	5'-TGGAGAAGGTTGAAGAGCAGAGTC-3'	
Mutant *Nod2*	oIMR4114 F	5'-TGACTGTGGCTAATGTCCTTTGTG-3'	1000
	oIMR6955 R	5'-TTCTATCGCCTTCTTGACGAGTTC-3'	
Mouse qRT-PCR primers			
Optn	mOptn2 F	5'-GAGCAGCTGGCCTTGCA-3'	73
	mOptn2 R	5'-ACTGTCTACTGCCTCCCTCTTCA-3'	
Tnf	mTnf F	5'-CTGAACTTCGGGGTGATCGG-3'	122
	mTnf R	5'-GGCTTGTCACTCGAATTTTGAGA-3'	
Cxcl1	mCxcl1 F	5'-ACTGCACCCAAACCGAAGTC-3'	114
	mCxcl1 R	5'-TGGGGACACCTTTTAGCATCTT-3'	
Il6	mIL6 F	5'-CGCTATGAAGTTCCTCTCTGCAA-3'	64
	mIL6 R	5'-CACCAGCATCAGTCCCAAGAA-3'	
Il10	mIL10 F	5'-GCTGGACAACATACTGCTAACC-3'	78
	mIL10 R	5'-ATTTCCGATAAGGCTTGGCAA-3'	
Ppia	mPpia F	5'-GGGCCGCGTCTCCTTT-3'	86
	mPpia R	5'-ATCCTTTCTCTCCAGTGCTCAGA-3'	
Mcm10	mMcm10 F	5'-TCCCAGCCAAGAGAAAACCA-3'	115
	mMcm10 R	5'-CCCTGGAGGCTGTTTAATTG-3'	
Ccdc3	mCcdc3 F	5'-CTACTTCTCCTGCCACTCCC-3'	93
	mCcdc3 R	5'-CCGTGTGGCAAGAGATTGTA-3'	
Mouse RT-PCR primers			
Optn	mOptn ex2-4 F	5'-CTGACTGAGAAGGGGGACAG-3'	367
	mOptn ex2-4 R	5'-ACCTGTAGCCACCTGTGAGG-3'	

Zebrafish primers, probes and morpholinos used

Gene	Primer pair	Primer sequence	Size (bp)
Zebrafish in situ hybridisation probe			
optn	optineurin Fw455	5'-GCCAGAACCAGACTGAACACTATGG-3'	-
	optineurin Rv1736	5'-GGACTTCCCCACATTTAGGACAAG-3'	
Zebrafish morpholinos (MO)			
optn	*optn* MO	5'-AGAGCCTCTGTGGGATGCATATAAT-3'	-
control	control MO	5'-CCTCTTACCTCAGTTACAATTTATA-3'	
Zebrafish qRT-PCR primers			
optn	optn qFw1163	5'-TCGATGAGATGAAGATGGAACTATTC-3'	77
	optn qRv1239	5'-TTCTGCCTGTGCCTGGAAA-3'	
ef1alpha	ef1alpha qFw	5'-TGCCTTCGTCCCAATTTCAG-3'	101
	ef1alpha qRv	5'-TACCCTCCTTGCGCTCAATC-3'	
Zebrafish RT-PCR primers			
optn	optn sFw62	5'-GGCTGACTGTAACGCACCAATC-3'	360
	optn sRv421	5'-CTCCTTCTGCTTCTCCTTCCAAG-3'	
ef1alpha	ef1alpha sFw	5'-ATCTACAAATGCGGTGGAAT-3'	299
	ef1alpha sRv	5'-ATACCAGCCTCAAACTCACC-3'	

Appendix 2 Address of Chemical Suppliers and Equipment Manufacturers

Abbott/AbbVie Ltd
Abbott House
Vanwall Business Park
Vanwall Road
Maidenhead
Berkshire SL6 4XE

Abcam plc
330 Cambridge Science Park
Milton Road
Cambridge CB4 0FL

ABR Affinity BioReagents
4620 Technology Drive
Suite 600
Golden, CO
United States of America

Agar Scientific/
Elektron Technology (UK) Ltd
Unit 7, M11 Business Park
Parsonage Lane
Stansted CM24 8GF

BD
The Danby Building
Edmund Halley Road
Oxford Science Park
Oxford OX4 4DQ

Beckman Coulter (UK) Ltd
Oakley Court
Kingsmead Business Park
London Road
High Wycombe HP11 1JU

Bioline Reagents Ltd
16 The Edge Business Center
Humber Road
London NW2 6EW

Bio-Rad Laboratories Ltd
Bio-Rad House
Maxted Road
Hemel Hempstead
Hertfordshire HP2 7DX

BMG Labtech Ltd
5 Alton House Office Park
Gatehouse Way
Aylesbury
Buckinghamshire HP19 8YB

Calbiochem/Merck Serono Ltd
Bedfont Cross
Stanwell Road
Feltham
Middlesex TW14 8NX

Cecil Instruments Ltd
Milton Technical Centre
Cambridge CB24 6AZ

CellPath Ltd
Unit 80 Mochdre Enterprise Park
Newtown
Powys SY16 4LE

Clontech/Takara Bio Europe SAS
2 Avenue du President Kennedy
78100 Saint-Germain-en-laye
France

CSL Behring UK Ltd
Hayworth House
Market Place
Haywards Heath
West Sussex RH16 1DB

Dako UK Ltd
Cambridge House
St Thomas Place
Ely
Cambridgeshire CB7 4EX

eBioscience Ltd
2nd Floor, Titan Court
3 Bishop Square
Hatfield
Hertfordshire AL10 9NA

Enzo Life Sciences (UK) Ltd/
Alexis Biochemicals
Palatine House
Matford Court
Exeter EX2 8NL

Eppendorf (UK) Ltd/Innova
Eppendorf House
Gateway 1000 Whittle Way
Arlington Business Park
Stevenage SG1 2FP

Eurofins Genomics
Anzingerstr. 7a
85560 Ebersberg
Germany

GE Healthcare Ltd/Amersham/
PAA Laboratories
Amersham Place
Little Chalfont
Buckinghamshire HP7 9NA

GraphPad Software, Inc.
7825 Fay Avenue
Suite 230
La Jolla, CA 92037
United States of America

Immunostics Inc.
1750 Brielle Ave
Ocean, NJ 07712
United States of America

LEEC
Private Road No. 7
Colwick Industrial Estate
Nottingham NG4 2AJ

Leica Microsystems (UK) Ltd
Larch House
Woodlands Business Park
Breckland
Linford Wood
Milton Keynes MK14 6FG

Life Technologies Ltd/
Gibco/Invitrogen/
Applied Biosystems/Ambion
3 Fountain Drive
Inchinnan Business Park
Paisley PA4 9RF

Lonza Biologics plc/Amaxa
Suite 3, Building A
The Courtyard
Severn Drive
Tewkesbury Business Park
Tewkesbury GL20 8GD

Merck Chemicals Ltd
Boulevard Industrial Park
Padge Road
Beeston
Nottingham NG9 2JR

Meso Scale Discovery
1601 Research Boulevard
Rockville, MD 20850-3173
United States of America

MP Biomedicals
Wellington House
East Road
Cambridge CB1 1BH

New England Biolabs Ltd
75-77 Knowl Piece
Wilbury Way
Hitchin SG4 0TY

Peprotech
Peprotech House
29 Margravine Road
London W6 8LL

Promega
Delta House
Southampton Science Park
Southhampton SO16 7NS

Qiagen
Qiagen House
Fleming Way
Crawley
West Sussex RH10 9NQ

R&D Ltd
19 Barton Lane
Abingdon Science Park
Abingdon OX14 3NB
Santa Cruz Biotechnology, Inc.
Bergheimer Str 89
2 Heidelberg
69115 Germany

Sigma-Aldrich Company Ltd
The Old Brickyard
New Road
Gillingham
Dorset SP8 4XT

Scientific Laboratory Supplies Ltd
Wilford Industrial Estate
Ruddington Lane
Wilford
Nottingham NG 11 7EP

Thermo Fisher Scientific UK/
RA Lamb
Bishop Meadow Road
Loughborough LE11 5RG

TreeStar, Inc.
385 Williamson Way
Ashland, OR 97520
United States of America

UVItec Ltd
Unit 36, St John's Innovation
Centre
Cowley Street
Cambridge CB4 0WS

VWR International Ltd/BDH
Prolabo
Hunter Boulevard
Magna Park
Lutterworth
Leicester LE17 4XN

Appendix 3 Gantt Chart of PhD Research Activity

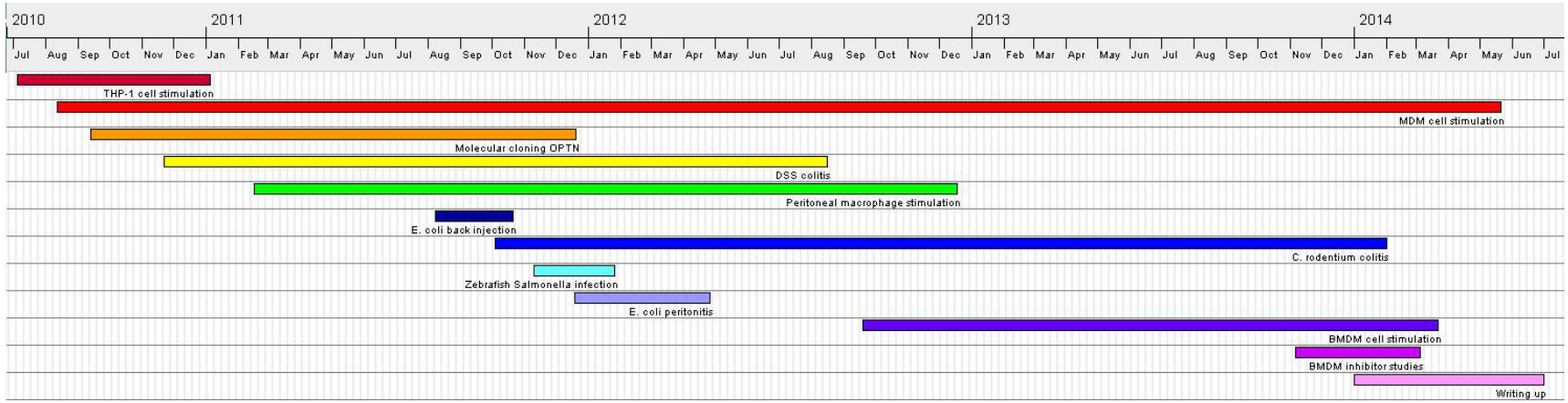

Appendix 4 Publications

Smith, A.M., Sewell, G.W., Levine, A.P., **Chew, T.S.**, Dunne, J., O'Shea, N.R., Smith, P.J., Harrison, P., McDonald, C.M., Bloom, S.L., Segal, A.W., Disruption of macrophage pro-inflammatory cytokine release in Crohn's disease is associated with reduced optineurin expression in a subset of patients. *Immunology* 2015. 144:45-55.

Chew, T.S., Sewell, G.W., O'Shea, N.R., Bloom, S.L., Segal, A.W., Smith, A.M., LB-003 The Role Of Optineurin In Macrophage Cytokine Secretion And Bowel Inflammation. *Gut* 2014. 63 Suppl 1: p. e2.

Appendix 5 Presentations & Prizes

Oral presentation
12th Annual North West Gastroenterology Meeting
Lytham St Annes, United Kingdom 2014

Best Oral Communication Prize
Gut and Liver Inflammation: A Translational Science Masterclass
British Society of Gastroenterology Annual Conference
Manchester, United Kingdom 2014

Oral presentation
12th Annual Bardhan Fellowship Meeting
Sheffield, United Kingdom 2014

Best digital oral poster award
9th European Crohn's and Colitis Organisation Congress
Copenhagen, Denmark 2014

Poster presentation
Keystone symposia: Molecular Cell Biology of Macrophages in Human Diseases
Santa Fe, United States of America 2014